Heat Transfer Enhancement using Ethylene Glycol and Water mixture based nanofluids in a Plate Heat Exchanger

Submitted in partial fulfilment of the requirements for the award of the degree of

DOCTOR OF PHILOSOPHY

in

CHEMICAL ENGINEERING

by

Yashawantha K M

Roll No: 718155

Under the Supervision of

Dr. A VENU VINOD

Professor

DEPARTMENT OF CHEMICAL ENGINEERING

NATIONAL INSTITUTE OF TECHNOLOGY WARANGAL

TELANGANA – 506004, INDIA.

November 2021

NATIONAL INSTITUTE OF TECHNOLOGY

Warangal – 506004, Telangana, INDIA.

CERTIFICATE

This is to certify that the thesis entitled **"Heat Transfer Enhancement using Ethylene Glycol and Water mixture based nanofluids in a Plate Heat Exchanger"** being submitted by Mr. **Yashawantha K M** for the award of the degree of Doctor of Philosophy (Ph.D) in Chemical Engineering to the National Institute of Technology, Warangal, India is a record of the bonafide research work carried out by him under my supervision. The thesis has fulfilled the requirements according to the regulations of this Institute and in my opinion has reached the standards for submission. The results embodied in the thesis have not been submitted to any other University or Institute for the award of any degree or diploma.

Date:

Dr. A. Venu Vinod
Thesis Supervisor
Professor
Department of Chemical Engineering
National Institute of Technology, Warangal, India.

DECLARATION

This is to certify that the work presented in the thesis entitled "**Heat Transfer Enhancement using Ethylene Glycol and Water mixture based nanofluids in a Plate Heat Exchanger**" is a bonafide work done by me under the supervision of Dr. A. Venu Vinod and was not submitted elsewhere for award of any degree.

I declare that this written submission represents my ideas in my own words and where others' ideas or words have been included, I have adequately cited and referenced the original source. I also declare that I have adhered to all principles of academic honesty and integrity and have not misrepresented or fabricated or falsified any idea/data/fact/source in my submission.

I understand that any violation of the above will be a cause for disciplinary action by the Institute and can also evoke penal action from the sources which have thus not been properly cited or from whom proper permission has not been taken when needed.

YASHAWANTHA K M
Roll No.718155

ACKNOWLEDGMENTS

First and foremost, I would like to thank my supervisor**,** ***Prof. A. Venu Vinod***, for his disciplined, patient guidance, timely appreciation, extraordinary support, enormous enlightening discussion with constructive criticism, inspiring, enticing pieces of advice, and sustained input throughout the research work and thesis preparation. The guidance has been a great learning experience for me throughout my stay at the National Institute of Technology Warangal, by strengthening me all the time. I owe a lot to him for his positive encouragement and guidance.

I would like to express gratitude to the university authorities, ***Prof. N.V. Ramana Rao***, Director, National Institute of Technology Warangal, and other officials who provided me with an opportunity to carry out research work.

I also sincerely thank ***Dr. S. Srinath,*** Head, Chemical Engineering Department, National Institute of Technology Warangal, for providing the necessary facilities to carry out research work in the department and for his valuable suggestions.

I wish to express my sincere thanks and gratitude to my doctoral scrutiny committee (DSC) members, ***Dr. S. Vidya Sagar*** and ***Dr. Raghu Raja Pandiyan Kuppusamy,*** Department of Chemical Engineering and ***Dr. D. Jaya Krishna,*** Department of Mechanical Engineering, National Institute of Technology Warangal, for their kind support, encouragement, and valuable suggestions for successful completion of this research work.

I would like to extend my thanks to all the faculty members in the Department of Chemical Engineering for their valuable suggestions and encouragement.

I take this opportunity to sincerely acknowledge the ***Aeronautics Research Development Board (AR & DB)*** of the ***Defence Research and Development Organisation (DRDO)***, ***Government of India*** for providing the financial assistance to conduct research work at the National Institute of Technology Warangal.

I would like to thanks ***Mr. Ramalingam, SVL Engineering services, Tamilnadu*** for providing the help for successful completion of my research work.

I would like to thank ***Mr. Sandeep, Application Specialist*****,** Malvern-Aimil Application Centre, Bengaluru, for help and useful conversations.

I would like to thank to my friends ***Dr. Patil Harshal Somnath, Mr. Ram Kishore Dora, Dr. B. Anil Kumar Naik, Dr. Gajanan Suryawanshi, Mr. Khiriod Kumar Mahapatro, Mr. Vikas Hakke, Mrs. Vividha Landage*** and ***Ms. Keerthi Sangamitra,*** for their companionship, many fruitful conversations, help, and quality time spent together throughout my stay at National Institute of Technology Warangal.

This thesis would not have been possible without the support of ***Mrs. Harini Yashawantha*** **(**Wife) and ***Honisha gowda K.Y*** (Daughter). I am grateful to them for their never-ending love, patience and encouragement.

Last but not least, I would like to express my deepest thanks to my family members ***Marigowda A*** (Father) and ***Radha K.P*** (Mother) for their understanding, patience, continuous support and heartiest love.

YASHAWANTHA K M

Abstract

Nanofluids have been proven to be superior heat transfer fluids due to their enhanced thermal properties. Plate heat exchangers have been used in many applications due to their very high heat transfer coefficients. Heat transfer rates in plate heat exchangers are higher as compared to those in shell and tube heat exchangers and are more compact. The addition of nanoparticles of higher thermal conductivity to the ethylene glycol (EG) and water mixture (base fluid, generally used for low temperature applications) enhances the thermal conductivity of the fluid and thereby increases the heat transfer coefficient.

Nanofluids of two materials (Al_2O_3 and TiO_2) were used in this study to perform experimental investigations on heat transfer and entropy generation in a plate heat exchanger. Thermophysical characteristics of nanofluid, such as thermal conductivity and rheological behaviour were determined experimentally. The effect of nanofluid concentration (0.2-2 wt.%) and inlet temperature (5-55 °C) on thermal conductivity and viscosity of nanofluids was studied. Using ultrasonication technique, nanofluids of various concentrations were prepared in ethylene glycol and water mixture (35/65 % volume). The thermal conductivity and viscosity of the nanofluid were measured using KD2 Pro thermal properties analyzer and rheometer respectively. The results showed that the thermal conductivity of nanofluid increased significantly as the concentration and temperature of the nanofluid increased. Thermal conductivity increased by 4.87% and 2.68% for Al_2O_3 and TiO_2 nanoparticles at 5 °C for 2 wt.% concentrations, respectively, as compared to EG:water. Similarly, the viscosity increase of 9.89% and 12.99% was observed for Al_2O_3 and TiO_2 nanofluid at 5 °C at 2 wt.% concentrations, respectively. The investigation revealed Newtonian behavior of the nanofluids in the shear rate range 10 – 1000 s^{-1}. The experimental results indicated that the viscosity of both nanofluids increases with increasing concentration and decreases with increasing temperature.

Correlations were developed for predicting the effective thermal conductivity and relative viscosity considering experimental data from the present study and literature results. Subsequently, machine learning models (artificial neural network (ANN) and adaptive neuro fuzzy inference system (ANFIS)) have been implemented to model the effective thermal conductivity (k_{nf}/k_{bf}) and relative viscosity (μ_{nf}/μ_{bf}) of nanofluids and compared with developed correlations. The models developed in this study are more generalized as literature results were

considered in addition to the results from the present study. ANN and ANFIS models performed better than the correlations developed.

Experimental studies were carried out in a plate heat exchanger to investigate heat transfer characteristics such as heat transfer rate, overall heat transfer coefficient, convective heat transfer coefficient, effectiveness and pumping power for EG: water - Al_2O_3 and TiO_2 nanofluids in the concentration range of 0.2 to 2 wt.%. Distilled water was used as a hot fluid and nanofluid as a cold fluid. The effect of nanopowder concentration on heat transfer was investigated at 20, 10 and - 5 °C inlet temperatures and the different flow rates of nanofluid. The results show a significant improvement in heat transfer using nanofluid compared to EG:water mixture (base fluid) considered in the study. The convective heat transfer coefficient showed an enhancement of 30.28%, 25.40% and 18.26% for Al_2O_3 nanofluid of 2 wt.% concentration compared to base fluid at 20°C, 10 °C and – 5 °C nanofluid inlet temperatures respectively. However, a slight increase in pumping power was observed due to the increase in particle concentration. The heat transfer rate, convective heat transfer coefficient and overall heat transfer coefficient increase with increase in nanoparticle concentration, nanofluid inlet temperature and Peclet number of nanofluid. The higher effectiveness of the plate heat exchanger was obtained with use of nanofliuids. A correlation was developed to predict the Nusselt number considering the experimental data. The prediction of the Nusselt number obtained from the present study showed good agreement with the experimental results.

Entropy generation due to heat transfer in plate heat exchanger was evaluated for Al_2O_3 and TiO_2 nanofluids. Thermal entropy generation and friction entropy generation showed descending and ascending trends respectively, for the considered weight concentration of nanofluid for the increased Peclet number. However, total entropy generation indicated significant reduction due to nanoparticle addition. Bejan number demonstrated the roles of heat transfer and fluid friction in the entropy generation.

Table of Contents

List of Figures

List of Tables

Nomenclature

A	Surface area (m^2)
b	Mean channel spacing (m)
Be	Bejan number
c_p	Specific heat capacity (J/kg.K)
D_h	Hydraulic diameter (m)
d	Particle diameter (nm)
f	Friction factor
G	Channel mass velocity (kg. m^2/s)
h	Convective heat transfer coefficient (W/m^2 .K)
k	Thermal conductivity (W/m .K)
L_{eff}	Effective length of plate (m)
m	Fluid mass flow rate (kg/s)
M	Molecular weight (grams/mole)
N_{cp}	Number of channels
Nu	Nusselt number
Pe	Peclet number
Pr	Prandtl number
Q	Heat transfer rate (W)
q	Heat transfer rate per unit length (W/m)
Re	Reynolds number
R	Correlation coefficient
R^2	Coefficient of determination
S_g	Total entropy generation (W/K)
T	Temperature (K)
U	Overall heat transfer coefficient (W/m^2 .K)
Δp	Pressure drop (Pa)
V	Volume ratio of EG and water mixture

Greek Letters

μ	Viscosity (cP)
β	Chevron angle
ρ	Density(kg/m^3)

α	Thermal diffusivity (m^2/s)
γ	Shear rate (1/s)
ε	Effectiveness
ϕ_w	Weight concentration
ϕ_v	Volume concentration

Subscripts

Avg	Average
bf	Base fluid
c	Cold side
exp	Experimental
eff	Effective
F	fluid friction
hf	Hot fluid
np	Nanoparticles
nf	Nanofluid
in	Inlet
out	Outlet
ref	Reference
rel	Relative
t	Thickness of plate
TH	Heat transfer
w	Water

Abbreviation

AI	Artificial intelligence
ASHARE	American society of heating, ventilation and air conditioning
ANFIS	Adoptive neuro - fuzzy inference system
ANN	Artificial neural network
BP	Backpropagation
BR	Base ratio
CAS	Chemical abstracts service
CTAB	Cetrimonium bromide
CHTC	Convective heat transfer coefficient (W/m^2)

DI	Distilled water
EG	Ethylene Glycol
FESEM	Field emission scanning electron microscopy
FEG	Frictional entropy generation (W/K)
FF	Feedforward
FIS	Fuzzy inference system
GA	Gum arabic
HTC	Heat transfer coefficient
HVAC	Heating, ventilation and air conditioning
LMTD	Logarithmic mean temperature difference (K)
MAPE	Mean absolute percentage error
MARS	Multivariate adaptive regression splines
MF	Membership function
MLP	Multi-layer perceptron
MPR	Multivariable polynomial regression
MWCNT	Multi-walled carbon nanotube
NTU	Number of transfer units
OHTC	Overall heat transfer coefficient (W/m^2)
PHE	Plate heat exchanger
PVP	Polyvinylpyrrolidone
RBF	Radial basis function
RMSE	Root mean square error
SDBS	Sodium dodecylbenzene sulfonate
SDS	Sodium dodecyl sulfate (SDS)
SVM	Support vector machines
TEG	Thermal entropy generation (W/K)

Chapter 1 Introduction

Extended surfaces, tube inserts, fins, tube deformation and baffles have been employed to improve the heat transfer capabilities of the heat transfer devices. Though, flow arrangement and increased surface area with various designs may improve performance significantly, the fabrication of these devices limits the use of complex designs. Water, engine oil, ethylene glycol (EG), mixtures of EG and water have been employed as heat transfer fluids. The thermal properties of these fluids are critical in improving heat transfer performance. Thermal conductivity of the fluids can be enhanced by suspending fine solid particles, as they have higher thermal conductivity than liquids (Choi and Eastman, 1995; Eastman et al., 1997). Such fluids containing nanoparticles are called nanofluids. Enhancement of heat transfer rates results in (i) smaller heat exchangers and (ii) shorter processing times. In this chapter, some of the heat transfer enhancement techniques and definitions of the systems are discussed.

1.1 Heat Transfer Enhancement

Heat transfer enhancement in heat exchangers can be accomplished by implementing additional surface or increasing heat transfer coefficient (HTC) depending on the applications. The main goal is to get a better rate of heat transfer in fixed conditions. Heat transfer rate between a fluid flowing past a surface is obtained using Eq. (1.1)

$$Q = hA\Delta T \tag{1.1}$$

To enhance the value of hA, the options are: The HTC can be enhanced without a considerable enhancement in the surface area. HTC maintained without any considerable change and surface area can be enhanced. Both the HTC and the surface area can be enhanced.

Heat transfer from an extended surface is obtained using Eq. (1.2)

$$Q = hA\eta\Delta T \tag{1.2}$$

In a heat exchanger, the two fluids are separated by a wall. The rate of heat transfer (Q) between two fluids can be determined using Eq. (1.3)

$$Q = UA(LMTD) \tag{1.3}$$

The heat transfer can be enhanced with either or both of the *hA* terms, that is, decreased convective resistance on both sides. From Eq. (1.3) increase of *UA* term will have following contribution (Kakac and Liu, 2003):

- Reduction of the size of the heat exchangers: If the heat duty is maintained constant under the same temperature circumstances, the size of heat exchangers can be reduced. If the size and the inlet temperatures are kept constant, then the rate of heat exchange will increase.
- If the heat duty *Q* and size are retained, then *LMTD* may be reduced. This delivers enhanced thermodynamic process efficiency and gives lower operating cost.

1.2 Heat Transfer Enhancement Techniques

The major challenge in designing heat transfer equipment is to make the equipment more compact and attain a high heat transfer rate by minimizing energy consumption. Intensification of heat transfer can help in meeting the challenge of designing a compact heat exchanger. The process of improving the performance of a heat exchanger is stated as the heat transfer enhancement technique. There are three types of heat transfer enhancement methods.

(i) Active technique: Aid of external power such as surface vibration, fluid vibration, mechanical aids, electric fields and jet impingement (Zimparov, 2002).

(ii) Passive technique: enhances heat transfer by changing or disrupting the existing flow behaviour such as use of rough surfaces, coating the surfaces, use of special surface geometry (e.g., coiled tubes, plate - fin, tube - fin heat exchanger), surface tension devices, displaced enhancement devices, fluid additives (e.g., nanoparticles), swirl flow devices (Dewan et al., 2004; Durmuş et al., 2009).

(iii) Compound technique: both active and passive techniques can be used simultaneously.

1.3 Heat Exchangers

Some of the important types of heat exchangers are double pipe heat exchanger, shell and tube heat exchanger and plate type heat exchanger. Plate heat exchangers are compact and give high heat transfer rates.

1.3.1 Plate heat exchangers

Plate heat exchangers (PHEs) are built of thin plates forming flow channels. The fluid streams are separated by flat plates which are smooth or between which lie corrugated fins. Plate heat exchangers are used for transferring heat for any combination of gas, liquid, and two-phase streams. These heat exchangers can further be classified as gasketed plate, spiral plate, or lamella (Kakac and Liu, 2003).

1.3.2 Gasketed Plate heat exchangers

Gasketed plate heat exchangers were developed in the 1930s, mostly for the food industry, due easiness in cleaning of plates. Later, in 1960s it gained lots of importance due to invention of effect geometries plates, superior gasket materials and assembly (Kakac and Liu, 2003). The scope of potential applications has expanded significantly, and it now overlaps and effectively competes in areas formerly perceived to be the domain of tabular heat exchangers under specific and appropriate conditions. They can perform a wide range of tasks in a variety of sectors. As a result, they can be used as a low and medium pressure liquid to liquid heat transfer alternative to shell and tube type heat exchangers. Fig.1.1 depicts a conventional plate and frame heat exchanger. Fig.1.2 depicts the flow pattern through a Gasketed PHE.

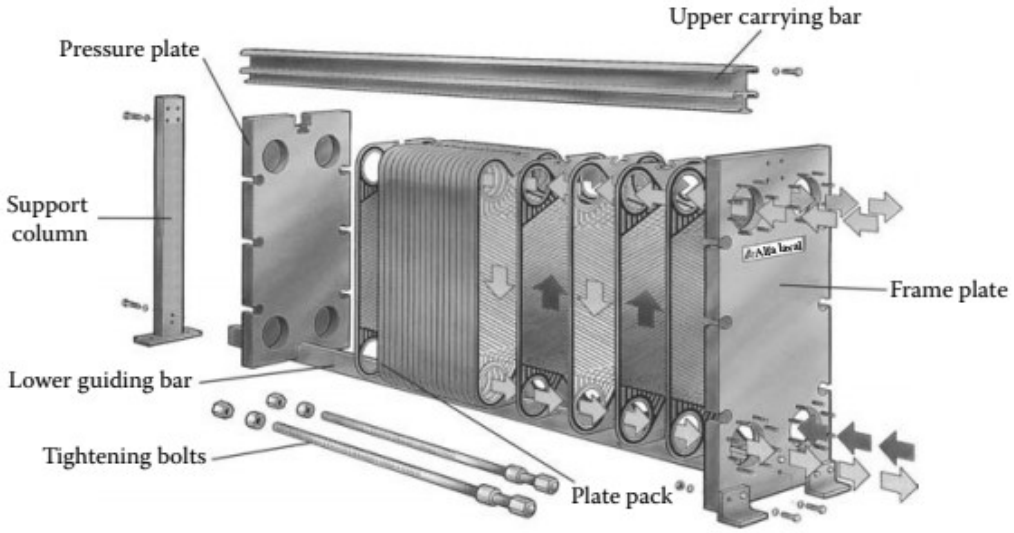

Fig. 1.1 Plate type heat exchanger (Kakac and Liu, 2003)

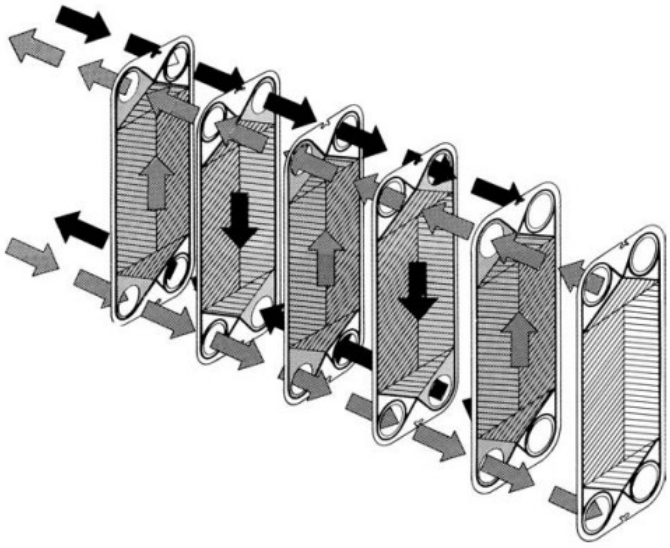

Fig. 1.2 Fluid flow diagram in a single-pass counterflow arrangement of plate type heat exchanger (Kakac and Liu, 2003)

The holes in the corners of a plate package provide continuous channels or manifolds that carry media from the inlet port of the PHE into the narrow tunnels created between the plates (Fig. 1.2). These passageways produced between the plates or corner ports are configured in such a way that the two heat transfer mediums can take alternative routes (counter-current flow). When the transit of flow phenomena takes place through the heat exchange device, the hot stream will transfer part of its heat energy to the colder stream on the opposite side via the thin plate wall (Gut and Pinto, 2003). Finally, the medium is discharged from the heat exchanger through exit hole tunnels (Gut and Pinto, 2004). The plate with corrugated design made precisely from a sheet of metal illustrated in Fig. 1.3, is the most fundamental component of the plate pack. A single plate's heat transfer area is in the range of 0.01-3.60 m^2. The gasket provided around the outside of the plate prevents leakage from the plate channels to the surrounding environment. Stainless steel, titanium, titanium-palladium, aluminium, and aluminium brass are the most common materials for plates (Kakac and Liu, 2003).

The most popular type of modern PHE is the chevron plate heat exchanger. The chevron pattern is formed by connecting neighbouring plates in such a way that the flow stream channel generates swirling motion for the fluids. This configuration has an angle known as the chevron angle. When the plates are clamped, the chevron angle on adjacent plates is reversed. The plates are used generally 0.6 mm due to numerous connecting point across the plate for the support.

The chevron angle of PHEs varies in the range of 20º to 65º (Kakac and Liu, 2003; Khan et al., 2009).

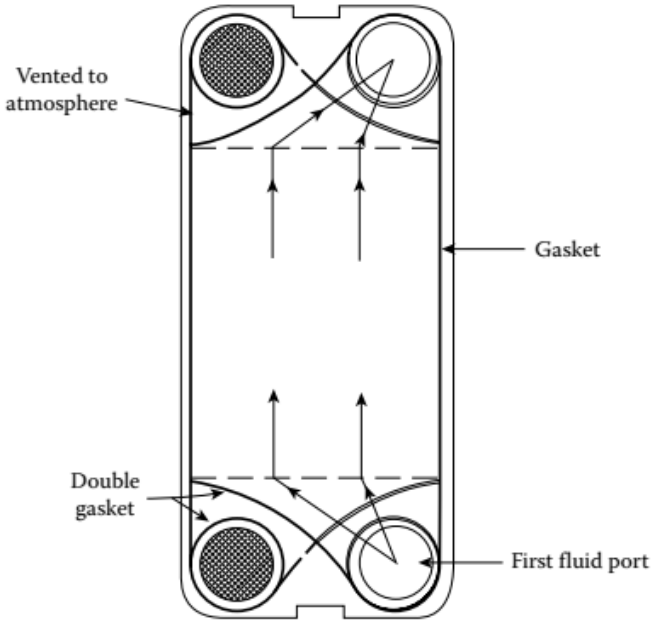

Fig. 1.3 Gasket arrangements in Plate type heat exchanger (Kakac and Liu, 2003)

The most common of these are chevron plate heat exchangers. Normally, a chevron plate generates a lot of turbulence, which allows for effective heat transfer (Tsai et al., 2009; Han et al., 2010). The heat transfer coefficients obtained in chevron plate heat exchangers can be equal to those produced by tubes with five times the Reynolds number (Kakac and Liu, 2003). For this reason, research on chevron plate heat exchangers with different chevron angles have been reported in literature.

1.3.3 Advantages of gasketed plate heat exchangers

The gasket design of PHEs is made such that the internal leakage is minimum. Moreover, the failure of such gaskets can be easily identified due to leaking into the environment as they are readily visible outside the unit. The following are the additional key advantages and benefits provided by gasketed PHEs:

- Design flexibility provided by a choice of plate sizes and pass configurations.
- Easily accessible heat transfer area, allowing for configuration adjustments to meet changing process needs by changing the number of plates.

- Efficient heat transmission; due to turbulence and the small hydraulic diameter, both fluids have high heat transfer coefficients.
- Compact in design, light in weight and only the edges of the plate are exposed to the environment. Heat losses are negligible, and no insulation is required.
- There can be no intermixing of the two fluids if the gasket fails and due to strong turbulence and a short residence period, plate units have minimal fouling properties.

1.4 Nanofluids

Nanofluids are novel fluids that contain solid particles with sizes smaller than 100 nm in the base fluid (Choi and Eastman, 1995). Conventional base fluids have a limited ability to transfer heat due to their low thermal conductivity. Materials having higher thermal conductivity can be dispersed in the base fluid to improve the heat transport properties (Saidur et al., 2011). The thermal conductivity of commonly used solids and liquids at room temperature for heat transfer applications is shown in Table 1.1 (Choi and Eastman, 1995; Paul et al., 2010; Nagarajan et al., 2014; Simpson et al., 2018).

Nanoparticles of metals, metal oxides and non-metal oxides have been used to prepare the nanofluids by dispersing them into the base fluid. Nanofluids are prepared using two methods; single step method and two step method. The most commonly used method of nanofluid preparation is the two step method. In the first step, nanoparticles are produced first in dry powder form by chemical or physical methods. In the second step, dry powders are dispersed into the base fluid using a magnetic stirrer, ultrasonication, high-profile mixing, homogenizing, and ball milling (Yu and Xie, 2012; Jama et al., 2016; Ali and Salam, 2020). Single step method employs a sequential cycle of nanoparticle synthesis and base fluid dispersion. This method will produce uniformly dispersed particles with good stability. This method entails simultaneously processing and dispersing nanoparticles into the base fluid (Zhu et al., 2004; Wu et al., 2009; Ghadimi et al., 2011; Yu et al., 2017; Ji et al., 2020).

The addition of nanoparticles to the conventional base fluid shows significant improvement of thermal properties and enhancement in heat transfer coefficients due to their high thermal conductivity and high specific surface area (Özerinç et al., 2010).Other characteristics of nanofluids include

- Greater heat transfer surface between particles and fluids due to high specific surface area.
- Due to their significantly smaller size, nanoparticles may be fluidized more easily and move faster in the base fluid without clogging.
- Can achieve high dispersion stability.
- Modifiable characteristics, including thermal conductivity and surface wettability, by adjusting particle concentrations to suit various applications.
- Enhanced efficiency in terms of manufacturing cost and size, energy consumption, and emission reduction.

Table 1.1 Thermal conductivity of solids and liquids at 30 °C

Material	Form	Thermal Conductivity (W/m.K)
Metals	Copper(Cu)	401
	Gold (Au)	315
	Silver	429
	Aluminium (Al)	237
Metal Oxides	Aluminium oxide (Al_2O_3)	36
	Copper oxide (CuO)	77
	Titanium oxide (TiO_2)	8.4
	Zinc oxide (ZnO)	29
Carbon	Carbon nanotubes (CNT)	2000
	Diamond	900-2320
Base fluids	Water	0.608
	Ethylene glycol	0.252
	Engine oil	0.145

1.4.1 Stability of nanofluids

Stability is one of the most important characteristics of any nanofluid, particularly in the application of heat transfer. Despite recent research on the stability of dispersions the synthesis

of higher stability homogenous nanofluids remains a major challenge (Ghadimi et al., 2011; Yu et al., 2017).There is a higher tendency for nanoparticles to form clusters in liquids, leading to microchannel blockage and degradation of nanofluid thermal characteristics (Ghadimi et al., 2011; Choudhary et al., 2017; Chakraborty and Panigrahi, 2020). The factors that may influence the stability of the nanofluid are use of surfactants, pH adjustment, nanofluid preparation technique, mixing / homogenization and nanoparticle loading.

Different methods have been used to evaluate the stability of nanofluids. Sediment photo capture method, zeta potential and UV-Visible spectrometer methods are used determine the stability of nanofluids. Some of the studies have considered the zeta potential method for stability analysis (Rashmi et al., 2011; Choudhary et al., 2017).The zeta potential represents electrostatic repulsion between nanoparticles. The particles are well distributed if the absolute zeta potential value is high. If the zeta potential is low, the nanoparticles tend to form a cluster and become poorly distributed. Sediment photography (Haghighi et al., 2013; Fuskele and Sarviya, 2017; Abdullah et al., 2018; Zhang et al., 2021) is an easy approach to assessing suspension stability. Using this approach, the photographs of the nanofluids are compared from time to time, resulting in an observable estimation of the nanofluids shelf life. The UV – Vis spectrophotometer (Rashmi et al., 2011; Sadeghi et al., 2015; Zhang et al., 2021) passes light through the suspension, and the absorbance graph versus the wavelength shows the absorption spectrum of samples.

1.4.2 Application of nanofluids

Nanofluids have superior heat transfer properties when compared to conventional heat transfer fluids. Wong and Leon (2010) and Saidur et al. (2011) reviews show the potential heat transfer application of nanofluids in industrial cooling applications, smart fluids, cooling electronics, nuclear reactors, extraction of geothermal power and other energy sources, cooling and heating in building, chillers and domestic refrigerators. The inclusion of nanoparticles into engine oils, coolants, automatic transmission fluids, lubricants, and other synthetic high-temperature heat transfer fluids may significantly benefit from the increased heat transfer by nanofluids (Wong and De Leon, 2010). This includes possible use of nanofluid coolant, nanofluid in fuel and brake and other vehicular nanofluids in automobile sector. Biomedical applications such as

nanodrug delivery, cancer theraupetics, cryopreservation, nanocryosurgery, sensing and imaging. Other applications such as in space, defense, ships and machining and grinding.

1.5 Thermo-Physical Properties of Nanofluids

The heat transfer behaviour of the nanofluid is determined based on its thermophysical properties such as thermal conductivity, viscosity, specific heat and density. The thermophysical properties of a nanofluid are dependent on nanoparticle loading, nanopowder material, temperature, morphology of nanoparticles and shear rate (viscosity) (Mahbubul et al., 2012; L Syam Sundar et al., 2013; Mishra et al., 2014; Meyer et al., 2015; W. H. Azmi et al., 2016; Murshed and Estellé, 2017).

1.6 Machine learning

The process of designing algorithms that allow a computers to learn is known as machine learning. Machine learning models are categorised as follows

1. Supervised learning - where the algorithm generates a function that maps inputs to desired outputs.
2. Unsupervised learning – A set of data that comprehends only inputs, and find arrangement of data, like grouping or clustering of data points.
3. Semi-supervised learning - It combines labelled and unlabelled instances to provide a suitable function or classifier.
4. Reinforcement learning - where the algorithm develops a strategy on how to operate based on world observation. Every action has an effect on the environment, and the environment offers feedback on the learning process.

1.6.1 Supervised learning

Supervised algorithms are classified into two types: regression and classification. The result of a regression type is a numerical value within a defined range, whereas the output of a classification type is a criteria within a specific range (Andrew Bagnell, 2005; Kotsiantis et al., 2006). The majority of mathematical models used in engineering problems and system modelling employ the regression type of supervised machine learning. A set of data known as the training set is analysed in order to determine the relationship between the input and output

variables. The obtained function, which may be computed using a variety of methods, is used to map the other datasets. In the following, commonly utilized machine learning methods have been used for modelling various kinds of nanofluids. These approaches are namely, multi-layer perceptron artificial neural network (MLP-ANN), radial basis function neural network (RBF-NN), group method of data handling (GMDH), adaptive neuro-fuzzy inference system (ANFIS), and support vector machine (SVM), respectively (Ramezanizadeh et al., 2019a). In this study, ANN and ANFIS model has been considered to model the experimental results.

1.6.1.1 Artificial neural network (ANN)

In recent years, the ANN technique has been applied for solving complex engineering problems (Longo et al., 2012). ANN modelling is a computational model based on the structure and functions of biological neural networks (Kurt and Kayfeci, 2009; Hemmat Esfe et al., 2015a). They are composed of three layers: the first (input) layer, the second (hidden) layer and the final (output) layer (Longo et al., 2012). Neurons are nodes that exist in each layer of the ANN. A node is a building block that uses a sum and transfer function to handle data in a network. Based on learning techniques, the ANN model is trained to characterise a dataset. The ANN model can be used for any type of relationship, including nonlinear, piecewise, discontinuous, and so on. The ANN model can be provided with an experimental dataset, which is split into training, validation, and testing points. In the process of ANN modelling, training and validation points may be used throughout the learning process, whereas the testing points may be utilised once the learning phase is completed to assess the model's ability to predict.

1.6.1.2 Adaptive Neuro Fuzzy Inference System (ANFIS)

Adaptive Neuro-Fuzzy Inference System (ANFIS) is a hybrid method used for optimizing the results by combining ANN and a fuzzy inference system (FIS). ANFIS approach has adaptation competence, nonlinear ability and rapid learning ability (Şahin and Erol, 2017). A fuzzy inference system considers the fuzzy if-then rules to model the complex systems (Jang, 1991). ANFIS system based on the Surgeno fuzzy model generates a set of fuzzy rule and membership functions automatically to establish strong relationship between inlet and output data. ANFIS model uses the combination of fuzzy logic and neural network to model the process. Prediction of data using ANFIS modelling is carried out in two stages - in the first stage fuzzy logic is formed (if-then rule), and then the neural network model of learning method is used to alter

these rules to optimize the model by reducing the error. The process involved in this model is data learning from the training data set using neural network theory, then by creating an ideal type of membership functions to map the input and output data established on the fuzzy if-then rules (Mehrabi et al., 2012; Hemmat Esfe, 2018; Aylı, 2020).

1.7 The present work and thesis organization

In this work, heat transfer studies were carried out in plate heat exchanger using nanopowder of two different materials (Al_2O_3 and TiO_2).

The thesis has been organized into five chapters. Chapter 1 deals with introduction to the work. In Chapter 2, a detailed literature review related to thermal conductivity, viscosity, stability, machine learning models and heat transfer studies in PHE has been presented to identify the gaps in literature and scope of study. In Chapter 3**,** materials used and methodology adopted for nanofluid preparation and its analyses for different important properties (thermal conductivity and viscosity) have been presented. Machine learning models (ANN and ANFIS) have been described. Experimental details of plate heat exchangers (heat transfer study) and data reduction are presented. Results obtained from the study are discussed in detail in chapter 4. In Chapter 5, the important conclusions drawn from the present work are mentioned.

Chapter 2 Literature Review

This chapter presents a detailed review of the previous work to identify the gaps in the literature regarding the thermophysical properties of nanofluids and heat transfer enhancement involving nanofluids. The chapter has been divided into the following sections.

1. **Thermophysical properties of nanofluids:** This section gives an overview of the studies on (i) thermophysical properties of nanofluids (ii) correlations for effective thermal conductivity and relative viscosity of nanofluids (ii) stability of nanofluids and (iv) ANN and ANFIS modelling.
2. **Heat transfer characteristics using nanofluids:** This section gives an account of literature relating to heat transfer studies using nanofluids.
3. **Thermodynamics analysis:** Previous work relating to entropy generation using nanofluids in heat exchangers has been mentioned.
4. **Scope and motivation:** This section sets up the objectives for the present study based on the gaps found in the literature.

2.1 Thermophysical Properties of Nanofluids

2.1.1 Thermal conductivity

Thermal conductivity of a fluid is the most important property for heat transfer studies. To enhance the property, researchers have developed a novel fluid by dispersing nanoparticles of higher thermal conductivity materials, of size below 100 nm. Such fluids containing nanoparticles are called nanofluids (Choi and Eastman, 1995). It is also known that the larger surface area (per volume) of the particles results in enhanced thermal conductivity of the fluid (Choi and Eastman, 1995).

Eastman et al. (1997) used water and HE 200 oil as a base fluid to disperse the Al_2O_3, CuO, and Cu nanoparticles. 5 vol.% of CuO nanoparticles suspended in water resulted in 60% enhancement in thermal conductivity compared to water without nanoparticles. Eastman et al. (2001) further extended their studies to carry out investigations on thermal conductivity of nanofluid using ethylene glycol (EG) as base fluid considering Cu particles (with less than 10 nm of size), and reported 40 % of enhancement for 0.3 vol.% concentration of nanofluid. Lee et al. (1999) considered Al_2O_3 and CuO dispersed in water and EG as base fluids to find the

thermal conductivity using the transient hot wire method. The findings of the experiments revealed that nanofluids have shown higher values of thermal conductivity than base fluids. For 4 vol. % of nanoparticles, the CuO/EG mixture showed a 20% increase in thermal conductivity. Hwang et al. (2006) used a transient hot wire method to evaluate the thermal conductivity to examine the thermal conductivities of four types of nanofluids: multi-walled carbon nanotube (MWCNT) in water, CuO in water, SiO_2 in water, and CuO in EG. They found maximum enhancement of thermal conductivity of 11.3% for water-based MWCNT nanofluid at 0.01 vol.%.

EG is generally used as a heat transfer fluid in cold regions due to its low freezing point (-12.9 °C). In cold regions, the mixture of EG:water is generally used in HVAC and automobiles as a heat transfer fluid due to its low freezing point and (Vajjha et al., 2009). Many studies have been carried out to enhance thermal conductivity by adding nanoparticles of different metals and metal oxides. Vajja and Das (2009) conducted an experimental study to report the role of two metal oxides (Al_2O_3 and CuO) in improving thermal conductivity when an EG:water mixture is considered as the base fluid. Their studies indicated a 69% improvement in thermal conductivity for 6 vol.% EG:water-CuO nanofluid and 10 vol.% EG:water-Al_2O_3 nanofluid.

Kole and Dey (2013) performed thermal conductivity measurement of functionalized graphene oxide nanoparticles dispersed in a mixture of EG and water (70:30 volume/volume). They performed thermal conductivity measurements in a temperature range of 10 to 70 ºC considering low volume concentrations (0.041 to 0.395 vol.%). It was found that the addition of 0.395 vol.% of graphene oxide resulted in 15% enhancement in thermal conductivity at 25 ºC. Similar study was performed by Reddy and Rao (2013) to report thermal conductivity of EG:water (40:60 and 50:50 by mass) - TiO_2 nanofluids at different volume concentrations and at different temperatures. Their study showed 1.94% and 4.38% enhancement in thermal conductivity for 0.2 vol.% and 1 vol.% of concentration, respectively, at 30 ºC.

Sundar et al. (2013) prepared EG:water (50:50) based Al_2O_3 and CuO nanofluid to examine the effect on thermal conductivity at different temperatures by considering the different volume concentrations. Both the nanofluids were found to have higher thermal conductivity values with respect to concentration and temperature compared with the base fluid of a selected mixture of EG:water for their study. However, enhancement for EG:water - CuO nanofluid was higher compared to EG:water - Al_2O_3 nanofluid. Further studies were reported for different ratios of

EG:water (20:80%, 40:60% and 60:40% in mass) to study the effect of EG and water mixture ratio, concentration of Al_2O_3 nanoparticles and temperature (Sundar et al., 2014). Their study indicated a maximum enhancement of 32.26% for a 20: 80 ratio of EG:water at 1.5 vol.%.

Azmi et al. (2016) conducted a conductivity measurement of EG:water-TiO_2 nanofluids for 0.5-1.5% volume concentrations and temperatures in the range of (30 - 80 ºC). Maximum enhancement of thermal conductivity of 15.4% at 1.5 vol.% concentration and temperature of 60 °C was obtained for the TiO_2 nanofluid.

Soltanimehr and Afrand (2016) studied the thermal conductivity of MWCNTs dispersed in EG:water mixture (40:60 vol%) and reported the effects of temperature and concentration on thermal conductivity. Their study indicated a 34.7% enhancement in thermal conductivity for 1 vol.% at 50 ºC.

Abdolbaqi et al. (2016) performed thermal conductivity studies involving TiO_2 nanoparticles in bioglycol and water mixtures (20:80% and 30:70% by volume) at different temperatures (30 ˚C to 80 ˚C) by changing the particle loading from 0.5 to 2 vol.% respectively. Their study showed thermal conductivity enhancement of 12.6% and 11% for 2 vol.% at 80 ˚C for 20:80 and 30:70 ratio of bioglycol and water-TiO_2 nanofluid.

Ahmadi Nadooshan (2017) reported thermal conductivity of EG:water based ZnO nanofluids for different temperatures and concentrations. Their study showed that an increase in temperature and concentration has a significant effect on improvement in thermal conductivity property compared to the base fluid.

Krishnakumar et al. (2019) performed thermal conductivity measurement of TiO_2 nanoparticles dispersed in the EG:water mixture (60:40) experimentally using the KD2 Pro thermal properties analyzer. The study showed a significant improvement in thermal conductivity when TiO_2 nanoparticles were added to the mixture. Furthermore, the increase in thermal conductivity was 11% for the volume concentration of 0.8% at a temperature of 20 ºC and the corresponding increase at 50 ºC was 24%.

Akilu et al. (2020) performed the thermal conductivity study of TiN nanofluids by considering EG:water mixture (60:40 and 40:60) as a base fluid. The study was carried out for concentrations of 0.25 to 1.0 vol.% in the temperatures range of 20-60 ºC. The study indicated

that TiN nanofluid with of 60:40 base mixture ratio of EG:water exhibited thermal conductivity enhancement of 22.5%.

Table 2.1 summarizes the studies carried out in literature on thermal conductivity of EG:water mixture based nanofluids.

Table 2.1 Thermal conductivity enhancement reported in the literature for different ratios of EG and water mixture

Reference	Nanoparticles /particle size	EG and water (volume/ volume)	Nanoparticle volume %	Temperature (^{o}C)	Enhancement (%) in *k*
Reddy and Rao (2013)	TiO_2/21 nm	40:60	0.2- 1	30-70	4.38-5 (for 1 vol.%)
Sundar et al. (2013)	CuO/27 nm Al_2O_3/36.5 nm	50:50	0.2-0.8	15–50	15.6-24.56 (for 0.8 vol.%) 9.8-17.89 (for 0.8 vol.%)
Elias et al. (2014)	Al_2O_3/13 nm	50:50	0-1	10–50	8.3 – 9.8 (for 1 vol.%)
Sundar et al. (2014)	Al_2O_3/36.5 nm	20:80 40:60 60:40	0.3-1.5 0.3-1.5 0.3-1.5	20-60	17.47-32.26 (for 1.5 vol.%) 14.60-30.51 (for 1.5 vol.%) 11.07-27.42 (for 1.5 vol.%)
Hamid et al. (2016)	TiO_2/50 nm	40:60	0.5-1.5	30-80	7-15.35 (1.5 vol.%)
Chiam et al. (2017)	Al_2O_3/53 nm	40:60 50:50 60:40	0.2-1 0.2-1 0.2-1	30-70	4.2-8 (1 vol.%) 5-12 (1 vol.%) 8-17 (1 vol.%)
Krishnakumar et al. (2019)	TiO_2/40 nm	60:40	0.2-0.8	20-50	8-24 (0.8% vol)

2.1.1.1 Correlations for effective thermal conductivity

The thermal conductivity of nanofluids is generally correlated in terms of effective thermal conductivity (ratio of thermal conductivity of nanofluid to that of base fluid at the same conditions). Researchers have developed several correlations considering the influencing parameters to predict the thermal conductivity of nanofluids. One of the correlations widely used in literature is the Maxwell (1873) model, which considers the basic mixture rule to estimate the thermal conductivity of the particles suspended in the base fluid.

$$k_{eff} = \frac{2k_{bf} + k_{np} + 2(k_{np} - k_{bf})\emptyset_v}{2k_{bf} + k_{np} - (k_{np} - k_{bf})\emptyset_v} \quad (2.1)$$

The correlation (Eq.2.1) proposed by Maxwell is simple and applicable for only spherical particles and does not consider factors like particle size, shape and Brownian motion etc. Hamilton and Crosser (1962) developed a correlation by extending Maxwell's work for estimating thermal conductivity of liquid-solid mixture of non-spherical particles. Lu and Lin (1996) established a simple correlation for the thermal conductivity of nanofluids that takes spherical and non-spherical particles into consideration. Bhattacharya et al. (2004) developed a correlation for effective thermal conductivity of the nanofluid using Brownian motion, particle thermal conductivity and base fluid thermal conductivity.

Reddy et al. (2013) developed a correlation to predict the thermal conductivity of EG:water (60:40-volume ratio) based TiO_2 nanofluids considering their experimental results. Sundar et al. (2013) proposed a correlation to predict the effective thermal conductivity of EG:water (50:50 volume ratio) based CuO nanofluids. Furthermore, a generalized correlation was developed for the different mixtures of EG:water based Al_2O_3 nanofluids (Chiam et al., 2017). Srinivas and Vinod (2016) proposed correlation considering temperature and nanoparticle concentrations for water based-Al_2O_3, CuO and TiO_2 nanofluids. Several correlations related to different nanoparticles and base fluid have been developed in literature to predict the thermal conductivity of nanofluids. Table 2.2 shows the correlations developed in literature to predict the thermal conductivity of nanofluids using the (i) classical models and (ii) models developed using the experimental results.

Table 2.2 Correlations reported in literature for the effective thermal conductivity of nanofluids

Reference	Correlation	Remarks
Maxwell (1873)	$k_{eff} = \frac{2k_{bf} + k_{np} + 2(k_{np} - k_{bf})\emptyset_v}{2k_{bf} + k_{np} - (k_{np} - k_{bf})\emptyset_v}$	For spherical particles
Hamilton-Crosser (1962)	$k_{eff} = \frac{k_{np} + k_{bf}(n-1) - (k_{bf} - k_{np})(n-1)\emptyset_v}{k_{np} + k_{bf}(n-1) + (k_{bf} - k_{np})\emptyset_v}$	Spherical and non-spherical particles. $n = 3$ for spherical particles
Bhattacharya (2004)	$k_{eff} = \left(\frac{k_{np}}{k_{bf}}\right)\emptyset_v + (1 - \emptyset_v)$	Spherical particles
Chandrasekar et al. (2010)	$k_{eff} = \left[\frac{C_{p,nf}}{C_{p,bf}}\right]^{-0.023}\left[\frac{\rho_{nf}}{\rho_{bf}}\right]^{1.358}\left[\frac{M_{nf}}{M_{bf}}\right]^{-0.126}$ $M_{nf} = M_{np}\emptyset_v + M_{bf}(1 - \emptyset_v)$	Considering the molecular weights and specific heats of nanoparticle and base fluid
Patel et al. (2010)	$k_{eff} = k_{bf}\left(1 + 0.135\left[\frac{k_{np}}{k_{bf}}\right]^{0.273}{\emptyset_v}^{0.467}\left[\frac{T}{20}\right]^{0.547}\left[\frac{100}{d_{np}}\right]^{0.234}\right)$	Oxide and metallic nanofluid
Reddy et al. (2013)	$k_{eff} = a + b\emptyset_v$ a and b are obtained from regression $\emptyset_v$=0.2 to 1 vol.% T= 30 to 70 ºC	For EG:water (40:60) mixture based TiO_2 based nanofluids
Sundar et al. (2013)	$k_{eff} = 1.262\left[\frac{T_{max}}{T_{min}}\right]^{-0.09214}\emptyset^{0.07379}$ $\emptyset_v$=0.2 to 0.8 vol.% T= 15 to 50 ºC	For EG:water (50:50) mixture based CuO nanofluids
Sundar et al. (2014)	$k_{eff} = 1.0806 + 10.164\emptyset_v$ $\emptyset_v$=0.3 to 1.5% T= 20 to 60 ºC	For EG:water (40:60) mixture based Al_2O_3 nanofluids

Hamid et al. (2016)	$k_{eff} = \left(1 + \frac{\emptyset_v}{100}\right)^7 \left(\frac{T}{80}\right)^{0.024}$ $\emptyset_v$=0.2 to 1 vol.% T= 30 to 70 ºC	For EG:water (60:40) mixture based TiO_2 based nanofluids
Khdher et al. (2016)	$k_{eff} = 1.268 \left(\frac{\emptyset_v}{100}\right)^{0.036} \left(\frac{T_{nf}}{80}\right)^{-0.074}$ $\emptyset_v$=0.1 to 1 vol.% T= 30 to 80 ºC	Bioglycol based Al_2O_3 nanofluids
Srinivas and Vinod (2016)	$k_{eff} = a\,(\emptyset_v)^b \left(\frac{T_{nf}}{T_0}\right)^c \left(\frac{d_{bf}}{d_{np}}\right)^d$ $\emptyset_w$= 0.3 to 2 wt.% T= 30 to 70 ºC	For water based nanofluids
Azmi et al. (2016)	$k_{eff} = \left(1 + \frac{\emptyset_v}{100}\right)^7 \left(\frac{T_{nf}}{80}\right)^{0.024}$ $\emptyset_v$=0.5 to 1.5 vol.% T= 30 to 80 ºC	For TiO_2 nanofluids of EG:water (40:60) mixture
Chiam et al. (2017)	$k_{eff} = 0.9683 \left(1 + \frac{\emptyset_v}{100}\right)^{11.13} \left(1 + \frac{T}{70}\right)^{0.1676} (1 + BR)^{0.00111} \left(\frac{d_p}{36}\right)^{0.0572}$ BR- Base ratio of EG water mixture(0.4 to 0.6) $\emptyset_v$=0 to 1.5vol.% T= 20 to 70 ºC	For Al_2O_3 nanofluids of EG:water mixture
Naik and Vinod (2018)	$k_{eff} = a \left(\frac{T_{nf}}{T_{ref}}\right)^b \left(\frac{\emptyset_{nf}}{\emptyset_{bf}}\right)^c$ $\emptyset_{nf}$=0 to 1 wt.% T= 30 to 50 ºC	For CMC-water based nanofluids

2.1.2 Viscosity

The viscosity of a fluid is one of the important parameter for heat transfer application as it directly affects heat transfer performance. The studies from literature show that the viscosity of nanofluids increases as the concentration of nanoparticles in nanofluid increases and reduces with the increase in temperature. Kulkarni et al. (2006) performed an experimental investigation

on the viscosity of water based CuO nanofluids for the 5 vol.% to 15 vol.% concentration. The results showed shear thinning, pseudoplastic behaviour of prepared nanofluid.

Namburu et al. (2007) carried out the viscosity measurement of EG:water (60:40 - by mass) based CuO nanofluid over a temperature range of -35 ºC to 50 ºC by considering 0 to 6.12 vol.%. The results obtained from their studies showed the Newtonian nature of nanofluid.

Sahoo et al. (2009) performed experimental investigations to study the rheological behavior of aluminum oxide nanoparticles dispersed in a base fluid of 60% and 40% (by mass) of ethylene glycol and water. Nanofluids of different volume concentrations (1, 2, 4, 6, 8, and 10%) were tested for determining the viscous properties in a temperure range of -35 ºC to 90 ºC. It was found from their study that the nanofluid behaved as non-Newtonian at lower temperatures (-35 ºC to 0 ºC) and Newtonian at higher temperatures (0 ºC to 90 ºC).

Duangthongsuk and Wongwises (2009) reported the viscosity of TiO_2-water nanofluids for volume concentration of 0.2 to 2%. The viscosity data of these nanofluids was obtained using a rotational viscometer in the temperature range of 15 ºC - 35 ºC at a shear rate of 100 to 10000 s^{-1}. According to their findings, the viscosity of TiO_2-water nanofluid was found to increase with volume concentration and decrease with temperature. Similarly, Yiamsawas et al. (2013) considered a mixture of EG:water (20/80, mass%) based TiO_2 and Al_2O_3 nanofluids to conduct the viscosity study at various concentrations (0 to 4 vol.%) in a temperature range of 15 to 60 ºC. The study indicated that viscosity for both nanofluids was found to be more due to nanoparticle loading.

LotfizadehDehkordi et al. (2013) considered a mixture of EG:water (60:40 by mass) based Al_2O_3 nanofluids to report the change in viscosity due to the addition of nanoparticles. They considered sodium dodecylbenzene sulfonate (SDBS) to improve the stability of the dispersion. It was found that the maximum increase in viscosity was 23% at 1 vol.%.

Sundar et al. (2014) presented the viscosity of different mixtures of EG:water based Al_2O_3 nanofluid over a temperature range of 0 to 60 ºC for a concentration of 0.3 to 1.5 vol.%. Their findings showed that the viscosity of nanofluids increases with particle loading and decreases with temperature rise. The maximum increase in viscosity was 2.58 times greater than that of the base fluid (40:60 – EG:water by mass) for 1.5 vol.% at 0 °C.

Li et al. (2015) investigated the viscosity of ethylene glycol based ZnO nanofluids at a concentration of 1.75% to 10.5 vol.% using Polyvinylpyrrolidone (PVP) as a dispersant. They conducted viscosity measurements in the temperature range of 15 ºC to 55 ºC. The results indicated that the prepared nanofluid of all concentrations demonstrated Newtonian behaviour.

Chaim et al. (2017) reported the viscosity of Al_2O_3 nanofluids for the different ratio of EG in water for a concentration of 0.1 to 1 vol.% by using a rheometer for a temperature range of 30 ºC to 70 ºC. The viscosity was found to increase by 50% for 40:60 (EG:water) for 1 vol.% of concentration. The study concluded that the base proportion of EG in water along with particle concentration and temperature significantly affected the viscosity.

Krishnakumar et al. (2019) investigated the viscosity of EG:water (60:40 by mass) by dispersing TiO_2 nanoparticles (0.2 to 0.8 vol.%). The results indicated a maximum increase in viscosity of 16% for 0.8 vol.% at 50 °C. Their findings also showed that the viscosity of nanofluids increases with particle loading and decreases with increase of temperature.

Ali et al. (2020) considered TiO_2 nanotubes in EG:water mixture to report the effect of different parameters such as the mass concentration (0 to 1%), temperature (25–65 °C), and shear rate (150 – 500 s^{-1}) on the viscosity behaviour. Their study indicated that, at 55 °C, increasing the mass concentration of nanotubes from 0 to 1% resulted in a 30% increase in viscosity, whereas at 25 °C, a 22% increase was observed against base fluid.

Akilu et al. (2020) considered two mixtures of EG and water (60:40 and 40:60 in volume ratio) as the base fluid to prepare the titanium nitride (TiN) based nanofluid by adding SDBS as the surfactant. They have considered the effect of volume concentration (0.25 to 1%) and temperature (20 to 60 ºC) on the viscosity variation. Their results indicated that the viscosity of EG:water (60:40) based TiN nanofluid was higher compared to EG:water (40:60) based TiN nanofluid.

Table 2.3 shows the instruments and parameters used for the measurement of the viscosity reported in the literature.

Table 2.3 Literature reported on the viscosity measurement of nanofluids

Reference	Nanoparticles / base fluid	Shear rate and temperature	Nanoparticle concentration	Behaviour	Rheometer
Sundar et al.(2014)	Al_2O_3 –EG and water mixture (20:80, 60:40,40:60 by mass)	20 °C to 60 °C	0-1.5 vol.%	Newtonian	AR-1000 rheometer (TA Instruments, UK) (Plate and cone (40 mm and cone angle 4°))
Elias et al. (2014)	Al_2O_3 – EG:water mixture (50:50 by volume)	10 °C to 50 °C	0 - 1 vol.%	-	Brookfield programmable viscometer (model: LVDV-III ultra) Ultra low adapter (ULA)
Li et al. (2015)	ZnO – EG	15 °C to 55 °C	1.75- 10.7 wt.%	Newtonian	Kinexus pro (Malvern Instruments Ltd, Britain)
Li et al. (2015)	SiC – EG	100-1000 s^{-1} 25 to 60 °C	0.2-1 vol.%	Newtonian	HAAKE MARS III rheometer
Efse et al. (2015d)	$Mg(OH)_2$ - EG	25 ºC to 55 ºC	0-2 vol.%	Newtonian	Brookfield viscometer (LVDV) (UL adapter)
Khedkar et al. (2016)	TiO_2 – EG	0-600 s^{-1} 283 to 323 K	0-7 vol.%	Newtonian	AR-G2 rheometer (TA instruments, USA)

Żyła et al. (2017)	MgO –EG	100 to 1000 s^{-1} at 298.15 K	1.6-7.2 vol.%	Newtonian	HAAKE MARS 2 rheometer Double cone geometry (60 mm diameter with 1 º cone angle)
Krishnakumar et al. (2019)	TiO_2 – EG:water mixture (40:60)	20 to 80 °C	0-0.8 vol.%	-	Brookfield LVDV-II +Pro, rheometer (plate and cone)

2.1.2.1 Correlations for relative viscosity

The resistance between two layers of fluids is characterised by viscosity. If the fluid is exposed to shear after the nanoparticles are distributed, there is a potential of increased resistance between the two layers of the fluid and increased viscosity of the nanofluid. This increase in viscosity of nanofluid may be estimated by considering the solid–fluid mixture equations. The simple theoretical formulae for estimating the viscosity of nanofluids is the Einstein (1906) model, which is based on the assumption of a viscous fluid containing spherical particle suspensions. This correlation is valid for non-interacting suspensions containing spherical particles at a relatively low volume fraction (less than 0.02). Other limitations of the Einstein model include that the form of the particles and particle-particle interactions inside the solution are not taken into consideration. Due to the limitations of this equation, researchers developed empirical correlations for estimating the viscosity of nanofluids while taking into account high particle concentrations, particle shape, particle-particle interaction within the solution, particle size and fluid temperature. Table 2.4 shows the summary of the studies on the theoretical and experimental models for viscosity of nanofluids.

Table 2.4 Correlations proposed in literature for the prediction of viscosity of nanofluid

Reference	Correlation	Remarks
Einstein (1906)	$\mu_{rel} = 1 + 2.5\emptyset_v$	For spherical particles and $\emptyset_v$<0:02
Brinkman (1952)	$\mu_{rel} = \frac{1}{(1-\emptyset_v)^{2.5}}$	For particle concentrations less than 4 %.
Batchelor (1977)	$\mu_{rel} = 1 + 2.5\emptyset_v + 6.5{\emptyset_v}^2$	Effect of Brownian motion for rigid and spherical particles
Kulkarni et al. (2006)	$ln\ \mu_{nf} = A\left(\frac{1}{T}\right) - B$ $A = 20587{\emptyset_v}^2 + 15857\emptyset_v + 1078.3$ $B = -107.12{\emptyset_v}^2 + 53.548\emptyset_v + 2.8715$	$\emptyset_v = 0.05\ to\ 0.15$ T=278-323 K water-CuO nanofluid
Yiamsawas et al. (2013)	$\mu_{nf} = 0.891{\emptyset_v}^{0.7391}T^{0.099}{\mu_{bf}}^{0.9844}$ $\mu_{nf} = 0.839{\emptyset_v}^{0.1882}T^{0.089}{\mu_{bf}}^{1.1}$	$\emptyset_v = 1\ to\ 4$ T=15-60 ºC EG:water (20:80 by mass) - Al_2O_3 and TiO_2
Sundar et al. (2014)	$\mu_{rel} = Ae^{B\emptyset_v}$ A = 0.9396 and B = 24.16 for 20:80% EG:water nanofluid A = 0.9299 and B = 67.43 for 40:60% EG:water nanofluid A = 1.1216 and B = 77.56 for 60:40% EG:water nanofluid	$\emptyset_v = 0.3\ to\ 1.5$ T=20-60 ºC EG:water - Al_2O_3
Chiam et al. (2017)	$\mu_{rel} = \left(1 + \frac{\emptyset_v}{100}\right)^{32}\left(\frac{T_{nf}}{80}\right)^{-0.001}(0.1 + BR)^{0.08}$	$\emptyset_v = 0.2\ to\ 1$ T=30-70 ºC EG:water - Al_2O_3

		BR- 0.4 to 0.6
Azmi et al. (2016)	$\mu_{rel} = 1.05\left(1 + \frac{\emptyset_v}{100}\right)^{14.61}\left(\frac{T_{nf}}{80}\right)^{0.0928}$	$\emptyset_v = 0.5\ to\ 1.5$ T=30-80 ºC EG:water (40:60 by mass) - TiO_2

2.1.3 Density

The addition of nanoparticles into the base fluid increases the density of the suspension due to the density of solid particles being greater than that of liquids. Several studies have reported the density of nanofluids as a function of temperature and volume concentrations. The density of nanofluid can be expressed theoretically based on conventional mixing theory as:

$$\rho_{nf} = (1 - \emptyset_v)\rho_{bf} + \emptyset_v\rho_{np} \tag{2.2}$$

The studies carried out by the various researchers (Pak and Cho, 1998; Vajjha et al., 2009; Ho et al., 2010; Heyhat et al., 2012; Teng and Hung, 2014) shows that Eq. (2.2) is consistent with the experimental results.

2.1.4 Specific heat

The specific heat capacity of fluids is critical in understanding heat transport and energy content in thermal systems. Xuan and Roetzel (2000) reported the following equation for modelling the specific heat of nanofluids (Eq. 2.3).

$$(c_p)_{nf} = (1 - \emptyset_v)(c_p)_{bf} + \emptyset_v(c_p)_{np} \tag{2.3}$$

Namburu et al. (2007) carried out a specific heat study of SiO_2 nanofluid based on the mixture of EG and water of 60:40% by mass for 0 to 10 vol.%. The results showed that the obtained specific heat data was very close to that predicted by Eq. (2.3). The study conducted by Zhou and Ni (2008) shows that the specific heat of water based Al_2O_3 nanofluids decreases with increase in nanoparticle loading. The specific heat obtained from the experimental study is consistent with the prediction obtained from the Eq. (2.3). Similarly, satisfactory performance of Eq.(2.3) was also reported in the literature for the different nanofluids (O'Hanley et al., 2011; Barbés et al., 2013, 2014; Mondragón et al., 2013; Teng and Hung, 2014; Cabaleiro et al.,

2015). Popa et al. (2017) performed extensive study on specific heat of nanofluids and concluded that the Eq. (2.3) was found to be accurate enough for estimating specific heat of EG:water based nanofluids. The lower specific heat of the nanofluids can be attributed to the lower specific heat of the nanoparticle material.

2.2 Stability of Nanofluids

The stability of nanofluids is critical for their use in practical application. To prepare a stable nanofluids, many approaches and procedures have been developed. In chapter 1, the techniques and influencing factors that affect the stability of nanofluids have been discussed. The major factor influencing many other characteristics of nanofluids, such as thermal conductivity, is nanoparticle sedimentation in the base fluid. As a result, the stability of nanofluids is an important consideration in the evaluation of nanofluids. The nanofluid must be ensured of nanoparticle dispersion in the liquid (base fluid), and the appropriate mechanism is required to maintain the suspension's stability against sedimentation.

Hwang et al. (2008) prepared Ag based silicon oil nanofluid using a modified magnetron sputtering system (one step method) and showed that particles were homogeneously dispersed in the base fluid with long term stability in base fluid. However, a two-step method used to prepare the nanofluid revealed that stable nanofluids can be obtained by high-pressure homogenizer. It was also reported that the surfactants (i.e. sodium dodecyl sulfate (SDS) or oleic acid) improve the stability of the nanofluids by increasing the magnitude of the zeta potential.

Wang et. (2009) investigated the stability of water based nanofluids involving Al_2O_3 and Cu nanoparticles. The analysis was considered under different pH values and different concentration of SDBS dispersant. An optimal pH value and SDBS concentration resulted in the highest thermal conductivity of the nanofluids.

Wang et al. (2011) investigated the absorbency and the zeta potential of Al_2O_3 and TiO_2 nanofluids under different pH conditions and different nanofluid concentrations. The results showed that for 0.05% alumina and 0.01% titanium dioxide nano suspensions, the absolute value of the zeta potential and the absorbency of the two nanofluids with SDS dispersant are highest. Nanofluid with pH $\approx$ 8 for Al_2O_3 and pH $\approx$ 10 for TiO_2 showed more stability compared to the lower pH.

Fadele et al. (2012) prepared the water based TiO_2 nanofluids by ultra-sonicating for 1 hour using acetic acid as the stabilizer. Stability was investigated using zeta potential method. They have found that the prepared nanofluid resulted in zeta potential value of 55 mV showing the good dispersion stability of prepared nanofluid.

Mahbubul et al. (2015) performed stability study of water based Al_2O_3 nanofluids by varying the ultrasonication time (1-5 hour) and power amplitude (25% and 50%) for 0.5 vol.% of concentration. The study showed that better particle dispersion, smaller aggregate sizes, and higher zeta potentials were found for the 3 hour (50% power amplitude) and 5 hour (25% power amplitude) of ultrasonication, respectively.

Asadi et al. (2017) investigated the effect of surfactant and sonication time on the stability of Mg $(OH)_2$-water nanofluid. They prepared nanofluid by applying different sonication time (10, 30, 50, 80, and 160 min) and three different surfactants (Cetrimonium bromide (CTAB), SDS, Oleic Acid). Zeta potential analysis indicated that CTAB surfactant showed good stability of the nanofluid with 30 min of ultrasonication.

Table 2.5 Summary of the various types of nanofluids, as well as their preparation methods and stability indicators

Reference	Nanofluid	Nanoparticle size (nm)	Surfactant	Stability duration (hrs) and zeta potential (mV)
Sahooli et al.(2012)	Water-CuO	4	PVP (steric)	168 h 32.3 mV
LotfizadehDehkordi et al.(2013)	Water-Al_2O_3	25	SDBS (Electrostatic)	−40.1 mV
Ghadimi and Metselaar (2013)	Water-TiO_2	25	SDS (Electrostatic	168 h -55 mv
Choudhury et al. (2017)	Water-Al_2O_3	20	SDS (Electrostatic	384 h -30 mV

2.3 Machine learning models

Machine learning models have been recently used by many researchers for modelling the thermophysical properties of nanofluid due to good accuracy in prediction of output data (Bahiraei et al., 2019). Machine learning approaches such as an ANN, RBF, multivariable polynomial regression (MPR), ANFIS, SVM and multivariate adaptive regression splines (MARS) has been used for modelling the thermophysical properties of nanofluids.

2.3.1 ANN modelling

In recent years, the ANN technique has been considered as one of the widely used machine learning approach for solving complex engineering problem. The multilayer feed-forward (FF) neural network technique was employed by Kurt and Kayfeci (2009) to predict the thermal conductivity of ethylene glycol/water based solutions. Hojjat et al. (2011) model the thermal conductivity of different oxide nanoparticles (Al_2O_3, TiO_2 and CuO) dispersed in 0.5 wt% of aqueous CMC solution using ANN. FF neural network model was developed to represent the thermal conductivity as a function of the nanoparticle concentration, temperature and the thermal conductivity of the nanoparticles. ANN model developed by them showed good agreement with the experimental data.

Longo et al. (2012) presented 3-input and 4-input FF- ANN models for the prediction of the thermal conductivity of Al_2O_3 and TiO_2–water nanofluid as a function of nanoparticle concentration, nanoparticle thermal conductivity, temperature and nanoparticle size. From the results, it was observed that both models show a reasonable agreement in predicting experimental data.

Esfe et al. (2014) developed ANN model to predict the effective thermal conductivity of EG based MgO nanofluids using experimental data and the results obtained were in good agreement with the measured data.

Ariana et al. (2015) presented an ANN model to predict the thermal conductivity of water based Al_2O_3 nanofluids. The modelling approach was implemented by considering thermal conductivity data for various particle sizes of Al_2O_3 at different concentration and temperature. They used FF-ANN model of two hidden layers having 14 neurons to predict the data and

results showed satisfactory prediction with a coefficient of determination (R^2) of 0.971, absolute average relative deviation (AARD %) of 1.27%, and mean square error (MSE) of 4.73×10^{-4}.

Esfe et al. (2015a) developed an empirical correlation and carried out FF-ANN modelling to predict the thermal conductivity of water based Al_2O_3 nanofluid. The correlation and ANN model performed well in predicting the thermal conductivity of nanofluid. One more study was carried out by them, in which ANN modelling proved better than correlation for EG:water (40:60) based MgO nanofluids (Hemmat Esfe et al., 2015b).

Tahani et al. (2016) performed ANN modelling for thermal conductivity of deionized water based graphite oxide nanoplatelets considering mass concentration and temperature as input variables. In their study, two hidden layers with eight neurons were used to predict the thermal conductivity. From the predicted data, root mean square error (RMSE), mean absolute percentage error (MAPE) and R^2 were determined to evaluate the performance of ANN. Results showed the accurate prediction of the thermal conductivity.

Zhao et al. (2017) adopted RBF-ANN approach to predict the thermal conductivity of water based Al_2O_3 nanofluids considering concentration and temperature as input variables. Their results concluded that ANN modelling can be used as an effective method to predict the thermophysical properties of nanofluids with an error of ±2%.

Alrashed et al. (2018) considered ANN model to model the viscosity, thermal conductivity and density of water based carboxylic diamond and MWCNT nanofluids. Model was developed based on three input variables consisting of volume fraction, temperature and particles type and three outputs, dynamic viscosity, density and thermal conductivity. Their results indicated that ANN model have the least MAPE and RMSE in all cases, in estimation of thermal conductivity, density and viscosity of both nanofluids. The ANN model results showed an excellent agreement with experimental results.

Ahmadi et al. (2019) proposed three methods (ANN, MARS, and MPR) for predicting the viscosity of water-silver nanofluid based on experimental data collected from the literature. Nanoparticle size, temperature and volume concentration of nanofluid were taken as the input variables for modelling. The study showed R^2 values of 0.9998, 0.9997 and 0.9996 for the ANN, MARS and MPR approaches, respectively. Thus, the viscosity data obtained from the modelling of nanofluid showed very good agreement with results reported in the literature.

Toghraie et al. (2019) presented an ANN model to forecast the dynamic viscosity of a EG-Silver nanofluid by taking the temperature and volume fraction as the input variables. The outcome of this model was then compared to the developed correlation, and results showed that ANN model prediction outperformed the correlation method.

Using literature data, Parashar et al. (2020) implemented ANN to forecast the viscosity of EG based nanofluids. They used nanoparticle diameter, temperature and nanoparticle concentration as input variables and relative viscosity (μ_{nf}/μ_{bf}) was considered as a target. Model was trained and tested with the various sets of neurons in the hidden layer and developed an optimal model with 2 hidden layers (45 neurons in both hidden layers). Their findings revealed that the ANN model's estimation of nanofluid viscosity was close to experimental results.

Afzal et al. (2021) proposed backpropagation (BP) modelling to predict the viscosity and shear stress of Ionic-MXene nanofluid considering the experimental data. The modelling was carried out considering the temperature, mass concentration and shear rate to predict viscosity and shear stress. The model was configured with different neurons (less than 5) in the hidden layer to estimate the viscosity and shear stress. The study concluded that BP modelling can be used to predict the viscosity and shear stress of Ionic-MXene nanofluid accurately with fewer neurons in the hidden layer.

2.3.2 ANFIS modelling

From literature review, it can be seen that ANN approach is the most widely used to estimate the thermal conductivity and viscosity of nanofluids. While many studies have employed a variety of artificial intelligent methods for predicting the thermophysical properties of nanofluids, novel artificial intelligent methods (hybrids) have yet to be extensively explored. Combining the ANN and fuzzy-set theory can provide advantages and overcome the disadvantages in both techniques. ANFIS also uses the ANN's ability to classify data and identify patterns. Compared to the ANN, the ANFIS model is more transparent to the user and causes less memorization errors. Consequently, several advantages of the ANFIS exist, including its adaptation capability, nonlinear ability, and rapid learning capacity (Şahin and Erol, 2017).

Sadi (2017) implemented a neuro fuzzy technique to predict thermal conductivity and viscosity of several Nanoparticle Enhanced Ionic Liquids (NEILs) using the input-output experimental

data as a function of temperature, nanoparticle concentration and molecular weight of ionic liquids. The obtained R^2 values for the prediction from the ANFIS model for thermal conductivity and viscosity of NEILs were 0.9959 and 0.9934 respectively.

Alrashed et al. (2018) considered the ANFIS modelling to predict the viscosity, density and thermal conductivity of Diamond-COOH and MWCNT-COOH nanoparticles dispersed in water. The model was implemented with the experimental data containing 70% of data points for training and 30% for testing. Their study also developed a non-linear correlation for predicting aforesaid properties. The models have considered the influence of material type, nanoparticle concentration and temperature on the aforesaid properties of nanofluids. Results demonstrated that the ANFIS model has the least MAPE and RMSE in all cases of prediction of properties of both nanofluids.

Baghban et al. (2019) developed an ANFIS-based swarm concept to create a general model for estimating the viscosity of nanofluids. Temperature, particle size, density, volume fraction and viscosity of base fluid were considered as input variables. ANFIS results have shown a very good prediction with R^2 value of 0.9999 (training and testing) and an absolute relative deviation of 0.42 %.

Razavi et al. (2019) presented ANFIS strategies for predicting the thermal conductivity of metal and metal oxide based nanofluids. Multiple input parameters such as nanoparticle diameter, temperature, thermal conductivity of the base fluid, thermal conductivity of nanoparticles and volume fraction that influences the thermal conductivity of nanofluids were considered for modelling. The Particle swarm optimization method was adopted to optimize the algorithm to obtain the best ANFIS model. Results obtained from the ANFIS model showed a high degree of accuracy in prediction of the thermal conductivity of different nanofluids.

Wole-Osho et al. (2020) performed the ANN and ANFIS modelling to predict the thermal conductivity of water/Al_2O_3–ZnO hybrid nanofluid using their experimental results. Out of the three modeling approaches viz., correlation model, the ANFIS model and ANN model approaches considered, the ANFIS model performed the best with an R^2 value of 0.9946 for the prediction of thermal conductivity.

2.4 Heat transfer studies

Researchers have reported on enhancement of heat transfer by suspending nanoparticles of materials such as CuO, Al_2O_3, TiO_2 etc., in liquids such as water, ethylene glycol etc., (Yiamsawas et al., 2013; Ray et al., 2014; Mukherjee et al., 2020). Heat transfer studies in PHEs considering these nanofluids have shown the significant improvement in the performance of PHE (Wang et al., 2018; Zhang et al., 2019). Plate heat exchangers of different kinds (brazed, gasket and spiral etc.) are used in many applications where heat transfer takes place between streams in relatively low and medium pressure range (Kakac and Liu, 2003).

Pandey and Nema (2012) carried out experimentation on heat transfer and frictional losses in a corrugated PHE using Al_2O_3-water with nanoparticle volume concentration of 2, 3 and 4%. Their results showed that heat transfer characteristics have improved when nanofluid was used. In another study, heat transfer characteristics in a corrugated PHE with water based Al_2O_3 nanofluids showed a noticeable improvement (13%) in HTC for a concentration of 4% in a laminar flow regime (Kabeel et al., 2013). The study also reported an increase in pumping power and pressure drop with increased nanofluid concentration and Reynolds number. The maximum increase in pressure drop of 45% was observed at highest concentration (4 vol. %).

Javadi et al. (2013) carried out experimentation on PHE using different metal oxides (SiO_2, TiO_2 and Al_2O_3) in liquid nitrogen. The addition of nanoparticles resulted in increased heat transfer rate with higher HTC. Al_2O_3 nanoparticles in liquid nitrogen have shown highest enhancement in HTC. However, the lowest pressure drop was obtained for SiO_2 nanofluids, about 50% smaller than the TiO_2 and Al_2O_3 nanofluids. Khairul et al. (2013) carried out an experimental study on heat transfer in corrugated PHE using water-CuO (1.5 vol%) nanofluids. Their study indicated that the HTC of water-CuO nanofluid increased by 27.2% against water.

Tiwari et al. (2015) reported performance study on plate heat exchanger when different metal oxides (CeO_2, Al_2O_3, TiO_2 and SiO_2) dispersed separately in water with different concentrations at the flow rate of 3 lpm. The study reported the optimized volume concentrations of 0.75%, 1%, 0.75% and 1.25% with a maximum enhancement of 35.9%, 26.3%, 24.1%, and 13.9% in heat transfer for corresponding nanofluids respectively.

Huang et al. (2015) carried out experimentation on Chevron type PHE using Al_2O_3/water and MWCNT/water nanofluids. Al_2O_3/water nanofluids exhibited better heat transfer

characteristics than MWCNT/water. However, the study showed that the pressure drop obtained for both nanofluids was considerably higher compared to water.

Behrangzade and Heyhat et al. (2016) carried out studies on PHE using nanosilver particles by investigating the effect of flow rate (cold flow rate (water) - 2,3 and 4 lpm and hot flow rate (nanofluid) - 4,6 and 8 lpm) and concentration on convective heat transfer and pressure drop. The results showed an overall heat transfer coefficient (OHTC) improvement of between 6.18% and 16.79%.

Taghizadeh-Tabari et al. (2016) performed a heat transfer study in PHE (specially designed for diary technology) using water based TiO_2 nanofluid by considering nanoparticle weight concentrations of 0.25%, 0.35% and 0.8%. Their study showed enhanced convective heat transfer coefficient (CHTC) with nanofluid compared to water.

Pourhoseini et al. (2018) studied the effect of silver-water nanofluid concentration on PHE at different flow rates. Their results indicated that nanofluid concentration and flow rate have significant effect on improvement of heat transfer coefficient. Wang et al. (2018) performed a study on the miniature plate heat exchanger (MPHE) to explore the heat transfer and pressure drop characteristics using water and ethylene glycol (50:50 by mass) as the base fluid by dispersing graphene nanoplatelets (GNPs) of different concentrations (0.01, 0.1, 0.5 and 1.0 wt.%). They placed nanofluids on the hot side and water on the cold side for experimental analysis. Their results showed higher heat transfer performance compared with the base fluid in the MPHE.

Zheng et al. (2020) considered many types of water based nanofluids (Fe_3O_4, Al_2O_3, CuO and SiC) to report heat transfer studies in PHE. Their study investigated the effect of weight concentration (0.05 to 1%) under different flow rates (3-9 liters/min). The results indicated a maximum enhancement in Nusselt number of 22.6% for 1 wt.% of Fe_3O_4-water nanofluid.

Saleh and Sundar (2021) performed heat transfer studies on corrugated PHE using nickel/water nanofluids of different weight concentrations (0.1%, 0.3% and 0.6%). The addition of nanoparticles to the base fluid has shown significant improvement in OHTC, HTC and Nusselt numbers.The study indicated that at the highest concentration (0.6%) of nanofluid at a Reynolds number of 707, the OHTC, CHTC and Nusselt's numbers were enhanced by 38.60%, 57.35% and 42.68% respectively when compared to the base fluid.

Table 2.6 shows some of the heat transfer studies in PHEs reported in literature for different types of nanofluids.

Table 2.6 Summery of heat transfer studies related to plate heat exchanger reported in literature

Reference	Nanofluid	Concentration	Significant findings
Javadi et al. (2013)	SiO_2/Liquid nitrogen	0.2 vol.%	TiO_2 and Al_2O_3 nanoparticles have shown higher heat transfer coefficient than SiO_2.
Tabari and Heris (2015)	MWCNT/water	0.25-0.55 wt.%	Experimental results at turbulent flow condition have indicated better improvement in Nusselt number when nanofluid used as hot fluid.
Sun et al. (2016)	Cu/water Fe_2O_3/water Al_2O_3/water	0.1-0.5 wt.%	Cu-water nanofluids exhibited better CHTC compared to Fe_2O_3 and Al_2O_3 nanofluids.
Kumar et al. (2017)	ZnO/water and CeO_2/water	0.5-2 vol.%	ZnO/water nanofluid have resulted with the better CHTC compared to CeO_2/water nanofluid
Arya et al. (2018)	MgO/water	0.1-0.3 wt.%	Heat transfer coefficient obtained was higher with particle loading and the effect of different inlet temperature of nanofluid in the study showed no influence on the pressure drop.

2.5 Entropy generation analysis

Thermodynamic analysis signifies the direct relationship between the irreversibility of an engineering method and the amount of available work destroyed by the process (Bejan, 1980). To calculate entropy generation, fluid flow and heat transfer properties of the thermal system must be known. The fluid flow properties of a system are represented by the pumping power and friction factor, whereas the heat transfer characteristics are represented by the heat transfer

coefficient and Nusselt number. Bejan (1980, 1987) introduced entropy generation concept to measure the thermodynamic performance of heat exchangers.

Huminic and Huminic (2018) presented the entropy analysis considering the MWCNT + Fe_3O_4/water and ND + Fe_3O_4/water hybrid nanofluids in a flattened tube based on the numerical study. Reynolds number (250-2000), nanofluid concentration (0-0.3 vol.%) and inlet temperature (30-60 ºC) was varied in their study. The results obtained by them showed that increase in volume concentration of hybrid nanofluids indicated decrease in total entropy generation of both hybrid nanofluids compared to base fluid. A reduction of entropy generation of 26.48% was obtained against base fluid at 0.3 vol.% MWCNT + Fe_3O_4 hybrid nanoparticles.

Shirav et al. (2020) performed the entropy generation analysis in helical coil heat exchangers under turbulent flow conditions considering carbon black nanofluid. The lowest entropy generation was reported for the 0.21% of mass concentration of nanofluid for the maximum value of Nusselt number. Bejan number obtained from their study showed that heat transfer effect is more dominant in entropy generation compared to fluid friction.

Saleh and Sundar (2021) performed entropy generation analysis in corrugated PHE using nickel/water nanofluids of different weight concentrations (0.1%, 0.3% and 0.6%). The study indicated that at highest concentration (0.6%) at a Reynolds number of 707, thermal entropy generation (TEG) was reduced by 15.70%, but frictional entropy generation (FEG) increased by 68.29%, when compared to base fluid.

Bizhaem (2021) performed the entropy generation analysis for three water based nanofluid (silver, MWCNT and graphene oxide (GO)) flow through helical tubes. Entropy generation results demonstrated that use of silver and MWCNT nanoparticles significantly reduces entropy generation, whereas, an increase in entropy generation was observed for water-GO nanofluids. Furthermore, the study also showed that Bejan number was decreased with an increase in Reynolds number.

Sundar et al. (2021) presented entropy generation analysis of nanodiamond dispersed in 40:60% propylene glycol and water mixture based nanofluid under transition flow condition. The study was carried out considering the volume concentration of 0.2 to 1 vol. % by varying the Reynolds number from 2000 to 8000. The study revealed that TEG obtained for the nanofluids was lower

than that of the base fluid, while the FEG of the nanofluid was higher. The study showed that TEG was found to be decreased by 26.92% at 1 vol.% for the Reynolds number of 5321.16.

2.6 Scope and motivation for the present study

Heat transfer can be improved in heat exchangers by enhancing the thermal conductivity of the base fluid. Researchers have found that various metal oxides such as CuO, Al_2O_3, TiO_2 etc in various base fluids (water, ethylene glycol, ethylene glycol and water mixture, propylene glycol etc) can be added to improve the heat transfer performance significantly by enhancing the thermal conductivity of the base fluid. Ethylene glycol and EG:water mixture provide excellent properties like low freezing point and high boiling temperature and are suitable as heat transfer fluids in extreme cold conditions. EG: water mixture of different proportions (base fluid) can be used in low temperature applications such as HVAC and chemical industries due to its low freezing point. However, there have not been many reports of PHEs in heat transfer enhancement and entropy generation studies using nanofluids considering EG:water mixture based nanofluids at low temperature conditions (<20 ºC). Most of the heat transfer studies reported for PHEs in literature have considered water based nanofluids. The use of nanofluids in the PHEs can improve heat transfer, leading to the more compact design of compact heat exchangers. EG:water based nanofluids assume importance because of its low freezing point (− 19.4 °C for 35v/65v of EG: water) and therefore as a potential heat transfer fluid at low temperatures.

As far as studies related to thermal conductivity and viscosity of nanofluids are concerned, for EG:water based nanofluids at lower temperature (<10 ºC) have been scarce. Hence, initially, thermophysical properties will be evaluated by considering Al_2O_3 and TiO_2 nanoparticles for a temperature range of 5 to 55 ºC. The effect of nanoparticle concentration in base fluid and temperature of nanofluid on effective thermal conductivity (ratio of thermal conductivity of nanofluid to base fluid) and relative viscosity (ratio of viscosity of nanofluid to base fluid) will be investigated. From the literature review, it can also be observed that there have been a few experimental and modelling (thermal conductivity and viscosity) studies on EG:water mixtures using various nanopowders. However, the modelling work reported by them only pertained to the respective experimental studies. No generalized models have been reported and compared with developed correlations. In this work, a generalized correlation and machine learning (ANN

and ANFIS) models will be developed to predict the effective thermal conductivity and relative viscosity of nanofluids using the experimental results from the present study and literature data for EG:water based nanofluids. Studies will be carried out using EG:water based nanofluid in a PHE to investigate the heat transfer characteristics. The effect of nanopowder concentration (0.2, 0.5, 1, 1.5, 2 wt.%) in the base fluid, fluid flow rates and inlet temperature of nanofluid on heat transfer and entropy generation will be investigated. Investigations will be carried out at, *inter alia,* low temperature of - 5 °C. Pressure drop, pumping power and friction factors will be assessed for nanofluids for aforesaid experimental conditions.

Chapter 3 Materials and Methods

This chapter presents details of work related to determinantion of thermal conductivity and viscosity of nanofluids, and heat transfer in PHE, data analysis methods and machine learning models for prediction of effective thermal conductivity and relative viscosity. It is broadly divided into the following sections.

1. Experimental work
2. Experimental data analysis
3. Machine learning models

3.1 Experimental work

The following experimental aspects have been described in this section:

3.1.1 Preparation of nanofluids

Preparation of nanofluid is the crucial step to achieve good stability of nanofluid and to have uniform thermophysical properties for longer time.

3.1.1.1 Materials

Ethylene glycol (Thermo Fisher Scientific, India) and water mixture containing 35% EG and 65% water by volume was considered as the base fluid for the preparation of nanofluid. This mixture was selected due its freezing point is low (−19.4 °C), and therefore can be used for low temperature applications. Thermophysical properties of the considered mixture are shown in Table 3.1.

Al_2O_3 (Alfa Aeaser, Lancashire-UK) and TiO_2 (Nanoshell, USA) nanoparticles were used for the preparation of nanofluids of different concentrations. The details of nanoparticles and base fluid considered for the study is shown in Tables 3.2 and 3.3 respectively.

Fig. 3.1 shows the Field Emission Scanning Electron Microscopy (FESEM) image for the Al_2O_3 (left) and TiO_2 (right) nanoparticles. The images show that most of the particles of two nanopowder materials are less than 50 nm.

Table 3.1 Thermophysical properties of 35:65 ratio (volume) of EG:water mixture from ASHRAE Data (ASHRAE, 2017)

Temperature, (ºC)	Thermal Conductivity (W/m.K)	Viscosity (mPa.s/cP)	Specific Heat (J/kg.K)	Density (kg/m^3)
5	0.41	4.15	3510.5	1057.77
10	0.415	3.495	3526	1056.12
15	0.42	2.985	3541	1054.36
20	0.4245	2.58	3556.5	1052.46
25	0.429	2.245	3572.5	1050.46
30	0.4335	1.975	3588	1048.32
35	0.437	1.745	3603	1046.43
40	0.441	1.56	3618.5	1043.7
45	0.4445	1.4	3634	1041.205
50	0.448	1.26	3649.5	1038.58
55	0.4505	1.14	3665	1035.84

Table 3.2 Properties details of EG and water at 25 ºC (ASHRAE, 2017)

Properties	Density	Chemical formula	Molecular weight	CAS
Ethylene glycol	1113 kg/m^3	$C_2H_6O_2$	62.07 gram/mol	107-21-1
Water	998.21 kg/m^3	H_2O	18.02 gram/mol	-

Table 3.3 Details of nanoparticles used for the preparation of nanofluid

Nanoparticle material	Particle size (nm)	True density (kg/m^3)	Thermal conductivity (W/m.K)	Specific surface area (m^2/g)	CAS number
Al_2O_3 (Alfa Aeaser, Lancashire-UK)	40-50	3970	40	32-40	1344-28-1
TiO_2 (Nanoshell, USA)	40-45	3900	8.4	>30	13463-67-7

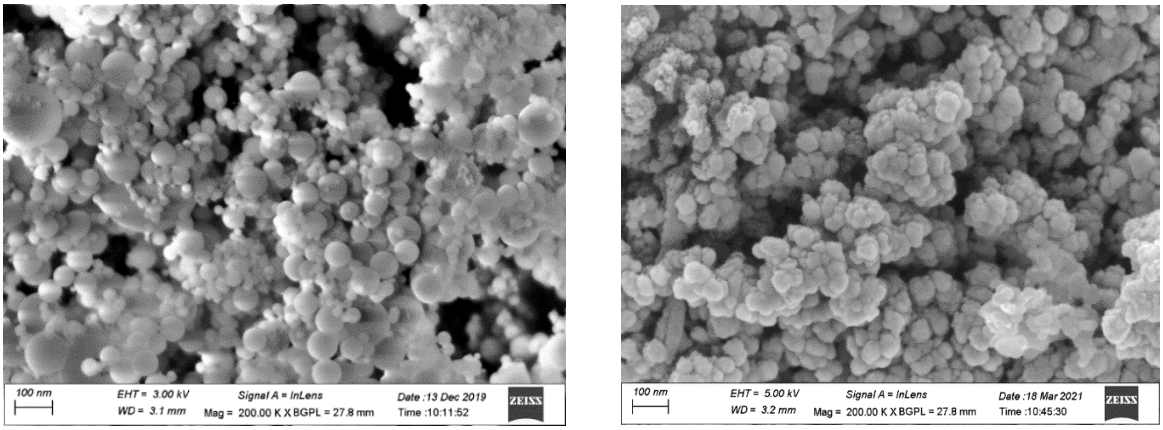

Fig. 3.1 FESEM image of Al_2O_3 nanoparticles (left) and TiO_2 nanoparticles (right).

3.1.1.2 Sample preparation

Initially, two nanopowders of Al_2O_3 and TiO_2 were dispersed separately in base fluid (EG:water) by stirring (120 min) and ultrasonication (120 min) by adding the different surfactants. Surfactants such as sodium lauryl sulphate (SLS), Sodium Dodecylbenzene Sulfonate Surfactant (SDBS), Polyvinylpyrrolidone (PVP) and Cetrimonium bromide (CTAB) were used separately to prepare a stable nanofluid. Surfactants of concentration 0.05, 0.1 and 0.2 wt.% in nanofluid were used to study the stability of all the nanofluid samples by visual observation over a period of 30 days. 0.2 wt.% SDBS has exhibited better stability compared to all other surfactants, as per the visual observation of sedimentation of nanopowder in the fluid, and therefore was used to prepare stable nanofluid in the study.

The two nanofluids of Al_2O_3 and TiO_2 of different concentrations (0.2, 0.5, 1, 1.5 and 2 wt.%) were prepared by dispersing nanoparticles in EG:water mixture. Eq. (3.1) was used to calculate the weight percentage of the nanoparticles in the samples:

$$100\emptyset_w = \frac{m_{np}}{m_{np}+m_{EG:water}} \tag{3.1}$$

where $\emptyset_w$, m_{np} and $m_{EG:water}$ are weight concentration, mass of nanoparticles and base fluid, respectively.

Sodium dodecyl benzenesulfonate (Sisco Research Lab, India) of 0.2 wt.% was added to the EG:water mixture before adding the nanoparticles. SDBS and EG:water mixture solution were mixed with the nanoparticles using a magnetic stirrer for 2 hr at 700–750 rpm at ambient conditions (25 to 30 °C). Using Hielscher (UP200H 200 W, 24 kHz) ultrasonic homogenizer,

ultrasonic probe with 50% amplitude and pulse ratio/burst ratio of 50% as parameters, the mixture of nanoparticles and base fluid with surfactant was homogenized for 2 hr to obtain a stable suspension. Fig. 3.2 shows the flow diagram for the nanofluid preparation method. Fig. 3.3 shows the Al_2O_3 and TiO_2 nanofluids prepared by this method. Visual inspection indicates over a period of time, prepared nanofluids were stable for more than 5 weeks without any sedimentation.

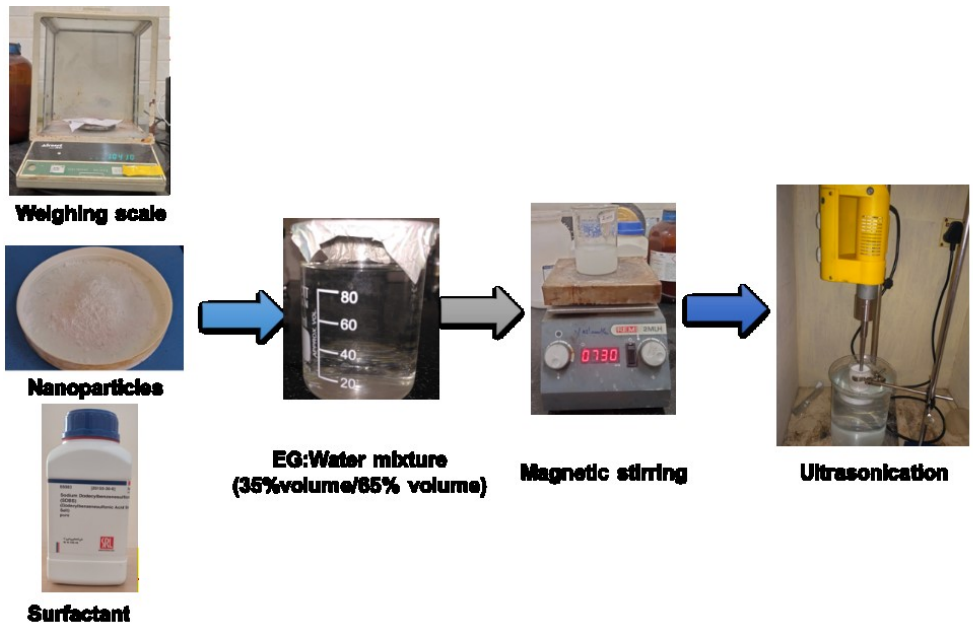

Fig. 3.2 Preparation of nanofluid

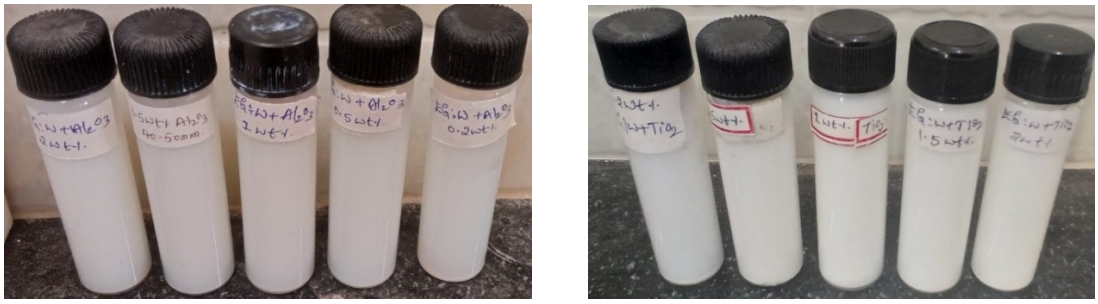

Fig. 3.3 Nanofluids of dfferent concentrations of EG:water – Al_2O_3 (left) and TiO_2 (right) after preparation

3.1.2 Stability of nanofluids

The stability of the EG:water based nanofluids was evaluated using visual observation, thermal conductivity measurement over a period of time and zeta potential measurements. Zeta potential

values for EG:water based Al_2O_3 and TiO_2 nanofluids were measured using Zetasizer Nano (Malvern Nano Z). The zeta potential represents electrostatic repulsion between nanoparticles. The particles are well distributed if the absolute zeta potential value is high (greater than ± 30 mv) (Rashmi et al., 2011; Choudhary et al., 2017). If the zeta potential is low, the nanoparticles tend to form a cluster and become poorly distributed.

3.1.3 Thermal conductivity measurement of nanofluid

Thermal conductivity of EG:water - Al_2O_3 and TiO_2 nanofluids of different concentration were determined using KD2 Pro thermal properties analyzer (Decagon Devices, Inc., USA). The instrument meets the requirements of ASTM D5334 and IEEE 442-1981 standards, and has been used by various researchers (L. Syam Sundar et al., 2013; Srinivas and Vinod, 2016; Chiam et al., 2017; Naik and Vinod, 2018; Krishnakumar et al., 2019; Yang et al., 2019b, 2019a). This instrument consists of a microcontroller and a KS-1 sensor needle with a size of 1.3 mm diameter and 60 mm long, capable of measuring the thermal conductivity in the range of 0.02 - 2.00 W/m.K. Prepared samples of specific nanofluid (volume = 30 ml) were taken in a glass tube of 30 mm diameter, which was equipped with a small opening (slightly larger than the sensor) through which the sensor needle was placed in it. The sensor was inserted into the fluid, oriented centrally and vertically inside the container without touching the side walls of the container as displayed in Fig.3.4. Each nanofluid sample of Al_2O_3 and TiO_2 of different concentration (0.2 - 2 wt.%) was taken into 30 ml glass bottle after preparation. Thermal conductivity at 5, 10, 15, 20, 25, 30, 35, 40, 45, 50 and 55 ºC was measured by keeping temperature constant as shown in Fig. 3.4 in a constant temperature bath. Fig. 3.5 depicts the arrangement made for maintaining the temperature below 30 °C for the measurement of thermal conductivity. This system consists of a tank filled with EG:water, temperature controller (PID) and a refrigeration system (R-134a). Temperature was maintained using refrigeration system for low temperatures. For each sample, 5 readings were taken by allowing 15 minutes for each reading for the temperature to equilibrate. The average of these readings was used for reporting the thermal conductivity of nanofluids. Table 3.4 shows the specification and accuracy of instruments used in the present study. The comparison of thermal conductivity measurement with the ASHRAE data was carried out. The measured values show a maximum deviation of ± 2.5%. Appendix-I shows the uncertainty involved in the thermal conductivity measurement.

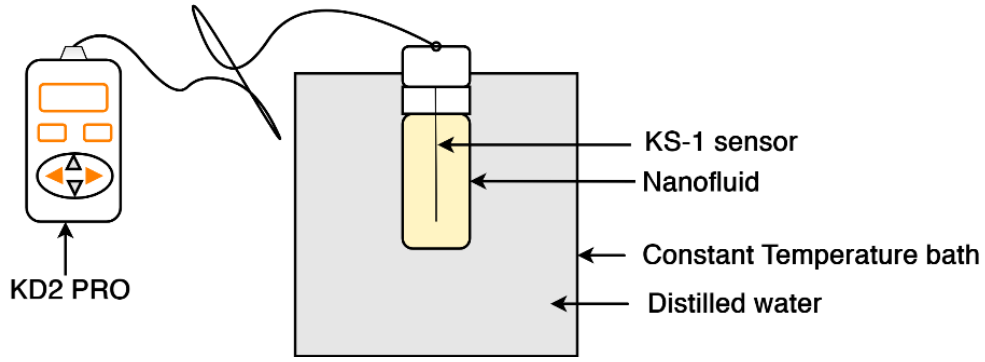

Fig.3.4 Experimental arrangement for thermal conductivity measurement of nanofluids for the temperature ≥ 30 ºC

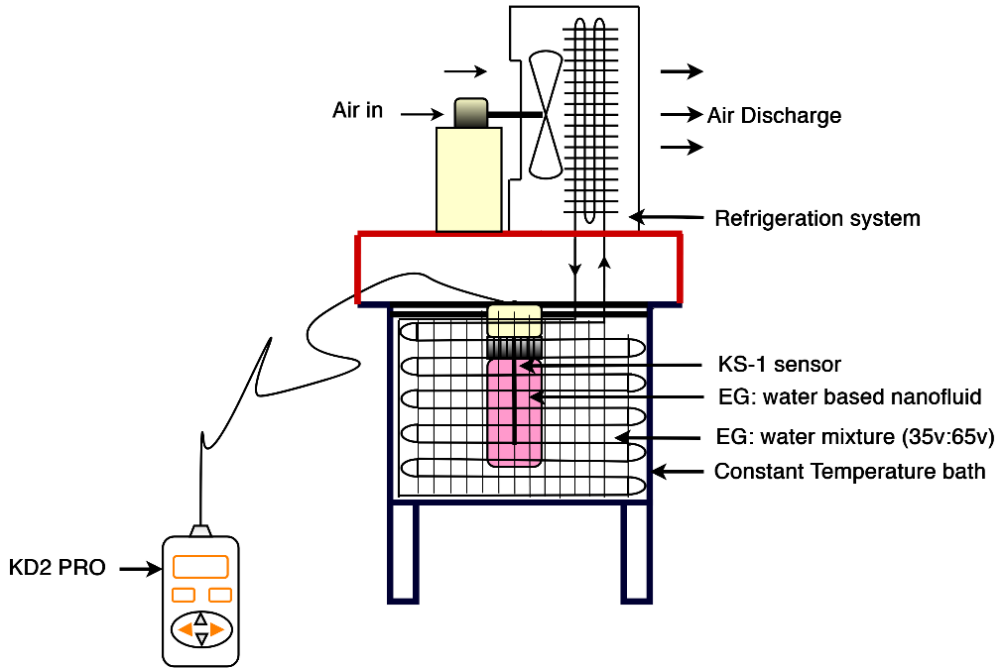

Fig.3.5 Experimental arrangement for thermal conductivity measurement of nanofluids at below 30 ºC

Table 3.4 Specification and accuracy of instruments used in the present study

Instrument	Precision balance (Afcoset, India)	KD2 Pro thermal Properties analyzer (Decagon Devices, Inc, USA)
Accuracy	0.001 g	± 5%
Measurement range	1 mg – 120 gram	0.02 - 2 W/m K

3.1.4 Viscosity measurement of nanofluid

Anton Paar (MCR 301) rheometer was used to measure the viscosity of EG:water nanofluids (Al_2O_3 and TiO_2) of different concentrations. Coaxial double gap measuring System (DG26.7-SN26991) was used for the measurement. Fig. 3.6 shows the rheometer used for the viscosity measurement. The rheometer was connected to a personal computer with RheoCompass software to record data. CoolPeltier, a peltier framework with a built-in cooling system was located in the measuring system to control the temperature in the rheometer with an accuracy of 0.01°C.

Fig. 3.6 Rheometer used for the study

Initially, viscosity of base fluid (EG:water) was measured at a fixed temperature (25 ºC) by varying the shear rate from 10 to 1000 s^{-1}(shear sweep). Then, a fresh sample of base fluid was poured into the measuring cell at a prescribed place (excess fluid was taken out carefully) to measure viscosity for the temperature range of 5 to 55 ºC (temperature sweep) by keeping the shear rate constant (100 s^{-1}). Procedure was repeated for all concentrations of nanofluid (Al_2O_3 and TiO_2) by keeping shear rate and temperature range same as that of the base fluid. The viscosity of the nanofluid for shear sweep, keeping the temperature constant, and the viscosity for temperature sweep, keeping the shear rate constant, were compared with the viscosity of EG:water base fluid measurement at identical conditions.

3.1.5 Experimental setup for heat transfer studies

Figs. 3.7 and 3.8 show the details of the plate heat exchanger experimental setup used in the present study. A commercial PHE (Sondex Heat Exchangers India Pvt. Ltd, India, model-S4A-1 G 10-22-TL-LIQUID) was used for the heat transfer studies. PHE contains stainless steel (SS316) plates with corrugation. The details of the PHE are shown in Table 3.5. Fig. 3.9 shows geometrical parameters of the plate considered for the heat transfer study.

(i) The experimental setup consists of nanofluid (cold fluid) and hot water loops as shown in Fig.3.8.

(ii) Hot water loop consists of a hot water tank and three immersion heaters (1.5 kW each) and a magnetic drive pump. Similarly, nanofluid flow loop consists of a magnetic drive pump and a separate refrigeration system (R134a) to cool the nanofluid for required inlet temperature before it is fed into the PHE.

(iii) The hot water and EG:water nanofluid tanks, each are of size 600 x 450 x 400 mm and are made of SS 316. The tanks were used as feed tanks for pumping fluids through the plate heat exchanger. Both the tanks are insulated and closed to prevent heat loss. The temperature of the hot and cold fluids in the tanks is maintained by two separate heating and cooling (refrigeration) systems using PID controllers.

(iv) Mechanical stirrers were used in both cold fluid (nanofluid) tank and hot water tank to maintain the uniform temperature.

(v) Magnetic drive pumps were used to circulate hot water and cold fluid (nanofluid) through PHE.

(vi) Flow rates of nanofluid and hot water were maintained by using rotameters (11-19 lpm).

(vii) Pressure drop across the hot and cold streams in plate heat exchanger was measured using pressure sensors (JUMO-Germany).

(viii) The inlets and outlets temperature of both the fluids in PHE were measured using PT-100 RTD sensor (0.1 °C resolution).

(ix) A data acquisition system was used to log all the data from the experiments.

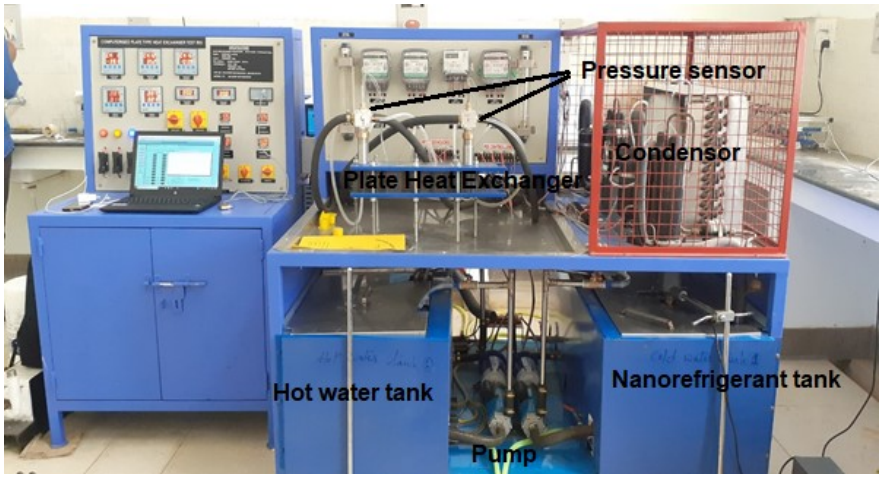

Fig. 3.7 Experimental setup of plate heat exchanger

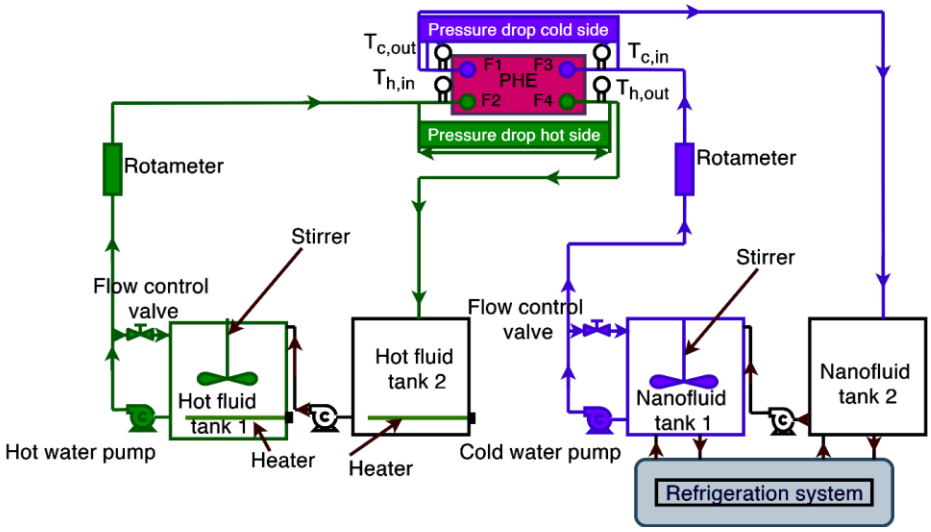

Fig. 3.8 Schematic diagram of arrangement made for plate heat exchanger for experimentation

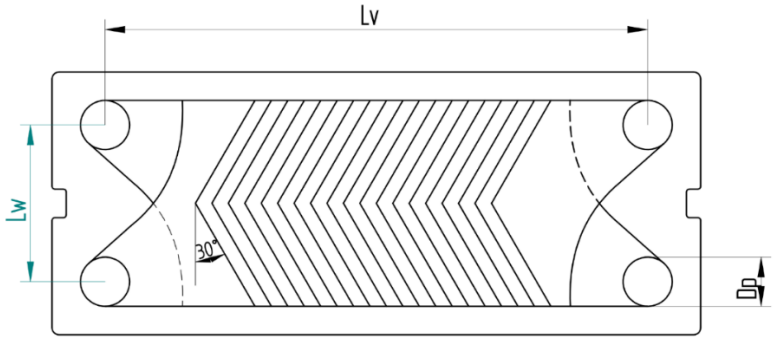

(a)

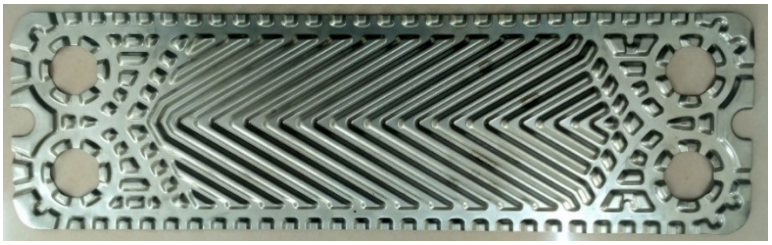

(b)

Fig. 3.9 Geometrical parameters of plate used in PHE in this study

Table 3.5 Geometrical parameters of the plate used for PHE in the present study

Parameter	Value
Plate width, L_w *(mm)*	110
Vertical distance between centres of ports, L_v *(mm)*	381
Horizontal distance between centres of ports, L_h *(mm)*	70
Port diameter, D_p *(mm)*	34.5
Mean channel spacing, *b (mm)*	2.8
Plate thickness, *t (mm)*	0.5
Chevron angle	30º
Number of plates	22
Number of channel (cold side)	10
Number of channel (hot side)	11
Heat exchanger area, $A\ (m^2)$	0.84

3.1.6 Experimental studies

The effect of the following on heat transfer enhancement (due to the use of nanofluid) has been investigated.

1) Concentration of Al_2O_3 and TiO_2 nanofluid (0.2, 0.5, 1, 1.5 and 2 wt.%).
2) Cold-side fluid flow rate: 11 to 19 lpm and hot fluid flow rate: 10 lpm and 12.5 lpm
3) Nanofluid inlet temperature: 20 ºC, 10 ºC and -5 ºC.

3.1.7 Experimental procedure

(i) Initially, experiments were carried out using the base fluid (EG:water mixture, cold fluid) and distilled water (hot fluid).

(ii) The heater for the hot water tank was switched on to bring the water temperature to 60 °C. Cold fluid was brought to a temperature of 20 °C. The inlet temperature of both the fluids was maintained at 60 °C and 20 °C throughout the experiment.

(iii) The flow rate of hot water is now set to 10 lpm using rotameter by operating flow control valve as shown in Fig. 3.8.

(iv) Experiments were carried out for cold fluid flow rates in the range of 11 lpm to 19 lpm, keeping the hot water flow rate constant. The experimental data (inlet and outlet temperatures, flow rate, inlet and outlet pressures) was collected at steady state condition.

(v) The above procedure was repeated for cold fluid (base fluid) inlet temperatures of 10 and -5 °C.

(vi) Similarly, the same procedure was followed for the hot fluid flow rate of 12.5 lpm without changing the other conditions (cold side flow rate, inlet temperature of cold fluid and hot fluid).

(vii) Subsequently, experiments were carried out to investigate enhancement in heat transfer using nanofluids of concentration of 0.2, 0.5, 1, 1.5 and 2 wt.%. Other experimental conditions for nanofluids were maintained the same as that of the base fluid.

3.2 Experimental Data analysis

3.2.1 Heat transfer studies

Table 3.6 shows correlations used to calculate the values of specific heat (Table 3.7) of nanoparticles at different temperatures. Density and specific heat of EG:water - Al_2O_3 and TiO_2 nanofluids were found using correlations proposed in the literature:

Density (Vajjha and Das, 2008) and Specific heat (Xuan and Roetzel (2000):

$$\rho_{nf} = (1 - \emptyset_v)\rho_{bf} + \emptyset_v \rho_{np} \tag{3.2}$$

$$(C_p)_{nf} = (1 - \emptyset_v)(C_p)_{bf} + \emptyset_v(C_p)_{np} \quad (3.3)$$

Conversion of nanofluids concentration from wt.% to vol.% is shown in Table 3.8. The calculated values of density and specific heat of nanofluids from Eq. (3.2) and Eq. (3.3) is tabulated in Tables 3.9 and 3.10 respectively.

Table 3.6 Equations for specific heat of nanoparticles (Perry and Green, 2008)

Material	Correlation (Cal/K.mol)	Temperature range (K)	Uncertainty (%)
Al_2O_3	$C_p = 22.08 + 0.008971\mathrm{T} - \left(\frac{522500}{T^2}\right)$	273 - 1973	3
TiO_2	$C_p = 11.81 + 0.00754\mathrm{T} - \left(\frac{41900}{T^2}\right)$	273 - 1973	3

Table 3.7 Specific heat (J/kg.K) of nanoparticles at different temperatures (Perry and Green, 2008)

Temperature (°C)	Al_2O_3	TiO_2
5	730.28	699.49
10	741.82	702.46
20	763.45	708.24
30	783.32	713.85
40	801.67	719.30

Table 3.8 Conversion of nanofluids concentration from wt.% to vol.%

Weight concentration of nanofluids (wt.%)	Volume concentration of corresponding nanofluid	
	Al_2O_3	TiO_2
0.2	0.0524	0.0533
0.5	0.1308	0.1332
1	0.2613	0.266
1.5	0.3914	0.3984
2	0.5212	0.5305

Table 3.9 Density (kg/m^3) of nanofluids at different temperatures and concentrations

Nanofluid	Temperature (°C)	Nanofluid concentration					
		EG: water	0.2 wt.%	0.5 wt.%	1 wt.%	1.5 wt.%	2 wt.%
EG:water-Al_2O_3	5	1057.7	1059.3	1061.5	1065.3	1069.1	1072.9
	10	1056.1	1057.6	1059.9	1063.7	1067.5	1071.3
	20	1052.4	1053.9	1056.2	1060.0	1063.8	1067.6
	30	1048.3	1049.8	1052.1	1055.9	1059.7	1063.5
	40	1043.7	1045.2	1047.5	1051.3	1055.1	1058.9
EG:water -TiO_2	5	1057.7	1059.2	1061.5	1065.3	1069.0	1072.8
	10	1056.1	1057.6	1059.9	1063.6	1067.4	1071.2
	20	1052.4	1053.9	1056.2	1060.0	1063.8	1067.5
	30	1048.3	1049.8	1052.1	1055.9	1059.6	1063.4
	40	1043.7	1045.2	1047.5	1051.3	1055.0	1058.8

Table 3.10 Specific heat (J/ kg K) of nanofluids at different temperatures and concentrations

Nanofluid	Temperature (°C)	Nanofluid concentration					
		EG: water	0.2 wt.%	0.5 wt.%	1 wt.%	1.5 wt.%	2 wt.%
EG:water -Al_2O_3	5	3510.5	3509.	3506.8	3503.2	3499.6	3496
	10	3541	3524.5	3522.3	3518.7	3515.1	3511.4
	20	3556.5	3555	3552.8	3549.2	3545.5	3541.9
	30	3588	3586.5	3584.3	3580.6	3577	3573.3
	40	3618.5	3617	3614.8	3611.1	3607.4	3603.8
EG:water -TiO_2	5	3510.5	3509	3506.8	3503.1	3499.5	3495.8
	10	3541	3524.5	3522.3	3518.6	3514.9	3511.2
	20	3556.5	3555	3552.7	3549	3545.3	3541.6
	30	3588	3586.5	3584.2	3580.4	3576.7	3573
	40	3618.5	3616.9	3614.7	3610.9	3607.1	3603.3

The data obtained from the experiments was used to calculate heat transfer rate, heat transfer coefficient and pressure drop. The Reynolds number on hot side and cold side (nanofluid) was calculated using Eqs. (3.4) and (3.5) considering channel mass velocity and hydraulic diameter.

$$Re_h = \frac{G_h D_h}{\mu_h} \tag{3.4}$$

$$Re_{nf} = \frac{G_{nf} D_h}{\mu_{nf}} \tag{3.5}$$

Where, $D_h = \frac{2b}{\emptyset}$, $\emptyset$ is the surface enlargement factor for PHE (Kakac and Liu, 2003) and channel mass velocity on both side was calculated using Eqs. (3.6) and (3.7)

$$G_{hf} = \frac{m_{hf}}{N_{cp}.b.L_w} \tag{3.6}$$

$$G_{nf} = \frac{m_{nf}}{N_{cp}.b.L_w} \tag{3.7}$$

Peclet number was calculated using Eq. (3.8). Peclet number (Pe) is a dimensionless number representing the ratio of heat transfer by motion of a fluid to heat transfer by thermal conduction. The Peclet number can be interpreted as the Reynolds number counterpart for thermal energy transfer.

$$Pe = \frac{u\, D_h}{\alpha} = RePr \tag{3.8}$$

Where u and α are the flow velocity and therml diffusivity. Heat transfer rate on the hot side and cold side was calculated using

$$Q_{hf} = m_{hf} c_{phf} \left(T_{hf,in} - T_{hf,out}\right) \tag{3.9}$$

$$Q_{nf} = m_{nf} c_{p,nf} \left(T_{nf,out} - T_{nf,in}\right) \tag{3.10}$$

The average heat transfer rate was calculated as the average of the above, for subsequent analysis, using Eq. (3.11)

$$Q_{avg} = \frac{Q_{hf} + Q_{nf}}{2} \tag{3.11}$$

The properties of fluids were evaluated at bulk fluid temperature

$$T_{b,hf} = \frac{T_{hf,in} + T_{hf,out}}{2} \tag{3.12}$$

$$T_{b,nf} = \frac{T_{nf,in} + T_{nf,out}}{2} \tag{3.13}$$

Convective heat transfer coefficient for hot side was found using Eq. (3.14) for plate heat exchanger (Kakaç and Liu, 2003)

$$\frac{hD_h}{k} = 0.348(Re)^{0.663}(Pr)^{0.333}\left(\frac{\mu}{\mu_w}\right)^{0.17} \tag{3.14}$$

Overall heat transfer coefficient was found using Eqs. (3.15) and (3.16)

$$U = \frac{Q_{avg}}{A.LMTD} \tag{3.15}$$

$$LMTD = \frac{(T_{hf,in} - T_{nf,out}) - (T_{hf,out} - T_{nf,in})}{\ln\left(\frac{T_{hf,in} - T_{nf,out}}{T_{hf,out} - T_{nf,in}}\right)} \tag{3.16}$$

To find the convective heat transfer coefficient on cold side, thermal resistance concept was used

$$U = \frac{1}{\frac{1}{h_{hf}} + \frac{t}{k_{plate}} + \frac{1}{h_{nf}}} \tag{3.17}$$

where, *t* is thickness of plate, *k* is the stainless steel thermal conductivity (16.5 W/m.K, Kakaç and Liu, 2003) of heat exchanger plate material, h_{nf} and h_{hf} are convective heat transfer coefficient of cold and hot fluid, respectively.

Prandtl number and Nusselt number were calculated using Eqs. (3.18) and (3.19)

$$Pr = {\mu c_p}/{k} \tag{3.18}$$

$$Nu = {hD_h}/{k} \tag{3.19}$$

Effectiveness of the plate heat exchanger was calculated using Eq. (3.20)

$$\varepsilon = \frac{Q_{avg}}{C_{\min}(T_{h,in} - T_{nf,in})} \tag{3.20}$$

Based on pressure drop obtained on the cold side, pumping power was found by taking the η_{pump} of pump 80% (Tiwari et al., 2015) using,

$$P_{pump} = \frac{\Delta p_{\,nf} m_{nf}}{\rho_{nf} \eta_{pump}} \tag{3.21}$$

Friction factor on the cold side (nanofluid) was calculated using Eq. (3.22) (Kakac and Liu, 2003; Behrangzade and Heyhat, 2016; Kumar and Singh, 2017; Sarafraz et al., 2017; Zahrani et al., 2019)

$$f = \frac{\Delta p_{nf}\, \rho_{nf}\, D_h}{2 L_{eff} G_{nf}^{2}} \tag{3.22}$$

Uncertianity involved in the heat transfer study is calculated by the method proposed by Moffat (1988) and details are given in appendix-I.

3.2.2 Entropy generation analysis

Thermal and frictional entropy generation are the two types that constitute entropy generation. The first term refers to irreversibility caused by heat transfer (TEG), whereas the second term refers to irreversibility caused by fluid flow (FEG). The total entropy generation can be calculated using the friction factor and Nusselt number of nanofluids from heat transfer investigation. The combined effect of TEG and FEG is total entropy generation. Bejan (1980, 1987) introduced entropy generation as a general measure for assessing the thermodynamic performance of heat exchanges. The rate of entropy generation per unit length is

$$S_g = \frac{q\Delta T}{T^2} + \frac{m}{\rho T}\left(-\frac{dp}{dx}\right) \tag{3.23}$$

Where q and (- dP/dx) are the heat transfer rate per unit length (W/m) and the longitudinal pressure gradient respectively.

The geometric parameters of the flow passage relate TEG and FEG to total entropy generation as shown in Eq. (3.24) (Mahian et al., 2013; Saleh and Sundar, 2021; Syam Sundar et al., 2021).

$$S_g = \frac{{q_{Avg}}^2 L}{\pi k_{nf} Nu_{nf} T_{c,in} T_{c,out}} + \frac{8\, m^3 f L}{\pi^2 \rho^2 (T_{c,out} - T_{c,in}) {D_h}^5} ln\left(\frac{T_{c,out}}{T_{c,in}}\right) \tag{3.24}$$

$$S_g = S_{g,TH} + S_{g,F} \tag{3.25}$$

S_g, q_{Avg} and f are the total entropy generation, average heat transfer per unit length and friction factor respectively. In the above equation (3.25) first term is the thermal entropy generation and the second term is the frictional entropy generation.

Bejan number (*Be*) was found using eq.(3.26) (Butt and Ali, 2013; Al-Rashed et al., 2019; Shiravi et al., 2020; Sodagar-Abardeh et al., 2020; Khosravi-Bizhaem et al., 2021)

$$Be = \frac{S_{g,TH}}{S_{g,TH} + S_{g,F}} \tag{3.26}$$

Bejan number ranges from 0 to 1. When *Be* is greater than 0.5, the irreversibility caused by heat transfer dominates, whereas when *Be* is less than 0.5, the irreversibility caused by viscous

effects dominates. Furthermore, $Be = 0.5$, corresponds to the case where the heat transfer irreversibility and the fluid friction irreversibility are equal (Butt and Ali, 2013; Shiravi et al., 2020).

3.3 Correlation development

3.3.1 Correlation for effective thermal conductivity

The thermal conductivity of nanofluid was measured at different concentrations and temperatures. Literature review mentions the different types of correlations reported in literature (Table 2.2, chapter 2). As mentioned in chapter 2, the generalized correlations were developed in the present study considering the results from the study and those reported in literature.

3.3.1.1 Considering experimental data from present study

Thermal conductivity of nanofluids is dependent on the material of nanoparticle, type of base fluid, nanoparticle concentration, particle size and temperature. In the present study, the following correlation is proposed, initially, for predicting the effective thermal conductivity (ratio of k_{nf}/k_{bf}) of nanofluids as a function of nanofluid concentration and temperature (two input parameters in non-dimensional form) as these two only were varied in the study.

$$k_{eff} = \frac{k_{nf}}{k_{bf}} = A\left(1 + \frac{\emptyset_v}{100}\right)^B \left(\frac{T_{nf}}{T_{ref}}\right)^C \tag{3.27}$$

where k_{nf} and k_{bf} represent thermal conductivity of nanofluids and EG:water respectively. T_{nf} (278 to 328 K) and T_r represent the temperature of nanofluid and reference temperature (273 K). $\emptyset_v$ (0.05 to 0.53) is volume fraction of nanofluids. *A, B* and *C* are the constants.

3.3.1.2 Considering experimental data from present study and literature data

The effective thermal conductivity (k_{eff}) model of EG:water based Al_2O_3 and TiO_2 proposed in Eq. (3.27) considers only temperature and volume concentration. The other variables viz., the volume ratios of EG:water mixture, temperature and size of nanoparticles which affect the thermal conductivity were not considered as they were kept constant. Hence, in order to develop more generalized correlation considering the experimental results from the present study and the results from literature reports (Table 3.11), the following correlation (Eq. 3.28) is proposed.

$$k_{eff} = a_1 \left(1 + \frac{\emptyset_v}{100}\right)^{a_2} \left(\frac{T_{nf}}{T_{ref}}\right)^{a_3} \left(\frac{d_{np}}{d_w}\right)^{a_4} (V_r)^{a_5} \quad (3.28)$$

Where k_{eff} is effective thermal conductivity, $\emptyset_v$ = volume concentration of EG:water based nanofluids, V_r = % of EG mixture (0.2 to 0.6) in water (in terms of volume), T_{nf} = the temperature of nanofluid in K (278 to 328 K) , T_{ref} =reference temperature in K (273 K), d_{np}= nanoparticle diameter (nm) and d_w=water molecule size in nm (0.27 nm). a_1 to a_5 are the corresponding constants to be determined by regression.

Table 3.11 Literature data related to thermal conductivity of EG:water mixture based Al_2O_3 and TiO_2 nanofluids considered for the correlation development

Reference	Nanoparticles /particle size	EG and water mixture (volume ratio)	Nanoparticle volume concentration	Temperature (ºC)	Number of data points
Sundar et al. (2013)	Al_2O_3/36.5 nm	50:50	0.2-0.8	15–50	32
Sundar et al. (2014)	Al_2O_3/36.5 nm	20:80 40:60 60:40	0.3-1.5 0.3-1.5 0.3-1.5	20-55	120
Chiam et al. (2017)	Al_2O_3/53 nm	40:60 50:50 60:40	0.2-1 0.2-1 0.2-1	30-50	45
Reddy et al. (2013)	TiO_2/21 nm	40:60	0.2- 1	30-50	30
Hamid et al. (2016)	TiO_2/50 nm	40:60	0.5-1.5	30-50	15
Azmi et al. (2016)	TiO_2/40 nm	60:40	0.2-0.8	20-50	28
Krishnakumar et al. (2019)	TiO_2/40 nm	60:40	0.2-0.8	20-50	28

3.3.2 Correlation for relative viscosity

Literature review on viscosity mentions the correlations reported in literature (Table 2.4, chapter 2). Generalized correlations were developed in the present study considering the results from the study and those reported in literature.

3.3.2.1 Considering experimental data from present study

The viscosity of nanofluids is dependent on the nanoparticle concentration, temperature, base fluid, size of nanoparticles and nanoparticle materials. In the present study, a correlation was developed for a specific material using the experimental results as a function of base fluid viscosity, nanofluid temperature and nanoparticle concentration. The size of nanoparticle was not varied in the study, and therefore not considered in the correlation. The correlation was developed for relative viscosity, i.e. the ratio of the viscosity of nanofluid to the viscosity of the base fluid.

$$\mu_{rel} = \frac{\mu_{nf}}{\mu_{bf}} = p\left(1 + \frac{\emptyset_v}{100}\right)^q \left(\frac{T_{nf}}{T_{ref}}\right)^r \tag{3.29}$$

where μ_{rel} is the relative viscosity of nanofluids. μ_{nf}, μ_{bf} and $\emptyset_v$ (0.05 to 0.53) are viscosity of nanofluids, base fluid viscosity and volume concentration respectively. T_{nf} and T_{ref} respectively, represent the temperature of nanofluids and reference temperature (273 K). *p, q* and *r* are the regression constants.

3.3.2.2 Considering literature data

The correlation proposed in Eq. (3.29) to predict the relative viscosity of nanofluids considers only temperature and volume concentration as input variables. Other variables such as EG and water mixture ratio and the size of nanoparticles that significantly affect the relative viscosity were kept constant and hence not considered in the previous equation. A more generalized correlation (Eq. 3.30) is proposed considering different volume ratios of the EG and water mixture, and size of nanoparticles. The correlation was developed by taking into account the experimental findings of the present work and the results of literature studies (Table 3.12).

$$\mu_{eff} = p_1 \left(1 + \frac{\emptyset_v}{100}\right)^{p_2} \left(\frac{T_{nf}}{T_{ref}}\right)^{p_3} \left(\frac{d_{np}}{d_w}\right)^{p_4} (V_r)^{p_5} \tag{3.30}$$

Where V_r, d_{np} and d_w are volume ratio of EG and water (0.18 to 0.6), nanoparticle diameter (13 - 50 nm) and water molecule size in nm respectively. p_1 to p_5 are the constants.

Table 3.12 Literature data for viscosity of Al_2O_3 and TiO_2 based nanofluids considered for the correlation development.

Reference	Nanoparticles and its size	EG:water mixture (volume ratio)	Volume concentration (%)	Temperature range	Number of data points
Yiamsawas et al. (2013)	Al_2O_3/21 nm	18:82	0-2	15-50 ºC	10
LotfizadehDehkordi et al. (2013)	Al_2O_3/13 nm	57.8:42.2	0.01-1	25-40 ºC	24
Sundar et al. (2014)	Al_2O_3/30 nm	20:80 40:60 60:40	0-1.5	5-55 ºC	164
Hamid et al. (2015)	Al_2O_3/13 nm	40:60 50:50 60:40	0-2	30-50 ºC	36
Yiamsawas et al. (2013)	TiO_2/21 nm	0.18:82	0-2	15-50 ºC	10
Azmi et al. (2016)	TiO_2/ 50 nm	40:60	0-1.5	30-50 ºC	15
Krishnakumar et al. (2019)	TiO_2/40 nm	60:40	0-0.8	20-50 ºC	32

The performance of regression models is affected by different factors such as the variables chosen as the input and number of data points used for the modeling process. Among different available methods, machine learning approaches have been broadly employed in modelling the thermophysical properties of nanofluids. Especially, artificial neural network is one of the most

attractive ones due to its ability to model complex systems. In addition to ANN models, other models such as ANFIS have shown promising performance in predicting the properties of nanofluids.

3.4 Machine learning models

3.4.1 ANN modelling

ANN modelling is a computational model based on the structure and functions of biological neural networks. The non-linear variation of data can be modelled using ANN. ANN model consists of three different layers with a number of neurons in each layer. Input neurons are in the first layer (input layer). These neurons send data to the second layer (hidden layer), which transmits data to the third layer (output layer). The neurons in all layers are interconnected with each other with a weight coefficient as shown in Fig. 3.10. The number of neurons in input layer is equal to the number of input variables. Each neuron (in hidden or output layer) multiplies the input received with weight coefficients and adds up to get the output using a transfer function. This can be represented in terms of ANN characterization parameters like weights (w), biases (b) and a function (f). The processing of output followed by the equation,

$$Y_k = f\left(\sum_{i=1}^{n} w_{ki} x_i + b_k\right) \tag{3.31}$$

Where $x_1, x_2, x_3, \ldots\ldots, x_n$ are the input.

$w_{k1}, w_{k2}, w_{k3}, \ldots\ldots, w_{kn}$ are the respective weights of neuron.

b_k is the bias.

f is the activation function.

In this study, a feed forward backpropagation ANN structure was considered for modelling effective thermal conductivity and relative viscosity of nanofluids. It is proposed to

(i) optimize the ANN model to predict the effective thermal conductivity and relative viscosity (material specific).

(ii) compare the experimental data with the that predicted by equations (3.27) and (3.29), and ANN model.

(iii) compare the ANN output with that predicted by generalized equations (3.28) and (3.30)

To accomplish the above, a neural network with a single hidden layer with a varying number of neurons was considered to obtain the optimized model. Table 3.13 shows the models considered in the current study to predict the effective thermal conductivity and relative viscosity of EG:water based nanofluids. Figs. 3.10 and 3.11 depict the corresponding ANN model structures.

Table 3.13 Model developed based on input variables

ANN model	Number of input variables	Input variables	Output / Target
Model 1T (considering experimental results of present study)	2	Volume concentration and temperature ratio	Effective thermal conductivity of EG:water-Al_2O_3/TiO_2 nanofluid
Model 2T (considering experimental results of present study and literature data (Table 3.11))	4	Volume concentration, Temperature ratio, ratio of nanoparticle size to water molecule size, EG:water mixture ratio (in terms of volume)	Effective thermal conductivity of EG:water-Al_2O_3/TiO_2 nanofluid
Model 1V (considering experimental results of present study)	2	Volume concentration and temperature ratio	Relative Viscosity of EG:water-Al_2O_3/TiO_2 nanofluid
Model 2V (considering experimental results of present study and literature data (Table 3.11))	4	Volume concentration, Temperature ratio, ratio of nanoparticle size to water molecule size, EG:water mixture ratio (in terms of volume)	Relative Viscosity of water:EG-Al_2O_3/TiO_2 nanofluid

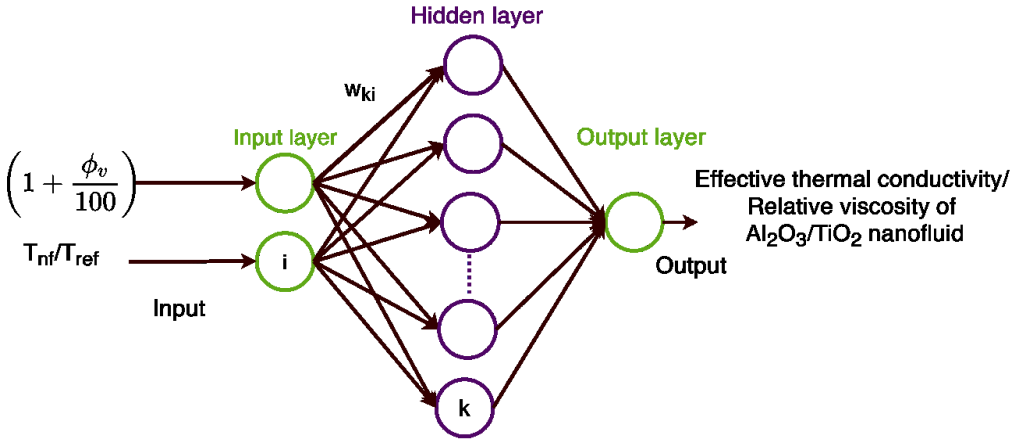

Fig. 3.10 ANN model for the experimental results of the present study for effective thermal conductivity / relative viscosity

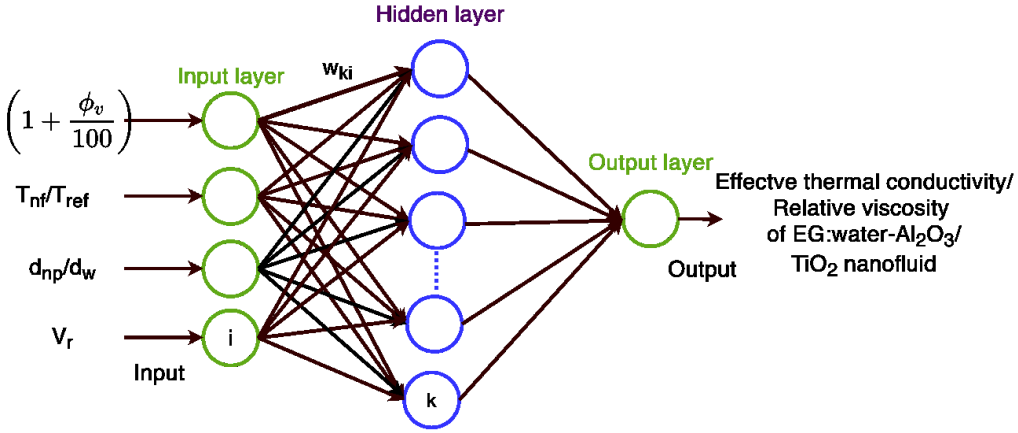

Fig. 3.11 Generalized ANN model considering experimental results of the present study and literature data for effective thermal conductivity / relative viscosity

ANN modelling was implemented in Matlab 2017a utilizing the nntool toolbox. The formulation of ANN modelling follows three steps training, testing and validation. Training is the process of choosing appropriate weights and biases in order to recognize the specific relationship between the target and input functions. The Levenberg-Marquardt training algorithm with a gradient descent with momentum weight and bias learning (LEARNGDM) function was used for the training process. The Tan-sigmoid function was considered in the hidden layer for modelling the effective thermal conductivity and relative viscosity of nanofluids. In the output layer, two functions, namely Tan-Sigmoid transfer function (TANSIG) and linear transfer function (PURELIN), were applied to determine an optimum model for the satisfactory prediction of the output. In this study, 70% of data (input)

was randomly taken for training and the remaining 30% of data was used for testing and validation. The performance of model and regression equation prediction was evaluated using coefficient of determination (R^2), root mean square error (RMSE) and mean absolute percentage error (MAPE) as follows.

$$R^2 = 1 - \frac{\sum_{k=1}^{n}\left(Y_k^o - Y_k^p\right)^2}{\sum_{k=1}^{n}\left(Y_k^o - \overline{Y_k^p}\right)^2} \tag{3.32}$$

$$RMSE = \sqrt{\frac{1}{n}\sum_{k=1}^{n}\left(Y_k^o - Y_k^p\right)^2} \tag{3.33}$$

$$MAPE(\%) = \left(\frac{100}{n}\right)\sum_{i=1}^{n}\left|\frac{Y_k^o - Y_k^p}{Y_k^o}\right| \tag{3.34}$$

Where $\overline{Y_k^p}$ is the mean value predicted data points, n is the number of data points, Y_k^0 is the k^{th} experimental data point and Y_k^p is the k^{th} predicted data point.

ANN has been widely used to estimate the thermal conductivity and viscosity of nanofluids. While many studies have employed a variety of artificial intelligent methods for predicting the thermophysical properties of nanofluids, novel artificial intelligent methods (hybrids) have yet to be extensively explored. Moreover, the suggested existence methods on literatures can cover limited ranges of operational conditions to predict the effective thermal conductivity and relative viscosity. Hence applying an exact method for the identification of the relationships between related parameters to predict the properties of nanofluid is a regularly problematic issue. Therefore, utilization of artificial intelligence methods such as ANFIS usually give us good results, has been recommended by many researchers (Razavi et al., 2019).

3.4.2 ANFIS modelling

A fuzzy inference system (Jang 1993) considers the fuzzy if-then rules to model the complex systems which are difficult to understand (Ramezanizadeh et al., 2019b). ANFIS system is based on the Sugeno fuzzy inference, also referred to as Takagi-Sugeno-Kang fuzzy inference which generates a set of fuzzy rule and membership functions automatically. ANFIS model uses the combination of fuzzy logic and neural network to model the process. Prediction of data using ANFIS modelling is carried out in two stages - in the first stage fuzzy logic is formed (if-then rule), and then the neural network model of learning method is used to alter these rules to optimize the model by reducing the error. The process involved in this model is data learning

from the training data set using neural network theory, then by creating an ideal type of membership functions to map the input and output data established on the fuzzy if-then rules.

The architecture of ANFIS consists of five layers as depicted in Fig. 3.12 (Hemmat Esfe, 2018; Aylı, 2020). ANFIS modelling for the effective thermal conducitivty and relative viscsoity of nanofluids was implemented similar to the ANN model as shown in Table 3.13. For a two input system, the base rule for a Sugeno fuzzy model is as follows

$$\text{Rule 1: } IF\ x = A_1\ AND\ \ y = B_1\ THEN\ f_1 = p_1x + q_1y + r_1 \tag{3.35}$$

$$\text{Rule 2: } IF\ x = A_2\ AND\ \ y = B_2\ THEN\ f_2 = p_2x + q_2y + r_2 \tag{3.36}$$

A_1, A_2, B_1, and B_2 are the four adaptive nodes showing the premise parameters. Where p_i, q_i and r_i are the consequent parameters and i=1, 2.

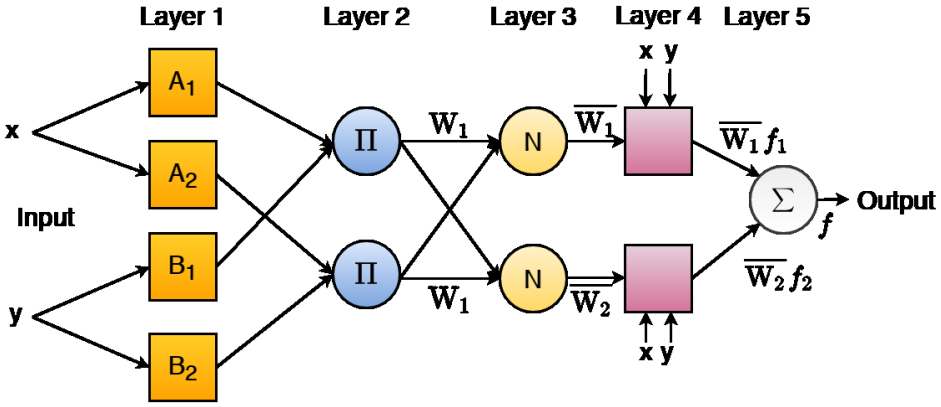

Fig. 3.12 Architecture of ANFIS for two input parameter

Layer 1 (Fuzzification): Each node in this layer is an adaptive node which includes a node membership function (MF) denoted as

$$O_i^1 = \mu_{Ai}(x)_{1i}\ ,\quad i = 1,2 \tag{3.37}$$

$$O_i^1 = \mu_{Bi}(y)_{1i}\ ,\quad i = 3,4 \tag{3.38}$$

This layer is an adaptive layer with the nodes of square shape. Every input of node i in this layer is adaptive membership function to generate the membership degree of linguistic variables. Membership function can be of any shape, i.e. Triangle, Trapezoidal, Gaussian, or generalized Bell function. The first layer has two inputs x and y representing the volume concentration and temperature ratio, respectively, with one output (either effective thermal conductivity or relative viscosity). The values in each input variable are changed to a membership value using the

assigned membership functions. The membership function applied in the present study for ANFIS is the Gaussian function. Here, x and y are the two inputs and if μ_{Ai} and μ_{Bi} are Gaussian MFs (Eq.3.39), they are specified by two parameters center c and width σ, which are referred to as premise parameters. O_i^1 is the output of layer l and the i^{th} node.

$$\text{Gaussian (x;c, σ)}=e^{-\frac{1}{2}\left(\frac{x-c}{\sigma}\right)^2} \tag{3.39}$$

Fuzzy membership function of different types such as Gaussian, trapezoidal, triangular, and generalized bell functions are commonly used for the modelling (Hemmat Esfe, 2018). However, many studies in the literature have shown Gaussian membership function is effective in the modelling. Hence, Gaussian MF result was considered in the present work.

Layer 2 (Product): Every node in this layer is a fixed node labelled Π, whose output is the product of all the incoming signals:

$$O_i^2 = W_i = \mu_{Ai}(x)\ \mu_{Bi}(x)_{1i}\ , i = 1,2 \tag{3.40}$$

Each node output represents the firing strength of a rule.

Layer 3 (Normalization): Nodes of layer 3 are also fixed nodes. All nodes in this layer are labeled as *N*.This layer determines the normalized firing strength of a rule from a previous layer

$$O_i^3 = \overline{W_i} = \frac{W_i}{\sum W_i}\ ; i = 1,2 \tag{3.41}$$

For convenience, outputs of this layer are called normalized firing strengths.

Layer 4 (Defuzzification): Each node in this layer represents a consequent part of the fuzzy rule and accountable for finding the output linguistic terms using Eq. (3.42). The linear coefficient of this rule consequent are trainable in the form given by

$$O_i^4 = \overline{W_i}\ f_i\ \ i = 1,2 \tag{3.42}$$

Layer 5 (Overall output): The single node in this layer is a fixed node labelled ∑, which computes the overall output as the summation of all incoming signals

$$O_i^5 = \sum_{i=1}^{n} \overline{W_i}\ f_i \tag{3.43}$$

For the ANFIS modelling, the data sets of nanofluids were divided into two parts. In the first part, 75% of the experimental data was considered for training purpose. In the second part, the remaining data (25%) was used for testing the model. FIS was generated considering the grid

partition method in MATLAB R2017a using the fuzzy logic designer toolbox. Generated FIS was trained using a hybrid optimization method by selecting the error tolerance and epochs as zero and 20 respectively. The hybrid optimization algorithm adopted in this study composed of a forward and a backward pass. In forward pass, the least square method was used to compute the values of a consequent parameter by keeping the premises parameter constant by propagating input patterns. Once the optimal consequent parameters are found, the backward pass starts immediately. In backward pass, keeping the consequent parameter constant, backpropagation was employed to adjust the premises parameter by propagating input patterns again using the gradient descent method. Table 3.14 summarizes the activities in each pass.

Table 3.14 Two passes in the hybrid learning algorithm for ANFIS.

Characteristic	Farward pass	Backward pass
Premise parameter	Fixed	Gradient descent
Consequent parameters	Least-squares estimator	Fixed
Signals	Node outputs	Error signals

ANFIS modelling was carried out separately for each material and combinedly (generalization), akin to correlation development. In the first approach, concentration and temperature ratio (similar to Model 1T and Model 1V) of nanofluids were considered as input parameters (two input parameters). For this study, the output MF of linear and constant types were used to obtain the best ANFIS model. Experimental results (effective thermal conductivity and relative viscosity) of EG:water nanofluids were taken as target data. The prediction of output (effective thermal conductivity and relative viscosity) was obtained with generated FIS for aforesaid method for EG:water based nanofluids for Al_2O_3 and TiO_2 materials separately. In the second approach, EG:water mixture ratio, volume concentration, ratio of nanoparticle size to water molecule size, and temperature ratio (four input parameters, similar to that of model 2T and model 2V) were considered as input parameters by combining the data from literature. Experimental effective thermal conductivity and relative viscosity were the target values for training and testing. Input and output membership functions were taken as the same as considered in the individual nanofluids ANFIS model. To evaluate the developed model, statistical criteria considered in the case of the ANN model (R^2, RMSE and MAPE) were employed.

Chapter 4 Results and Discussion

The results of experimental studies are presented and analysed in this section. This chapter is divided into the following sections:

1. **Stability of nanofluids:** This section presents results of the study on stability over a period of time of EG:water - Al_2O_3 and TiO_2 nanofluids.
2. **Thermal conductivity and viscosity of nanofluids:** Determination of thermal conductivity and viscosity of EG:water - Al_2O_3 and TiO_2 nanofluids at different temperatures and concentrations is discussed. Experimental results of thermal conductivity and viscosity of EG:water nanofluids are compared with several thermal conductivity and viscosity models in literature. New correlations were developed from the experimental data.
3. **Machine learning models to model effective conductivity and relative viscosity of nanofluids:** In this section two machine learning models (ANN and ANFIS) were implemented to model the effective thermal conductivity and relative viscosity of EG:water - Al_2O_3 and TiO_2 nanofluids by considering several influencing parameters.
4. **Heat transfer characteristics using nanofluids:** This section deals with the study on heat transfer enhancement in plate heat exchanger using nanofluids.
5. **Entropy generation analysis:** This section deals with the effect of nanofluid concentration and nanomaterials on the entropy generation in plate heat exchanger.

4.1 Stability of nanofluids

Stability of the nanofluids was evaluated through visual inspection, thermal conductivity investigation and zeta potential analysis.

4.1.1 Visual inspection of stability

The prepared nanofluids were observed visually for any sedimentation over a period of 30 days. The photographs of two nanofluids of different concentration captured right after preparation of nanofluid and during the 30 days (kept at static condition) are shown in Figs 4.1 and 4.2. The nanofluid stability was inspected by naked eyes. Nanofluids of both the materials showed good stability.

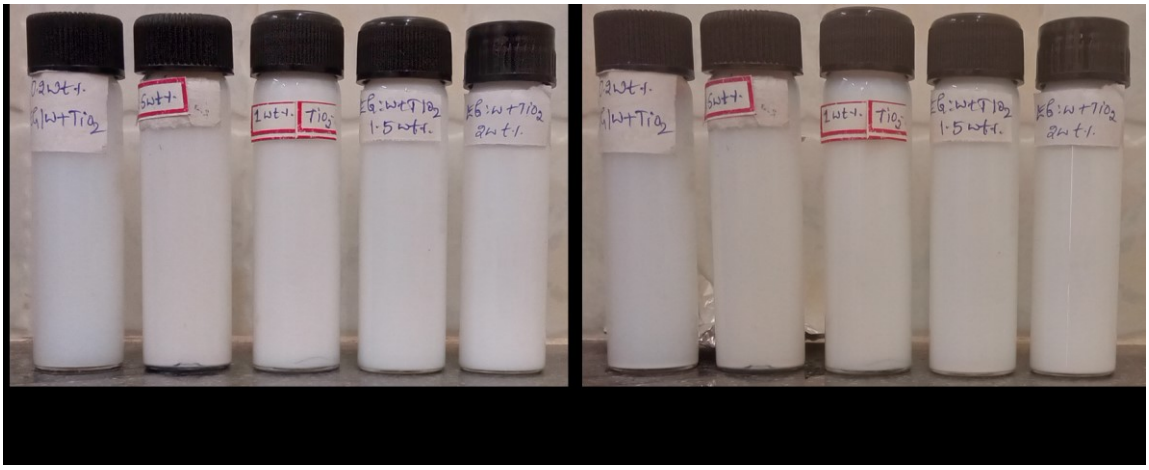

Fig. 4.1 Stability condition of the EG:water- Al_2O_3 nanofluids

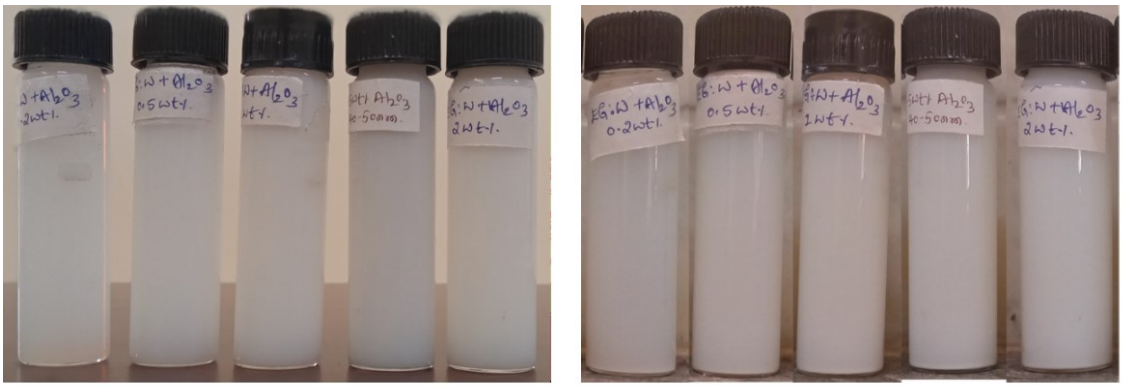

Fig. 4.2 Stability condition of the EG:water- TiO_2 nanofluids

4.1.2 Zeta potential analysis

The zeta potential values for Al_2O_3 and TiO_2 (0.2 wt.%) nanofluids are shown in Table 4.1. For EG:water-Al_2O_3 nanofluids, the sample without surfactant is the most unstable (7.44 mV), followed by the sample with SDBS (-41.1 mV). For EG:water-TiO_2 nanofluids, the zeta potential was –37.2 mV. After six weeks, the zeta potential values for Al_2O_3 and TiO_2 nanofluids were -39.1 and -35.7 mV, indicating that both nanofluids are stable. Figs. 4.3 to 4.6 show the zeta potential results obtained for the 0.2 wt.% of Al_2O_3 and TiO_2 nanofluids. A study conducted by Leong et al. (2017) on water based Al_2O_3 and TiO_2 nanofluids showed a superior value of zeta potential with SDBS surfactant compared to PVP and gum arabic surfactant.

Table 4.1 Zeta potential values (mV) of samples tested in present study (0.2 wt.% concentration)

Sample	After preparation (with SDBS surfactant)	After 6 weeks (with SDBS surfactant)	After preparation (without any surfactant)
EG:water-Al_2O_3	-41.1	-39.1	7.44
EG:water-TiO_2	-37.2	-35.7	8.86

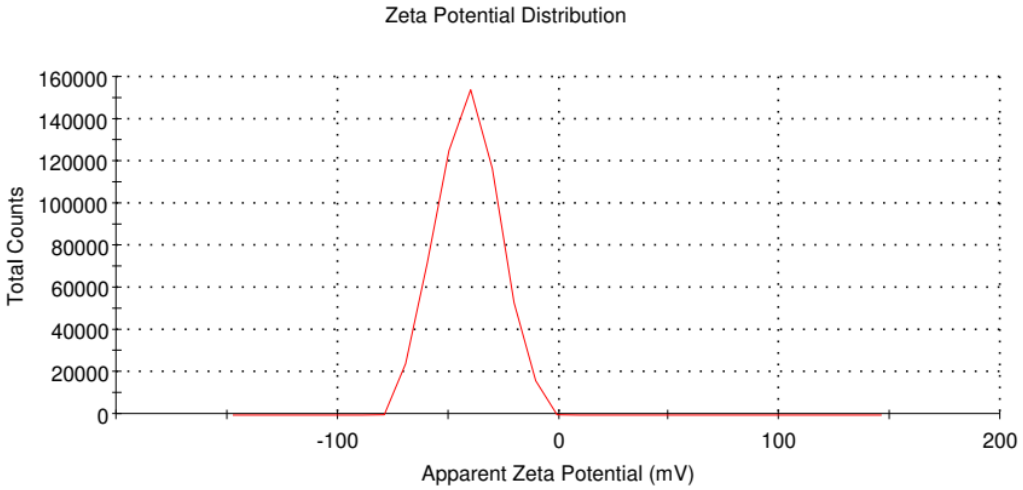

Fig. 4.3 Zeta potential result for EG:water- Al_2O_3 (0.2 wt.%) nanofluids (after preparation)

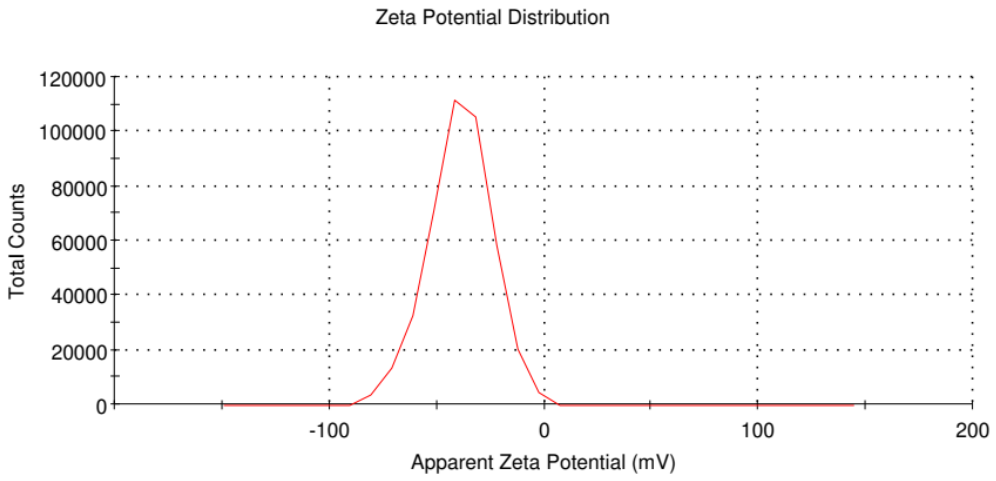

Fig. 4.4 Zeta potential result for EG:water- Al_2O_3 (0.2 wt.%) nanofluids (after six weeks)

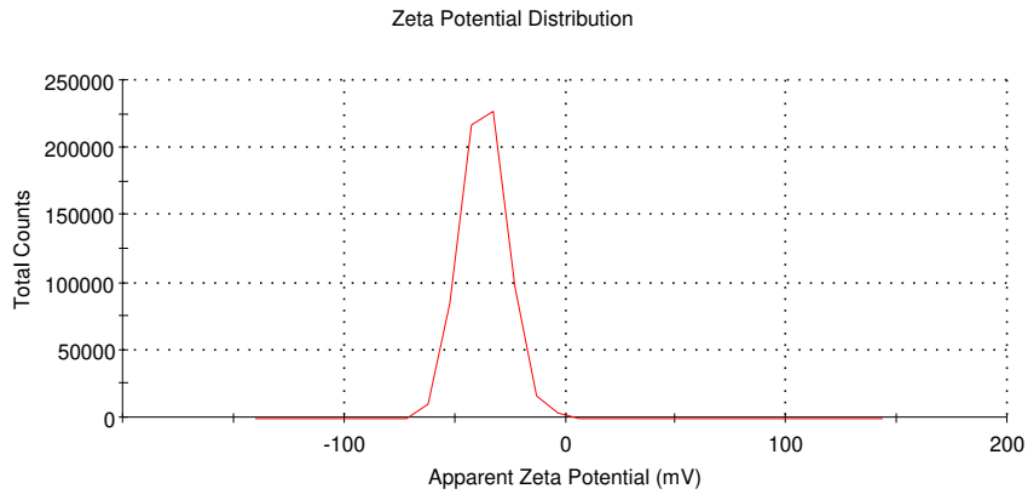

Fig. 4.5 Zeta potential result for EG:water- TiO_2 (0.2 wt.%) nanofluids (after preparation)

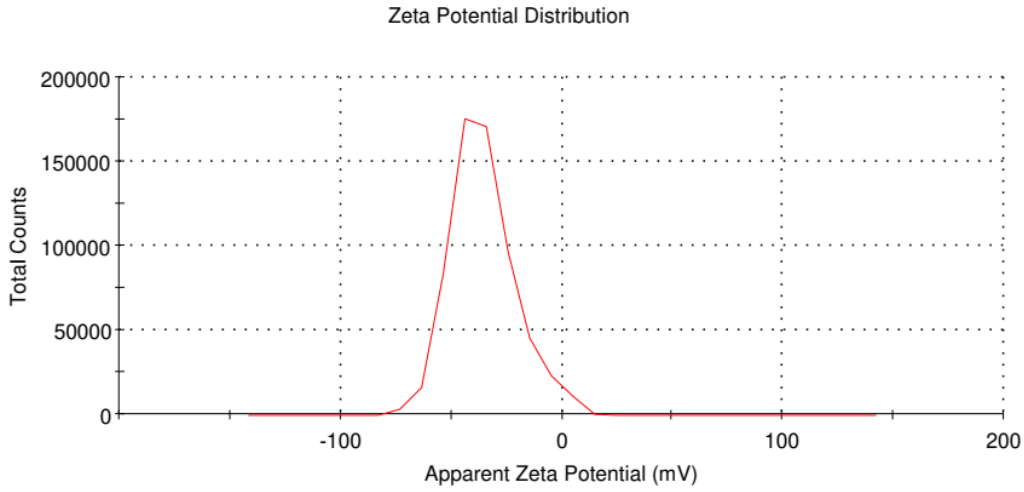

Fig. 4.6 Zeta potential result for EG:water- TiO_2 (0.2 wt.%) nanofluids (after six weeks)

4.1.3 Thermal conductivity investigation

The stability of nanofluids was investigated by measuring their thermal conductivity with respect to sedimentation time (for 32 days). The thermal conductivity measurement of various concentrations of the nanofluids of two materials was carried out. It is expected that the sedimentation of particles results in a decrease in the thermal conductivity of the nanofluid. Figs 4.7 and 4.8 show the thermal conductivity of the nanofluid during the 30-day period. Variation in thermal conductivity is an indication of the stability of the nanofluid. From these figures, it can be observed that the thermal conductivity slightly decreased after the 27^{th} and

30th day for Al_2O_3 and TiO_2 nanofluid respectively. After 27 days and 30 days, the decrease in thermal conductivity was found to be 0.3 to 0.8 % for two nanofluids. This shows that the nanofluids prepared in the study can be assumed to be stable for 30 days after preparation in view of the very small decrease in the value of thermal conductivity.

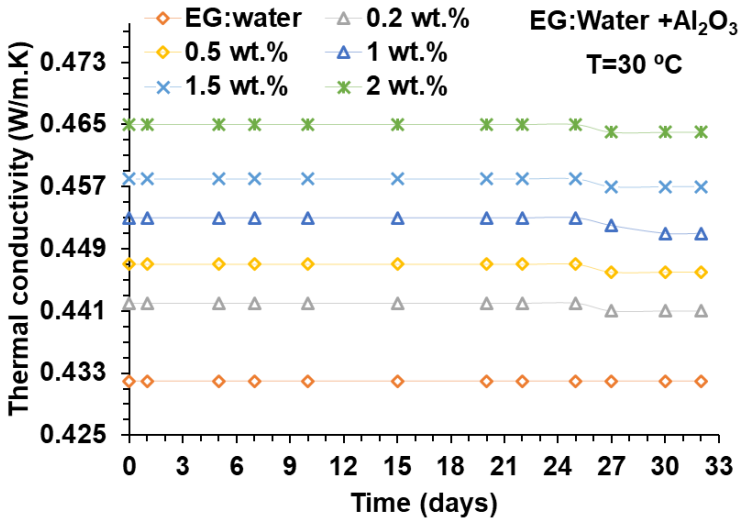

Fig. 4.7 Thermal conductivity of the EG:water- Al_2O_3 nanofluids as a function of time

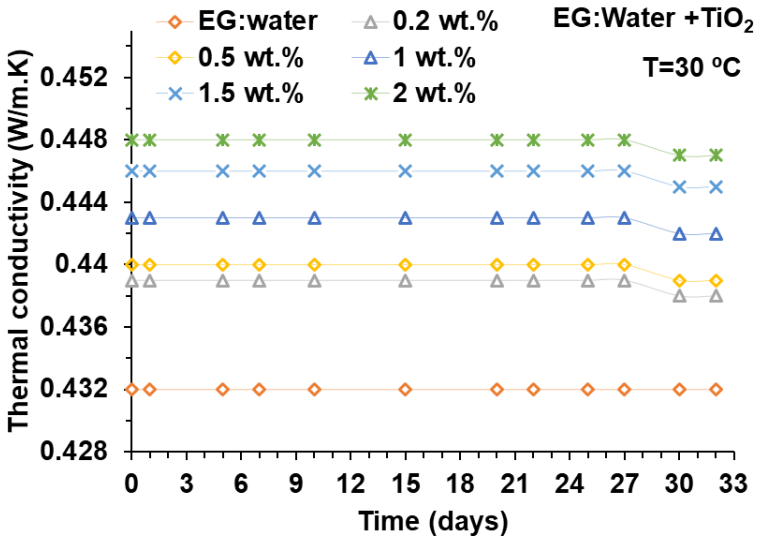

Fig. 4.8 Thermal conductivity of EG:water- TiO_2 nanofluids as a function of time

4.2 Thermal conductivity and viscosity of nanofluid

4.2.1 Thermal conductivity

In this study, thermal conductivity measurements at various temperatures (5 to 55 ºC) were carried out for nanofluids of two materials (Al_2O_3 and TiO_2) with different weight concentrations in the range 0 – 2 wt.%. The enhancement of thermal conductivity is presented in the form of effective thermal conductivity (k_{nf}/k_{bf}).

Figs. 4.9 to 4.12 show the effect of concentration and temperature on the thermal conductivity and effective thermal conductivity of EG:water nanofluids. From Fig. 4.9 and 4.10, it can be found that the thermal conductivity of nanofluids increases with an increase in nanoparticle loading. From Fig. 4.9, it can be found that the thermal conductivity of Al_2O_3 nanofluid increases by 1.21% to 4.87% for 0.2 to 2 wt.% concentration at 5 °C (compared to base fluid). Similarly, at the same concentration range, thermal conductivity enhancement of 0.48% to 2.68% was found for TiO_2 nanofluid at 5 °C (Fig. 4.10). Furthermore, thermal conductivity was found to increase as temperature increased (Fig. 4.9 and Fig.4.10). A similar behavior was reported by Esfe et al. (2015c) for EG:water mixture of 40:60 (volume/volume) based nanofluids.

At 5 °C, 20 °C, 30 °C, 40 °C and 55 °C, the thermal conductivity of EG: water – Al_2O_3 nanofluid is 0.415, 0.433, 0.442, 0.453 and 0.470 W/m.K, respectively (Fig. 4.9) for 0.2 wt.% concentration.The corresponding values for base fluid (EG:water) are 0.410, 0.423, 0.432, 0.441, and 0.450 W/m.K. For Al_2O_3 nanofluid containing 2 wt.% concentration, thermal conductivity values obtained were 0.430, 0.452, 0.465, 0.476, and 0.490 W/m.K in that order. Similarly, for the TiO_2 nanofluid (From Fig.4.10), thermal conductivity values at 2 wt.% were 0.421, 0.439, 0.448, 0.459 and 0.474 W/m.K for 5 °C, 20 °C, 30 °C, 40 °C and 55 °C respectively. This shows the increase in temperature has significant effect on the thermal conductivity values for both the nanofluids.

From Fig. 4.11, the increase in thermal conductivity of Al_2O_3 nanofluid was 4.87% and 9.29% for nanofluid concentration of 2 wt.%, corresponding to 5 °C and 55 °C, respectively compared to base fluid. Similarly, for TiO_2 nanofluid (Fig. 4.12) indicated thermal conductivity enhancements of 2.68% to 4.86% in that order for 2 wt.% concentration. From the figures (Fig.4.11 and 4.12), it can be observed that the effective thermal conductivity values are more

than 1, indicating enhancement in the thermal conductivity of nanofluid compared to base fluid (EG:water) both nanofluids. As the temperature and concentration of nanofluid increase, the effective thermal conductivity is found to be more. When compared to the base fluid, the maximum enhancement obtained for Al_2O_3 (Fig. 4.12) and TiO_2 (Fig. 4.13) nanofluids at 55 °C for 2 wt.% concentration was 9.29% and 4.86%, respectively. Out of two nanofluids considered in the study, the highest enhancement was found to be for Al_2O_3 nanofluid at low temperature and high temepature (Fig. 4.13). This can be attributed to its higher thermal conductivity of Al_2O_3 compared to TiO_2. Table 4.2 shows the percentage of enhancement in thermal conductivity for two materials in the temperature range of 5 – 55 ºC.

The enhanced thermal conductivity of nanofluids can be attributed to the Brownian motion of nanoparticles and liquid layering of liquid / particle interfaces (Özerinç et al., 2010; Qiu et al., 2020). According to Lee et al. (2010) two forms of Brownian motion in nanofluids that could possibly enhance the thermal conductivity are – (i) collision between nanoparticles (diffusion process) and nanoscale convection caused by the motion of nanoparticles and (2) liquid layering at the interface of liquid/particle. It is well known that liquid molecules form a layered structure very near to the surface of the particles and behave more like solids. The formation of these layer structures also possibly enhances the thermal conductivity of nanofluid by providing a thermal bridge between particles and liquid (Liang and Tsai, 2011). Previously Yu et al. (2012) and Mojarrad et al. (2014) studies have reported enhancement in thermal conductivity for EG:water - Al_2O_3 nanofluid.

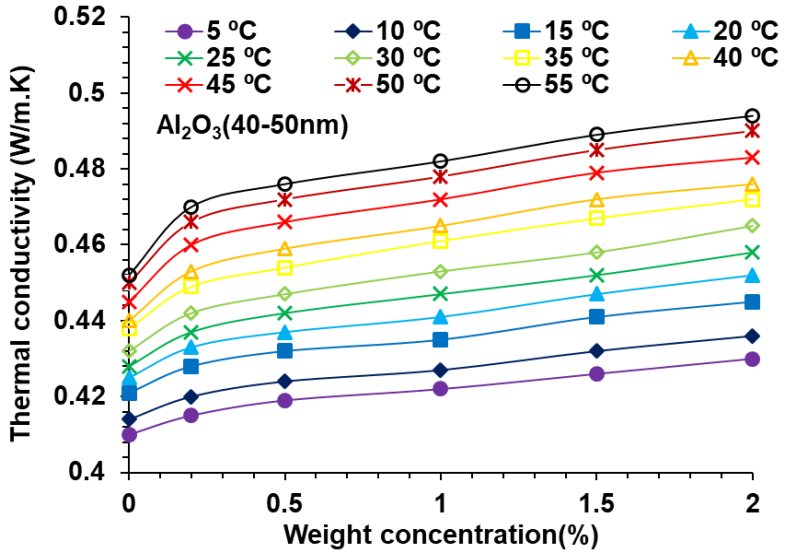

Fig. 4.9 Thermal conductivity of the EG:water- Al_2O_3 nanofluids vs. concentration at different temperatures

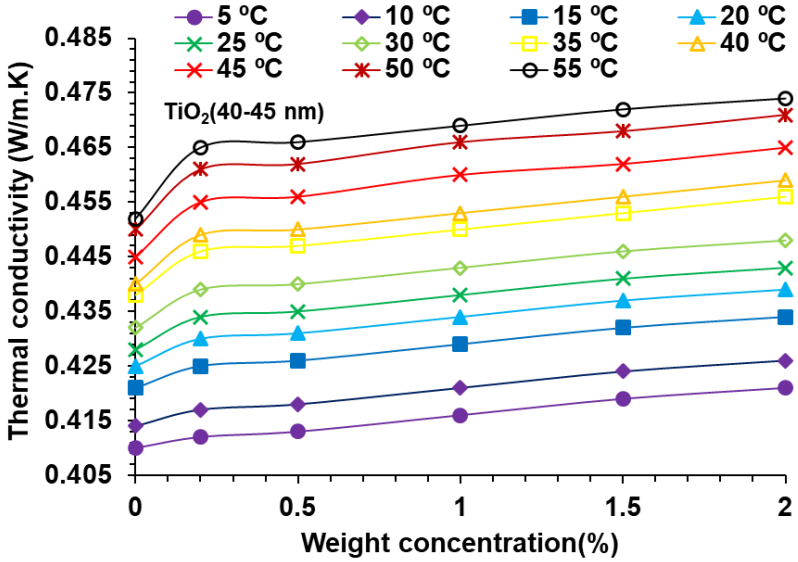

Fig. 4.10 Thermal conductivity of the EG:water- TiO_2 nanofluids vs. concentration at different temperatures

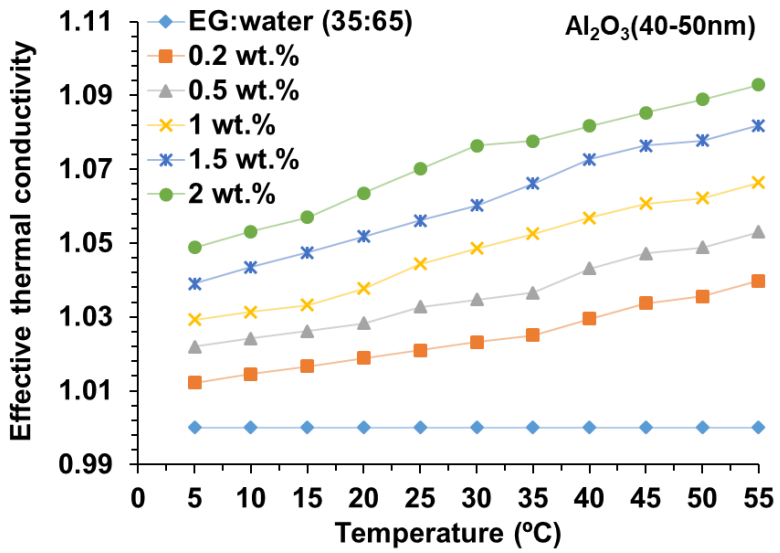

Fig. 4.11 Effective thermal conductivity of the EG:water- Al_2O_3 nanofluids as a function of temperature at different weight concentrations

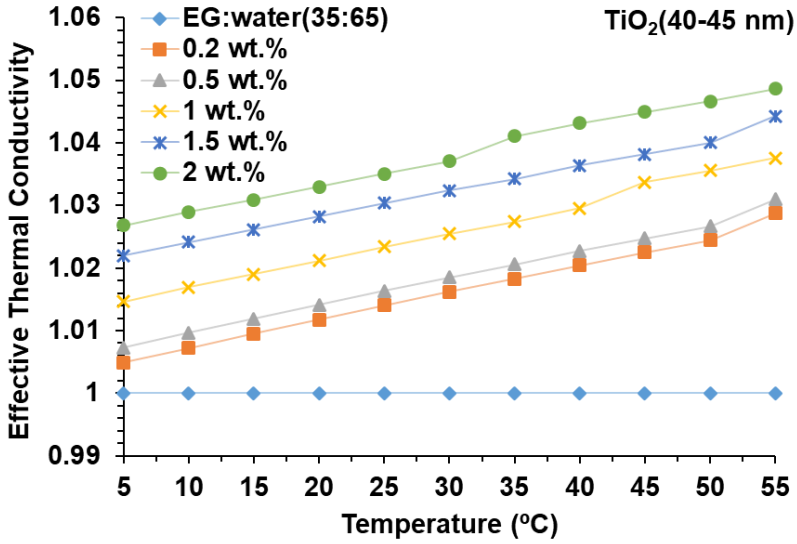

Fig. 4.12 Effective thermal conductivity of the EG:water- TiO_2 nanofluids vs. temperature at different concentrations

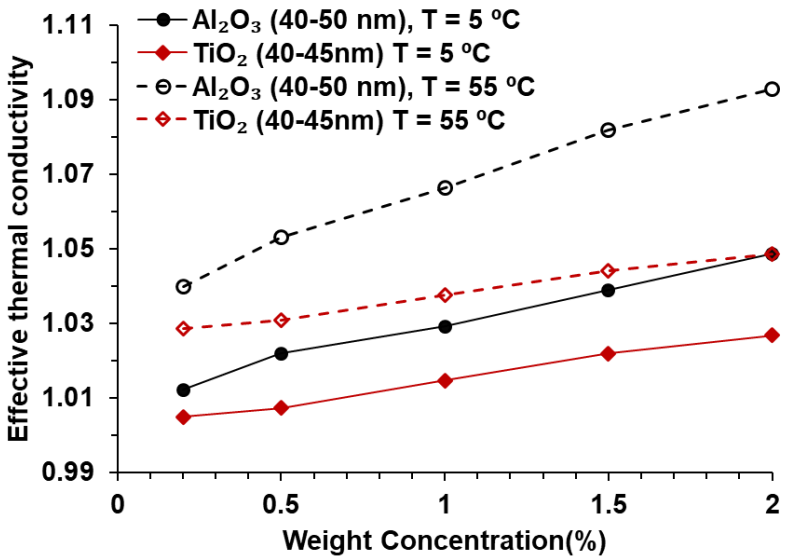

Fig. 4.13 Effect of two oxide nanopowder on effective thermal conductivity with respect to weight concentration at 5 ºC and 55 ºC

Table 4.2 Enhancement (%) in thermal conductivity of EG:water based nanofluids at temperature range of 5 – 55 ºC.

Nanofluid	**Nanofluid concentration (wt.%)**				
	0.2 wt.%	**0.5 wt.%**	**1 wt.%**	**1.5 wt.%**	**2 wt.%**
Al_2O_3	1.21-3.98	2.19-5.30	2.92-6.63	3.9-8.18	4.87-9.29
TiO_2	0.48-2.87	0.73-3.09	1.46-3.76	2.19-4.42	2.68-4.86

4.2.2 Viscosity

Viscosity is an important physical property in heat transfer. As the addition of nanoparticles to the base fluid can alter its viscosity, it is imperative that the effect of addition of nanoparticles on the viscosity of nanofluids has to be investigated. In this study, viscosity of Al_2O_3 and TiO_2 nanoparticles dispersed in the EG:water was measured experimentally considering the effect of the shear rate and temperature.

4.2.2.1 Effect of weight concentration on viscosity

The viscosity of nanofluids depends on the nanofluid concentration, shear rate and temperature. Figs. 4.14 to 4.21 show the viscosity behaviour of the aforementioned parameters for EG:water nanofluids. From these figures, it can be observed that the viscosity is a strong function of

nanofluid concentration and temperature. The viscosity of nanofluids was found to increase with an increase in the concentration of nanofluid. Similar behaviour has been reported in the literature (Kwak and Kim, 2005; Pastoriza-Gallego et al., 2011). The addition of nanoparticles to the base fluid increases the interactions between the molecules of the base fluid and the nanoparticles, leading to higher viscosity of the nanofluid. The measured viscosities of Al_2O_3 nanofluids were found to increase by 9.89% for the maximum nanoparticle loading of 2 wt.% at 5 ºC against base fluid. A similar behavior (12.99% increase) of the viscosity of TiO_2 nanofluids was observed for the same weight concentration (2 wt.%) and temperature (5 ºC). For the low weight concentration (0.2 wt.% in the present study), the measured viscosities for Al_2O_2 and TiO_2 nanofluid were found to increase by 2.05% and 2.94% against the base fluid at 5 ºC respectively. This shows that the increased weight concentration of nanoparticles have significant effect on the viscosity rise of resultant nanofluid.

4.2.2.2 Effect of shear rate on viscosity

Figs. 4.14 and 4.15 depict the effect of shear rate on the viscosity of EG:water based Al_2O_3 and TiO_2 nanofluid, respectively. The measurement was carried out for the base fluid and nanofluids of 0.5, 1 and 2 wt.% concentration. The base fluid considered in the present study (EG:water mixture) shows that viscosity does not vary with the applied shear rate at 25 ºC (Fig. 4.14). It is observed that for Al_2O_3 nanofluid (0.5, 1 and 2 wt.%), the trend appears similar to that of the base fluid, but viscosity is slightly more than that of the base fluid. The increase in viscosity is caused by a disseminated nanoparticle in the base fluid, which results in more flow resistance. However, the viscosity remained constant at range of applied shear rate for both the nanofluids. It can also be observed from the study that the viscosity of the TiO_2 nanofluid was slightly higher than that of the Al_2O_3 nanofluid at an identical shear rate. This can be attributed to the particle size, shape, specific surface area and density of nanoparticles of a specific material (Meyer et al., 2015; W. H. Azmi et al., 2016; Dey et al., 2017; Qiu et al., 2020).

Figs. 4.16 and 4.17 indicate the shear stress variation of Al_2O_3 and TiO_2 nanofluids for with shear rate at different weight concentrations at 25 ºC. Fluids either behave like a Newtonian fluid or a non-Newtonian fluid, depending on whether the relationship between shear stress and shear rate is linear or non-linear. From Figs. 4.16 and 4.17, it can be clearly observed that a linear relationship between shear stress and shear rate that follows Newton's law of viscosity. Similar linear behaviour can be observed for all concentrations of both nanofluids. Shear stress

is higher in the case of nanofluid and it increased with increase in weight concentration. Similar behaviour of nanofluids have been reported by many researchers for EG based nanofluids (Hemmat Esfe et al., 2015d; Khedkar et al., 2016). The viscosity study carried out by Sundar et al. (2014) also shows the Newtonian behaviour when Al_2O_3 nanoparticles were dispersed in the different ratios of EG and water mixtures.

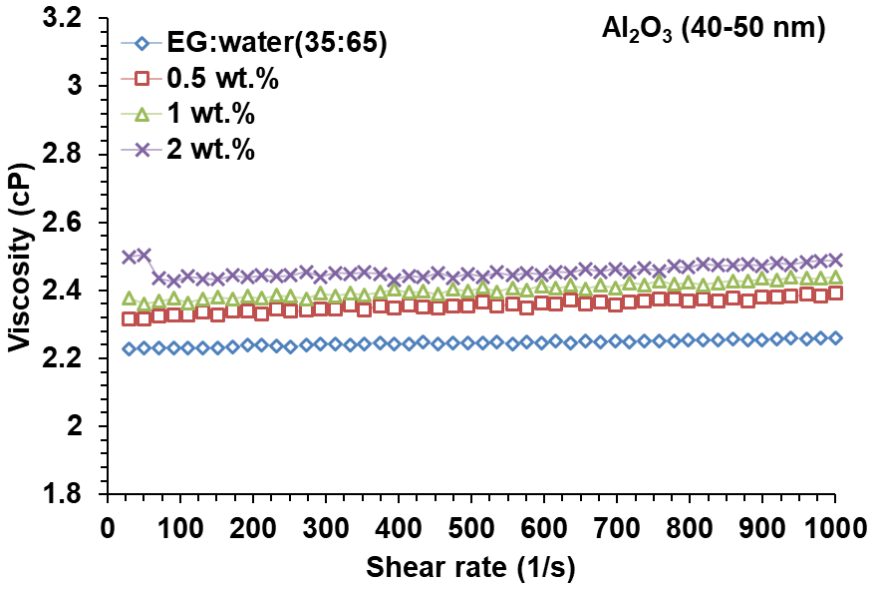

Fig. 4.14 Viscosity of EG:water - Al_2O_3 nanofluid vs. shear rate at different concentrations (25°C)

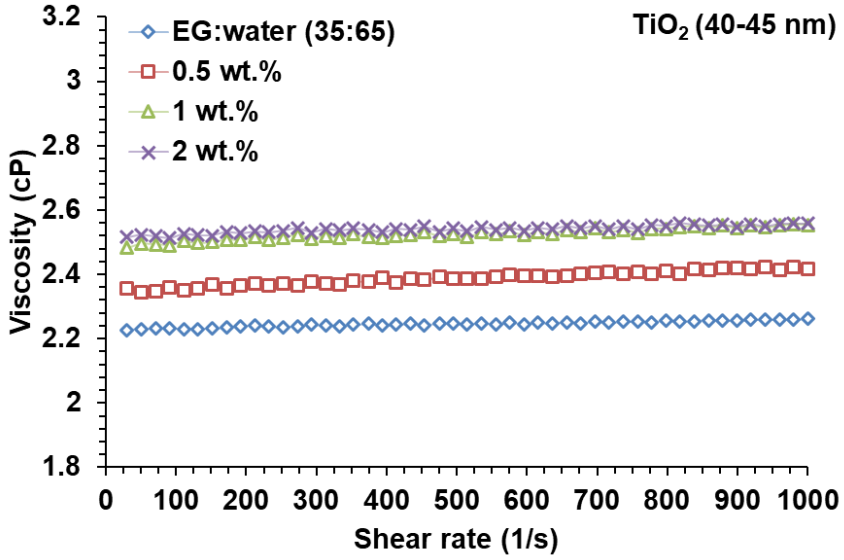

Fig. 4.15 Viscosity of EG:water – TiO_2 nanofluid vs. shear rate at different concentrations (25°C)

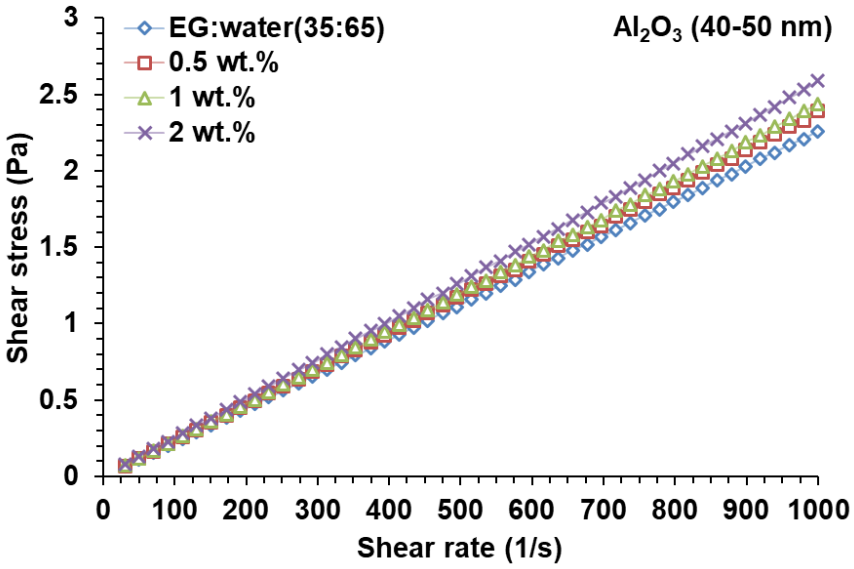

Fig. 4.16 Shear stress variation of EG:water – Al_2O_3 nanofluid at different concentrations (25°C

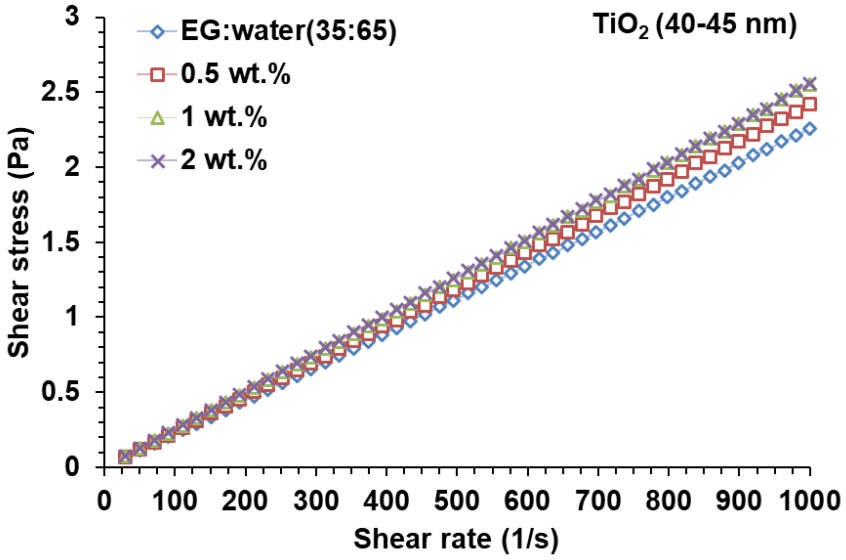

Fig. 4.17 Shear stress variation of EG:water – TiO_2 nanofluid a different concentrations (25 °C)

4.2.2.3 Effect of temperature on viscosity

The viscosity of EG:water based Al_2O_3 and TiO_2 nanofluids was measured in a temperature range of 5 to 55 ºC at a constant shear rate of 100 s^{-1}. Figs. 4.18 to 4.21 depict the effect of the temperature on viscosity and relative viscosity of nanofluids at different concentrations for Al_2O_3 and TiO_2 nanofluids. From Fig. 4.18, it can be observed that the behaviour is similar to

that of a liquid, i.e., decrease in viscosity with the increase in temperature. However, the viscosity of the Al_2O_3 nanofluid at lower temperatures was found to be higher than that of the base fluid. On the other hand, at higher temperatures, the viscosity increase of Al_2O_3 nanofluid was lower compared to the lower temperatures. Several researchers have previously reported the effect of temperature on the viscosity of nanofluids, which showed a similar trend to the present study (Suganthi et al., 2014; Hemmat Esfe et al., 2015d; Krishnakumar et al., 2019).

Fig. 4.19 shows the effect of relative viscosity variation on increasing temperature at different weight concentrations of Al_2O_3 nanofluid. It is evident from Fig. 4.15 that the relative viscosity is >1 at all concentrations. However, relative viscosity was found to decrease as the temperature increased for all concentrations. The relative viscosity values for Al_2O_3 nanofluid obtained at the lowest temperature (5 °C) are 1.0205, 1.0409, 1.0759, 1.0874, and 1.0989 for 0.2, 0.5, 1, 1.5, and 2 wt.% concentrations, respectively. Similarly, at the highest temperature of the study (55 °C), the corresponding relative viscosity values for the aforementioned concentrations are 1.0012, 1.0025, 1.023, 1.049, and 1.0748, respectively.

Fig. 4.20 depicts the temperature-dependent viscosity variation of EG:water - TiO_2 nanofluid at various weight concentrations.The trends are similar to that of Al_2O_3. Fig. 4.21 depicts the relative viscosity variation as a function of temperature for EG:water - TiO_2 nanofluid at various weight concentrations. For 0.2, 0.5, 1, 1.5 and 2 wt.% concentrations, the relative viscosity values obtained at the lowest temperature (5 °C) are 1.0294, 1.0588, 1.0940, 1.112, and 1.1299, respectively. In that order of weight concentration, the corresponding relative viscosity values at the highest temperature (55 °C) are 1.0025, 1.0051, 1.0473, 1.0654, and 1.0834.

The study shows that viscosity is highly influenced by temperature and weight concentration. Brownian motion and van der Waals forces are the primary contributors for the viscosity increase (Chen et al., 2007; Chandrasekar et al., 2010; Kanti et al., 2020a). If the weight concentration of nanoparticles in the base fluid increases, the suspended cluster causes flow retardation. Enhancement in viscosity of nanofluid can also be due to the interface created between the liquid molecules and nanoparticles and the adhesive intermolecular forces between the particles (Kole and Dey, 2013; L Syam Sundar et al., 2013; Akilu et al., 2020; Kanti et al., 2020a). Because of stronger repulsive forces at higher temperatures, energised nanoparticles remain away from one another, resulting in greater dispersion in the base fluid (Kanti et al., 2020b). As a result, the higher temperature of nanofluid results in the lower viscosity of

nanofluid. The study shows that the maximum increase in viscosity is 9.89% and 12.99% for Al_2O_3 and TiO_2 nanofluid at 5 ºC for 2 wt.% concentration respectively. Moreover, at higher temperature (55 ºC) maximum increase in viscosity were found to be 7.48% and 8.34% respectively at 2 wt.% concentration. Because of the small increase in viscosity, it is unlikely to have a significant impact on pressure drop or pumping power.

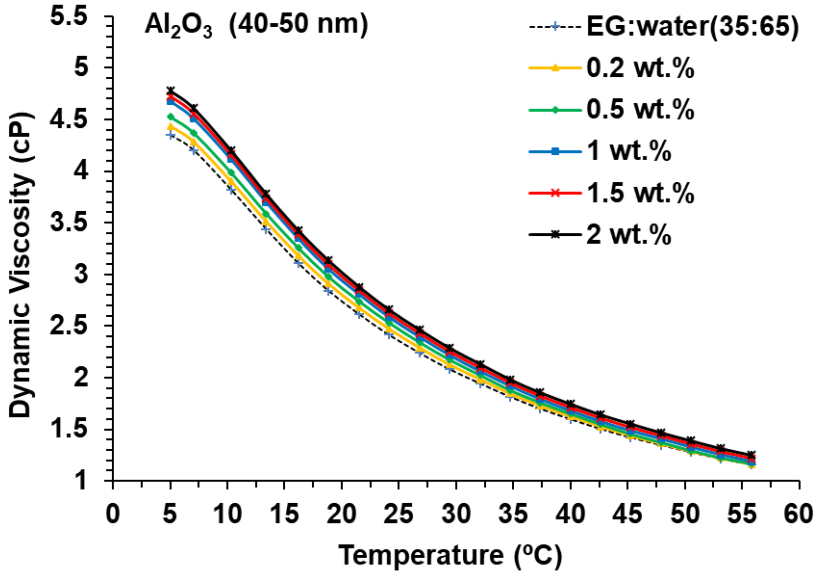

Fig. 4.18 Viscosity variation of EG:water - Al_2O_3 nanofluid vs. temperature at different concentration

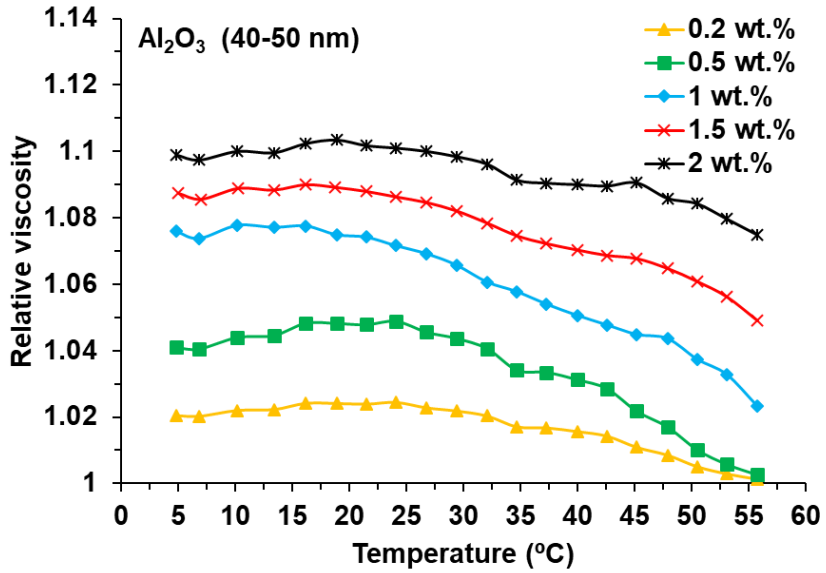

Fig. 4.19 Effect of temperature on relative viscosity of EG:water - Al_2O_3 nanofluid with respect to temperature at different concentration

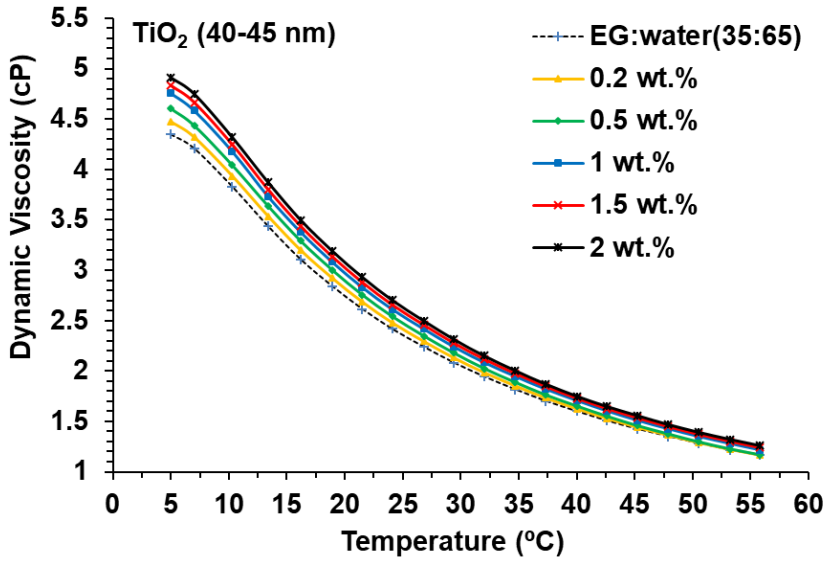

Fig. 4.20 Viscosity variation of EG:water – TiO_2 nanofluid vs. temperature at different concentration

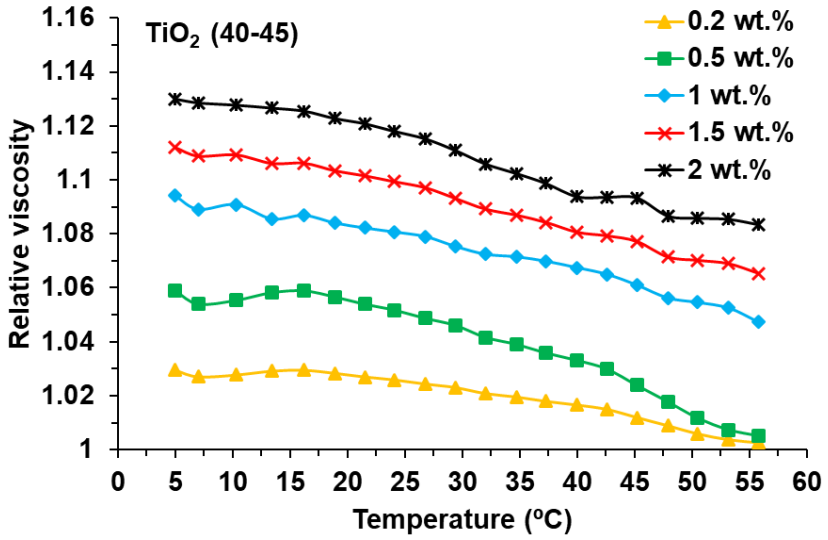

Fig. 4.21 Effect of temperature on relative viscosity of EG:water – TiO_2 nanofluid with respect to temperature at different concentration

4.2.3 Correlations for effective thermal conductivity

4.2.3.1 Considering experimental data from present study

Regression was performed in Microsoft (MS) Excel using experimental data to determine the correlation constants of A, B and C in Eq. (3.27). The correlation constants R^2 and adjusted R^2 values for the EG:water based nanofluids are given in Table 4.3. The performance of the model

was evaluated by comparing the experimental data (55 data points). The obtained model is valid for 0.05 vol.% to 0.54 vol.% (corresponding to 0.2 wt.% to 2 wt.%), temperature range of 5 to 55 ºC for the Al_2O_3 and TiO_2 nanoparticles and the base fluid (EG:water) considered in the present work. R^2 and RMSE values (in Table 4.3) obtained for this model show the accuracy of prediction of effective thermal conductivity. Fig. 4.22 shows that predicted values of effective thermal conductivity fit well with the experimental data.

Table 4.3 Constants, R^2, adjusted R^2 and RMSE values for Eq. (3.27)

Nanofluids	EG:water - Al_2O_3	EG:water - TiO_2
A	0.9983	0.9988
B	9.62	4.611
C	0.2194	0.132
R^2	0.981	0.990
Adjusted R^2	0.980	0.990
RMSE	0.002831	0.001064

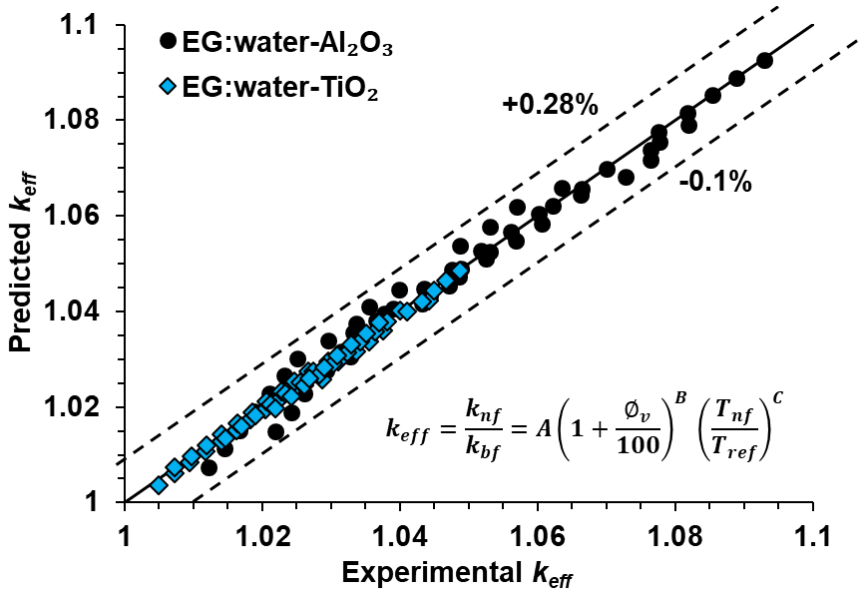

Fig.4.22 Predicted results of Eq. (3.27) vs. experimental results of effective thermal conductivity for EG:water nanofluid

4.2.3.2 Considering experimental data from present study and literature data

The correlation proposed previously (Eq. 3.27) considers two input parameters (temperature and concentration) only. However, thermal conductivity also depends on factors such as volume ratio of EG:water, nanoparticle size and thermal conductivity of nanoparticles. In the present experimental study these parameters were kept constant, and therefore not considered in the model developed previously. However, a generalized correlation considering all the above factors will be more useful. Therefore, considering results of present study data and literature data (Table 3.11) a generalized correlation for each nanolfuid (Al_2O_3 and TiO_2) separately, was developed considering temperature, concentration, nanoparticle size and EG:water mixture ratio. Regression was carried out for Eq. (3.28) for the two materials separately. Regression constants, correlation coefficients, and performance parameters are given in Table 4.4. The Eq. (3.28) is valid for the concentration of 0.05-1.5 vol.%, temperature range of 5-55 ºC, EG in the base fluid from 20% to 60% (V_r=0.2 to 0.6) and nanoparticle size 20 - 50 nm (Table 3.11, Chapter 3) of Al_2O_3 (252 data points) and TiO_2 (143 data points) nanoparticles. From Table 4.4 and Fig. 4.23, it can be observed that the combined results of the literature data on thermal conductivity for individual nanoparticles of two materials show reasonable prediction with experimental results.

Table 4.4 Constants, R^2, adjusted R^2 and RMSE values for Eq. (3.28)

Nanofluids	EG:water - Al_2O_3	EG:water - TiO_2
a_1	0.7737	1.082
a_2	11.32	3.906
a_3	0.544	0.1255
a_4	0.0394	0.00873
a_5	-0.0337	0.124
R^2	0.849	0.662
Adjusted R^2	0.847	0.652
RMSE	0.0256	0.02445

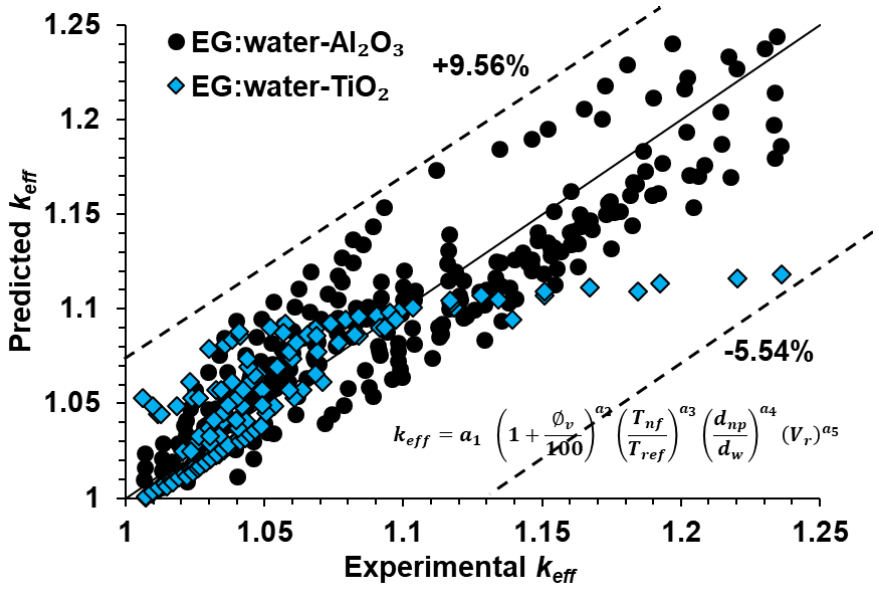

Fig.4.23 Predicted results of Eq. (3.28) vs. experimental results of effective thermal conductivity for EG:water nanofluid

4.2.4 Correlations for relative viscosity

4.2.4.1 Considering experimental data from present study

The constants for Eq. (3.29) were obtained by performing regression in MS excel. The corresponding constants, correlation of determination *(R^2)* and adjusted R^2 values for the EG:water based nanofluids (Al_2O_3 and TiO_2) are given in Table 4.5. Eq. (3.29) is valid for the temperature range of 5 to 55 ºC and a concentration of 0.05 vol.% to 0.53 vol.% of EG:water (35%/65% by volume) - Al_2O_3 and TiO_2 nanofluids. To compare the prediction obtained from the correlation with the experimental results, a graph was drawn with predicted relative viscosity versus experimental relative viscosity for both nanofluids (100 data points). Fig. 4.24 indicates the data distribution of relative viscosity obtained from the prediction (Eq. 3.29 - two input variables) and experimental relative viscosity of EG:water - Al_2O_3 and TiO_2 nanofluids. It is clear from this figure that most of the data is very close to the fit line, showing a good prediction of the present experimental data of both nanofluids.

Table 4.5 Constants, R^2, adjusted R^2 and RMSE values obtained for Eq.(3.29)

Nanofluids	EG:water - Al_2O_3	EG:water - TiO_2
p	1.033	1.044
q	15.55	17.75
r	-0.191	-0.259
R^2	0.944	0.958
Adjusted R^2	0.943	057
RMSE	0.00724	0.00848

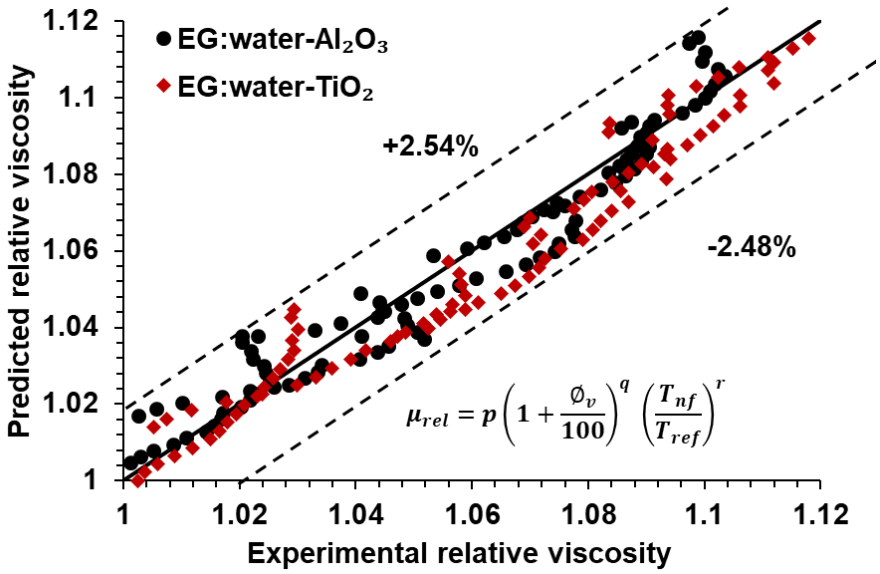

Fig.4.24 Predicted results of Eq. (3.29) vs. experimental results of relative viscosity for EG:water nanofluid

4.2.4.2 Considering experimental data from present study and literature data

Previous correlation for viscosity considered only the nanofluid concentration and temperature which were varied in the experiment. A more generalized correlation (Eq. 3.30) was developed considering particle size, EG:water mixture ratio, temperature, and concentration using the literature data (Chapter 3,Table 3.12). The corresponding constants R^2 and adjusted R^2 values obtained for generalised correlation are given in Table 4.6. From this table, it can be observed that the R^2 value obtained in the case of two input variables (volume concentration and temperature- Eq. 3.29) is greater than that of the four input variables, Figs. 4.25 and 4.26 show

the data distribution of relative viscosity obtained from the prediction (Eq. 3.30 - four input variables, generalised correlation) and experimental relative viscosity of Al_2O_3 (334 data points) and TiO_2 (157 data points) nanofluids, respectively. It is clear from these figures that predicted data are scarttered which shows the large deviation in predicting the relative viscosity of both nanofluids.

Table 4.6 Constants, R^2, adjusted R^2 and RMSE values for Eq. (3.30)

Nanofluids	EG:water - Al_2O_3	EG:water - TiO_2
p_1	0.6619	1.27
p_2	60.82	6.752
p_3	0.2014	-0.211
p_4	0.1721	-0.0214
p_5	0.5176	0.0109
R^2	0.829	0.552
Adjusted R^2	0.826	0.539
RMSE	0.2947	0.06658

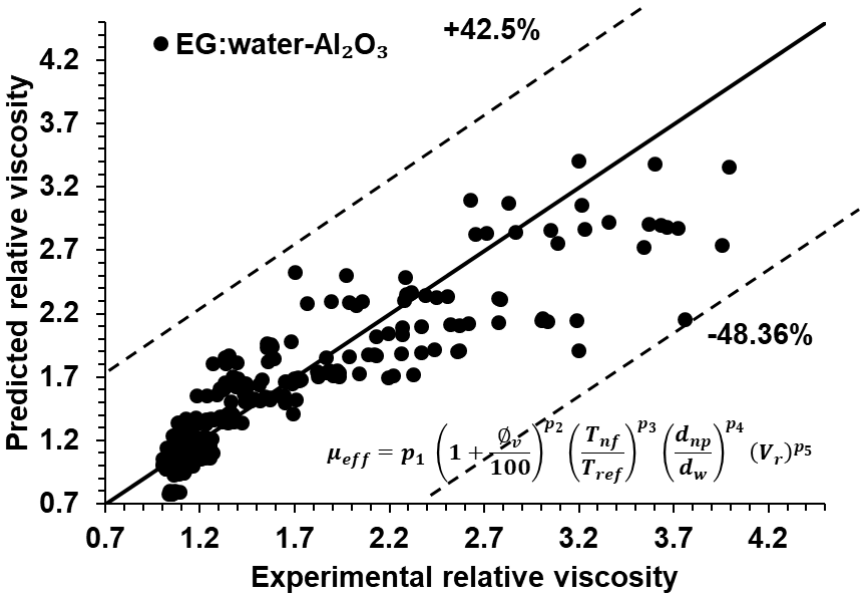

Fig. 4.25 Comparison of predicted relative viscosity (Eq.3.30) of EG:water – Al_2O_3 nanofluid with experimental results of present study and literature work

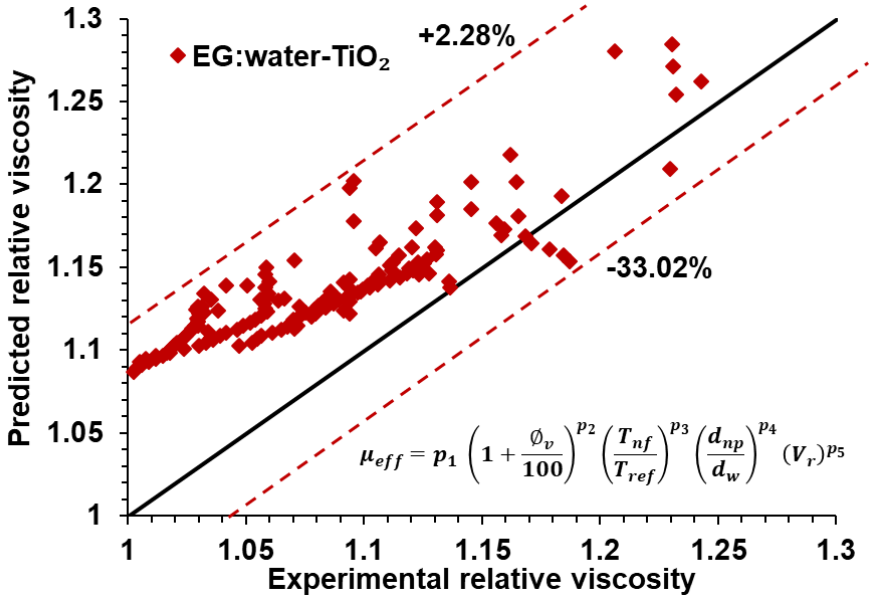

Fig. 4.26 Comparison of predicted relative viscosity (Eq.3.30) of EG:water – TiO_2 nanofluid with experimental results of present study and literature work

4.2.5 Validation of developed correlations and comparison with existing models

4.2.5.1 Effective thermal conductivity

To predict the effective thermal conductivity results of the present study, the performance of the proposed correlations (3.27 and 3.28) was compared with the literature correlations for Al_2O_3 and TiO_2 nanoparticles in EG:water base fluid. The comparison is shown in Figs. 4.27 and 4.28. It can be observed from Fig. 4.27, that at lower concentrations (compared to literature, Table 2.1, Chapter 2), Sundar et al. (2013) correlation largely deviated in terms of predicting the effective thermal conductivity of EG:water - Al_2O_3 which is used in the present study. This is due to the correlation proposed by them was for higher concentration. It can be seen from Fig. 4.27 that the model of Patel et al. (2010) prediction is slightly better than the one by Chiam et al. (2017). Correlation proposed by Patel et al. (2010) considers particle size, temperature and particle thermal conductivity effects.

Fig. 4.28 shows the effective thermal conductivity comparison for EG:water - TiO_2 nanofluids for different models proposed in the literature. From Fig.4.28, it can be clearly noted that Reddy and Rao (2013) correlation showed very close values of prediction compared to present experimental values and the proposed correlation (Eq. 3.27). This can be attributed to the close

ratio of EG:water mixture (EG:water - 40:60) considered in their study with TiO_2 nanoparticles to develop the model. A generalised correlation proposed by Patel et al. (2010) also predicts the close values as their studies considered particle size, temperature and particle thermal conductivity effects. The experimental results from the present study showed higher thermal conductivity than the model proposed by Maxwell and Hamilton - Crosser for all weight concentrations of the nanofluids. In fact, these two models have shown almost the same values of effective thermal conductivity for both nanofluids. However, the calculated thermal conductivity for all nanofluids by the Maxwell model and Hamilton - Crosser is lower than the current experimental data. This is due to the fact that the classical model does not consider other factors affecting thermal conductivity, such as the size of the particle, and the Brownian motion of the particles. It can also be noted from the observation that thermal conductivity increases with an increase in weight concentration in both experimental data and developed models. Furthermore, it is also seen from the study that the prediction by generalised form of correlation proposed in the present work (Eq. (3.28) - material specific) for both nanofluids has slightly deviated due to the several input parameters used to develop the model.

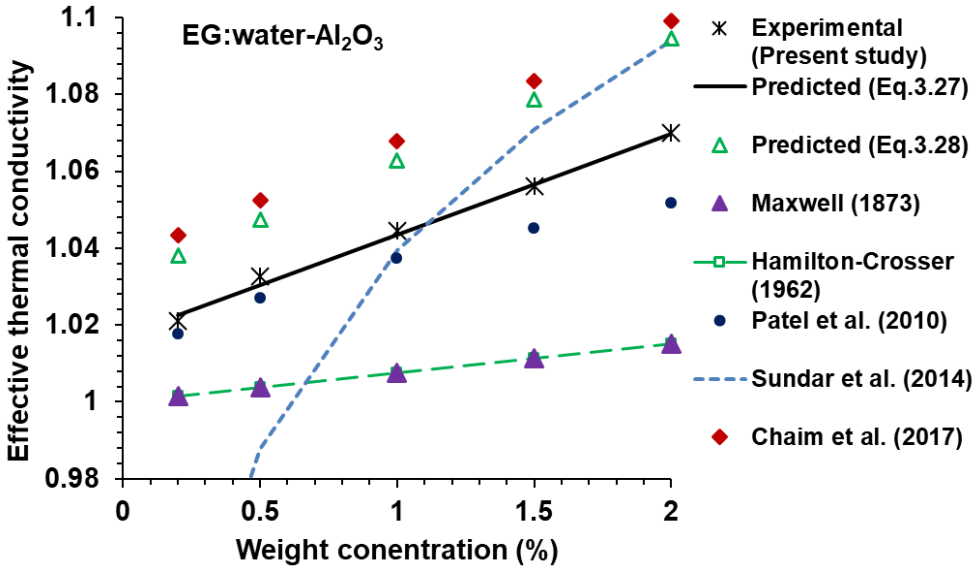

Fig. 4.27 Comparison of effective thermal conductivity of Al_2O_3 nanofluid from the present study and literature models at 25 ºC

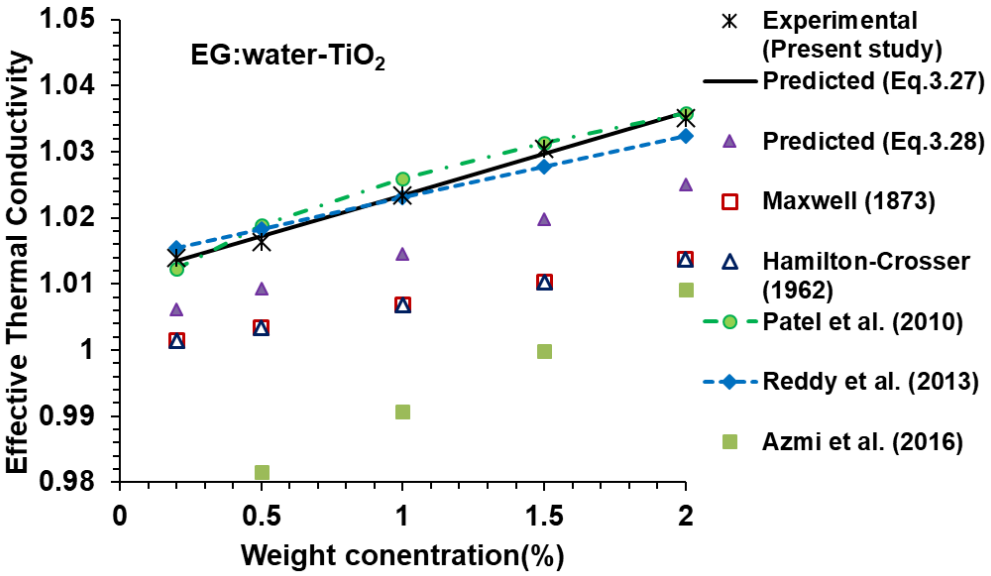

Fig. 4.28 Comparison of effective thermal conductivity of TiO_2 nanofluid from the present study and literature models at 25 ºC

4.2.5.2 Relative viscosity

Figs. 4.29 and 4.30 show comparison between the relative viscosity at various concentrations at 25 ºC of Al_2O_3 and TiO_2 nanofluids obtained from the experiment and those obtained from models reported in the literature. As can be seen from Fig. 4.29, the correlation proposed by Chaim et al. (2017) shows a similar behaviour as that of the Eq. (3.29) for Al_2O_3 nanofluid. It is also noted that the base fluid used in the Chaim et al. (2017) study corresponds to the ratio of the water and EG mixture in the range of 0.4 to 0.6. In case of TiO_2 nanofluids (Fig.4.30), the model proposed by Azmi et al. (2016) was for higher concentrations compared to the present scope of study, hence prediction is not similar to that of present study. The relative viscosity found from the classical models (Einstein (1906), Brinkman (1952) and Batchelor (1977)) have demonstrated similar results at various concentrations and for both nanofluids. However, the prediction from the present study and correlation (Eq. 3.30) show higher viscosity compared to these models. This may be due to low concentrations of nanofluids used in the present study. In addition, the classical models proposed in the literature do not consider the effect of the particle sizes and shape.

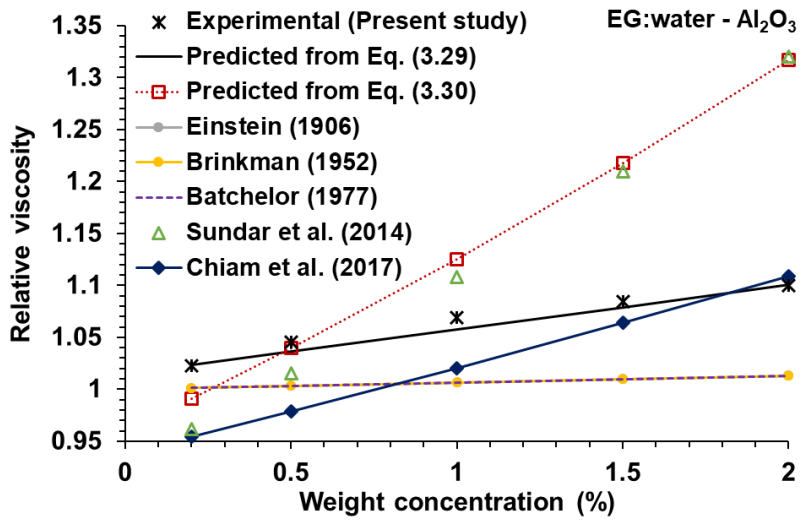

Fig. 4.29 Comparison of the experimental relative viscosity of EG:water - Al_2O_3 nanofluid with different models presented in literature for different concentrations at 25 ºC.

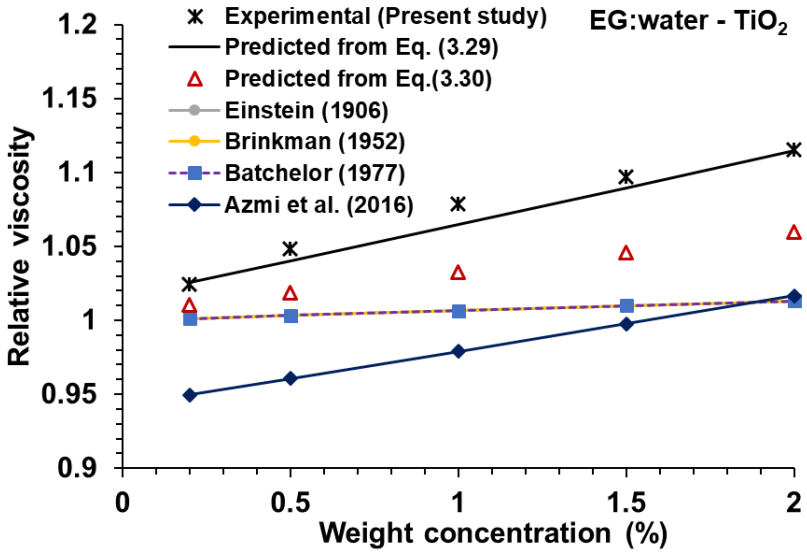

Fig. 4.30 Comparison of the experimental relative viscosity of EG:water – TiO_2 nanofluid with different models presented in literature for different concentrations at 25 ºC.

4.3 Machine learning models

4.3.1 ANN modelling

Out of the four correlations developed (Eq. 3.27 to 3.30) prediction by Eq. (3.27) is the best as indicated by R^2 value in the range of 0.98 – 0.99 for the two materialsc, compared to the peformance of the other three correlations (Eq. 3.28 – 3.30) as indicated by R^2 values (<0.96).

Morever, traditional models for particle suspensions in liquids are not able to account for all the different parameters and mechanisms affecting the thermal conductivity and viscosity of nanofluids. For better prediction of the results ANN modelling was carried out.

4.3.1.1 Effective thermal conductivity

Considering present experimental results

ANN modelling was performed as described in Material and Methods (Chapter 3). Neural networks were created (two input parameters as described in Chapter 3, Table 3.13) with a single hidden layer having 5, 7, 9 and 10 neurons for modelling the experimental results to predict the effective thermal conductivity. The performance of output layer functions (TANSIG and PURELIN) for the prediction of effective thermal conductivity with a developed model 1T for Al_2O_3 and TiO_2 nanofluids are shown in Tables 4.7 and 4.8 respectively. The coefficient of determination (R^2) of ANN model for training set, validation set, testing set, and finally the entire experimental data are shown in Table 4.7 and 4.8. It can be noted from the tables that both the transfer functions used in the hidden layer indicate good prediction of effective thermal conductivity of nanofluid for individual materials. However, the TANSIG-PURELIN (hidden layer and output layer) combination with 10 and 9 neurons in the hidden layer exhibited the best results for the prediction of effective thermal conductivity of Al_2O_3 and TiO_2 nanofluids respectively. It can also be observed from the tables that, RMSE values obtained at optimum number of neurons in hidden layer are the lowest, indicating the superiority of prediction of data compared to others. The corresponding optimized results of model 1T for Al_2O_3 and TiO_2 nanofluids in training, testing, validation and all data are shown in Fig. 4.31 and 4.32 respectively.

Figs. 4.33 and 4.34 show a comparison of predicted data of effective thermal conductivity of Al_2O_3 and TiO_2 nanofluid from developed correlation (Eq. 3.27) and Model 1T respectively. From these figures, it can be seen that the most of the output data predicted from the ANN model (optimized neural network structure from Table 4.7 and 4.8) are very close to the fit line. This shows the accuracy of neural network modelling in the prediction of experimental data considered in the present study. Moreover, the predicted data from the regression method (Eq. 3.27) was found to be slightly away from the fit line and shows less accuracy than ANN model 1T.

Table 4.7 ANN modelling results for effective thermal conductivity of EG:water – Al_2O_3 nanofluid for Model 1T

Hidden layer function	Output layer function	Neuron in hidden layer	Coefficient of determination (R^2)				RMSE (All data)
			Training	Validation	Test	All	
TANSIG	PURELIN	5	0.9968	0.9984	0.9994	0.9972	0.00111
TANSIG	PURELIN	7	0.9984	0.9970	0.9996	0.9986	0.00079
TANSIG	PURELIN	9	0.9994	0.9986	0.9980	0.9988	0.00071
TANSIG	**PURELIN**	**10**	**0.9992**	**0.9996**	**0.9986**	**0.9992**	**0.00058**
TANSIG	TANSIG	5	0.9980	0.9978	0.9984	0.9980	0.00090
TANSIG	TANSIG	7	0.9984	0.9990	0.9978	0.9986	0.00078
TANSIG	TANSIG	9	0.9976	0.9968	0.9984	0.9974	0.00108
TANSIG	TANSIG	10	0.9980	0.9978	0.9996	0.9982	0.00088

Bold indicates the best result

Table 4.8 ANN modelling results for effective thermal conductivity EG:water – TiO_2 nanofluid for Model 1T

Hidden layer function	Output layer function	Neurons in hidden layer	Coefficient of determination (R^2)				RMSE (All data)
			Training	Validation	Test	All	
TANSIG	PURELIN	5	0.9980	0.9988	0.9992	0.9982	0.000445
TANSIG	PURELIN	7	0.9992	0.9992	0.9982	0.9988	0.000358
TANSIG	**PURELIN**	**9**	**0.9994**	**0.9996**	**0.9996**	**0.9994**	**0.000251**
TANSIG	PURELIN	10	0.9992	0.9996	0.9982	0.9990	0.000315
TANSIG	TANSIG	5	0.9984	0.9982	0.9980	0.9982	0.000447
TANSIG	TANSIG	7	0.9982	0.9988	0.9982	0.9994	0.000447
TANSIG	TANSIG	9	0.9986	0.9990	0.9972	0.9984	0.000505
TANSIG	TANSIG	10	0.9986	0.9994	0.9998	0.9988	0.000431

Bold indicates the best result

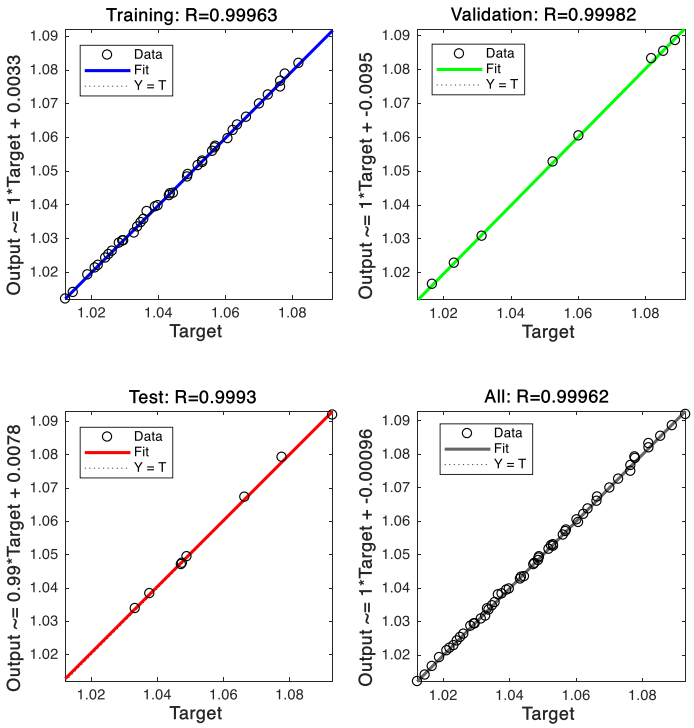

Fig. 4.31 Optimized ANN model 1T results obtained for the effective thermal conductivity of Al_2O_3 nanofluids

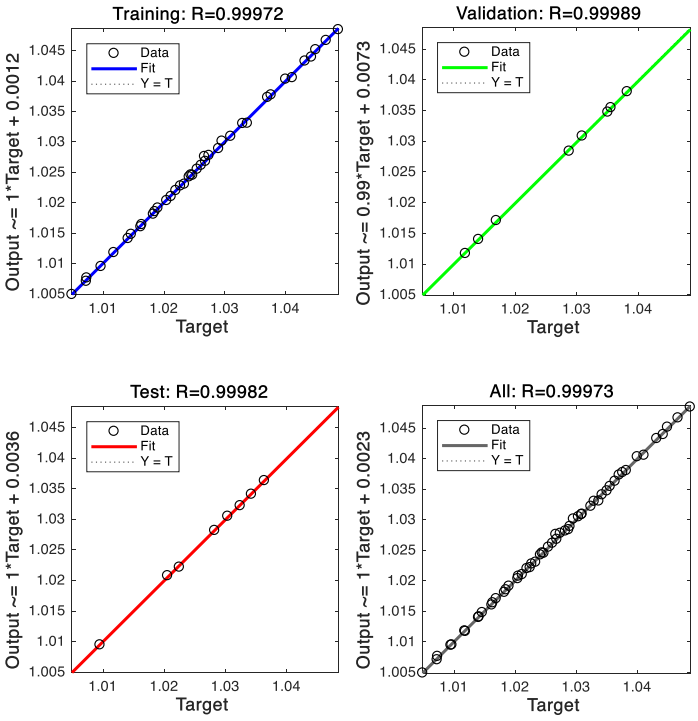

Fig. 4.32 Optimized ANN model 1T results for the effective thermal conductivity of TiO_2 nanofluids

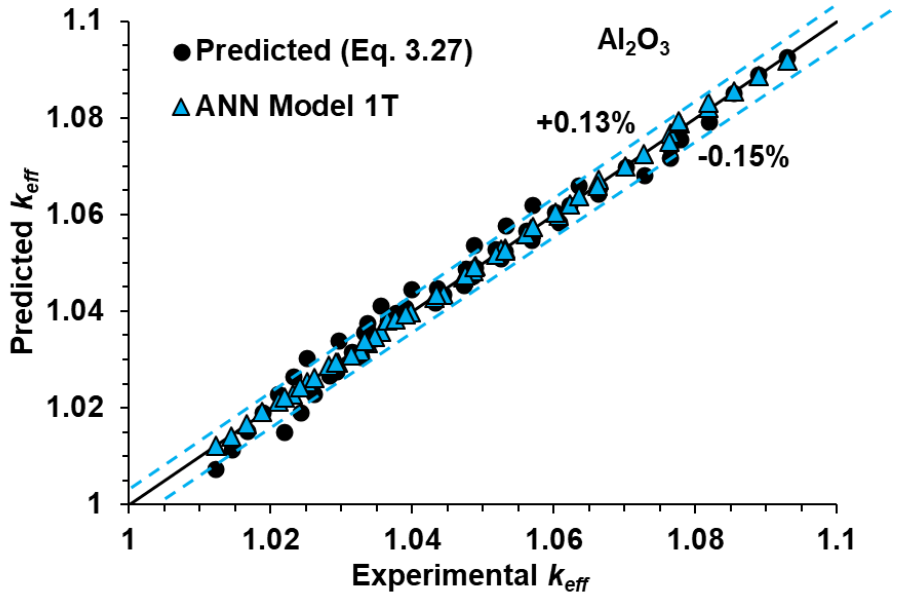

Fig. 4.33 Correlation prediction vs. ANN model 1T prediction of effective thermal conductivity with experimental data for Al_2O_3 nanofluid

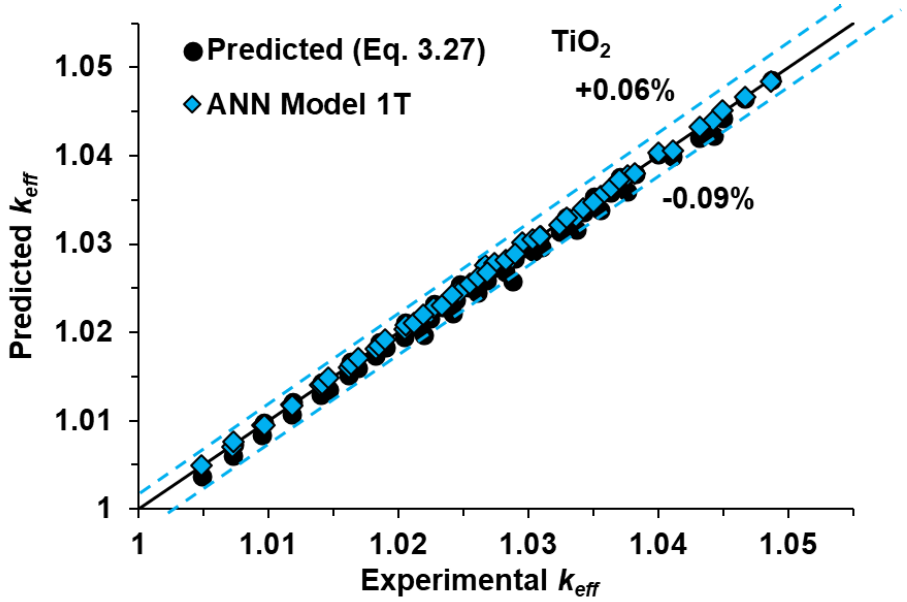

Fig. 4.34 Correlation prediction vs. ANN model 1T prediction of effective thermal conductivity with experimental data for TiO_2 nanofluid

Considering present experimental results and literature data

The ANN model presented previously is especially for individual materials using experimental results from the present study only, considering non-dimensional temperature and concentration as input variables. The proposed Eq. (3.28) presents the generalized regression model for each material by combining present work and the literature data to predict the effective thermal conductivity by considering additional variables such as nanoparticle size and different ratios of EG:water mixtures for the Al_2O_3 and TiO_2. The R^2 values for this equation for both materials are less than 0.85 (Table 4.4), indicating scope for a better model. Hence, ANN modelling was carried out by combining the results of the present study with literature data, as mentioned in Table 3.13 as Model 2T in Chapter 3.

The results for different configurations implemented to determine the best neural network structure for predicting the effective thermal conductivity for each material are shown in Tables 4.9 and 4.10. A single hidden layer with neurons 5, 7, 9, 10, 12, 15, 17, 19, 20, 22 and 25 was used to find the best results for TANSIG and PURELIN functions at the output layer for Al_2O_3 and TiO_2 nanofluids. The best result was obtained for the TANSIG-PURELIN (hidden layer-outlet layer) with 22 neurons in the hidden layer, which showed the highest R^2 value and lowest RMSE value (Table 4.9) for Al_2O_3 nanofluid. Similarly, for the TiO_2 nanofluid, the best neural structure obtained was with the same combination of functions as that of Al_2O_3 nanofluid with 12 neurons in the hidden layer. The corresponding optimized ANN results are shown in Figs. 4.35 and 4.36 for Al_2O_3 and TiO_2 nanofluids, respectively.

Figs. 4.37 and 4.38 show a comparison of the predicted effective thermal conductivity of EG:water - Al_2O_3 and TiO_2 nanofluid from developed correlation (Eq. 3.28 - four input variables) and Model 2T (four input variables) respectively. From these two figures, it can be observed that most of the data points of the ANN model (best results from Table 4.9 and 4.10) are very close to the fit line. This shows the better accuracy of neural network model to predict the effective thermal conductivity with multi input variables accurately compared to the regression model.

Table 4.9 ANN modelling results for effective thermal conductivity of EG:water - Al_2O_3 nanofluid for Model 2T

Hidden layer function	Output layer function	Neurons in hidden layer	Coefficient of determination (R^2)				RMSE (All data)
			Training	Validation	Test	All	
TANSIG	PURELIN	5	0.9922	0.9922	0.9944	0.9926	0.00571
TANSIG	PURELIN	7	0.9954	0.9938	0.9930	0.9948	0.00473
TANSIG	PURELIN	9	0.9966	0.9920	0.9920	0.9952	0.00457
TANSIG	PURELIN	10	0.9916	0.9940	0.9960	0.9926	0.00563
TANSIG	PURELIN	12	0.9922	0.9962	0.9932	0.9930	0.00551
TANSIG	PURELIN	15	0.9954	0.9952	0.9914	0.9950	0.00467
TANSIG	PURELIN	17	0.9952	0.9946	0.9960	0.9952	0.00454
TANSIG	PURELIN	19	0.9958	0.9970	0.9936	0.9954	0.00445
TANSIG	PURELIN	20	0.9962	0.9964	0.9976	0.9964	0.00389
TANSIG	**PURELIN**	**22**	**0.9972**	**0.9970**	**0.9968**	**0.9970**	**0.00355**
TANSIG	PURELIN	25	0.9948	0.9958	0.9980	0.9956	0.00442
TANSIG	TANSIG	5	0.9898	0.9886	0.9809	0.9886	0.00710
TANSIG	TANSIG	7	0.9924	0.9946	0.9934	0.9928	0.00556
TANSIG	TANSIG	9	0.9950	0.9962	0.9926	0.9948	0.00478
TANSIG	TANSIG	10	0.9960	0.9940	0.9845	0.9938	0.00518
TANSIG	TANSIG	12	0.9974	0.9930	0.9855	0.9948	0.00475
TANSIG	TANSIG	15	0.9982	0.9956	0.9803	0.9950	0.00463
TANSIG	TANSIG	17	0.9982	0.9916	0.9906	0.9962	0.00407
TANSIG	TANSIG	19	0.9980	0.9910	0.9914	0.9958	0.00422
TANSIG	TANSIG	20	0.9990	0.9896	0.9884	0.9954	0.00448
TANSIG	TANSIG	22	0.9972	0.9908	0.9900	0.9950	0.00466
TANSIG	TANSIG	25	0.9970	0.9952	0.9886	0.9958	0.00422

Bold indicates the best result

Table 4.10 ANN modelling results for effective thermal conductivity of EG:water – TiO_2 nanofluid for Model 2T

Hidden layer function	Output layer function	Neurons in hidden layer	Coefficient of determination (R^2)				RMSE (All data)
			Training	Validation	Test	All	
TANSIG	PURELIN	5	0.9868	0.9685	0.9675	0.9819	0.00562
TANSIG	PURELIN	7	0.9797	0.9829	0.9916	0.9825	0.00551
TANSIG	PURELIN	9	0.9821	0.9930	0.9332	0.9831	0.00547
TANSIG	PURELIN	10	0.9835	0.9637	0.9843	0.9789	0.00607
TANSIG	**PURELIN**	**12**	**0.9853**	**0.9843**	**0.9817**	**0.9849**	**0.00513**
TANSIG	PURELIN	15	0.9726	0.9952	0.9894	0.9799	0.00591
TANSIG	PURELIN	17	0.9789	0.9874	0.9892	0.9825	0.00552
TANSIG	PURELIN	19	0.9777	0.9765	0.9914	0.9803	0.00588
TANSIG	PURELIN	20	0.9803	0.9702	0.9954	0.9817	0.00568
TANSIG	PURELIN	22	0.9823	0.9862	0.9754	0.9823	0.00558
TANSIG	PURELIN	25	0.9837	0.9797	0.9720	0.9811	0.00574
TANSIG	TANSIG	5	0.9811	0.9866	0.9827	0.9827	0.00551
TANSIG	TANSIG	7	0.9815	0.9910	0.9827	0.9825	0.00555
TANSIG	TANSIG	9	0.9771	0.9934	0.9862	0.9813	0.00573
TANSIG	TANSIG	10	0.9769	0.9918	0.9545	0.9811	0.00575
TANSIG	TANSIG	12	0.9847	0.9532	0.9813	0.9827	0.00553
TANSIG	TANSIG	15	0.9763	0.9982	0.9938	0.9821	0.00561
TANSIG	TANSIG	17	0.9855	0.9718	0.9823	0.9833	0.0054
TANSIG	TANSIG	19	0.9738	0.9938	0.9884	0.9815	0.00569
TANSIG	TANSIG	20	0.9795	0.9884	0.9821	0.9805	0.00585
TANSIG	TANSIG	22	0.9805	0.9817	0.9880	0.9817	0.00567
TANSIG	TANSIG	25	0.9868	0.9779	0.9720	0.9837	0.00533

Bold indicates the best result

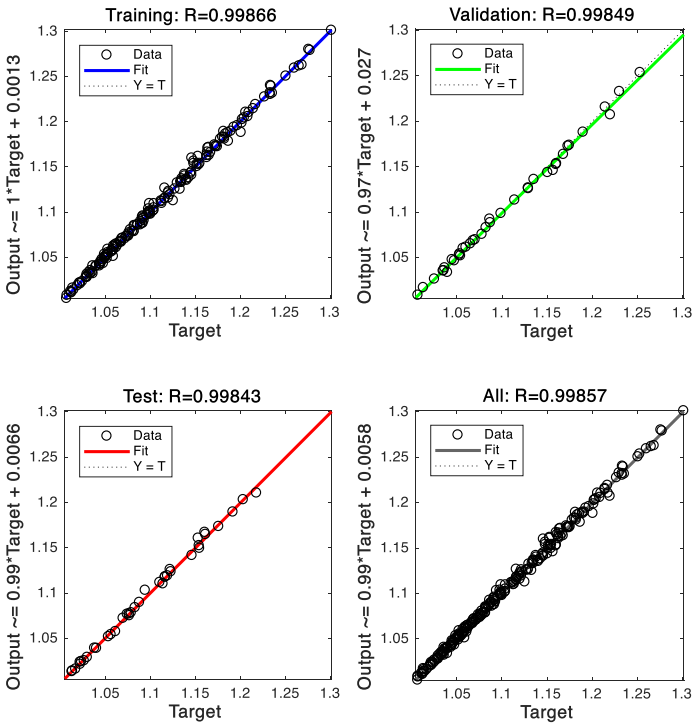

Fig. 4.35 Optimized ANN model 2T results for effective thermal conductivity of Al_2O_3 nanofluids

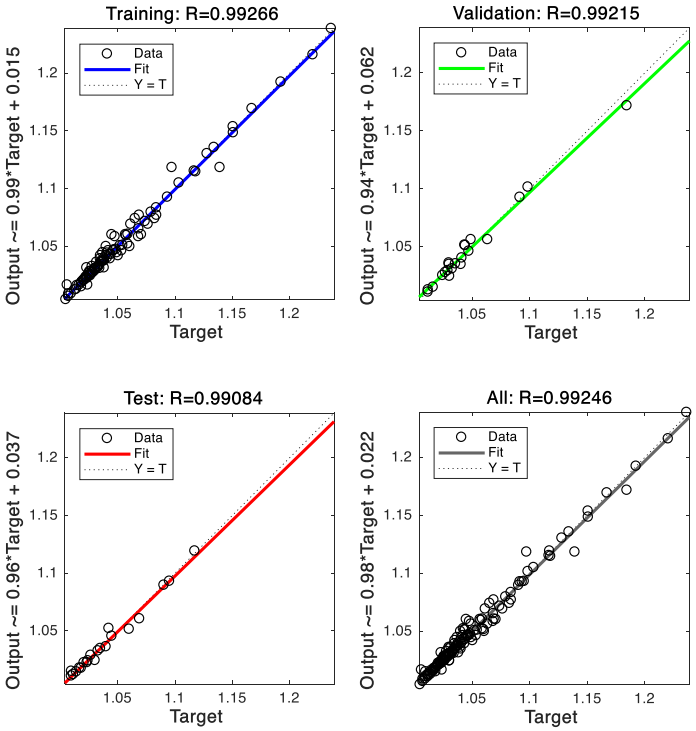

Fig. 4.36 Optimized ANN model 2T results for effective thermal conductivity of TiO_2 nanofluids

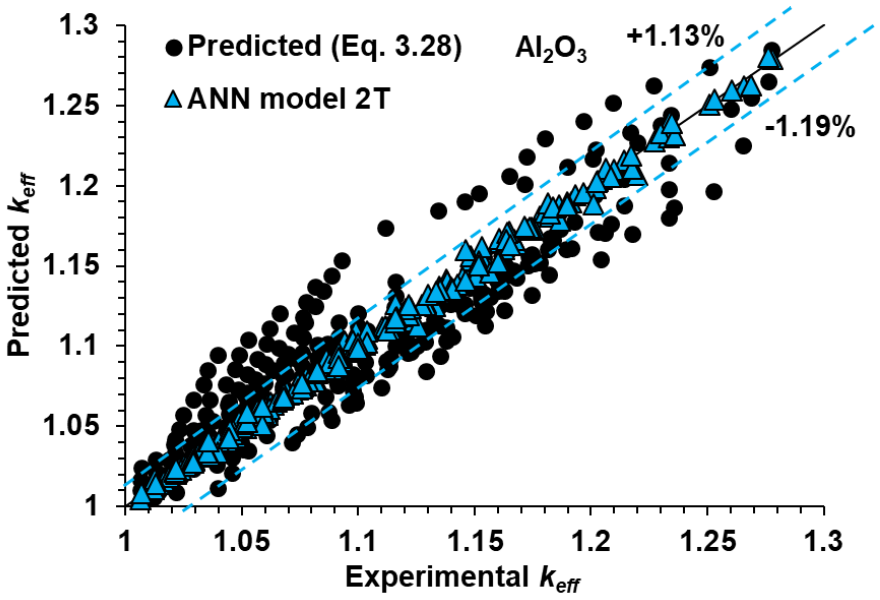

Fig. 4.37 Comparison of correlation prediction and best ANN model 2T prediction of effective thermal conductivity for Al_2O_3 nanofluid

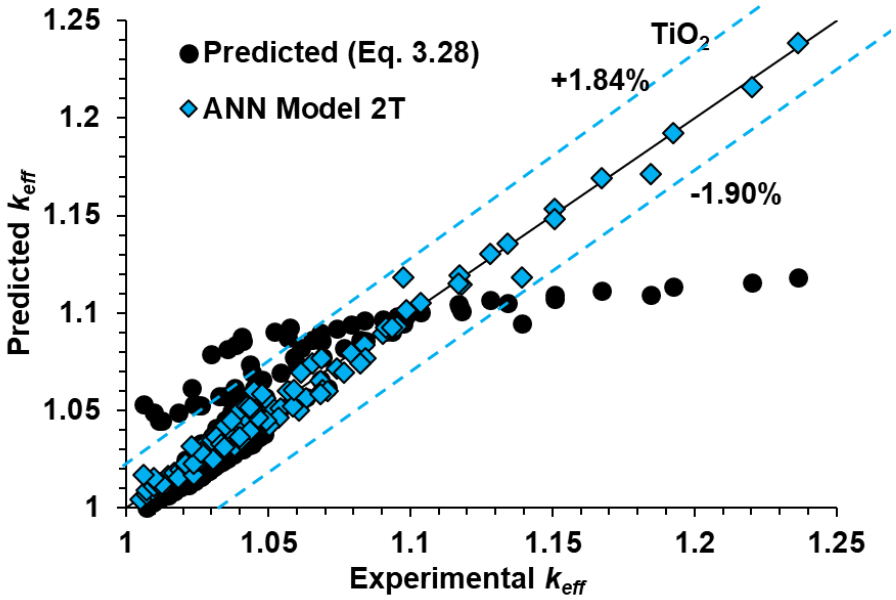

Fig. 4.38 Comparison of correlation prediction and best ANN model 2T prediction of effective thermal conductivity for TiO_2 nanofluid

4.3.1.2 Relative viscosity

As seen from the correlations developed for relative viscosity, the prediction accuracy (in terms of R^2 value) of EG:water nanofluid in the case of the two input variables (Eq. 3.29) is less than 0.95. Furthermore, the R^2 value was found to be reduced (< 0.82) for generalized correlation (Eq. 3.30), indicating the scope for a better model.

Considering present experimental results

Model 1V (Table 3.13) was implemented similar to that of the previous model (effective thermal conductivity), considering the two inputs and one output variable as described earlier (Materials and Methods). To obtain the best model in terms of getting better prediction of output data, the number of neurons in the hidden layer was varied, similar to the effective thermal conductivity model. The neurons and transfer functions were used similar to those of the effective thermal conductivity model. Tables 4.11 and 4.12 show the variation of R^2 and RMSE values for relative viscosity data during training, testing, validation and all data for EG:water - Al_2O_3 and TiO_2 nanofluids, respectively. The best ANN result for Al_2O_3 was found to be 10 neurons with TANSIG function in both hidden and output layers. A similar approach was implemented in the case of TiO_2 nanofluid and the best results were obtained with 10 neurons in the hidden layer (TANSIG) with a PURELIN activation function in the output layer. The corresponding model results for the two nanofluids are shown in Figs. 4.39 and 4.40 respectively. For the optimized model, RMSE values obtained are 0.001697 and 0.002654 for Al_2O_3 and TiO_2 nanofluids respectively. This also confirms the accuracy of the model with the lowest RMSE value compared to other models having a different configuration of a neural network (Table 4.11 and 4.12). Furthermore, Figs. 4.41 and 4.42 show the comparison of best model (Model 1V) with the Eq. (3.29) for Al_2O_3 and TiO_2 nanofluids, respectively. These figures show that both the regression model and the ANN model perform well with two input variables. However, the ANN model shows better prediction than Eq. (3.29).

Table 4.11 ANN modelling results for relative viscosity of EG:water - Al_2O_3 nanofluid for Model 1V

Hidden layer function	Output layer function	Neurons in Hidden layer	Coefficient of determination (R^2)				RMSE (All data)
			Training	Validation	Test	All	
TANSIG	PURELIN	5	0.9938	0.9976	0.9968	0.9948	0.002196
TANSIG	PURELIN	7	0.9944	0.9986	0.9974	0.9956	0.002034
TANSIG	PURELIN	9	0.9922	0.9994	0.9994	0.9948	0.002196
TANSIG	PURELIN	10	0.9948	0.9962	0.9992	0.9954	0.002032
TANSIG	TANSIG	5	0.9966	0.9752	0.9988	0.9942	0.002310
TANSIG	TANSIG	7	0.9982	0.9994	0.9732	0.9942	0.002326
TANSIG	TANSIG	9	0.9970	0.9932	0.9992	0.9968	0.001709
TANSIG	**TANSIG**	**10**	**0.9976**	**0.9994**	**0.9930**	**0.9968**	**0.001697**

Bold indicates the best result

Table 4.12 ANN modelling results for relative viscosity of EG:water-TiO_2 nanofluid for Model 1V

Hidden layer function	Output layer function	Neurons in Hidden layer	Coefficient of determination (R^2)				RMSE
			Training	Validation	Test	All	
TANSIG	PURELIN	5	0.9926	0.9970	0.9781	0.9920	0.003200
TANSIG	PURELIN	7	0.9978	0.9516	0.9984	0.9922	0.003149
TANSIG	PURELIN	9	0.9936	0.9986	0.9956	0.9944	0.002656
TANSIG	**PURELIN**	**10**	**0.9932**	**0.9992**	**0.9946**	**0.9944**	**0.002654**
TANSIG	TANSIG	5	0.9886	0.9970	0.9968	0.9908	0.003434
TANSIG	TANSIG	7	0.9944	0.9988	0.9912	0.9944	0.002656
TANSIG	TANSIG	9	0.9892	0.9992	0.9992	0.9926	0.003065
TANSIG	TANSIG	10	0.9992	0.9992	0.9563	0.9932	0.00293

Bold indicates the best result

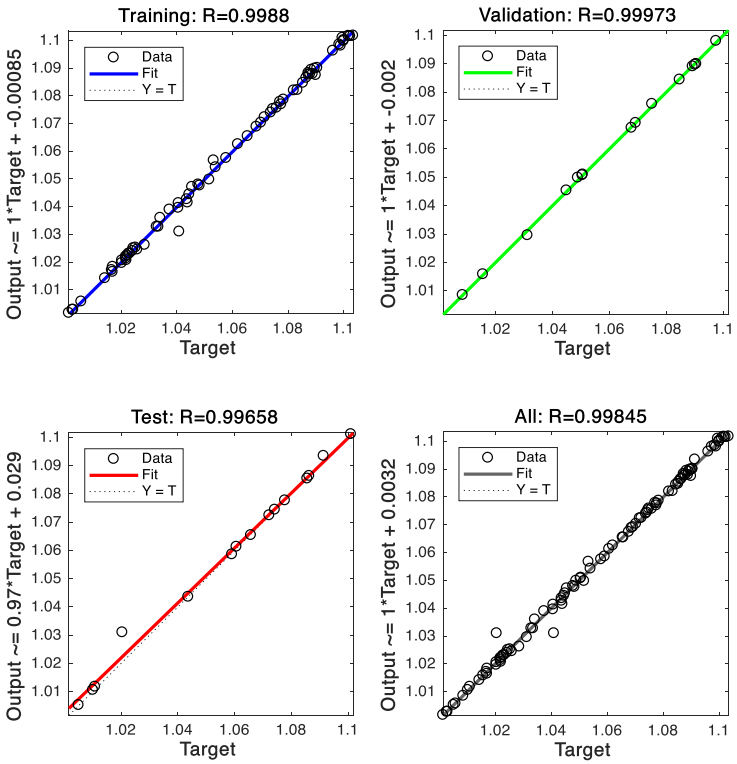

Fig. 4.39 Optimized ANN model 1V results for relative viscosity of Al_2O_3 nanofluids

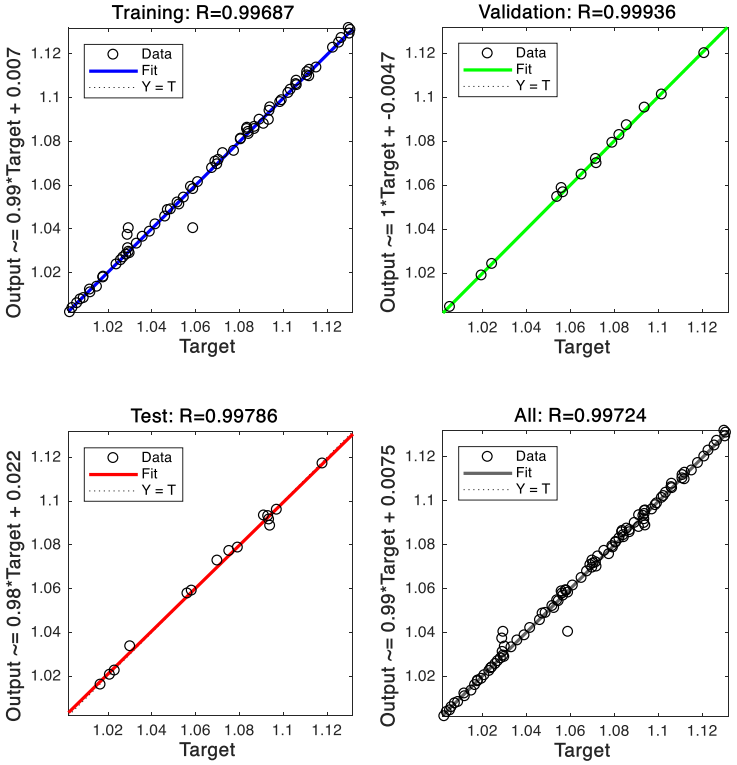

Fig. 4.40 Optimized ANN model 1V results for relative viscosity of TiO_2 nanofluids

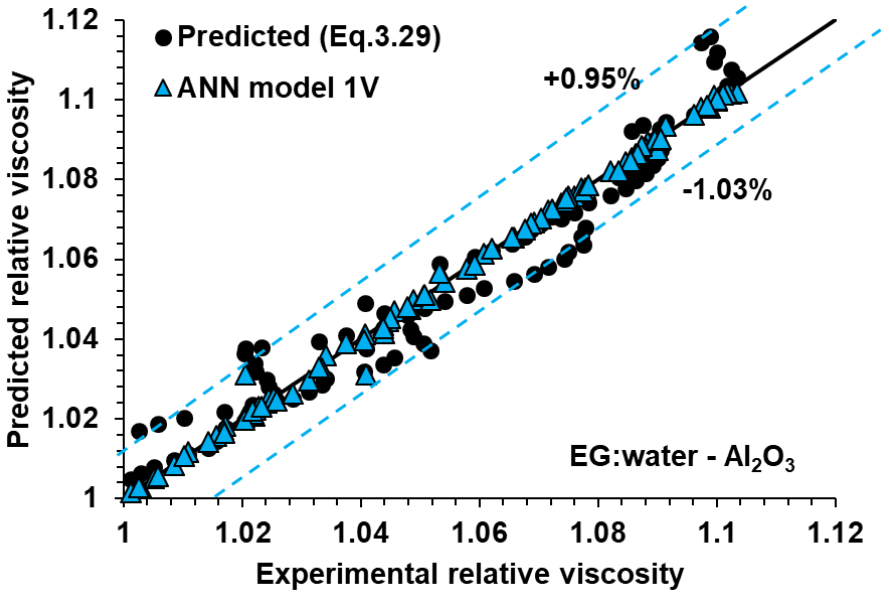

Fig. 4.41 Comparison of correlation prediction and best ANN model 1V prediction of relative viscosity for Al_2O_3 nanofluid

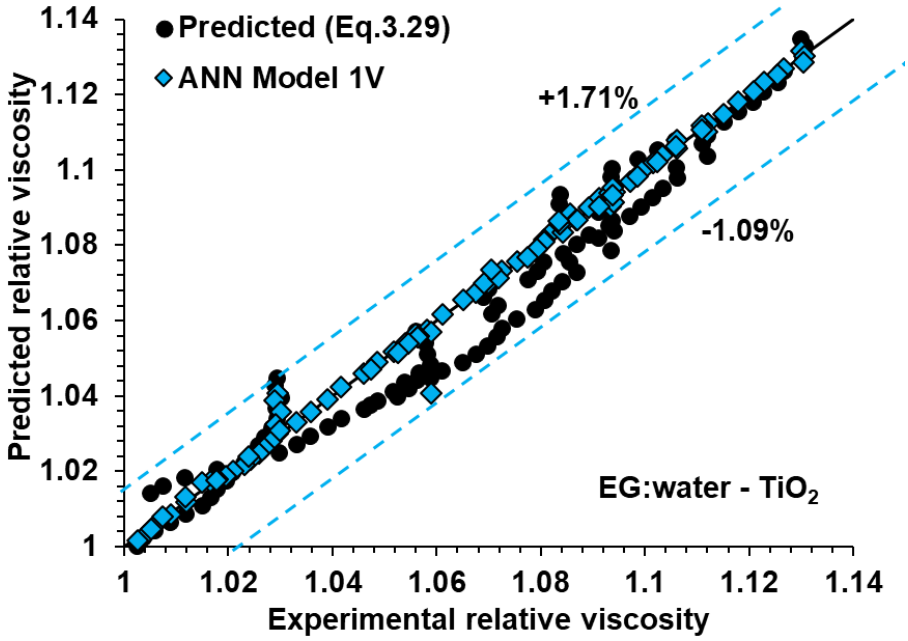

Fig. 4.42 Comparison of correlation prediction and best ANN model 1V prediction of relative viscosity for TiO_2 nanofluids

Considering present experimental results and literature data

ANN modelling was performed for Model 2V (Table 3.13) for the Al_2O_3 and TiO_2 nanofluids in a similar way as Model 1V. Model 2V was developed with combining experimental results from this study and literature data to model relative viscosity with multiple input parameters (four input variables). Tables 4.13 and 4.14 show the corresponding values of R^2 and RMSE values for a variable number of neurons in the hidden layer for both nanofluids for PURELIN and TANSIG activation functions at the output layer (training, validation, testing, and all data). The optimized ANN structure was found to have 25 neurons in a hidden layer with a TANSIG activation function at the output layer for Al_2O_3 nanofluids. On the other hand, the best results were obtained for TiO_2 nanofluids with 22 neurons in the hidden layer and a PURELIN function in the hidden layer. The corresponding results obtained for the optimized model from the ANN structure for considered literature results and experimental results of present work (Model 2V) of Al_2O_3 and TiO_2 nanofluids are shown in Fig. 4.43 and 4.44 respectively.

Figs. 4.45 and 4.46 depict the comparison of the prediction from the correlation (Eq. 3.30) of relative viscosity and the ANN model obtained from Model 2V for EG:water - Al_2O_3 and TiO_2 nanofluids, respectively. As can be seen from these figures, the majority of the data predicted by the ANN model are very close to the fit line when compared to Eq. (3.30). From Tables 4.13 and 4.14, it is evident that the least values of RMSE were found in the case of the ANN model compared to the Eq. (3.30) (Table 4.6) for corresponding nanofluids. This shows the superiority of ANN model for better prediction of output with multiple input variables.

Table 4.13 ANN modelling results for EG:water-Al_2O_3 nanofluid for Model 2V

Hidden layer function	Output layer function	Neurons in hidden layer	Coefficient of determination (R^2)				RMSE
			Training	Validation	Test	All	
TANSIG	PURELIN	5	0.9624	0.9688	0.9452	0.9582	0.13866
TANSIG	PURELIN	7	0.9592	0.9567	0.9655	0.9571	0.13983
TANSIG	PURELIN	9	0.9777	0.9669	0.9825	0.9767	0.10273
TANSIG	PURELIN	10	0.9769	0.9940	0.9815	0.9795	0.09671
TANSIG	PURELIN	12	0.9763	0.9813	0.9872	0.9787	0.09883
TANSIG	PURELIN	15	0.9742	0.9868	0.9847	0.9771	0.10252
TANSIG	PURELIN	17	0.9884	0.9825	0.9916	0.9880	0.07401
TANSIG	PURELIN	19	0.9914	0.9942	0.9898	0.9902	0.06648
TANSIG	PURELIN	20	0.9920	0.9845	0.9902	0.9906	0.06523
TANSIG	PURELIN	22	0.9910	0.9886	0.9950	0.9912	0.06321
TANSIG	PURELIN	25	0.9746	0.9880	0.9744	0.9765	0.10483
TANSIG	TANSIG	5	0.9543	0.9366	0.9726	0.9526	0.14732
TANSIG	TANSIG	7	0.9746	0.9845	0.9765	0.9679	0.12087
TANSIG	TANSIG	9	0.9878	0.9645	0.9686	0.9807	0.09445
TANSIG	TANSIG	10	0.9724	0.9807	0.9827	0.9752	0.10738
TANSIG	TANSIG	12	0.9754	0.9829	0.9783	0.9756	0.10583
TANSIG	TANSIG	15	0.9653	0.9712	0.9839	0.9706	0.11668
TANSIG	TANSIG	17	0.9829	0.9870	0.9894	0.9843	0.08482
TANSIG	TANSIG	19	0.9688	0.9767	0.9675	0.9675	0.12144
TANSIG	TANSIG	20	0.9629	0.9968	0.9974	0.9732	0.11006
TANSIG	TANSIG	22	0.9870	0.9950	0.9592	0.9829	0.08827
TANSIG	**TANSIG**	**25**	**0.9934**	**0.9972**	**0.9930**	**0.9936**	**0.05361**

Bold indicates the best result

Table 4.14 ANN modelling results for EG:water-TiO_2 nanofluid for Model 2V

Hidden layer function	Output layer function	Neuron in hidden layer	Coefficient of determination (R^2)				RMSE
			Training	Validation	Test	All	
TANSIG	PURELIN	5	0.8208	0.9857	0.9870	0.8666	0.0193097
TANSIG	PURELIN	7	0.9954	0.9874	0.9465	0.9896	0.0053611
TANSIG	PURELIN	9	0.9783	0.9837	0.9934	0.9813	0.0071689
TANSIG	PURELIN	10	0.9908	0.9916	0.9795	0.9892	0.0054117
TANSIG	PURELIN	12	0.9819	0.9862	0.9920	0.9835	0.0067536
TANSIG	PURELIN	15	0.9944	0.9980	0.9982	0.9956	0.003495
TANSIG	PURELIN	17	0.9942	0.9938	0.9902	0.9928	0.0044307
TANSIG	PURELIN	19	0.9884	0.9952	0.9882	0.9888	0.005533
TANSIG	PURELIN	20	0.9876	0.9839	0.9928	0.9855	0.0063539
TANSIG	**PURELIN**	**22**	**0.9974**	**0.9974**	**0.9956**	**0.9972**	**0.0027981**
TANSIG	PURLIN	25	0.9886	0.9942	0.9651	0.9878	0.0057668
TANSIG	TANSIG	5	0.9827	0.9920	0.9914	0.9851	0.0064299
TANSIG	TANSIG	7	0.9726	0.9920	0.9748	0.9746	0.0083674
TANSIG	TANSIG	9	0.9872	0.9920	0.6705	0.9249	0.0146452
TANSIG	TANSIG	10	0.9942	0.9857	0.9214	0.9801	0.0074912
TANSIG	TANSIG	12	0.9825	0.9958	0.9890	0.9851	0.0064751
TANSIG	TANSIG	15	0.9859	0.9960	0.9829	0.9870	0.006018
TANSIG	TANSIG	17	0.9793	0.9801	0.9757	0.9785	0.0077416
TANSIG	TANSIG	19	0.9900	0.9948	0.9916	0.9908	0.005103
TANSIG	TANSIG	20	0.9910	0.9868	0.9926	0.9908	0.0050365
TANSIG	TANSIG	22	0.9849	0.9878	0.9930	0.9866	0.0062122
TANSIG	TANSIG	25	0.9926	0.9976	0.9908	0.9932	0.0043699

Bold indicates the best result

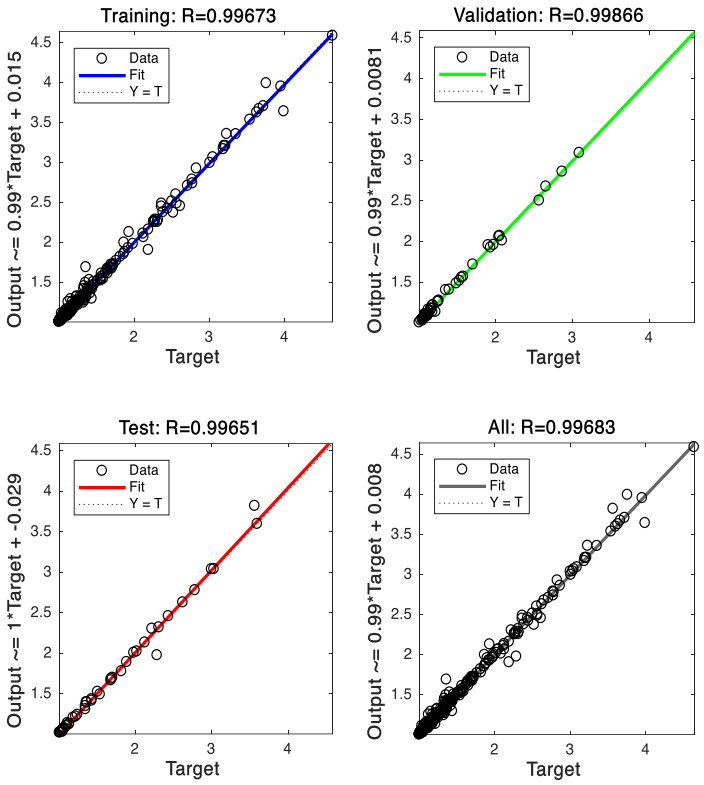

Fig. 4.43 Optimized ANN model 2V results for relative viscosity of Al_2O_3 nanofluids

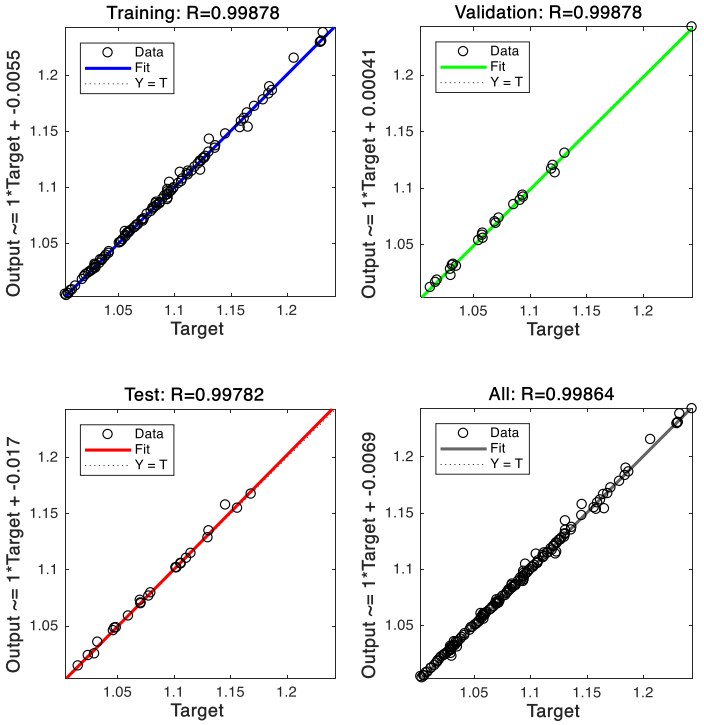

Fig. 4.44 Optimized ANN model 2V results for relative viscosity of TiO_2 nanofluids

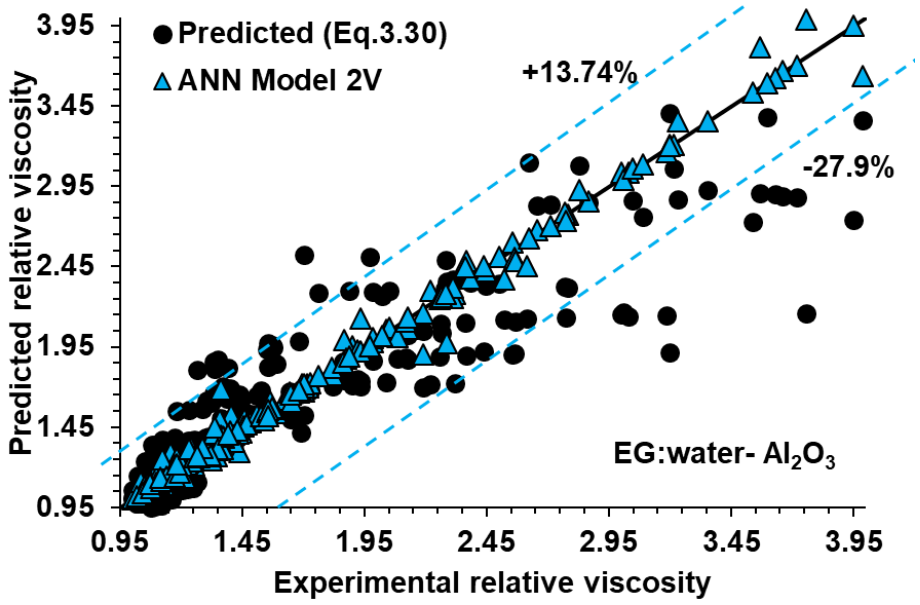

Fig. 4.45 Comparison of correlation prediction and best ANN model 2V prediction of relative viscosity for Al_2O_3 nanofluids

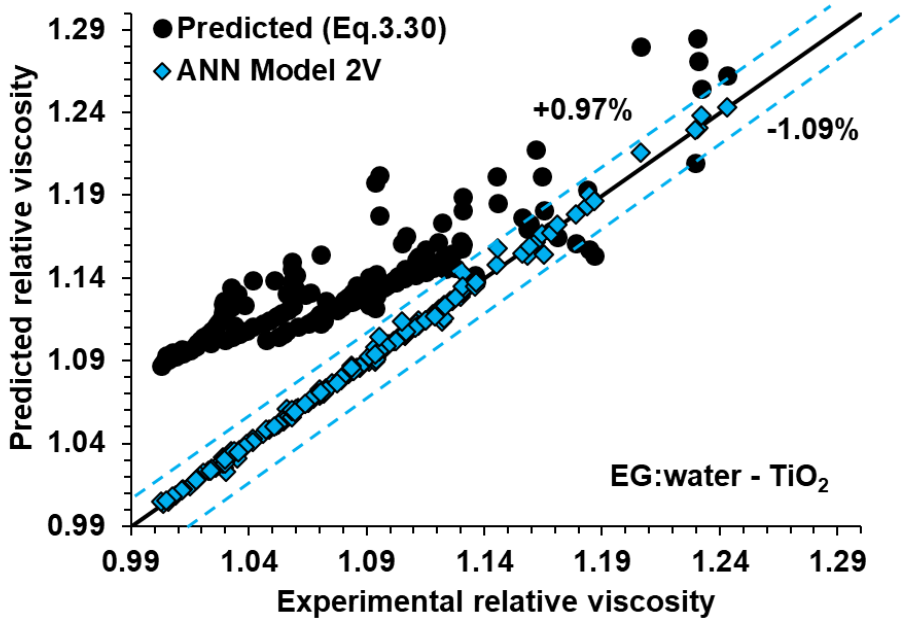

Fig. 4.46 Comparison of correlation prediction and best ANN model 2V prediction of relative viscosity for TiO_2 nanofluids

4.3.2 ANFIS modelling

4.3.2.1 Effective thermal conductivity

Considering present experimental results

ANFIS modelling of effective thermal conductivity was performed for EG:water-Al_2O_3 and TiO_2 nanofluids separately with two input parameters as mentioned in the case of ANN modelling previously (Table 3.13, input parameters as described in Model 1T). The FIS was developed for individual nanofluids with membership functions (input and output) to predict the output (k_{eff}). Table 4.15 shows statistical parameters (R^2 and RMSE) obtained from ANFIS modelling for training, testing and entire data for the two nanofluids. The R^2 value (0.99) is an indicator of the strong correlation between the predictions from the ANFIS model and the experimental results, not only for the training data but also for the testing data. Table 4.15 indicates that both linear and constant functions have performed well in predicting the effective thermal conductivity data. The best R^2 and least RMSE values are obtained for the constant output MF of the ANFIS structure. The corresponding structure is shown in Fig. 4.47. The best model prediction data obtained from this ANFIS (two input parameters) for EG:water nanofluid (Al_2O_3 and TiO_2) has excellent agreement with experimental data as shown in Fig. 4.48 and Fig. 4.49.

Table 4.15 ANFIS modelling results for effective thermal conductivity of EG:water nanofluid for two input parameter

Nanofluid	Output MF	Training	Testing	All data	RMSE (All data)
		R^2			
EG:water-Al_2O_3	**Constant**	**0.9960**	**0.9886**	**0.9961**	**0.00129**
EG:water-TiO_2		**0.9930**	**0.9774**	**0.9925**	**0.00093**
EG:water-Al_2O_3	Linear	0.9954	0.9708	0.9940	0.0016
EG:water-TiO_2		0.9982	0.8282	0.9736	0.001756

Bold indicates the best result

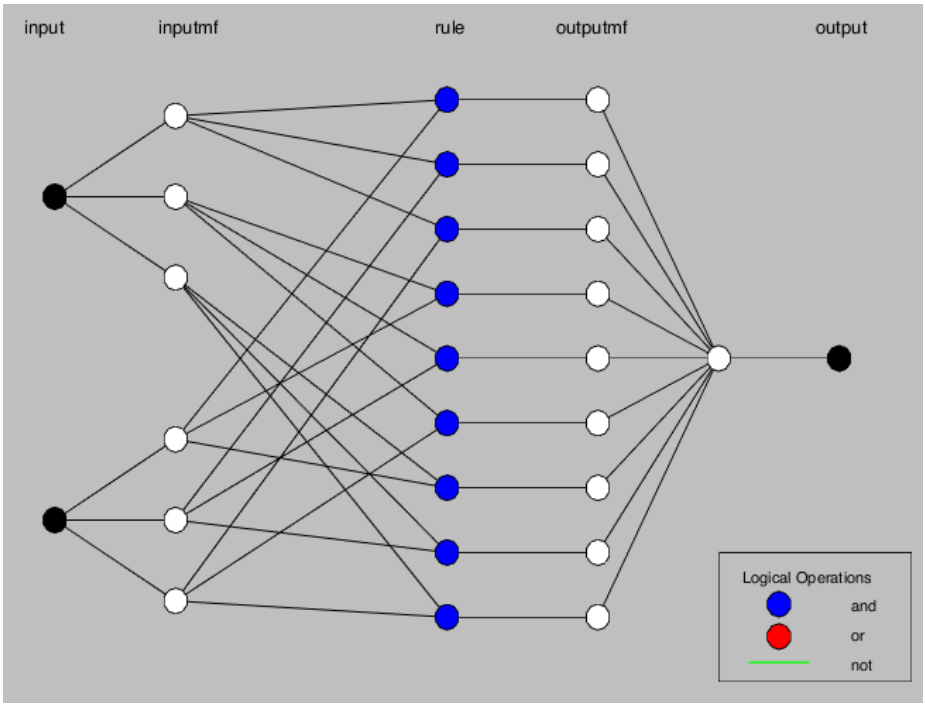

Fig. 4.47 ANFIS structure (two input) for effective thermal conductivity for EG:water - Al_2O_3/TiO_2 nanofluids

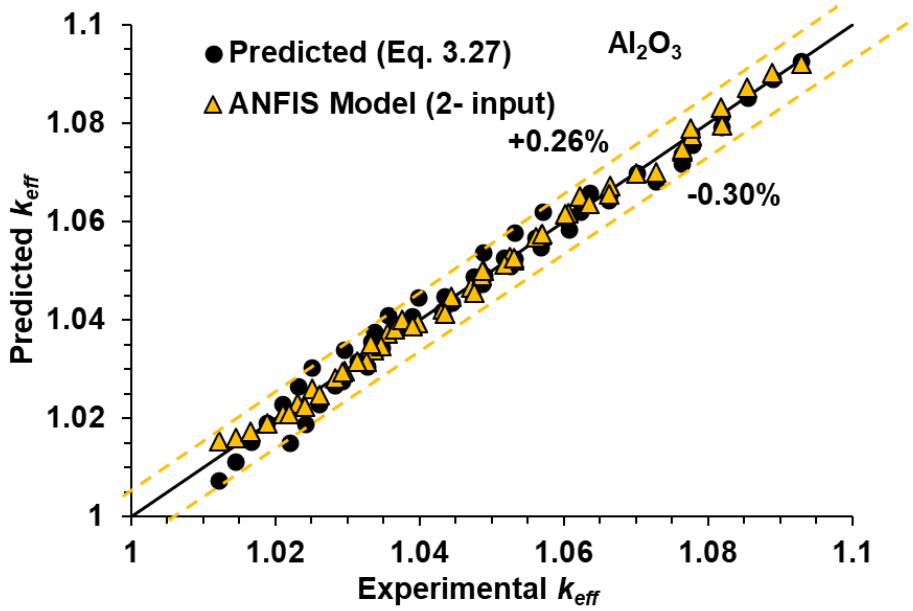

Fig. 4.48 Comparison of correlation prediction and ANFIS model (two input) prediction of effective thermal conductivity for EG:water - Al_2O_3 nanofluids

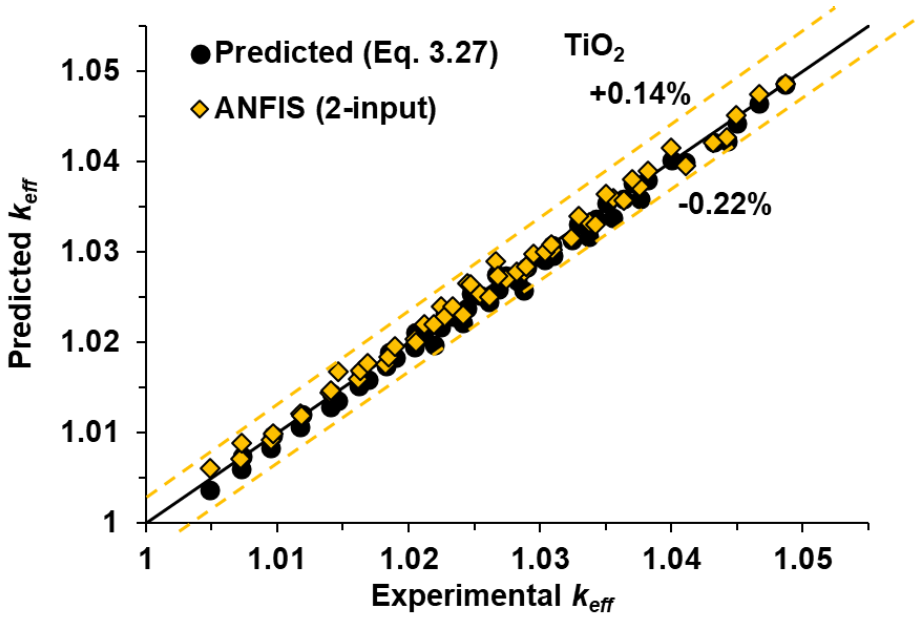

Fig. 4.49 Comparison of correlation prediction and ANFIS model (two input) prediction of effective thermal conductivity for EG:water –TiO_2 nanofluids

Considering present experimental results and literature data

The regression approach (Eq.3.28) to predict the effective thermal conductivity of nanofluids increases the complexity of the equation because of multiple input data (more than two variables). As a result, similar to ANN modelling, an intelligent approach, ANFIS modelling, was explored in this work to predict the effective thermal conductivity of nanofluids. Four input parameters ($1+\emptyset_w/100$, T_{nf}/T_{ref}, Vr,k_{np}/k_{bf})) involving input MF of Gaussian, constant and linear MF at output were used to model the data (training and testing) of nanofluids. Based on the R^2 and RMSE values, the optimised ANFIS model prediction result for Al_2O_3 nanofluids was obtained with a Gaussian MF at the input and a constant MF at the output (Table 4.16). For TiO_2 nanofluid, the optimized results were obtained with a Gaussian MF in the input and a linear MF in the output (Table 4.16). Fig. 4.50 depicts the corresponding ANFIS structure formed with membership functions. Other membership functions, such as trapezoidal, triangular, and generalized bell functions, produced higher RMSE values and were therefore not reported. Figs. 4.51 and 4.52 shows the comparision of correlation (Eq.3.28) and ANFIS model (four input) predictions of effective thermal conductivity for Al_2O_3 and TiO_2 nanofluids, respectively. These figures show that the majority of the data predicted by the ANFIS model is

very close to the fit line, demonstrating superiority in prediction compared to correlation (3.28) for both nanofluids.

Table 4.16 ANFIS modelling results for effective thermal conductivity of EG:water nanofluid for four input parameters

Nanofluid	Output MF	Training	Testing	All data	RMSE
		R^2			(All data)
EG:water-Al_2O_3	**Constant**	**0.9921**	**0.9944**	**0.9905**	**0.006431**
EG:water-TiO_2		0.9766	0.9829	0.9785	0.0061
EG:water-Al_2O_3	Linear	0.9978	0.9699	0.9879	0.007262
EG:water-TiO_2		**0.9819**	**0.9822**	**0.9821**	**0.005583**

Bold indicates the best result

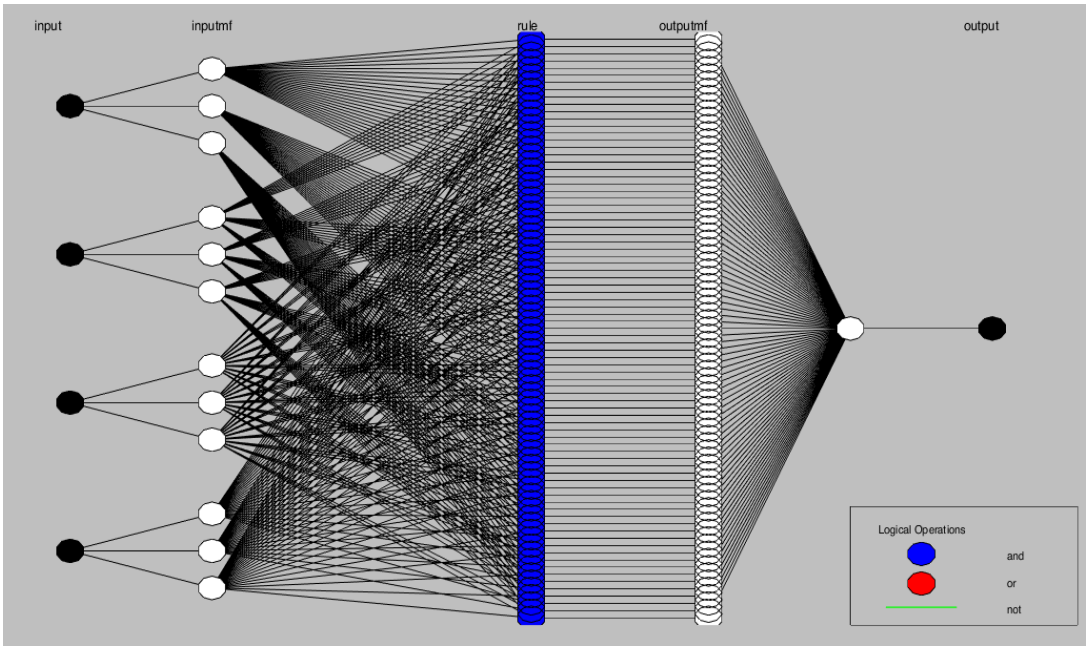

Fig. 4.50 ANFIS structure (four input) for effective thermal conductivity for EG:water – Al_2O_3/TiO_2 nanofluids

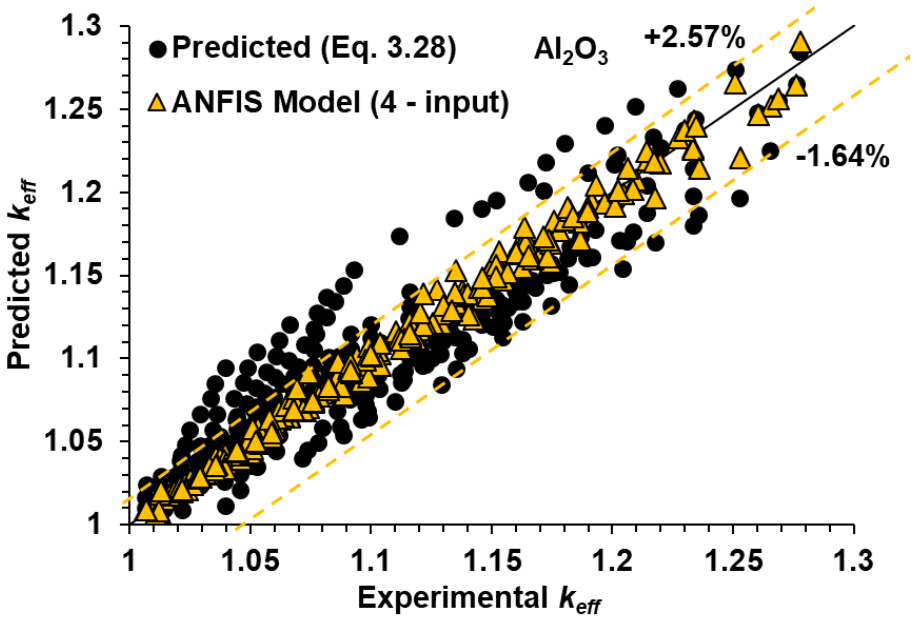

Fig. 4.51 Comparison of correlation prediction and ANFIS model (four input) prediction of effective thermal conductivity for EG:water –Al_2O_3 nanofluids

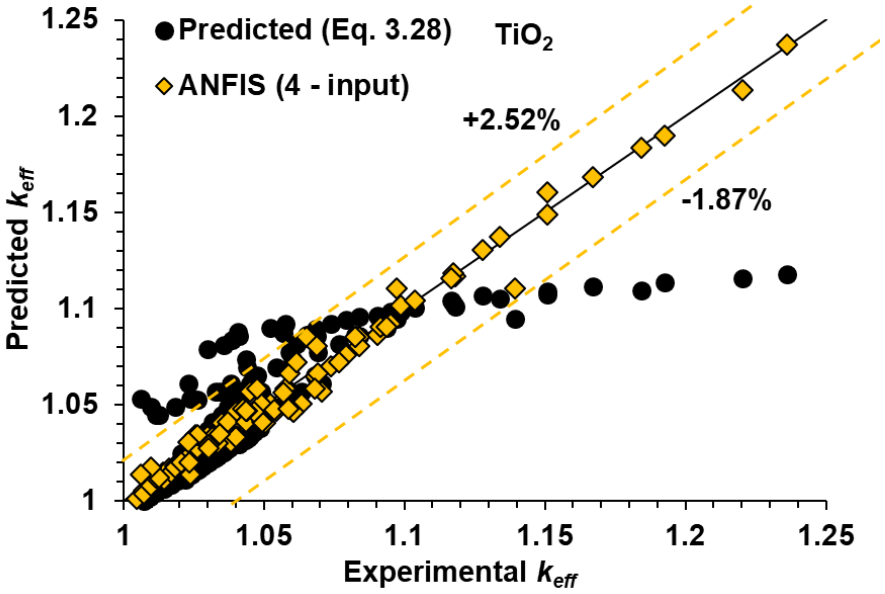

Fig. 4.52 Comparison of correlation prediction and ANFIS model (four input) prediction of effective thermal conductivity for EG:water –TiO_2 nanofluids

4.3.2.2 Relative viscosity

Considering present experimental results

ANFIS modelling of relative viscosity was performed for EG:water-Al_2O_3 and TiO_2 nanofluids separately with two input parameters as mentioned in the case of ANN modelling (volume concentration and temperature ratio). The FIS was formed using a similar method as that of effective thermal conductivity conditions for individual nanofluids with membership functions (input and output). Table 4.17 shows statistical parameters (R^2 and RMSE) obtained from ANFIS modelling for training, testing and entire data for both nanofluids. From this table, it is evident that the input and output MF obtained for best results were Gaussian function and linear functions respectively for both the nanofluids. The corresponding structure used in the model is shown in Fig. 4.53. The best results of ANFIS model prediction for EG:water nanofluid (Al_2O_3 and TiO_2) have indicated excellent agreement with experimental data as shown in Fig. 4.54 and Fig. 4.55.

Table 4.17 ANFIS modelling results for relative viscosity of EG:water nanofluid for two input variables

Nanofluid	Output MF	Training	Testing	All data	RMSE (All data)
		R^2			
EG:water-Al_2O_3	Constant	0.9791	0.9753	0.9792	0.004398
EG:water-TiO_2		0.9819	0.9779	0.9817	0.00482
EG:water-Al_2O_3	**Linear**	**0.9932**	**0.9746**	**0.9880**	**0.003336**
EG:water-TiO_2		**0.9923**	**0.9633**	**0.9836**	**0.004558**

Bold indicates the best result

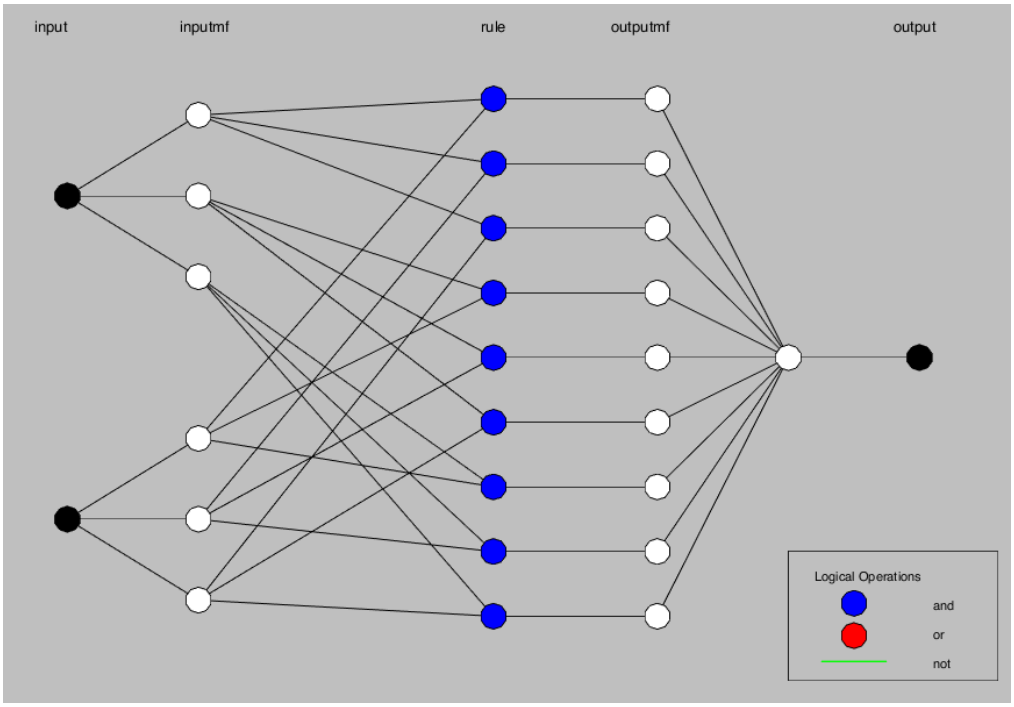

Fig. 4.53 ANFIS structure (two input) for relative viscosity for EG:water – Al_2O_3/TiO_2 nanofluids

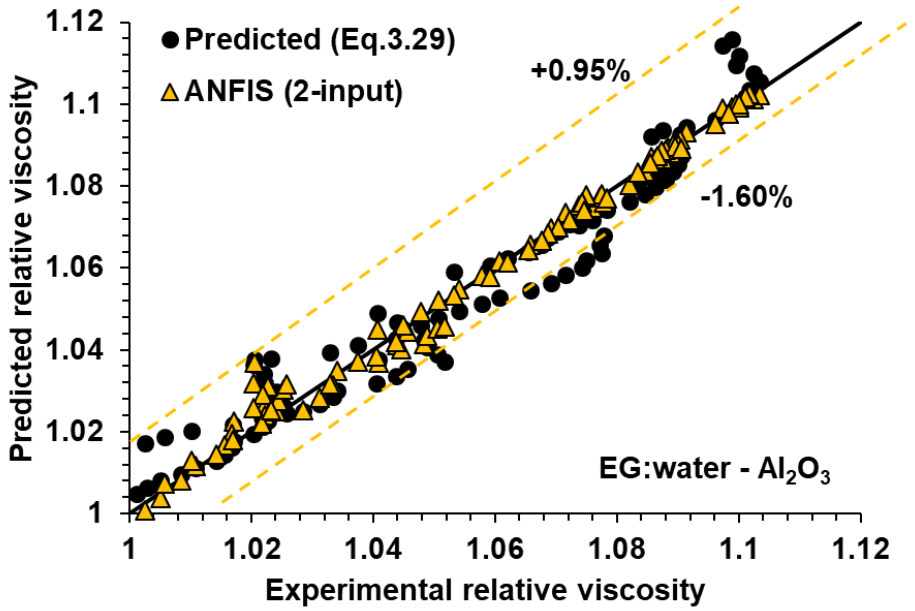

Fig. 4.54 Comparison of correlation prediction and ANFIS model (two input) prediction of relative viscosity for EG:water-Al_2O_3 nanofluids

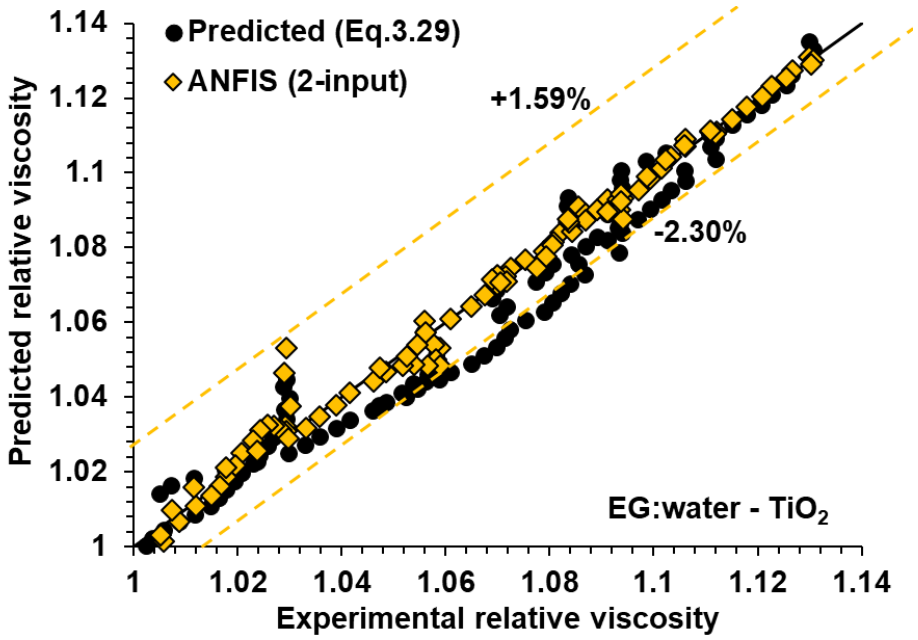

Fig. 4.55 Comparison of correlation prediction and ANFIS model (two input) prediction of relative viscosity for EG:water-TiO_2 nanofluids

Considering present experimental results and literature data

ANFIS modelling was carried out in this study to model the relative viscosity of nanofluids considering four input parameters. The structure of ANFIS was implemented with a Gaussian function in input. Constant and linear functions at output were used to model the data of nanofluids. Table 4.18 shows ANFIS modelling performance for two functions in training, testing and all data for Al_2O_3 and TiO_2 nanofluids. From Table 4.18, the optimized ANFIS prediction result was found at a constant MF in the output for both nanofluids, as evident from the comparison of R^2 and RMSE values of both functions. The corresponding ANFIS structure is shown in Fig. 4.56. Figs. 4.57 and 4.58 show the comparison of correlation prediction (Eq.3.30) and ANFIS model (four input) prediction of relative viscosity for Al_2O_3 and TiO_2 nanofluids respectively. It can be observed from these figures that most of the relative viscosity data predicted by the ANFIS model shows a better fit with experimental and literature results than the correlation (Eq. 3.30) results for both nanofluids.

Table 4.18 ANFIS modelling results for relative viscosity of EG:water nanofluid for four input parameter

Nanofluid	Output MF	Training	Testing	All data	RMSE (All data)
		R^2			
EG:water-Al_2O_3	**Constant**	**0.9959**	**0.9832**	**0.9552**	**0.1425**
EG:water-TiO_2		**0.9918**	**0.9746**	**0.9883**	**0.005678**
EG:water-Al_2O_3	Linear	0.9987	0.9675	0.9424	0.1618
EG:water-TiO_2		0.9941	0.660	0.9239	0.01449

Bold indicates the best result

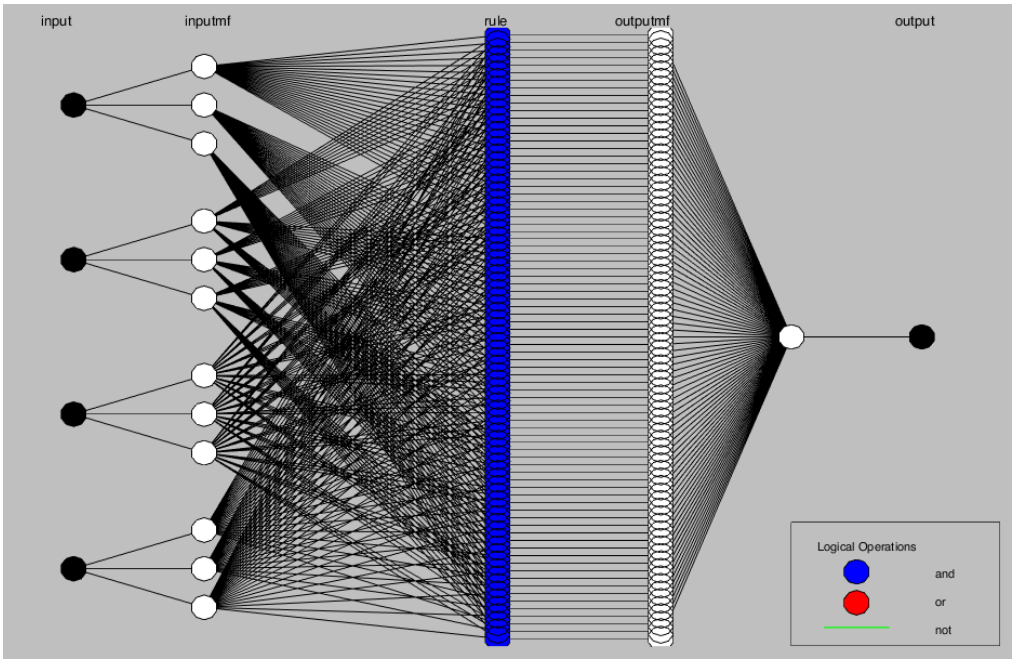

Fig. 4.56 ANFIS structure (four input) for relative viscosity for EG:water – Al_2O_3/TiO_2 nanofluids

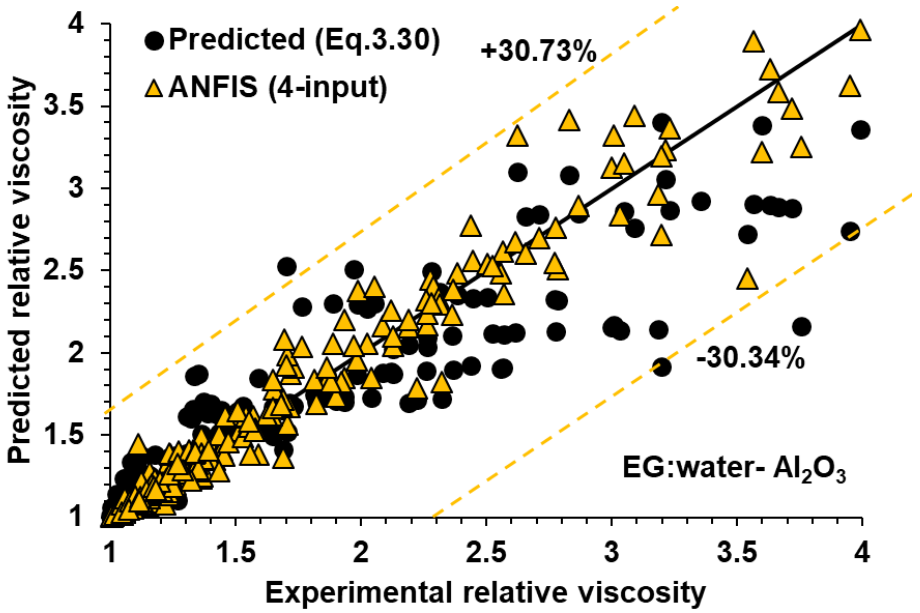

Fig. 4.57 Comparison of correlation prediction and ANFIS model (two input) prediction of relative viscosity for EG:water-Al_2O_3 nanofluids

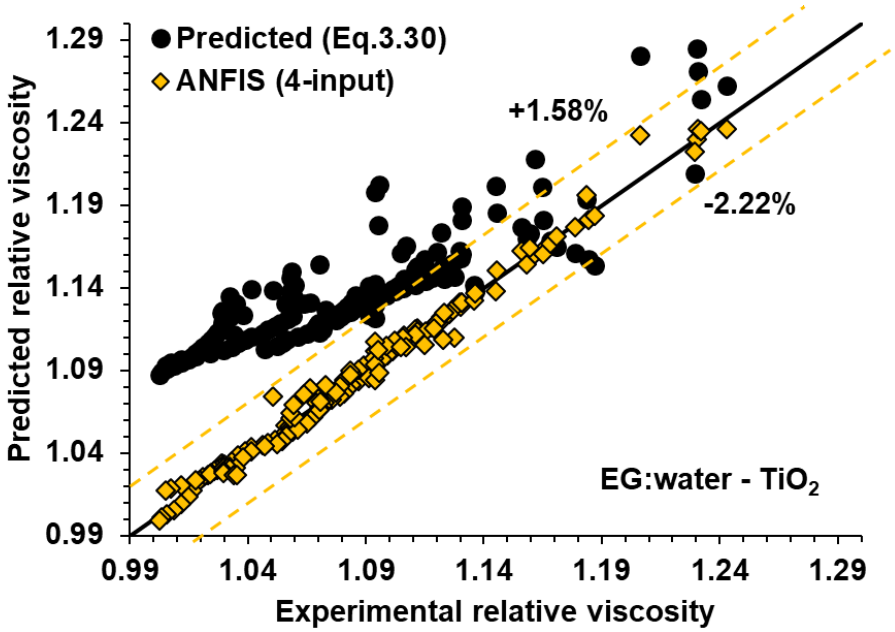

Fig. 4.58 Comparison of correlation prediction and ANFIS model (four input) prediction of relative viscosity for EG:water-TiO_2 nanofluids

4.3.3 Comparison of machine learning models with regression methods by statistical parameters

The closeness of predicted results to actual results can be measured using the mean absolute percentage error. The MAPE is one of the most commonly used performance indicators to measure prediction accuracy. The MAPE values of the regression models (Eq. 3.27 to 3.30), ANN model and ANFIS model obtained for effective thermal conductivity and relative viscosity of nanofluids are shown in Figs.4.59 and 4.60. It can be seen from Fig. 4.59 that the MAPE values for ANN model with two and four inputs are lower than the regression model as well as the ANFIS model. Similarly, for the relative viscosity of nanofluids, the best results were found with the ANN and ANFIS models, compared to the regression approach, as can be seen from Fig. 4.60. This demonstrates that the ANN and ANFIS models can be used as an accurate tool with more number of dependent parameters for forming a predefining structure for the prediction of effective thermal conductivity and relative viscosity of nanofluids. The details of statistical parameters for the optimized models for effective thermal conductivity and relative viscosity are shown in Tables 4.19 and 4.20 respectively. Margin of deviation (MOD) obtained for effective thermal conductivity and relative viscosity for all approaches are given in the Tables 4.21 and 4.22 respectivley.

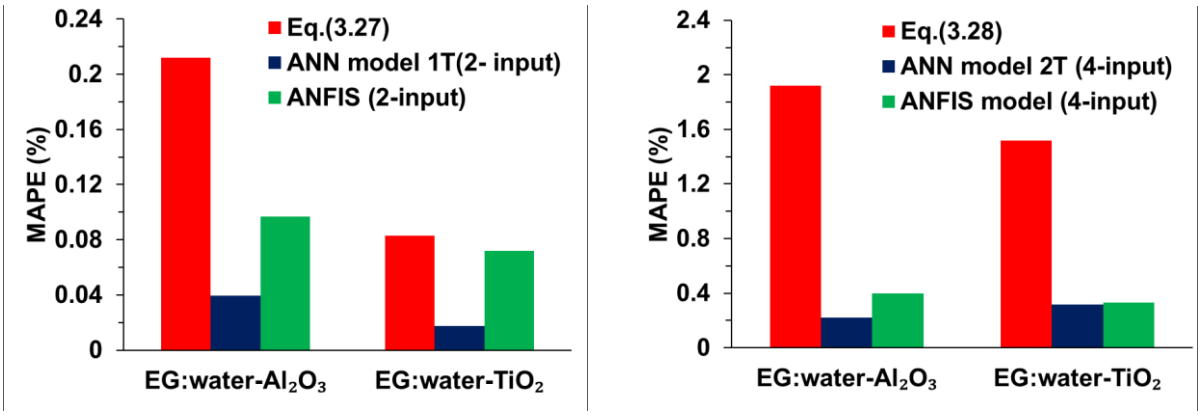

Fig. 4.59 MAPE variation for regression, ANN and ANFIS model for effective thermal conductivity (two input (left), four input (right)) of nanofluids

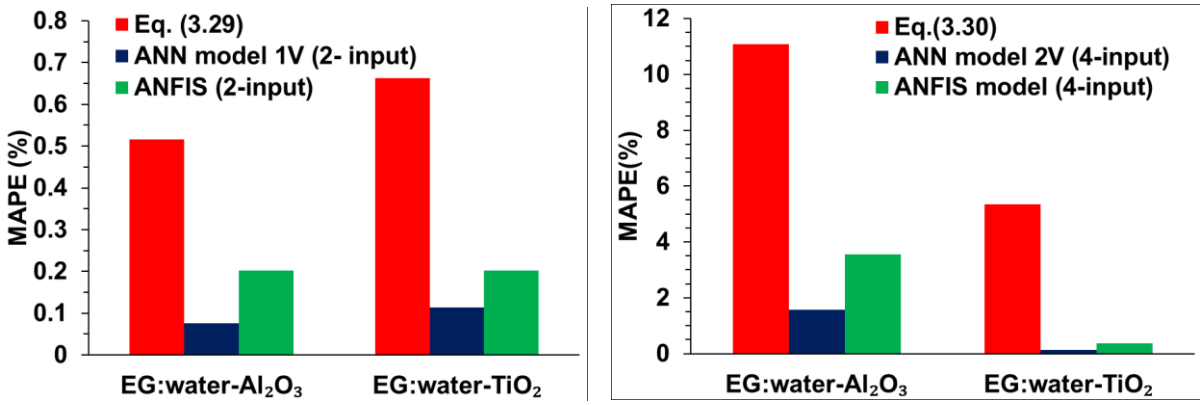

Fig. 4.60 MAPE variation for regression, ANN and ANFIS model for relative viscosity (two input (left), four input (right)) of nanofluids

Table 4.19 Statistical parameter for the optimized models effective thermal conductivity of nanofluids

Input parameter	Models	EG:water - Al_2O_3			EG:water - TiO_2		
		R^2	RMSE	MAPE	R^2	RMSE	MAPE
2-input	Eq.(3.27)	0.9813	0.00283	0.212	0.9905	0.00106	0.083
	ANN	0.9992	0.00058	0.039	0.9994	0.00025	0.017
	ANFIS	0.9961	0.00129	0.097	0.9925	0.00093	0.072
4-input	Eq.(3.28)	0.849	0.02560	1.921	0.6626	0.02445	1.520
	ANN	0.9970	0.00355	0.221	0.9849	0.00513	0.316
	ANFIS	0.9905	0.00643	0.396	0.9821	0.00558	0.329

Table 4.20 Statistical parameter for the optimized models relative viscosity of nanofluids

Input parameters	Models	Al_2O_3			TiO_2		
		R^2	RMSE	MAPE	R^2	RMSE	MAPE
2-input	Eq.(3.29)	0.944	0.00724	0.5154	0.9585	0.00848	0.6623
	ANN	0.9968	0.00169	0.0761	0.9944	0.00265	0.1142
	ANFIS	0.988	0.00334	0.2027	0.9837	0.00456	0.2596
4-input	Eq.(3.30)	0.829	0.29475	11.067	0.552	0.06658	5.3549
	ANN	0.9936	0.0536	1.570	0.9972	0.00279	0.1369
	ANFIS	0.9552	0.1452	3.547	0.9883	0.00568	0.3798

Table 4.21 Margin of deviation for the models to predict effective thermal conductivity of nanofluids

Input parameter	Models	Al_2O_3	TiO_2
2-input	Eq.(3.27)	-0.53% to 0.68%	-0.1% to 0.28%
	ANN	-0.15% to 0.13%	-0.09% to 0.06%
	ANFIS	-0.50% to 0.26%	-0.1% to 0.14%
4-input	Eq.(3.28)	-5.54% to 4.52%	-4.76% to 9.56%
	ANN	-1.19% to 1.13%	-1.90% to 1.84%
	ANFIS	-1.64% to 2.57%	-1.87% to 2.52%

Table 4.22 Margin of deviation for the models to predict relative viscosity of nanofluids

Input parameter	Models	Al_2O_3	TiO_2
2-input	Eq.(3.29)	-1.69% to 1.39%	-2.48% to 2.54%
	ANN	-1.031% to 0.95%	-1.09% to 1.71%
	ANFIS	-1.60% to 0.95%	-2.30% to 1.59%
4-input	Eq.(3.30)	-48.36% to 42%	-33.02%to 2.28%
	ANN	-27.9% to 13.74%	-1.09% to 0.97%
	ANFIS	-30.34% to 30.73%	-2.22% to 1.58%

4.4 Heat transfer characteristics

The heat transfer performance of the EG:water - Al_2O_3 and TiO_2 nanofluids in PHE was evaluated in terms of heat transfer rate, OHTC and CHTC. The study was carried out at a fixed flow rates of hot fluid (10 lpm and 12.5 lpm) and different flow rates of nanofluid (11-19 lpm). The corresponding range of Reynold number and Peclet nmber for the hot fluid and cold fluid (nanofluid) flow rates are given in the Table 4.23 and 4.24. Peclet number values were calculated using flow rate (velocity) and thermal diffusivity. At a given flow rate as the nanofluid concentration increases, the thermal diffusivity (representing thermal conductivity, density and specific heat) increases, leading to slight reduction in Peclet number value. The same can be observed in Fig. 4.61.

Table 4.23(a) Range of Reynolds number for base fluid

Inlet temperature	Hot fluid (water)		Base fluid (EG:water)	
	Flow rate, lpm	Reynolds number range	Flow rate, lpm	Reynolds number range
20 ºC	10	545-500	11-19	145-233
	12.5	674-632		168-265
10 ºC	10	500-460		125-200
	12.5	623-582		148-220
-5 ºC	10	460-420		97-136
	12.5	575-533		115-168

Table 4.23(b) Range of Reynolds number for weight concentration of nanofluid (0.2 to 2 wt.%)

Nanofluid	Inlet temperature	Hot fluid (water)		Cold fluid (nanofluid)	
		Flow rate, lpm	Reynolds number range	Flow rate, lpm	Reynolds number range
EG:water - Al_2O_3	20 ºC	10	545-500	11-19	152-245
		12.5	674-632		152-245
	10 ºC	10	500-460		113-195
		12.5	623-582		132-211
	-5 ºC	10	460-420		88-136
		12.5	575-533		103-163
EG:water – TiO_2	20 ºC	10	545-500		130-211
		12.5	674-632		151-245
	10 ºC	10	500-460		112-194
		12.5	623-582		120-202
	-5 ºC	10	460-420		86-133
		12.5	575-533		103-163

Table 4.24(a) Range of Peclet number for base fluid

Inlet temperature	Hot fluid (water)		Base fluid (EG:water)	
	Flow rate, lpm	Peclet number range	Flow rate, lpm	Peclet number range
20 ºC	10	1959-1974	11-19	2508-4358
	12.5	2449-2468		2501-4332
10 ºC	10	1977-1998		2529-4380
	12.5	2471-2491		2523-4378
-5 ºC	10	1998-2027		2534-4447
	12.5	2498-2518		2541-4434

Table 4.24(b) Range of Peclet number for weight concentration of nanofluid (0.2 to 2 wt.%)

Nanofluid	Inlet temperature	Hot fluid (water)		Cold fluid (nanofluid)	
		Flow rate, lpm	Peclet number range	Flow rate, lpm	Peclet number range
EG:water - Al_2O_3	20 ºC	10	1959-1974	11-19	2328-4277
		12.5	2449-2468		2304-4255
	10 ºC	10	1977-1998		2354-4297
		12.5	2471-2491		2323-4274
	-5 ºC	10	1998-2027		2401-4392
		12.5	2498-2518		2440-4359
EG:water – TiO_2	20 ºC	10	1959-1974		2416-4306
		12.5	2449-2468		2384-4276
	10 ºC	10	1977-1998		2433-4385
		12.5	2471-2491		2420-4307
	-5 ºC	10	1998-2027		2462-4423
		12.5	2498-2518		2444-4359

4.4.1 Heat transfer rate

Heat transferred to the cold fluid was calculated using Eq.(3.10). Figs. 4.61 and 4.62 depict the effect of nanofluid concentration at various nanofluid inlet temperatures (20 ºC, 10 ºC and -5 ºC) on heat transfer rate for Al_2O_3 and TiO_2 nanofluids, respectively. Figs. 4.61 (a), (b), and (c) show that the heat transfer rate of nanofluid increases with increase in concentration and Peclet number of nanofluid. The Peclet number is the measure of the relative importance of advection (bulk motion of a fluid) versus diffusion (random motions of nanoparticles), where a large number indicates an advectively dominated distribution, and small number indicates a diffuse flow. The Peclet number for a heat exchanger depends on the thermal diffusivity and flow rate of fluid. An enhancement of 6.85%, 5.53%, and 4.19% in heat transfer rate compared to that for base fluid (EG:water), was obtained for 2 wt.% Al_2O_3 nanofluid (Fig. 4.61) at highest Peclet number (corresponding to 19 lpm of nanofluid flow) for inlet temperatures of 20 ºC, 10 ºC and -5 ºC, respectively. At low Peclet number (flow rate = 11 lpm) lower enhancement in heat transfer rate was noticed. Fig. 4.62 shows the heat transfer rate results for TiO_2 nanofluid. The figure shows a similar trend to that of Al_2O_3 nanofluid. A maximum enhancement of 5.30%, 3.87%, and 2.91% was observed for inlet temperatures of 20 ºC, 10 ºC and -5 ºC, respectively. Enhanced heat transfer rates can be attributed to the enhanced thermal conductivity of nanofluid due to the addition of nanoparticles.The presence of nanoparticles in the base fluid modifies the flow structure by increasing the chaotic and random motions. Consequently, the turbulence created due to nanoparticles in the channels of the PHE enhances the rate of heat transfer between plate walls and the fluid. Furthermore, at high flow rates (higher Peclet number), mixing creates greater turbulence due to random motions of nanoparticles, resulting in improved heat transfer (Taghizadeh-Tabari et al., 2016).

The material of the nanoparticle used for heat transfer studies has a significant influence on the properties of the nanofluid, notably thermal conductivity. In this study, two materials, Al_2O_3 and TiO_2 have been used. The properties of nanofluid, particularly thermal conductivity, are strongly dependent on the material of the nanoparticle used. The effect of the material at 2 wt.% concentration, temperature -5 ºC and at flow rates of hot fluid (10 lpm and 12.5 lpm) , on heat transfer rate is shown in Fig. 4.63. For the two nanofluids Al_2O_3 and TiO_2 the heat transfer rate increased by 3.62% and 2.62% compared to that of base fluid, respectively for the hot fluid

flow rate of 12.5 lpm (Fig. 4.63). Among the two materials studied, Al_2O_3 had the maximum thermal conductivity. This is reflected in the higher values of heat transfer rate.

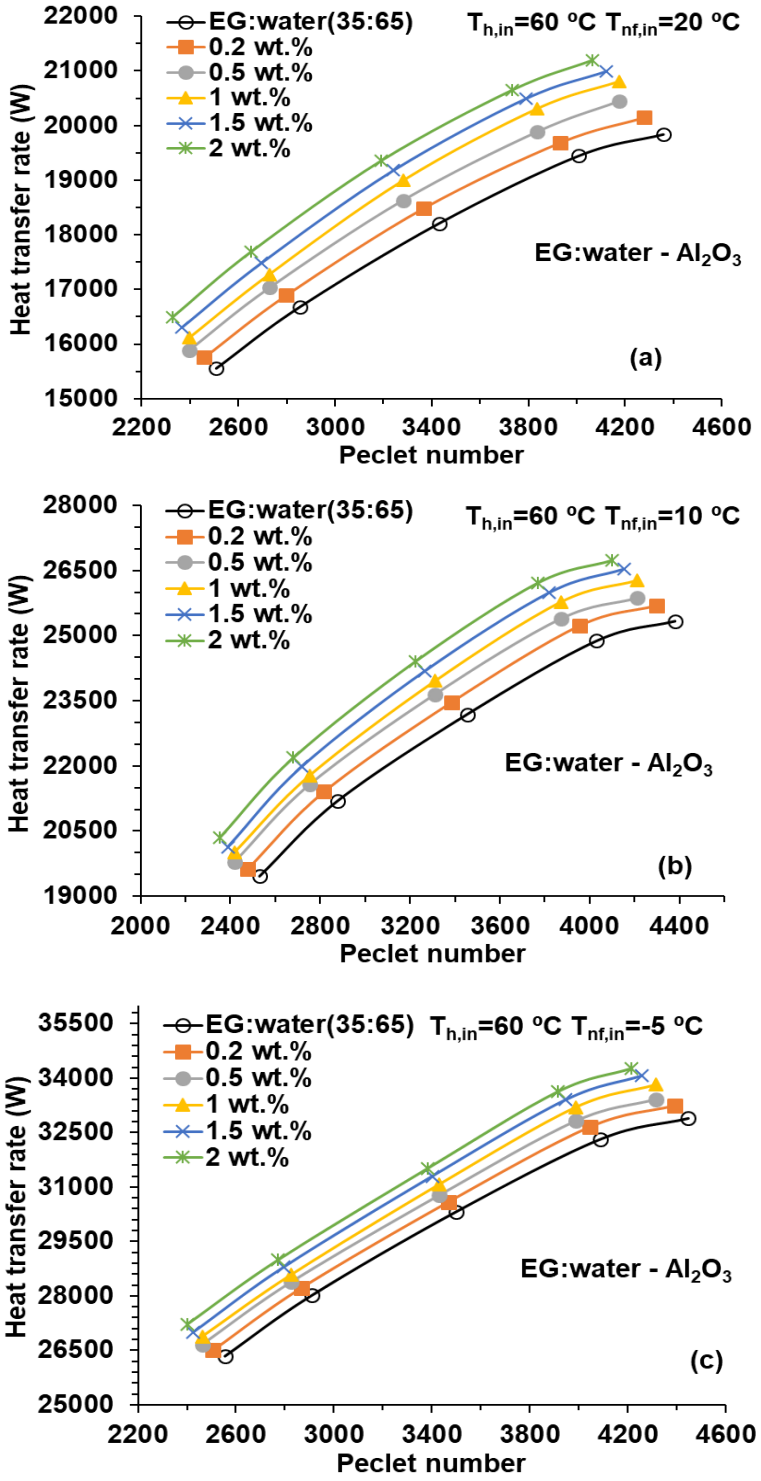

Fig. 4.61 Heat transfer rate vs. Peclet number for Al_2O_3 nanofluids (at nanofluid inlet temperatures $T_{nf,\,in}$ =20 ºC(a) 10 ºC(b) and -5 ºC (c), Hot fluid flow rate = 10 lpm)

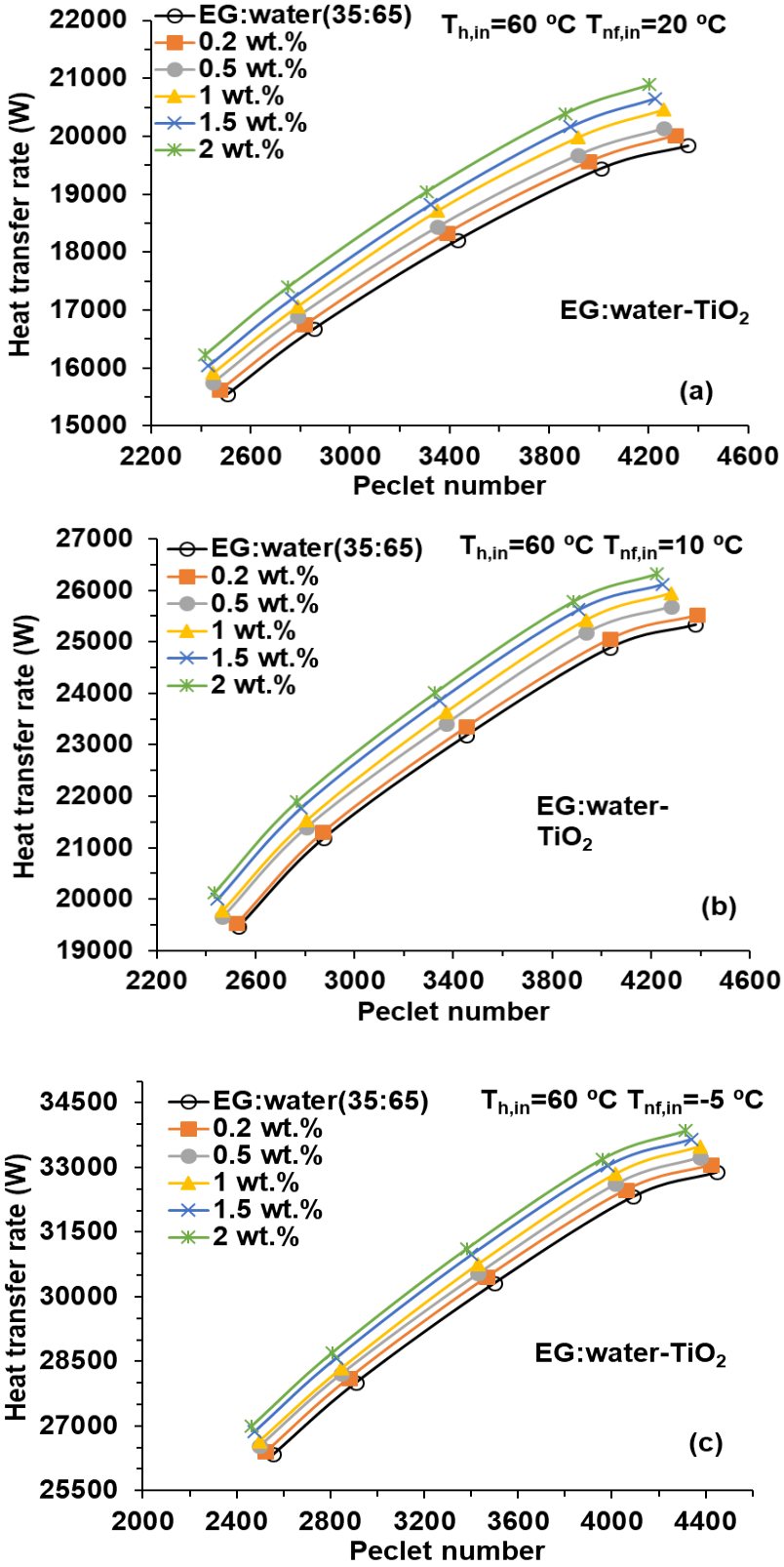

Fig. 4.62 Heat transfer rate vs. Peclet number for TiO_2 nanofluids (at nanofluid inlet temperatures $T_{nf,\,in}$ =20 ºC(a) 10 ºC(b) and -5 ºC (c) , Hot fluid flow rate = 10 lpm)

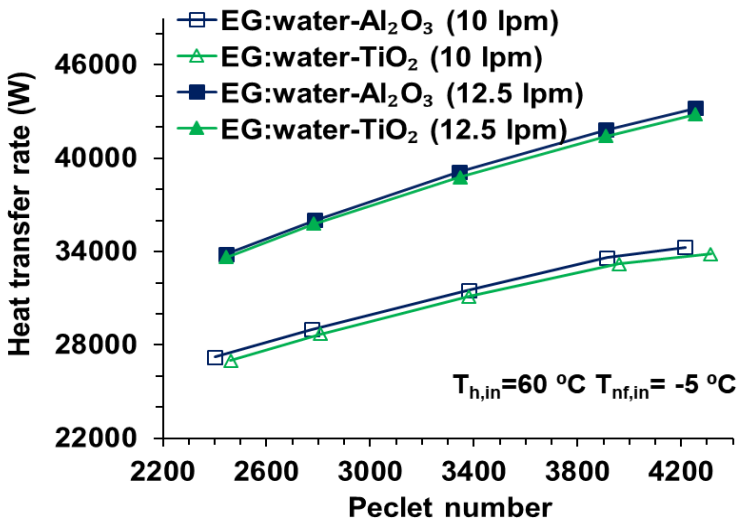

Fig. 4.63 Variation of heat transfer rate for two nanofluids for 2 wt.% nanofluid concentration, at -5 ºC nanofluid inlet temperature

4.4.2 Convective heat transfer coefficient

Figs. 4.64 and 4.65 show the effect of the flow rate (in terms of Peclet number) of EG:water-Al_2O_3 and TiO_2 nanofluid on CHTC at a fixed flow rate of hot water (10 lpm) for a nanofluid inlet temperature of 20, 10 and -5 ºC respectively. From the figures it can be seen that as the nanofluid concentration increases, the CHTC from hot fluid to cold fluid increased. The CHTC of the EG:water - Al_2O_3 nanofluid is higher than that of the EG:water base fluid at all inlet temperatures. Similar trend to that of Al_2O_3 nanofluid was observed for TiO_2 nanofluid (Fig. 4.65 (a), (b), and (c)). The enhancement in CHTC for both nanofluids can be attributed to the Brownian motion of nanoparticles in the base fluid, nanoparticle collisions and thermophoresis effects(Tabari and Heris, 2015; Li et al., 2016; Arya et al., 2018; Bhattad et al., 2020).

At 19 lpm (corresponding Peclet numbers of 4306, 4294, 4260, 4226, 4203), the increase in CHTC values for 0.2, 0.5, 1, 1.5, and 2 wt.% of Al_2O_3 nanofluid concentration is 5.7%, 12.1%, 19.04%, 24.15% and 30.28%, respectively, compared to the base fluid at a nanofluid inlet temperature of 20 ºC. CHTC increased by 30.28%, 25.40% and 18.26% when the nanofluid inlet temperatures are 20, 10 and -5 ºC respectively at highest Peclet number (flow rate of 19 lpm) of Al_2O_3 nanofluid for 2 wt.% concentration. Similalry, for TiO_2 nanofluid, CHTC increased by 19.77%, 16.75% and 11.99% in that order. It can be seen that at a lower

temperature (-5 ºC) the CHTC obtained for both nanofluids is less compared to that at a higher temperature (20 ºC). The effect of the increase in the inlet temperature of nanofluid on CHTC is due to the corresponding change in the thermophysical properties of the nanofluid (thermal conductivity, viscosity and density). A similar trend has been reported by Bhattad et al. (2020) when different combination of water based hybrid nanofluids were tested in PHE at different inlet temperatures (10, 15, 20 and 25 ºC). However, the observed enhancement in CHTC of nanofluid at below sub-zero temperature has shown significant improvement.

Figure 4.66 depicts the effect of nanoparticle materials on the CHTC at 2 wt.% concentration, -5 ºC nanofluid inlet temperature and two hot fluid flow rates (10 and 12.5 lpm). From this figure, it is evident that Al_2O_3 nanofluid exhibited higher CHTC values compared to TiO_2 nanofluid. This is due to the superior thermal conductivity of Al_2O_3 material compared to TiO_2. A maximum enhancement of 22.73% and 16.08% of CHTC was obtained for 2 wt.% of Al_2O_3 and TiO_2 nanofluids for the lowest inlet temperature, respectively, at a hot fluid flow rate of 12.5 lpm.

The Nusselt number was calculated using Eq. (3.19). For given conditions on PHE (nanofluid concentration, nanofluid inlet temperature and material and flow rate) use of nanofluid resulted in increased heat transfer rate and higher values CHTC. Fig 4.67 shows the effect of Al_2O_3 and TiO_2 nanofluid concentration at -5 ºC nanofluid inlet temperatures on Nusselt number for two hot fluid rates considered in the study. Nusselt number was found to increase with increase in nanofluid concentration. This illustrates that the key purpose of heat transfer enhancement is the development of molecular thermal diffusion as a result of introducing nanoparticles into the base fluid (Khairul et al., 2013). Wang et al. (2018) reported a similar trend when EG:water based graphene nanofluid was used with a weight concentration of up to 1 wt.% in a miniature PHE. Similar observations were also made by Tiwari et al. (2015) who used different nanoparticles dispersed in water to report the effect of concentration and flow rates in PHE. Similar studies have been reported in the literature stating that for nanofluids the CHTC can be enhanced with flow rate (Tiwari et al., 2013a; Sun et al., 2016; Pourhoseini et al., 2018). Out of the two types of nanofluids used, Al_2O_3 nanofluid gave the maximum values of Nusselt number due to its higher thermal conductivity.

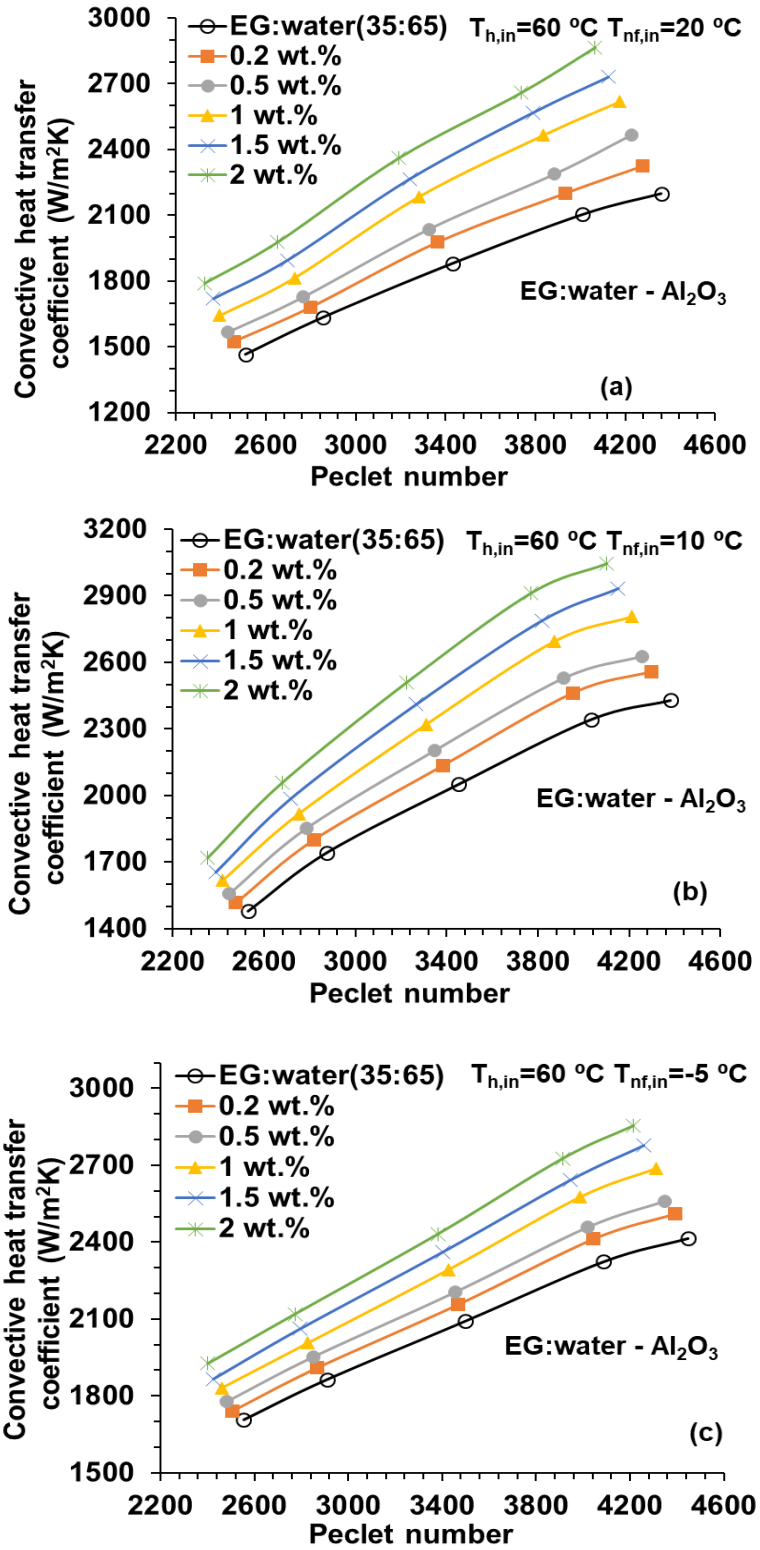

Fig. 4.64 Convective heat transfer coefficient vs. Peclet number for Al_2O_3 nanofluids (at nanofluid inlet temperatures $T_{nf,\,in}$ =20 ºC (a) 10 ºC(b) and -5 ºC (c) , Hot fluid flow rate = 10 lpm)

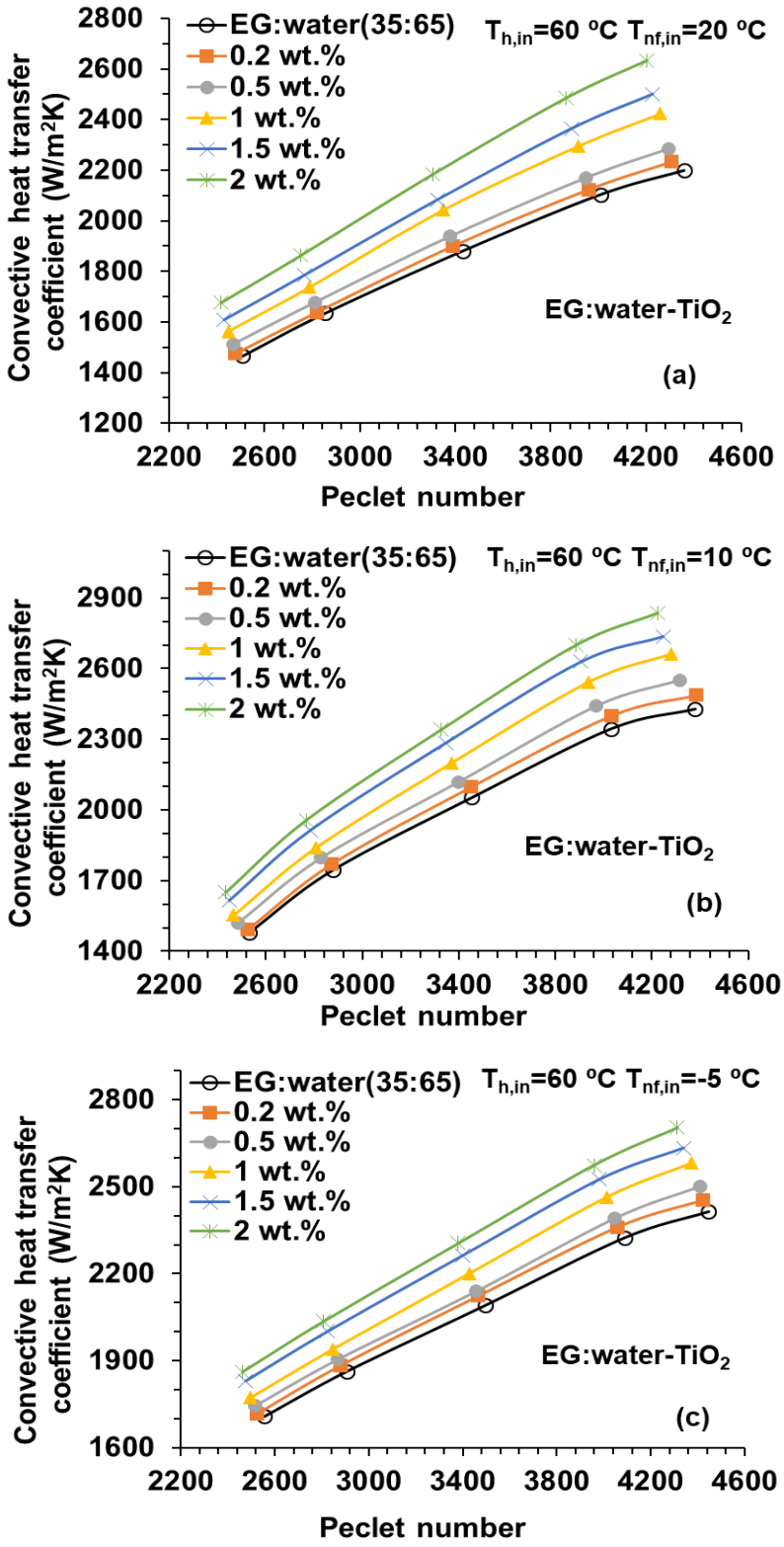

Fig. 4.65 Convective heat transfer coefficient vs. Peclet number for TiO_2 nanofluids (at nanofluid inlet temperatures $T_{nf,\,in}$ =20 ºC(a) 10 ºC(b) and -5 ºC (c), Hot fluid flow rate = 10 lpm)

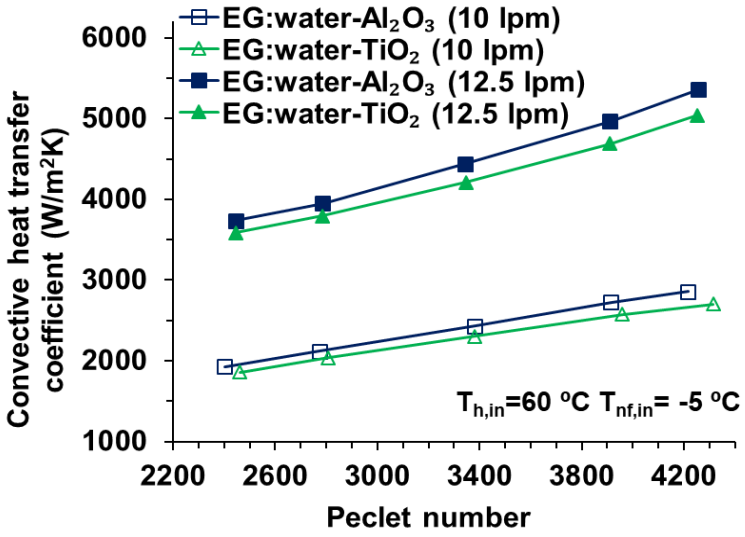

Fig. 4.66 Effect of nanoparticles materials on CHTC for varied Peclet number of EG:water nanofluids for different hot fluid flow rates at lowest nanofluid inlet temperature

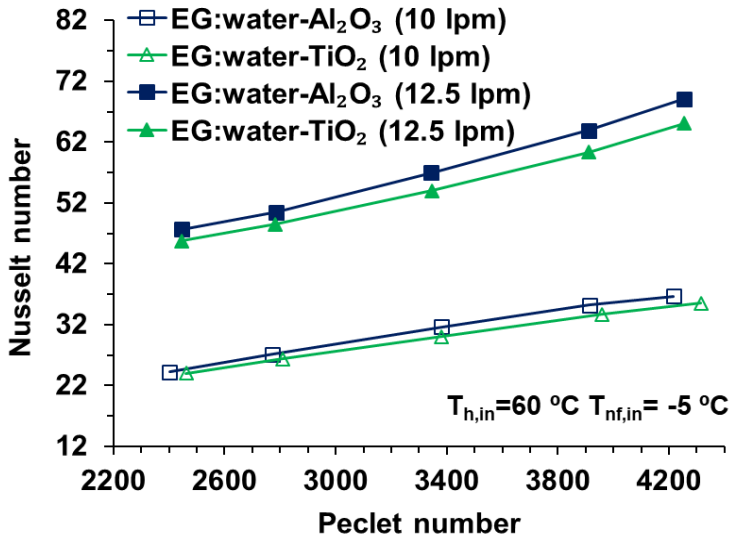

Fig. 4.67 Effect of nanoparticles materials on Nusselt number for varied Peclet number of EG:water nanofluids for different hot fluid flow rates at lowest nanofluid inlet temperature

4.4.3 Overall heat transfer coefficient

Overall heat transfer coefficient was calculated from the average heat transfer rate using Eq. (3.15). The variation of OHTC with experimental conditions is shown in Figs.4.68 and 4.69. It can be seen that use of nanofluid has resulted in significantly higher values of OHTC. Higher values of OHTC indicate lower heat transfer surface requirement, making the heat exchanger compact. Therefore the application of nanofluids has great potential for intensification in heat

exchangers. The heat transfer rate and LMTD are the influencing parameters on the OHTC. The experiment study showed that LMTD decreases as the weight concentration of the nanofluid increases. OHTC was found to increase with increasing the weight concentration of nanofluid. The study reported using water based nanofluids shows a similar kind of trend in enhancement of OHTC (Pandey and Nema, 2012; Tiwari et al., 2013b, 2015). The OHTC increased by 18.61%, 15.30% and 11.99% for Al_2O_3 nanofluid concentration of 2 wt.% compared to base fluid, at a flow rate of 19 lpm (corresponding to highest Peclet number) for nanofluid inlet temperature 20, 10 and -5 ºC repectivley (Fig. 4.68). Fig. 4.69 shows the similar nature of OHTC enhancement behaviour with nanoopaticle loading for TiO_2 nanofluid. The OHTC values obtained for TiO_2 nanofluid are 13.96%, 10.68% and 8% for 20, 10 and -5 ºC repectivley for corresponding weight concentration (2 wt.%) and highest Peclet number (flow rate of 19 lpm).

It can also be observed from the study that the OHTC reduces as the nanofluid inlet temperature decreases. Pourhoseini et al. (2018) made a similar observation with regard to water-based silver nanofluids. The study carried out by Arya et al. (2018) also shows the similar kind of decrease in OHTC for EG based MgO nanofluids. The effect at higher temperatures is predominant as the viscosity of nanofluids reduces and thermal conductivity rises, resulting in an increase in OHTC.

The effect of hot flow rate on OHTC has been investigated at 10 lpm and 12.5 lpm. Fig 4.70 shows the results of the study for 2 wt.% of Al_2O_3 and TiO_2 nanofluid. From the figure, it can be observed that the increasing flow rate on hot fluid increases the overall heat transfer coefficient. OHTC increased by 11.99% for the 10 lpm of hot fluid rate and 11.82% for the 12.5 lpm at highest Peclet number (corresponding to the highest flow rate of 19 lpm in the study). Similar trends were observed for TiO_2 nanofluids.

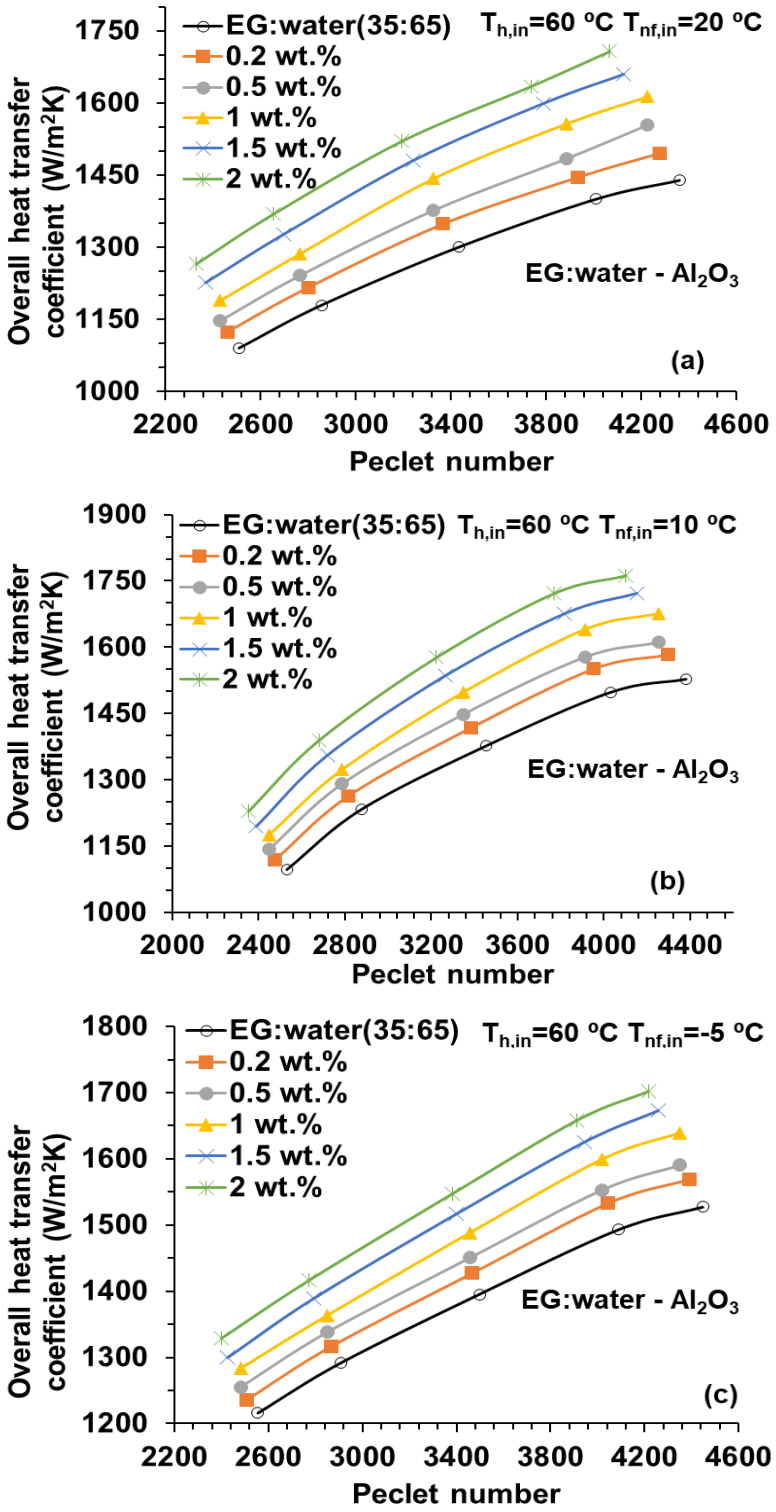

Fig. 4.68 Overall heat transfer coefficient vs Peclet number for Al_2O_3 nanofluids (at nanofluid inlet temperatures $T_{nf,\,in}$ =20 ºC (a) 10 ºC (b) and -5 ºC (c) , Hot fluid flow rate = 10 lpm)

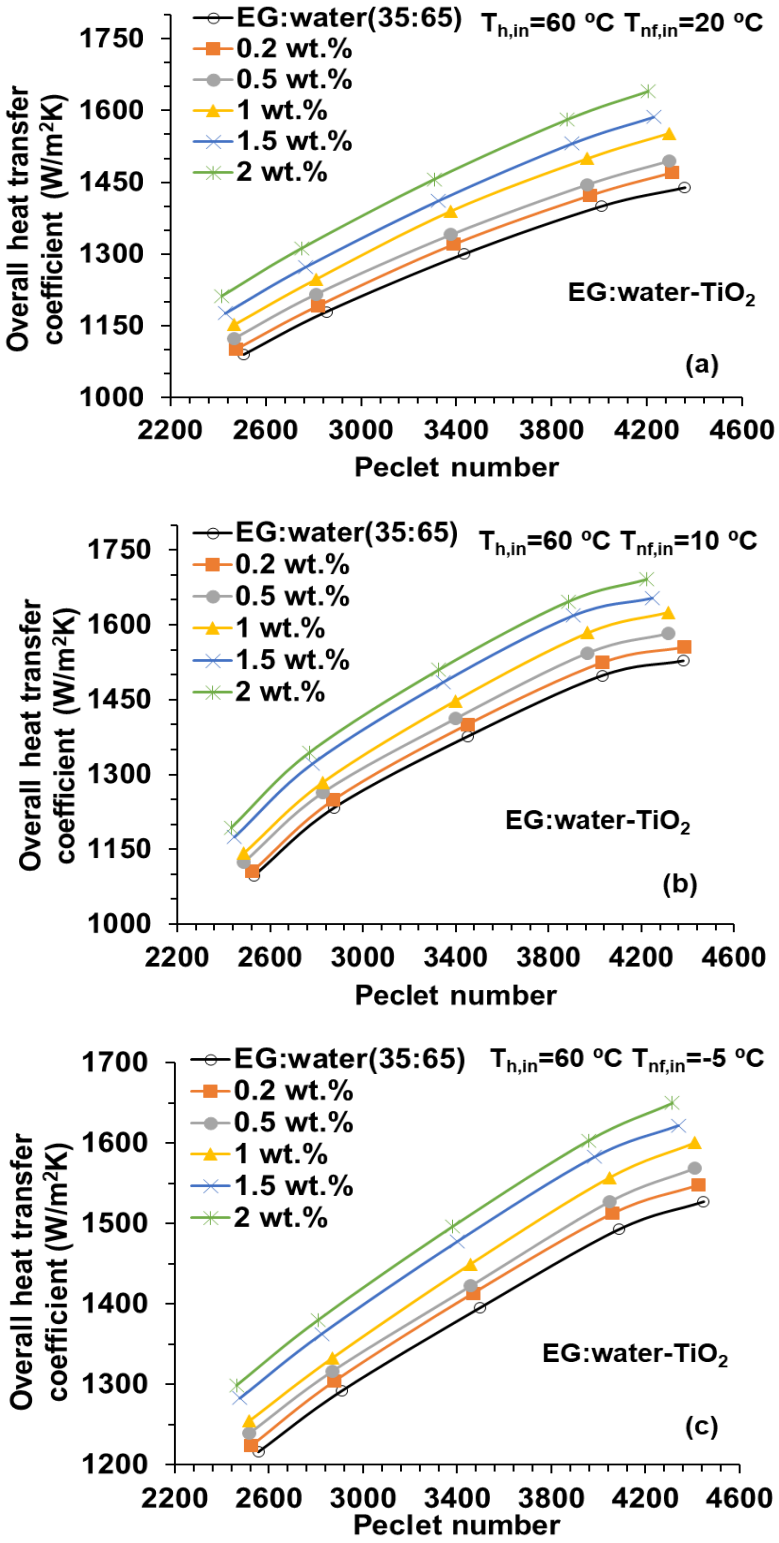

Fig. 4.69 Overall heat transfer coefficient vs Peclet number for TiO_2 nanofluids (at nanofluid inlet temperatures $T_{nf,\,in}$ =20 ºC (a) 10 ºC (b) and -5 ºC (c), Hot fluid flow rate = 10 lpm)

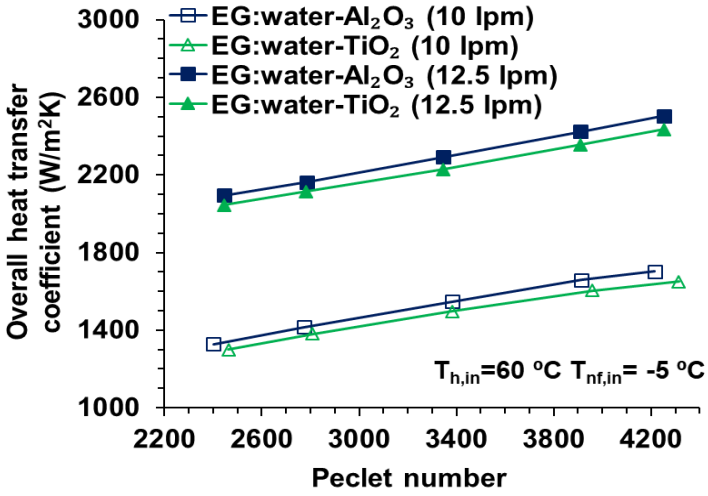

Fig. 4.70 Effect of nanoparticles materials on OHTC for varied Peclet number of EG:water nanofluids for different hot fluid flow rates at lowest nanofluid inlet temperature for 2 wt.% of concentration

4.4.4 Effectiveness

Effectiveness is a qualitative measure of heat transfer for cold fluid approaching the inlet temperature of the hot fluid, i.e., the higher the outlet temperature of the cold stream, the greater the effectiveness. Figs. 4.71 and 4.72 illustrate the variation of effectiveness with nanofluid Peclet number and concentration for three nanofluid inlet temperatures tested in the present study. Effectiveness was found to be higher at all concentrations of nanofluid compared to the base fluid at all Peclet numbers of both nanofluids. In this study, enhancement in effectiveness was found to be 6.85%, 5.53% and 4.19% for Al_2O_3 nanofluid at inlet temperatures of 20 ºC, 10 ºC and -5 ºC for 2 wt.% concentration, respectively. Similarly, for TiO_2 nanofluids, enhancement in effectiveness was found to be 5.29%, 3.87% and 2.91% in that order. From Figs. 4.71 and 4.72, it can be clearly noticed that the effectiveness obtained for the PHE increases with the increase in the Peclet numbers of the nanofluid.

Figs. 4.73 and 4.74 show material (Al_2O_3 and TiO_2) effect on the effectiveness for 2 wt.% concentration of nanofluid for different Peclet numbers at hot fluid flow rates of 10 lpm and 12.5 lpm, respectively. In both cases of fixed hot flow rate, Al_2O_3 nanofluid showed higher effectiveness compared to TiO_2 nanofluids. This can be attributed to higher thermal conductivity values of Al_2O_3 nanofluids compared to TiO_2 nanofluids at corresponding temperatures.

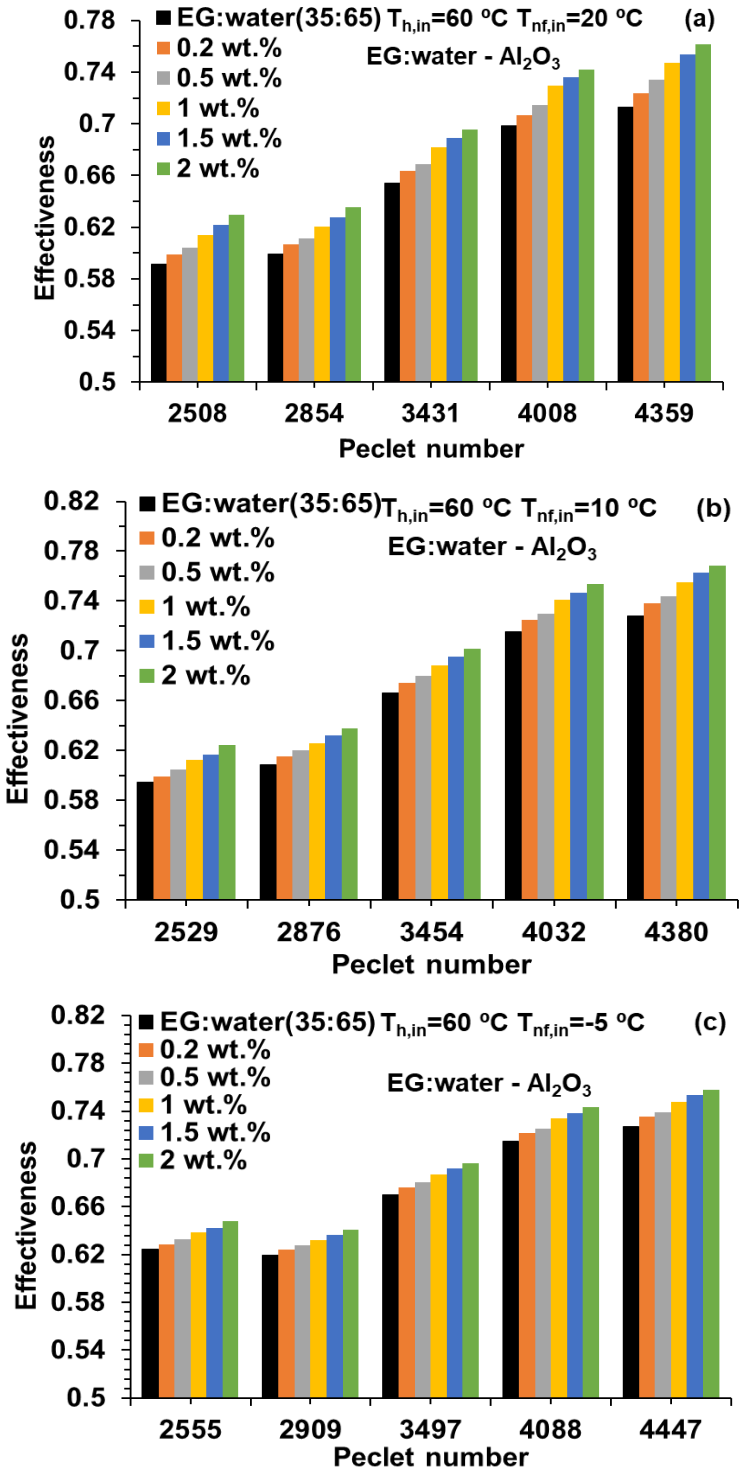

Fig. 4.71. Effectiveness vs. Peclet number for Al_2O_3 nanofluids (at nanofluid inlet temperatures $T_{nf,\,in}$ =20 ºC (a), 10 ºC (b) and -5 ºC (c), Hot fluid flow rate = 10 lpm)

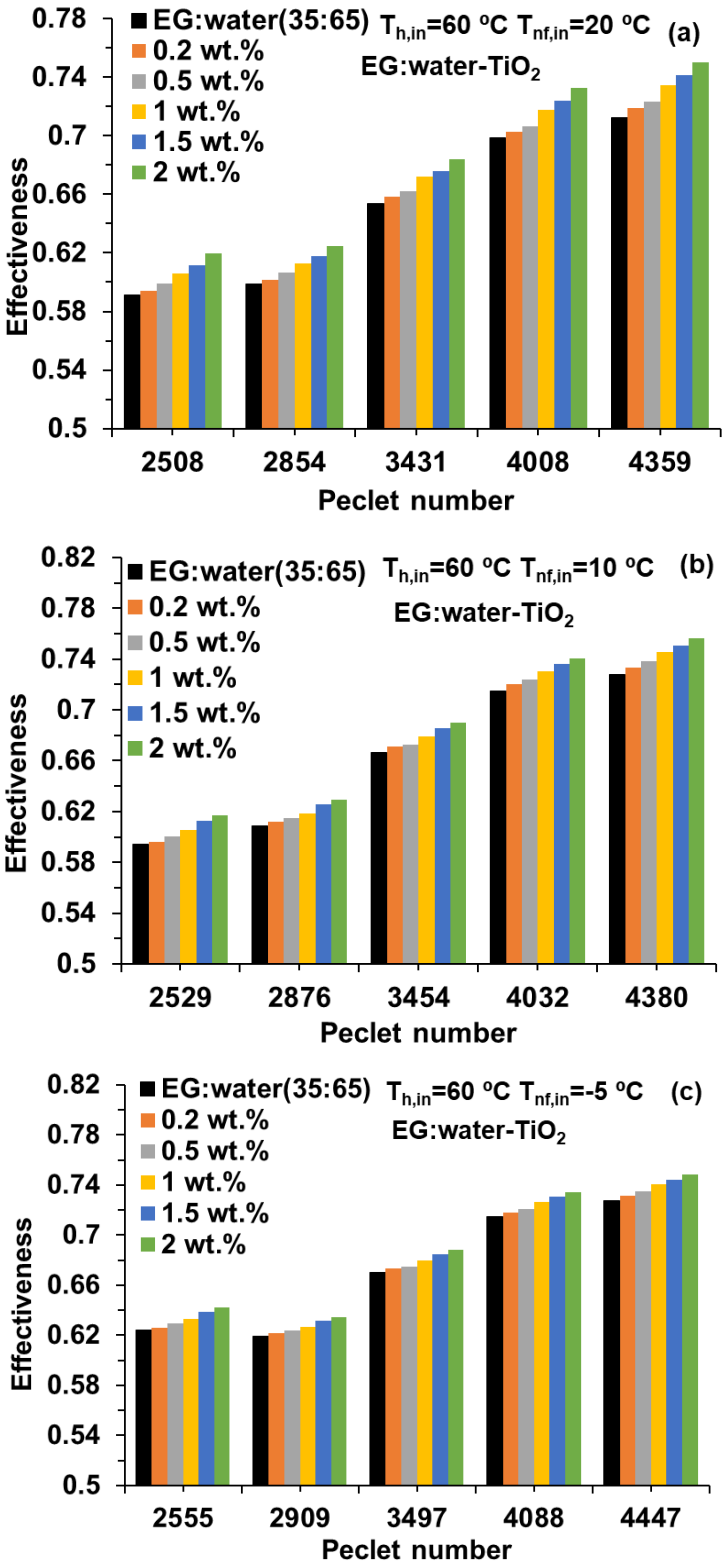

Fig. 4.72. Effectiveness vs. Peclet number for TiO_2 nanofluids (at nanofluid inlet temperatures $T_{nf,\,in}$ =20 ºC (a), 10 ºC (b) and -5 ºC (c), Hot fluid flow rate = 10 lpm)

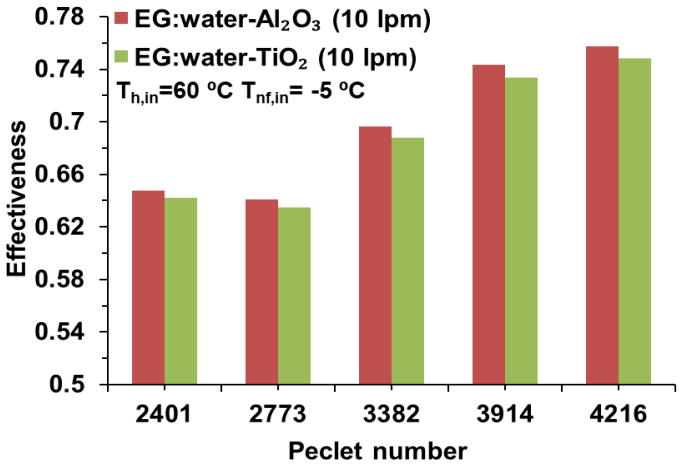

Fig. 4.73 Effect of nanoparticles materials on effectiveness for varied Peclet number of nanofluids for hot fluid flow rate of 10 lpm at lowest nanofluid inlet temperature for 2 wt.% of concentration

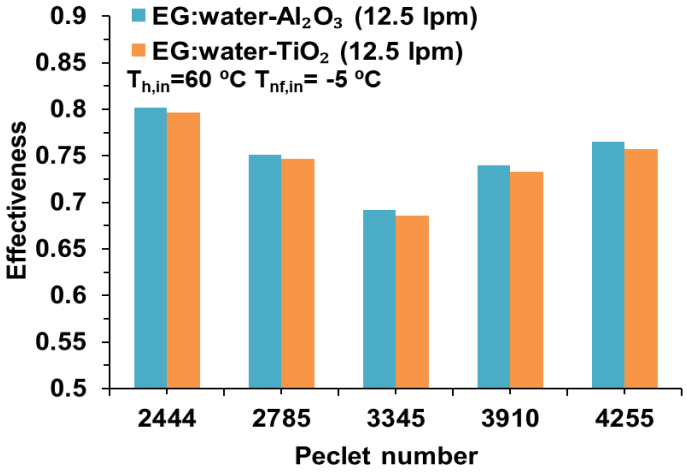

Fig. 4.74 Effect of nanoparticles materials on effectiveness for varied Peclet number od nanofluids for hot fluid flow rate of 12.5 lpm at lowest nanofluid inlet temperature for 2 wt.% of concentration

4.4.5 Pressure drop and pumping power

Pressure drop plays an important role in heat transfer application as it effects the pumping power required to operate the PHE at different environmental conditions. In the present study, the pressure drop was measured experimentally at various flow rates (11-19 lpm) of nanofluid in PHE. The pressure drop for nanofluid was found to be greater than that of base fluid (EG:water). The highest increase in pressure drop was observed for 2 wt.% of nanofluid concentration with 15.38%, 17% and 17.72% compared to EG:water at 20 ºC, 10 ºC and -5 ºC

(nanofluid inlet temperatures) respectively for Al_2O_3 nanofluids. Similarly, for TiO_2 nanofluids, the corresponding pressure drop was 20.5%, 23.8% and 27.22% in that order.

The pressure drop measured experimentally was used to calculate the pumping power for the varied nanofluid flow rate using Eq. (3.21). Fig. 4.75 (a), (b) and (c) illustrate the effect of Al_2O_3 nanofluid concentration on pumping power at 20 ºC, 10 ºC and -5 ºC (nanofluid inlet temperature) respectively. It can be seen from these figures that the pumping power increases with an increase in nanofluid concentration. This is due to the presence of nanoparticles in EG:water, which exhibits greater viscosity compared to the base fluid. The increase in power consumption for the Al_2O_3 nanofluids at 2 wt.% for the 20 ºC, 10 ºC and -5 ºC inlet temperature conditions is 13.74%, 15.47% and 16.05% respectively. TiO_2 nanofluids containing 2 wt.% of concentration have shown an increase in power consumption by 18.80%, 21.91% and 25.48% for 20 ºC, 10 ºC and -5 ºC inlet temperature conditions respectively (Fig.4.76) at highest Peclet number (corresponding floe rate of 19 lpm) compared to EG:water.

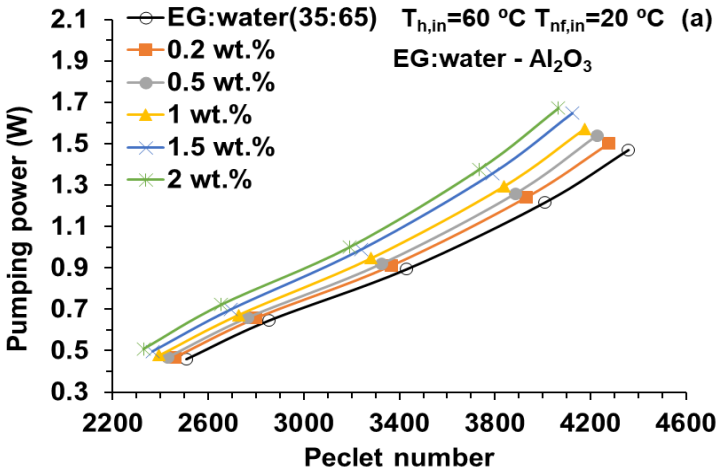

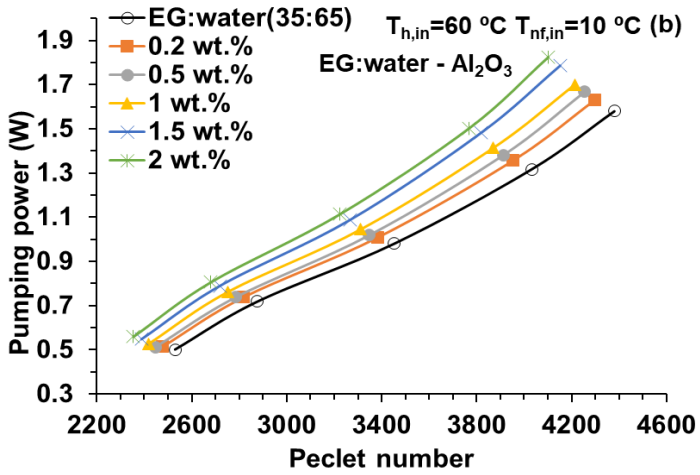

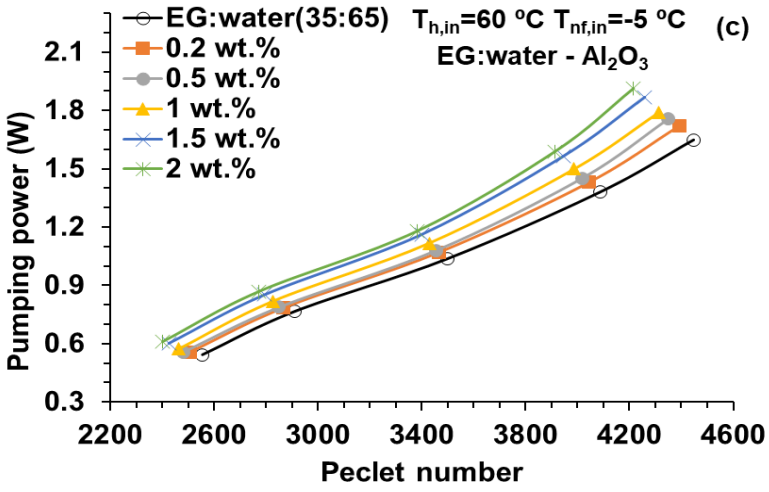

Fig. 4.75 Pumping power vs. Peclet number for Al_2O_3 nanofluids (at nanofluid inlet temperatures $T_{nf,\,in}$ =20 ºC (a), 10 ºC (b) and -5 ºC (c), Hot fluid flow rate = 10 lpm)

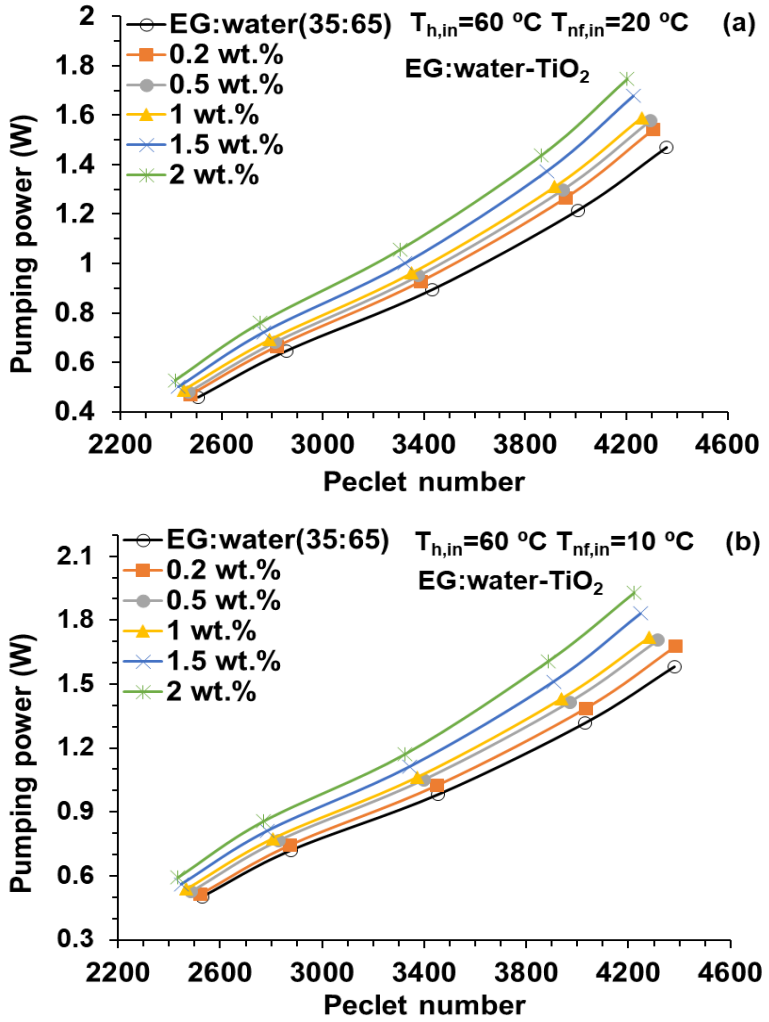

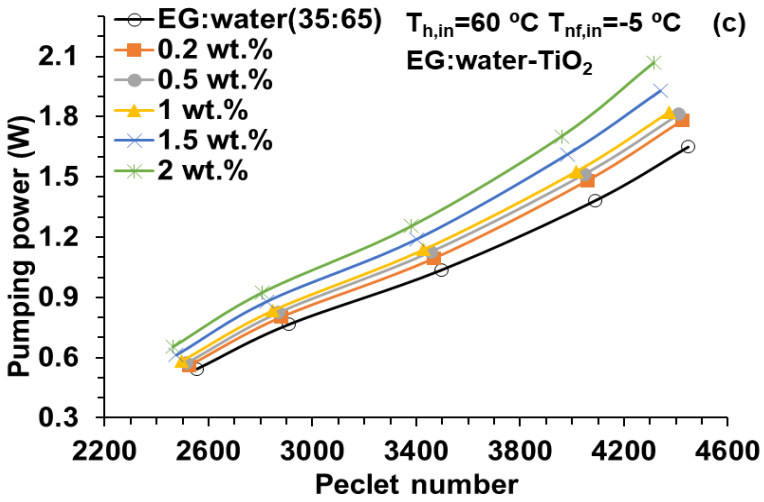

Fig. 4.76. Pumping power vs. Peclet number for TiO_2 nanofluids (at nanofluid inlet temperatures $T_{nf,\,in}$ =20 ºC (a), 10 ºC (b) and -5 ºC (c), Hot fluid flow rate = 10 lpm)

Fig. 4.77 indicates comparision of two nanoparticle materials on pumping power for a varied Peclet number of nanofluids for two hot fluid flow rates (10 lpm and 12.5 lpm) at -5 ºC inlet temperature (lowest nanofluid inlet temperature in the study) at 2 wt.% concentration. It can be seen from this graph that in both the fixed hot fluid flow conditions, TiO_2 nanofluids exhibited higher values of pumping power. This is due to the higher values of viscosity compared to Al_2O_3 nanofluids at corresponding bulk temperatures.

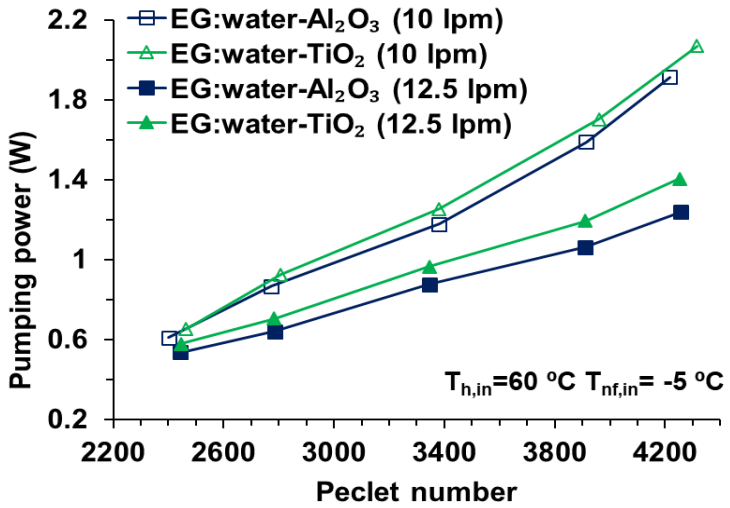

Fig. 4.77 Effect of nanoparticle materials on pumping power for varied Peclet number of EG:water nanofluids for two hot fluid flow rate at lowest nanofluid inlet temperature for 2 wt.% of concentration

4.4.6 Friction factor

The friction factor for the different flow rates was determined using Eq. (3.22) (Pandey and Nema, 2012; Tiwari et al., 2013b; Goodarzi et al., 2015). Figs. 4.78 and 4.79 show the effect on friction factor with different concentrations of Al_2O_3 nanofluid at varied Peclet numbers. The experimental results indicated that the friction factor of Al_2O_3 nanofluid is higher than that of EG:water. Similarly, the same trend has been observed for TiO_2 nanofluids. At the identical Peclet numbers, the friction factor increased with increasing weight concentration of nanofluids. At lower temperatures, it is observed that the friction factor is slightly higher than that at higher nanofluid inlet temperatures. This effect is more pronounced at lower inlet temperatures, where more density change and pressure drop occurred than at higher temperatures. However, trends in both temperatures are similar.

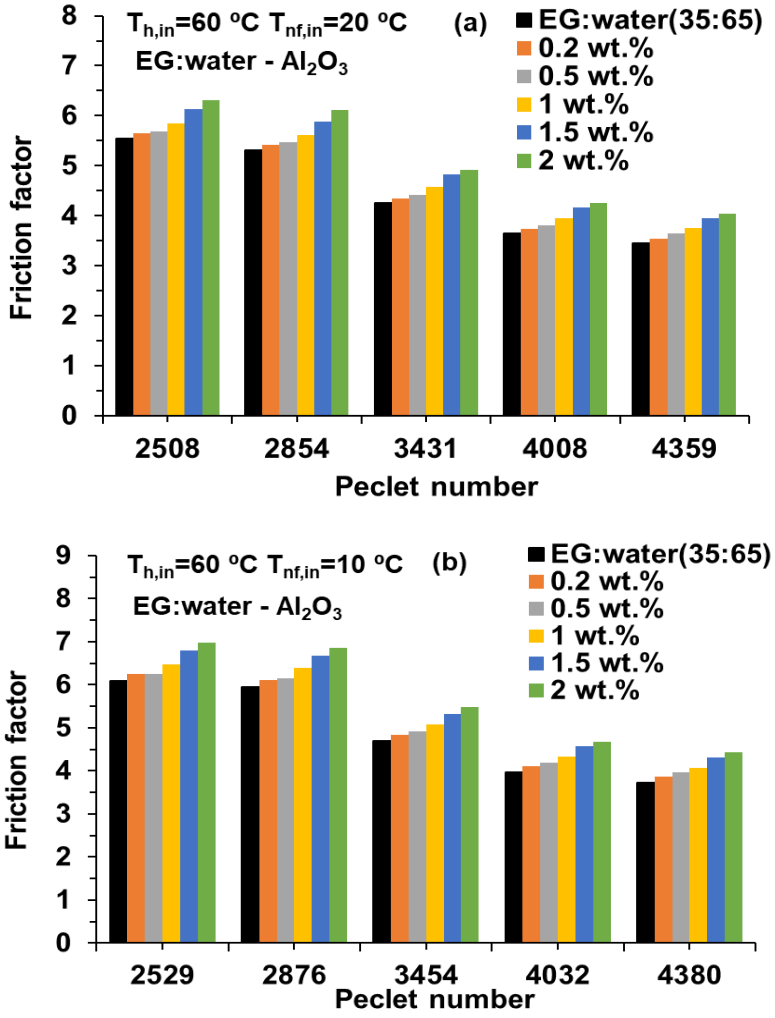

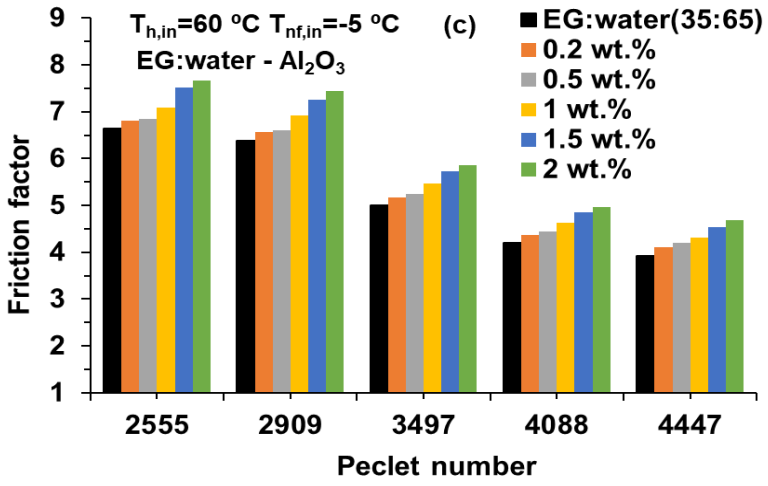

Fig. 4.78. Friction factor vs Peclet number for Al_2O_3 nanofluids (at nanofluid inlet temperatures $T_{nf,\,in}$ =20 ºC (a), 10 ºC (b) and -5 ºC (c), Hot fluid flow rate = 10 lpm)

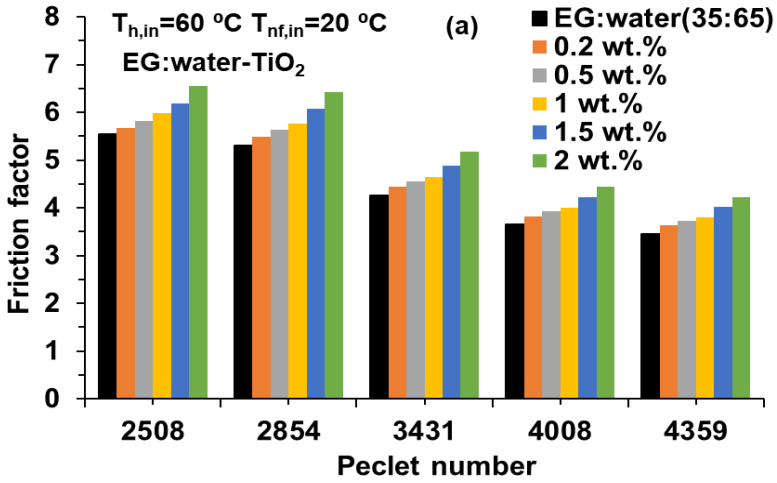

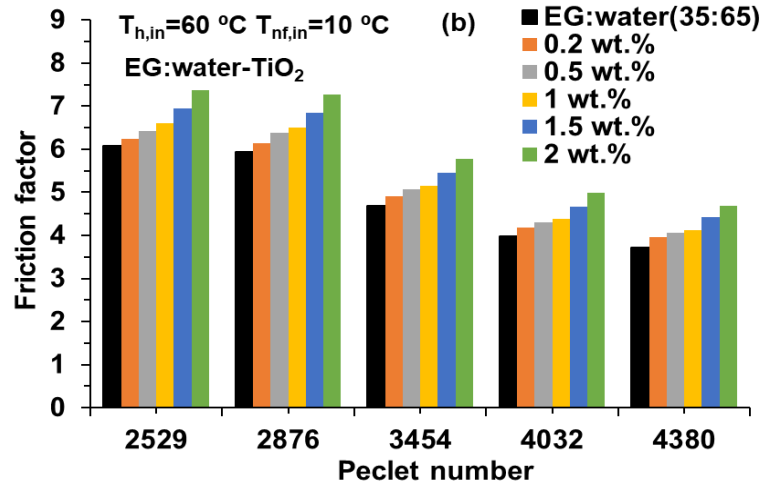

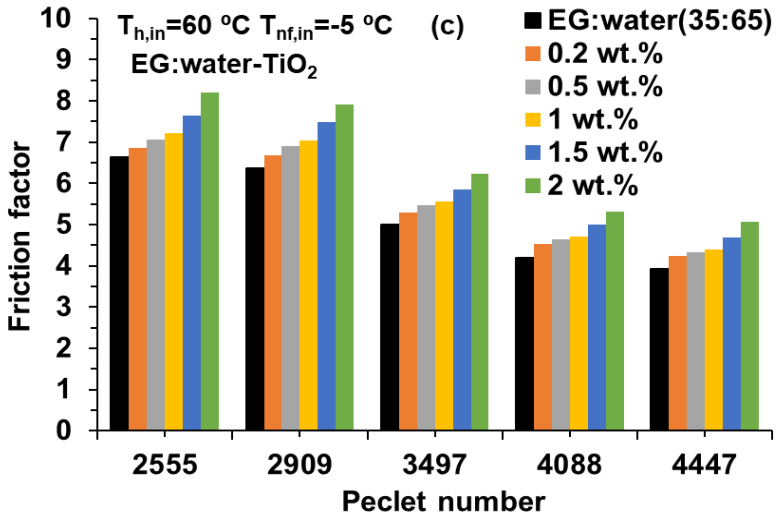

Fig. 4.79. Friction factor vs Peclet number for TiO_2 nanofluids (at nanofluid inlet temperatures $T_{nf,\,in}$ =20 ºC (a), 10 ºC (b) and -5 ºC (c), Hot fluid flow rate = 10 lpm)

The material influence on the friction factor for the 2 wt.% concentration of nanofluid at different Peclet numbers at the lowest inlet temperature and hot fluid flow rates (10 and 12.5 lpm) considered in the study are shown in Fig. 4.80. Friction factor of TiO_2 nanofluids was found to be higher at both fixed flow rate of the hot fluid. This is due to a rise in the viscosity and density of nanofluids at the corresponding temperature, which results in a higher pressure drop at the corresponding concentration.

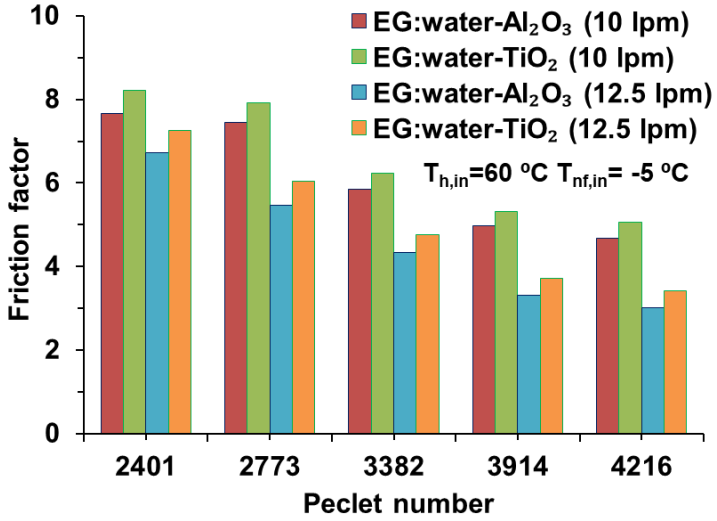

Fig. 4.80 Effect of nanoparticle materials on fricition factor for varied Peclet number of EG:water nanofluids for two hot fluid flow rate at lowest nanofluid inlet temperature for 2 wt.% of concentration

4.5 Entropy generation

Entropy generation is a common characteristic and a crucial aspect of every heat transfer process. Lowering the irreversibility of the process is desirable for effective use of nanofluids in heat transfer application. Heat transfer caused by temperature gradients and viscous effects may contribute to entropy generation in heat exchangers.

4.5.1 Thermal entropy generation

TEG of the PHE was determined using Eq. (3.24). The TEG values obtained for the nanofluid at different Peclet numbers for Al_2O_3 and TiO_2 nanofluids are shown in Figs. 4.81 and 4.82 respectively for the lowest nanofluid inlet temperature (-5 ºC). It is clearly seen from the study that for both nanofluids, the TEG is decreased with the nanoparticle loading. Furthermore, the corrugation structure of PHE promotes recirculation and mixing of the nanofluid flow (Huminic and Huminic, 2012; Kumar et al., 2015). Therefore, the heat transfer rate of nanofluids increases and the thermal entropy generation decreases. The TEG value obtained for the base fluid is higher compared to nanofluids. The present study shows the similar results previously reported by Huminic (2018) for hybrid nanofluid (water - MWCNT + Fe_3O_4 and water - ND + Fe_3O_4) used in a flattened tube. Similarly, a decrease in TEG was observed with the use of Ni-water and EG:water-nanodiamond+Fe_3O_4 nanofluids compared to based fluid (Saleh and Sundar, 2021; Syam Sundar et al., 2021). The reduction in thermal entropy generation is 1.86%, 2.84%, 5.41%, 7.15% and 8.69% for 0.2, 0.5, 1, 1.5, and 2 wt.% of concentration respectively at Peclet numbers of 4392, 4348, 4314, 4258, and 4215 against base fluid for Al_2O_3 nanofluids. For TiO_2 nanofluids, the reduction in TEG is 0.65%, 1.57%, 3.28%, 4.33% and 5.77% for 0.2, 0.5, 1, 1.5, and 2 wt.% of concentration respectively at Peclet numbers of 4423, 4410, 4374, 4339 and 4314 against the base fluid.

Fig. 4.83 shows the effect of two nanoparticle materials on TEG for the varied Peclet numbers of nanofluid for two hot fluid rates (10 lpm and 12.5 lpm) at 2 wt.% concentration for the lowest nanofluid inlet temperature. From this figure, it is evident that the Al_2O_3 nanofluids exhibited lower TEG compared to TiO_2 nanofluids for both fixed flow rates of hot fluid. It is obvious that the superior thermal properties (thermal conductivity) of Al_2O_3 resulted in a significant reduction in TEG.

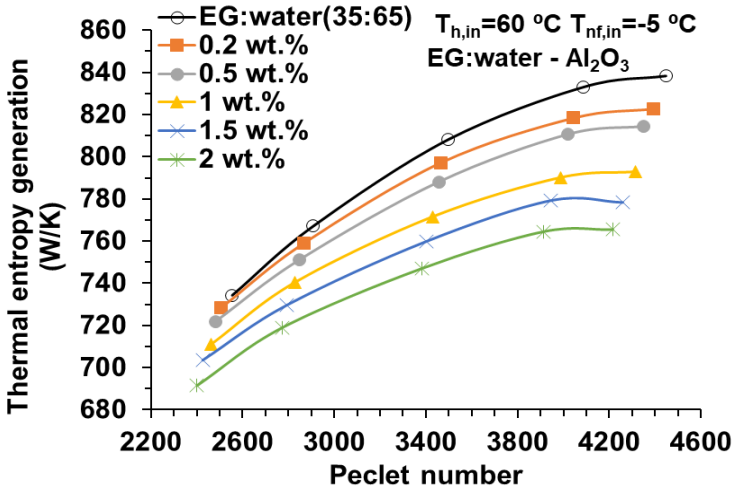

Fig. 4.81 Thermal entropy generation vs. Peclet number for EG:water-Al_2O_3 nanofluid

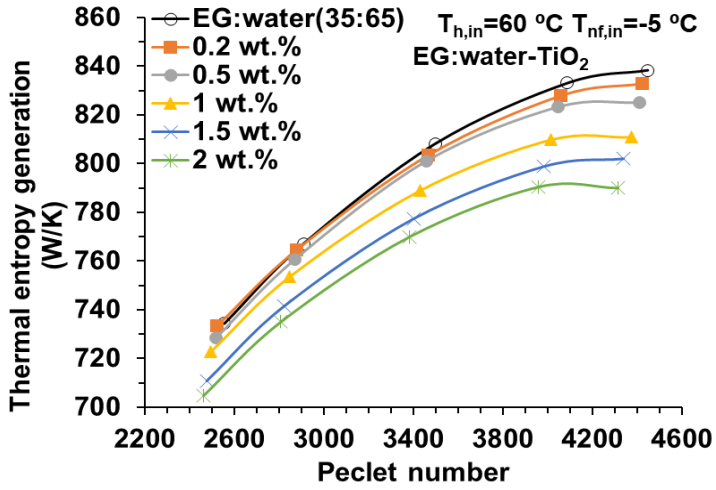

Fig. 4.82 Thermal entropy generation vs. Peclet number for EG:water-TiO_2 nanofluid

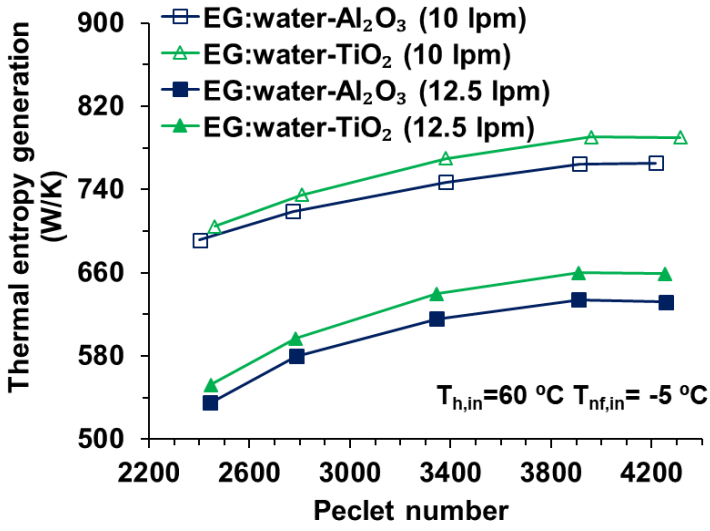

Fig. 4.83 Effect of nanoparticle materials on thermal entropy generation for varied Peclet number for EG:water nanofluid for two hot fluid rate at 2 wt.% concentration

4.5.2 Frictional entropy generation

The FEG of the base fluid and nanofluids was calculated from Eq. (3.24). Figs. 4.84 and 4.85 show the FEG obtained for base fluid and nanofluid at different Peclet numbers. From the figures, it is observed that the FEG increased with the increase in Peclet number and nanoparticle concentration. The effect of the friction factor in the case of nanofluids is more dominant because of the increase in the flow resistance in the small channels of the PHEs. As a result of this, the concentration of nanofluid increases the friction factor for the fixed geometry of the PHE. The increase in FEG is 4.17%, 6.15%, 8.18%, 12.86% and 15.58% for 0.2, 0.5, 1, 1.5, and 2 wt% of concentration respectively at Peclet numbers of 4392, 4348, 4314, 4258, and 4215 against base fluid for Al_2O_3 nanofluid. Similarly, for TiO_2 nanofluids, the increase in FEG is 7.83%, 9.58%, 10.28%, 16.56% and 25.08% for 0.2, 0.5, 1, 1.5, and 2 wt% of concentration respectively at Peclet numbers of 4423, 4410, 4374, 4339 and 4314 against base fluid.

Fig. 4.86 shows the effect of two nanoparticle materials on FEG for the varied Peclet numbers of nanofluid for two hot fluid rates (10 and 12.5 lpm) at 2 wt.% concentration for the lowest nanofluid inlet temperature. From this figure, it is evident that the Al_2O_3 nanofluids exhibited lower FEG compared to TiO_2 nanofluids for both fixed flow rates of hot fluid. The frictional resistance offered by the Al_2O_3 nanofluids is significantly less compared to the TiO_2 nanofluids due to a reduction in viscosity and an increase in thermal conductivity.

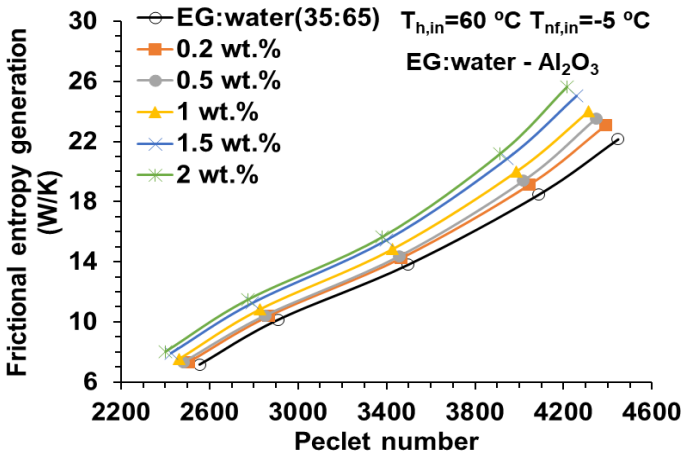

Fig. 4.84 Frictional entropy generation vs Peclet number for EG:water-Al_2O_3 nanofluid

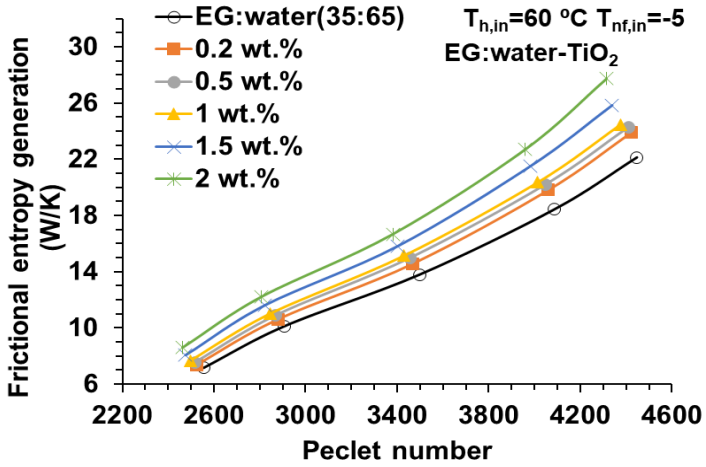

Fig. 4.85 Frictional entropy generation vs Peclet number for EG:water-TiO_2 nanofluid

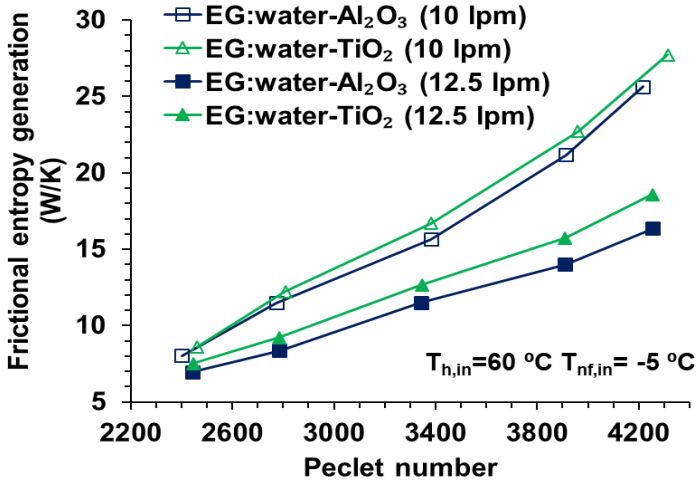

Fig. 4.86 Effect of nanoparticle materials on frictional entropy generation for varied Peclet number for EG:water nanofluid for two hot fluid rate at 2 wt.% concentration

4.5.3 Total entropy generation

The combined effect of TEG and FEG results in total entropy generation. Figs. 4.87 and 4.88 depict the overall entropy generation results for the nanofluid concentration at various Peclet numbers for two nanofluids. The total entropy generation decreases as the weight concentration of the nanofluid increases. The effect of TEG dominates the reduction of total entropy generation for the nanofluid. Total energy generation is reduced by 1.71%, 2.61%, 5.06%, 6.64% and 8.07% for concentrations of 0.2, 0.5, 1, 1.5, and 2 wt.% at Peclet numbers of 4392, 4348, 4314, 4258, and 4215 against the base fluid for Al_2O_3 nanofluid. Similarly, for TiO_2 nanofluid, the reduction in total entropy generation is 0.44%, 1.29%, 2.94%, 3.79% and 4.97%

for 0.2, 0.5, 1, 1.5, and 2 wt.% of concentration respectively at Peclet numbers of 4423, 4410, 4374, 4339 and 4314 against the base fluid. From a thermodynamic point of view, the system with lower entropy generation will have greater efficiency. TEG and FEG of nanofluids exhibit a decreasing and increasing trend in entropy generation for increased Peclet numbers for both nanofluids. As can be seen from the study (Fig. 4.87 and 4.88), for all concentrations, total entropy generation showed a descending trend at the investigated range of Peclet numbers. This shows that the nanofluid used in the PHE significantly reduces the generation of entropy. Fig. 4.89 shows the effect of two nanoparticle materials on total entropy generation for the varied Peclet numbers of nanofluid for two hot fluid rates (10 and 12.5 lpm) at 2 wt.% concentration for the lowest nanofluid inlet temperature. The combined effect of TEG and FEG shows that a significant reduction in total entropy can be obtained using Al_2O_3 nanofluids.

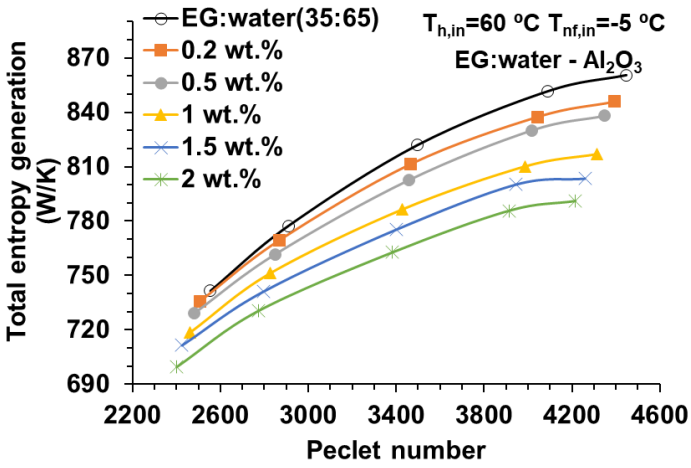

Fig. 4.87 Total entropy generation vs Peclet number for EG:water-Al_2O_3 nanofluid

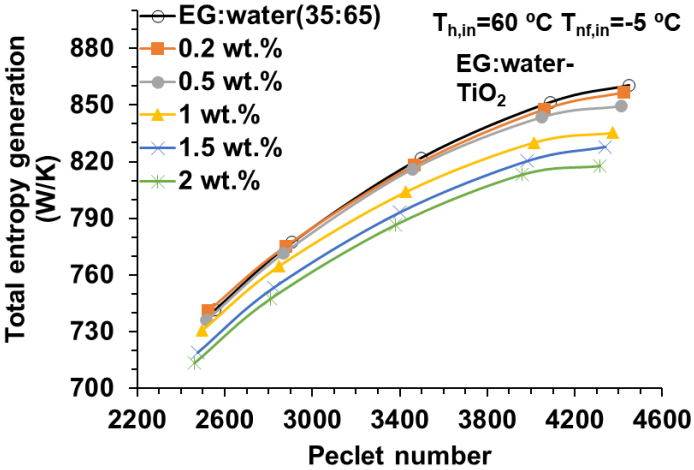

Fig. 4.88 Total entropy generation vs Peclet number for EG:water-TiO_2 nanofluid

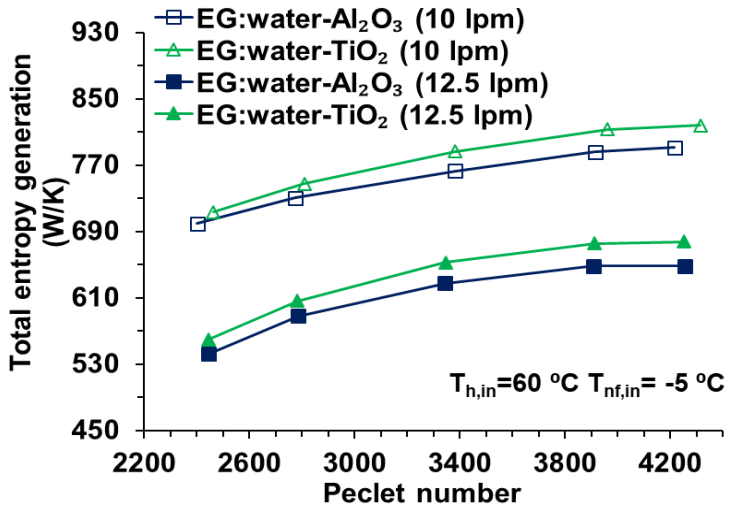

Fig. 4.89 Effect of nanoparticle materials on total entropy generation for varied Peclet number for EG:water nanofluid for two hot fluid rate at 2 wt.% concentration

4.5.4 Bejan number

The Bejan number is the ratio of TEG to the total entropy generation. The Bejan number (Eq. (3.25)) of the base fluid and nanofluids is presented in Figs.4.90 and 4.91 for different Peclet numbers of two nanofluids. From these figures, it can be observed that the Bejan number decreases as the Peclet number increases for the nanofluid and base fluid. The Bejan numbers obtained for the base fluid and nanofluid (2 wt.%) are 0.974 and 0.967, respectively, at Peclet numbers of 4447 and 4314 for Al_2O_3 nanofluids. Similarly, TiO_2 nanofluids, Bejan numbers found for the base fluid and nanofluid (2 wt.%) are 0.974 and 0.966, respectively, at Peclet numbers of 4447 and 4215. A higher Bejan number suggests that heat transfer generates more entropy than FEG and internal irreversibilities. The Bejan number value decreases as the Peclet number of the nanofluid increases due to increasing pressure drop and pumping power.

Fig. 4.92 shows the effect of two nanoparticle materials on Bejan number for the varied Peclet numbers of nanofluid for two hot fluid rates (10 and 12.5 lpm) at 2 wt.% concentration for the lowest nanofluid inlet temperature. From this figure, it is evident that the Al_2O_3 nanoparticles effect on TEG is greater compared to TiO_2.

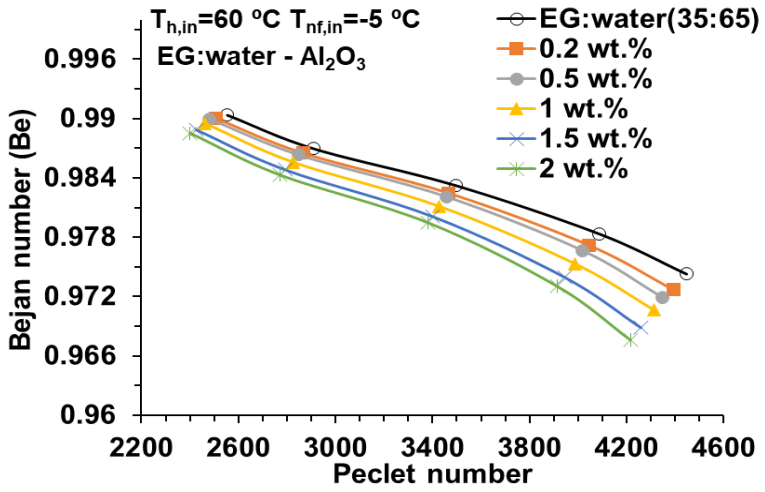

Fig. 4.90 Bejan number vs Peclet number for EG:water-Al_2O_3 nanofluid

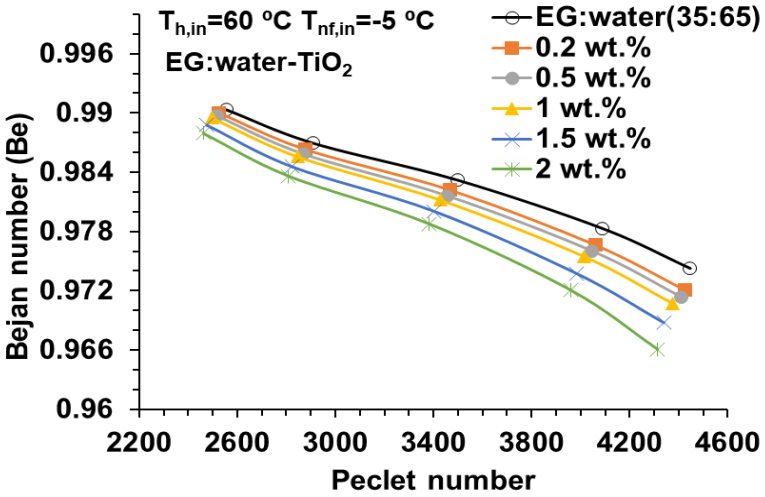

Fig. 4.91 Bejan number vs Peclet number for EG:water-TiO_2 nanofluid

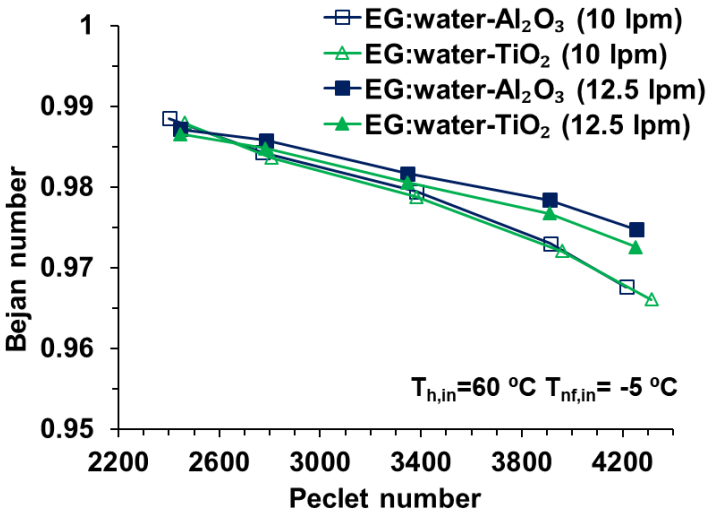

Fig. 4.92 Effect of nanoparticle materials on Bejan number for varied Peclet number for EG:water nanofluid for two hot fluid rate at 2 wt.% concentration

4.6 Performance index

The present study shows that the convective heat transfer coefficient increases with an increase in Peclet number and weight concentration. On the other hand, pressure drop also increases as a result of the addition of nanoparticles. Performance index was used to analyze the relative effect of heat transfer and fluid friction. The performance index is defined in the following form (Taghizadeh-Tabari et al., 2016).

$$PI = \frac{\frac{h_{nf}}{h_{bf}}}{\frac{\Delta p_{nf}}{\Delta p_{bf}}} = \frac{RE_h}{RE_{\Delta p}} \tag{4.1}$$

In above equation RE_h is the ratio of heat transfer enhancement by the application of nanofluid instead of EG:water (base fluid) and $RE_{\Delta p}$ is the ratio of nanofluid pressure drop to that of basefluid. A value of the performance index that is greater than 1 indicates that heat transfer enhancement is greater compared to the pressure drop increase, thereby indicating a favourable condition.

Figs. 4.93 and 4.94 depict the performance index obtained for three nanofluid inlet temperatures (20 ºC, 10 ºC and -5 ºC) of EG:water-Al_2O_3 nanofluid at different concentrations and Peclet number for two hot fluid rates respectively. It can be clearly noted from these two figures that for all concentrations of Al_2O_3 nanofluid, the performance index values are more than 1 for the two hot fluid flow rates. This shows the benefit of using Al_2O_3 nanofluids instead of EG:water (basefluid) for the heat transfer application.

Figs. 4.95 and 4.96 show the performance index obtained for the TiO_2 nanofluids at different concentrations and the Peclet number for three nanofluid inlet temperature conditions at two hot fluid flow rates, respectively. From the figures, it can be seen that at higher Peclet numbers with higher nanofluid inlet temperatures (20 °C) are beneficial for the practical use of nanofluids. However, at lower inlet temperatures, the effect of viscosity is more dominant and shows a performance index of less than 1. Hence, it can be concluded that Al_2O_3 nanofluids have shown superior thermal conductivity and lower viscosity compared to TiO_2 nanofluids, thus delivering more beneficial results at the inverstigated experimental conditions of the present study.

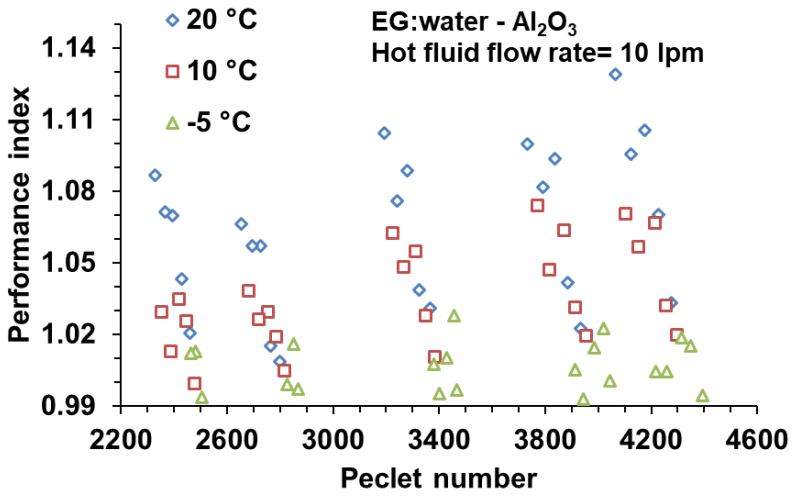

Fig. 4.93 Performance index versus Peclet number for EG:water- Al_2O_3 nanofluid for hot fluid rate of 10 lpm

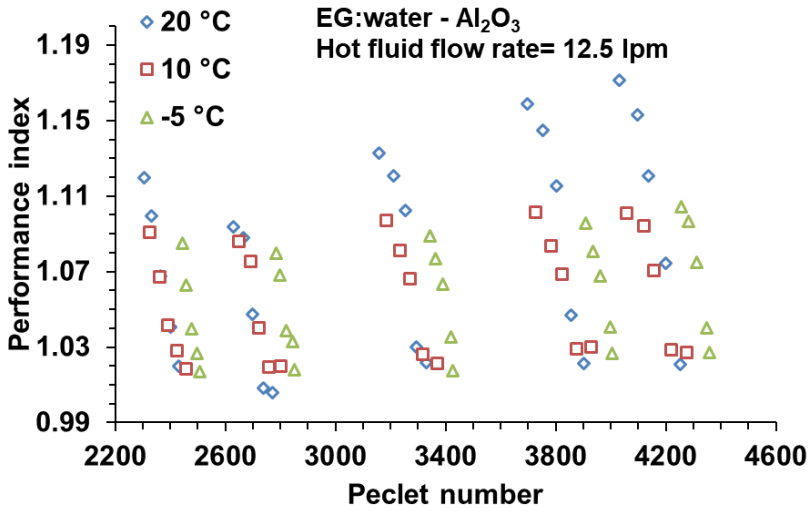

Fig. 4.94 Performance index versus Peclet number for EG:water- Al_2O_3 nanofluid for hot fluid rate of 12.5 lpm

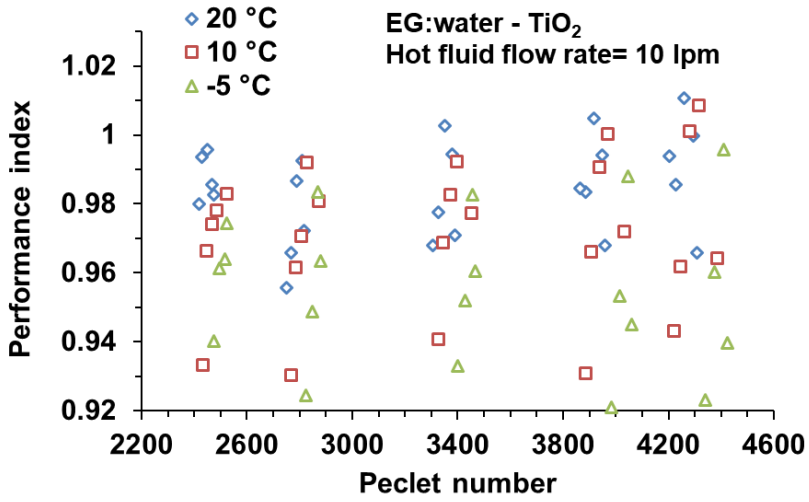

Fig. 4.95 Performance index versus Peclet number for EG:water- TiO_2 nanofluid for hot fluid rate of 10 lpm

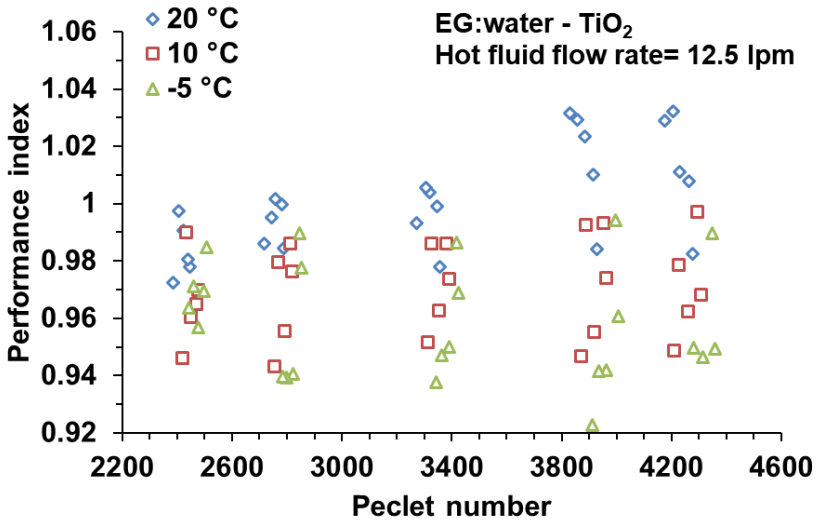

Fig. 4.96 Performance index versus Peclet number for EG:water- TiO_2 nanofluid for hot fluid rate of 12.5 lpm

4.7 Proposed correlation for Nusselt number

The Nusselt number of EG:water based nanofluids are developed based on the equations proposed by Saleh and Sundar (2021), Zheng et al. (2020), Bhattad et al. (2020) and Kanti et al. (2021). The mass velocity, hydraulic diameter, and viscosity of the cold fluid (EG: water or nanofluid) are used to determine the Reynolds number. The heat transfer coefficient of a nanofluid is calculated and converted into a non-dimensional Nusselt number based on the

overall heat transfer coefficient. Nusselt number of nanofluid is enhanced due to the increase in Reynolds number, Prandtl number, and volume concentration, then the below function is used to develop a correlation equation.

$$Nu = f(Re, Pr, \emptyset_v) \tag{4.2}$$

If the base fluid data is used for the equation, the term $\emptyset_v$ is replaced with $1 + \emptyset_v$, then Eq. (4.3) is written as

$$Nu = k_1 \, Re^m Pr^n \left(1 + \frac{\emptyset_v}{100}\right)^{k_2} \tag{4.3}$$

The above equation valid for the $80 < Re < 240$; $17 < Pr < 34$; $0 < \varphi < 0.53\%$. The constant *C* and the exponents *m, n* and *p* are estimated based on the non-linear regression analysis by considering the experimental results of present study. Table 4.25 shows the corresponding values of constants and performance values for the Al_2O_3 and TiO_2 nanofluids.

Figs. 4.97 and 4.98 show a comparison of the predicted Nusselt number by Eq. (4.3) with the experimental Nusselt number. Based on the experimental data of EG:water and nanofluid, the empirical formula was developed and shown to have a margin of deviation of -7.52% to 8.31% and -9.19% to 7.39% for Al_2O_3 and TiO_2 nanofluids respectively. It can be clearly noted that empirical correlation proposed in this work delivers predictions that are quite close to the experimental data for both nanofluids (Figs. 4.97 and 4.98).

Table 4.25 Constants, R^2 and adjusted R^2 values for Eq. (4.3)

Nanofluids	K_1	*m*	*n*	K_2	R^2	*Adjusted* R^2
EG:water - Al_2O_3	0.0235	0.792	0.975	31.02	0.952	0.951
EG:water - TiO_2	0.0232	0.797	0.969	27.29	0.957	0.956

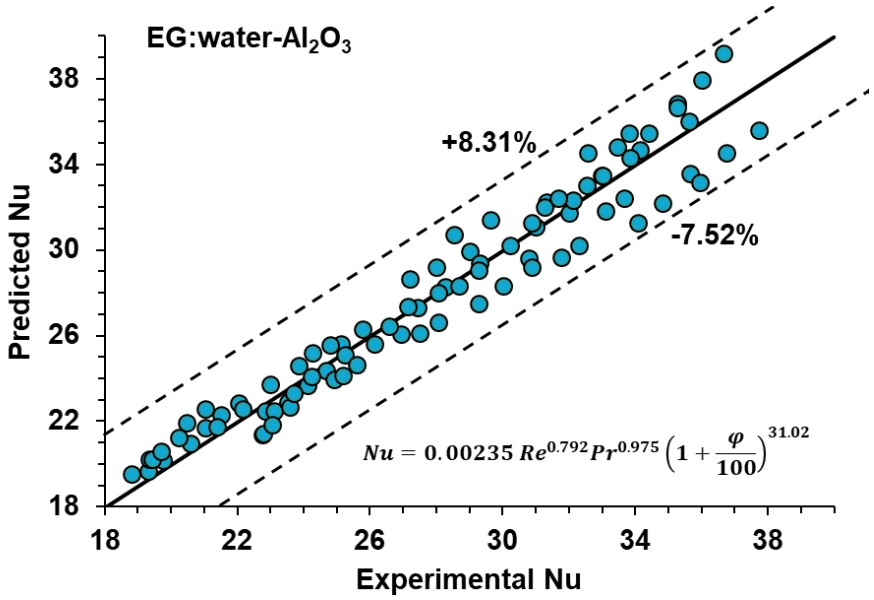

Fig. 4.97 Comparison between experimental and predicted Nusselt number for EG:water – Al_2O_3 nanofluids

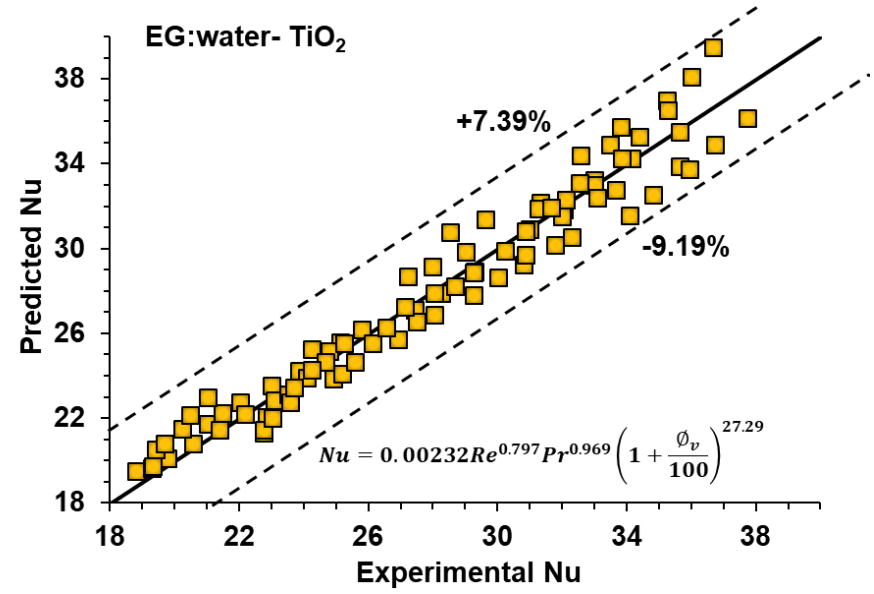

Fig. 4.98 Comparison between experimental and predicted Nusselt number for EG:water – TiO_2 nanofluids

Chapter 5 Conclusions and Future work

5.1 Conclusions

Studies have been carried out to investigate the heat transfer and entropy generation due to the addition of nanoparticles to EG:water (35v:65v) mixture. The following are the conclusions drawn from the study:

Thermophysical Properties:

- The thermal conductivity and effective thermal conductivity of nanofluids (EG:water-Al_2O_3 and TiO_2) increase with an increase in concentration and temperature for both nanopowder materials.
- The maximum enhancement obtained for Al_2O_3 and TiO_2 nanofluid was 9.29% and 4.86% at 55 °C for 2 wt.% concentration respectively compared to the base fluid.
- The addition of nanoparticles to the base fluid (EG:water) did not alter the characteristic behaviour of the fluid. It exhibited Newtonian behaviour over the investigated range of shear rate.
- The viscosity of nanofluids increased with an increase in nanofluid concentration and decreased with an increase in temperature.
- From the study, maximum increase in viscosity of 9.89% and 12.99% was found for Al_2O_3 and TiO_2 nanofluid at 5 °C for 2 wt.% of concentration respectively.
- Among two the nanofluids studied, EG:water - Al_2O_3 nanofluid was found to have superior properties, with the lowest viscosity and the highest effective thermal conductivity.
- Correlations developed by considering the experimental results showed satisfactory results. Whereas, generalized correlation showed relatively poor performance in prediction of effective thermal conductivity and relative viscosity of nanofluids.
- ANN and ANFIS models showed better agreement with the experimental results compared to empirical correlations developed using regression for the present experimental results and for the generalized correlations.

Heat Transfer Studies:

Heat transfer studies were carried out for heat transfer from nanofluid to water in a plate heat exchanger. Al_2O_3 and TiO_2 nanofluids have been used in the study.

- Addition of nanoparticles to a base fluid resulted in a significant improvement in heat transfer enhancement.
- Heat transfer rate, convective heat transfer coefficient, overall heat transfer coefficient and Nusselt number increase with increasing Peclet number and inlet temperature of nanofluid.
- Enhancement in heat transfer rates was 4.19% and 2.91% for Al_2O_3 and TiO_2 nanofluids respectively for nanofluid inlet temperature of -5 ºC 2 wt.% concentration at highest Peclet number.
- Enhancement in convective heat transfer coefficient was 18.26% and 11.99% for Al_2O_3 and TiO_2 nanofluid respectively for -5 ºC of nanofluid inlet temperature at 2 wt.% concentration at highest Peclet number.
- Enhancement in overall heat transfer coefficient was 11.99% and 8% for Al_2O_3 and TiO_2 nanofluid respectively for -5 ºC of nanofluid inlet temperature at 2 wt.% concentration at highest Peclet number. Higher overall heat transfer coefficient values lead to compact heat exchangers.
- Enhancement in Nusselt number was observed for both nanofluids shows remarkable potential for nanofluid as a cooling fluid to enhance heat transfer significantly for low temperature application.
- Effectiveness of heat exchangers can be improved by using nanofluids. The highest effectiveness of heat exchanger was found for EG:water-Al_2O_3
- Pressure drop and friction factor increased with the addition of nanoparticles. The result showed pumping power was increased by 16.05% and 25.48% for 2 wt.% concentration at -5 °C (nanofluid inlet temperature) for Al_2O_3 and TiO_2 nanofluids respectively at highest Peclet number.
- Performance index values were greater than 1 for Al_2O_3 nanofluids showing applicability of nanofluid for practical use.

- Correlation was developed for Nusselt number considering the Reynolds number, Prandtl number and concentration as variables. The correlation showed good agreement with the experimental results.

The thermal performance of a plate heat exchanger using Al_2O_3 and TiO_2 nanofluid has been evaluated in terms of the entropy generation when nanofluid used as cooling medium.

- Thermal entropy generation and frictional entropy generation were found to be decreasing and increasing trends, respectively, with an increase in weight concentration.
- The thermal entropy generation decreased by 8.69% and 5.77%; the frictional entropy generation increased by 15.58% and 25.08% at 2 wt.% of Al_2O_3 and TiO_2 nanofluid respectively compared to EG:water for the inlet temperature of -5 °C for the 2 wt.% concentration at highest Peclet number.
- The total entropy generation decreased by 8.07% and 4.97% at 2 wt.% of concentration for Al_2O_3 and TiO_2 nanofluid, respectively, compared to EG:water for the inlet temperature of -5 °C at highest Peclet number.
- According to the Bejan number found in the study, heat transfer effects are dominant in the generation of entropy.

5.2 Recommendations for Future work

The following are the scope for the future work and suggestion for improvement

1. In the present study, Al_2O_3 and TiO_2 nanoparticles of low volume concentrations were considered for the heat transfer analysis. Further experiments may be carried out by considering different hybrid nanofluids.
2. In the present study, only EG:water mixture of 35%/65% was considered for the heat transfer study. Studies for different base fluid mixture ratios may be carried out.
3. Different machine learning models approaches (support vector machines, decision tress and random forest) can be tried to further optimize the prediction of thermophysical properties of nanofluids.

References

Abdolbaqi, M.K., Sidik, N.A.C., Aziz, A., Mamat, R., Azmi, W.H., Yazid, M.N.A.W.M., Najafi, G., 2016. An experimental determination of thermal conductivity and viscosity of BioGlycol/water based TiO2 nanofluids. International Communications in Heat and Mass Transfer 77, 22–32.

Abdullah, M., Malik, S.R., Iqbal, M.H., Sajid, M.M., Shad, N.A., Hussain, S.Z., Razzaq, W., Javed, Y., 2018. Sedimentation and stabilization of nano-fluids with dispersant. Colloids and Surfaces A: Physicochemical and Engineering Aspects 554, 86–92.

Afzal, A., Yashawantha, K.M., Aslfattahi, N., Saidur, R., Abdul Razak, R.K., Subbiah, R., 2021. Back propagation modeling of shear stress and viscosity of aqueous Ionic-MXene nanofluids. Journal of Thermal Analysis and Calorimetry.

Ahmadi, M.H., Mohseni-Gharyehsafa, B., Farzaneh-Gord, M., Jilte, R.D., Kumar, R., Chau, K. wing, 2019. Applicability of connectionist methods to predict dynamic viscosity of silver/water nanofluid by using ANN-MLP, MARS and MPR algorithms. Engineering Applications of Computational Fluid Mechanics 13, 220–228.

Ahmadi Nadooshan, A., 2017. An experimental correlation approach for predicting thermal conductivity of water-EG based nanofluids of zinc oxide. Physica E: Low-dimensional Systems and Nanostructures 87, 15–19.

Akilu, S., Baheta, A.T., Sharma, K. V., 2020. Characterization and modelling of density, thermal conductivity, and viscosity of TiN–W/EG nanofluids. Journal of Thermal Analysis and Calorimetry 140, 1999–2010.

Al-Rashed, A.A.A.A., Ranjbarzadeh, R., Aghakhani, S., Soltanimehr, M., Afrand, M., Nguyen, T.K., 2019. Entropy generation of boehmite alumina nanofluid flow through a minichannel heat exchanger considering nanoparticle shape effect. Physica A: Statistical Mechanics and its Applications 521, 724–736.

Ali, A., Ilyas, S.U., Garg, S., Alsaady, M., Maqsood, K., Nasir, R., Abdulrahman, A., Zulfiqar, M., Mahfouz, A. Bin, Ahmed, A., Ridha, S., 2020. Dynamic viscosity of Titania nanotubes dispersions in ethylene glycol/water-based nanofluids: Experimental evaluation and predictions from empirical correlation and artificial neural network. International Communications in Heat and Mass Transfer 118, 104882.

Ali, A.R.I., Salam, B., 2020. A review on nanofluid: preparation, stability, thermophysical properties, heat transfer characteristics and application. SN Applied Sciences 2, 1–17.

Alrashed, A.A.A.A., Gharibdousti, M.S., Goodarzi, M., de Oliveira, L.R., Safaei, M.R., Bandarra Filho, E.P., 2018. Effects on thermophysical properties of carbon based nanofluids: Experimental data, modelling using regression, ANFIS and ANN. International Journal of Heat and Mass Transfer 125, 920–932.

Andrew Bagnell, J., 2005. Robust supervised learning. Proceedings of the National Conference on Artificial Intelligence 2, 714–719.

Ariana, M.A., Vaferi, B., Karimi, G., 2015. Prediction of thermal conductivity of alumina water-based nanofluids by artificial neural networks. Powder Technology 278, 1–10.

Arya, H., Sarafraz, M.M., Arjomandi, M., 2018. Heat transfer and fluid flow of MgO/ethylene glycol in a corrugated heat exchanger. Journal of Mechanical Science and Technology 32, 3975–3982.

Asadi, A., Asadi, M., Siahmargoi, M., Asadi, T., Gholami Andarati, M., 2017. The effect of surfactant and sonication time on the stability and thermal conductivity of water-based nanofluid containing Mg(OH)2 nanoparticles: An experimental investigation. International Journal of Heat and Mass Transfer 108, 191–198.

ASHRAE, 2017. Handbook - Fundamentals (SI Edition), American Society of Heating, Refrigerating and Air-Conditioning Engineers, Inc.

Aylı, E., 2020. Modeling of mixed convection in an enclosure using multiple regression, artificial neural network, and adaptive neuro-fuzzy interface system models. Proceedings of the Institution of Mechanical Engineers, Part C: Journal of Mechanical Engineering Science 234, 3078–3093.

Azmi, W.H., Abdul Hamid, K., Mamat, R., Sharma, K.V., Mohamad, M.S., 2016. Effects of working temperature on thermo-physical properties and forced convection heat transfer of TiO 2 nanofluids in water – Ethylene glycol mixture. Applied Thermal Engineering 106, 1190–1199.

Azmi, W. H., Sharma, K. V., Mamat, R., Najafi, G., Mohamad, M.S., 2016. The enhancement of effective thermal conductivity and effective dynamic viscosity of nanofluids - A review. Renewable and Sustainable Energy Reviews 53, 1046–1058.

Baghban, A., Jalali, A., Shafiee, M., Ahmadi, M.H., Chau, K. wing, 2019. Developing an ANFIS-based swarm concept model for estimating the relative viscosity of nanofluids. Engineering Applications of Computational Fluid Mechanics 13, 26–39.

Bahiraei, M., Heshmatian, S., Moayedi, H., 2019. Artificial intelligence in the field of nanofluids: A review on applications and potential future directions. Powder Technology 353, 276–301.

Barbés, B., Páramo, R., Blanco, E., Casanova, C., 2014. Thermal conductivity and specific heat capacity measurements of CuO nanofluids. Journal of Thermal Analysis and Calorimetry 115, 1883–1891.

Barbés, B., Páramo, R., Blanco, E., Pastoriza-Gallego, M.J., Piñeiro, M.M., Legido, J.L., Casanova, C., 2013. Thermal conductivity and specific heat capacity measurements of Al 2O3 nanofluids. Journal of Thermal Analysis and Calorimetry 111, 1615–1625.

Batchelor, G.., 1977. The effect of Brownian motion on the bulk stress in a suspension of spherical particles. Journal of Fluid Mechanics 83, 97–117.

Behrangzade, A., Heyhat, M.M., 2016. The effect of using nano-silver dispersed water based nanofluid as a passive method for energy efficiency enhancement in a plate heat exchanger. Applied Thermal Engineering 102, 311–317.

Bejan, A., 1987. The thermodynamic design of heat and mass transfer processes and devices. International Journal of Heat and Fluid Flow 8, 258–276.

Bejan, A., 1980. Second law analysis in heat transfer. Energy 5, 720–732.

Bhattacharya, P., Saha, S.K., Yadav, A., Phelan, P.E., Prasher, R.S., 2004. Brownian dynamics simulation to determine the effective thermal conductivity of nanofluids. Journal of Applied Physics 95, 6492–6494.

Bhattad, A., Sarkar, J., Ghosh, P., 2020. Hydrothermal performance of different alumina hybrid nanofluid types in plate heat exchanger: Experimental study. Journal of Thermal Analysis and Calorimetry 139, 3777–3787.

Brinkman, H.C., 1952. The viscosity of concentrated suspensions and solutions. The Journal of Chemical Physics 20, 571.

Butt, A.S., Ali, A., 2013. Thermodynamical Analysis of the Flow and Heat Transfer over a Static and a Moving Wedge. ISRN Thermodynamics 2013, 1–6.

Cabaleiro, D., Gracia-Fernández, C., Legido, J.L., Lugo, L., 2015. Specific heat of metal oxide nanofluids at high concentrations for heat transfer. International Journal of Heat and Mass Transfer 88, 872–879.

Chakraborty, S., Panigrahi, P.K., 2020. Stability of nanofluid: A review. Applied Thermal

Engineering 174.

Chandrasekar, M., Suresh, S., Bose, A.C., 2010. Experimental investigations and theoretical determination of thermal conductivity and viscosity of Al2O3/water nanofluid. Experimental Thermal and Fluid Science 34, 210–216.

Chen, H., Ding, Y., Tan, C., 2007. Rheological behaviour of nanofluids. New Journal of Physics 9.

Chiam, H.W., Azmi, W.H., Usri, N.A., Mamat, R., Adam, N.M., 2017. Thermal conductivity and viscosity of Al2O3 nanofluids for different based ratio of water and ethylene glycol mixture. Experimental Thermal and Fluid Science 81, 420–429.

Choi, S.U.S., Eastman, J.A., 1995. Enhancing thermal conductivity of fluids with nanoparticles, in: ASME International Mechanical Engineering Congress & Exposition.

Choi, S.U.S., Li, S., Eastman, J.A., 1999. Measuring thermal conductivity of fluids containing oxide nanoparticles. Journal of Heat Transfer 121, 280–289.

Choudhary, R., Khurana, D., Kumar, A., Subudhi, S., 2017. Stability analysis of Al2O3/water nanofluids. Journal of Experimental Nanoscience 12, 140–151.

Dewan, A., Mahanta, P., Raju, K.S., Suresh Kumar, P., 2004. Review of passive heat transfer augmentation techniques. Proceedings of the Institution of Mechanical Engineers, Part A: Journal of Power and Energy 218, 509–527.

Dey, D., Kumar, P., Samantaray, S., 2017. A review of nanofluid preparation, stability, and thermo-physical properties. Heat Transfer - Asian Research 46, 1413–1442.

Duangthongsuk, W., Wongwises, S., 2009. Measurement of temperature-dependent thermal conductivity and viscosity of TiO2-water nanofluids. Experimental Thermal and Fluid Science 33, 706–714.

Durmuş, A., Benli, H., Kurtbaş, İ., Gül, H., 2009. Investigation of heat transfer and pressure drop in plate heat exchangers having different surface profiles. International Journal of Heat and Mass Transfer 52, 1451–1457.

Eastman, J.A., Choi, S.U.S., Li, S., Yu, W., Thompson, L.J., 2001. Anomalously increased effective thermal conductivities of ethylene glycol-based nanofluids containing copper nanoparticles. Applied Physics Letters 78, 718–720.

Eastman, J.A., Choi, U.S., Li, S., Thompson, L.J., Lee, S., 1997. Enhanced thermal conductivity through the development of nanofluids, in: Materials Research Society Symposium -

Proceedings. pp. 3–11.

Einstein, A., 1906. Eine neue Bestimmung der Moleküldimensionen. Annalen der Physik 324, 289–306.

Elias, M.M., Mahbubul, I.M., Saidur, R., Sohel, M.R., Shahrul, I.M., Khaleduzzaman, S.S., Sadeghipour, S., 2014. Experimental investigation on the thermo-physical properties of Al2O3 nanoparticles suspended in car radiator coolant. International Communications in Heat and Mass Transfer 54, 48–53.

Fedele, L., Colla, L., Bobbo, S., 2012. Viscosity and thermal conductivity measurements of water-based nanofluids containing titanium oxide nanoparticles. International Journal of Refrigeration 35, 1359–1366.

Fuskele, V., Sarviya, R.M., 2017. Recent developments in Nanoparticles Synthesis, Preparation and Stability of Nanofluids. Materials Today: Proceedings 4, 4049–4060.

Ghadimi, A., Metselaar, I.H., 2013. The influence of surfactant and ultrasonic processing on improvement of stability, thermal conductivity and viscosity of titania nanofluid. Experimental Thermal and Fluid Science 51, 1–9.

Ghadimi, A., Saidur, R., Metselaar, H.S.C., 2011. A review of nanofluid stability properties and characterization in stationary conditions. International Journal of Heat and Mass Transfer 54, 4051–4068.

Goodarzi, M., Amiri, A., Goodarzi, M.S., Safaei, M.R., Karimipour, A., Languri, E.M., Dahari, M., 2015. Investigation of heat transfer and pressure drop of a counter flow corrugated plate heat exchanger using MWCNT based nanofluids. International Communications in Heat and Mass Transfer.

Gut, J.A.W., Pinto, J.M., 2004. Optimal configuration design for plate heat exchangers. International Journal of Heat and Mass Transfer 47, 4833–4848.

Gut, J.A.W., Pinto, J.M., 2003. Modeling of plate heat exchangers with generalized configurations. International Journal of Heat and Mass Transfer 46, 2571–2585.

Haghighi, E.B., Nikkam, N., Saleemi, M., Behi, M., Mirmohammadi, S.A., Poth, H., Khodabandeh, R., Toprak, M.S., Muhammed, M., Palm, B., 2013. Shelf stability of nanofluids and its effect on thermal conductivity and viscosity. Measurement Science and Technology 24.

Hamid, K.A., Azmi, W.H., Mamat, R., Usri, N.A., 2016. Thermal conductivity enhancement

of TiO 2 nanofluid in water and ethylene glycol (EG) mixture. Indian Journal of Pure & Applied Physics 54, 651–655.

Hamid, K.A., Azmi, W.H., Mamat, R., Usri, N.A., Najafi, G., 2015. Investigation of Al2O3 Nanofluid Viscosity for Different Water / EG Mixture Based. Energy Procedia 79, 354–359.

Hamilton, R.L., Crosser, O.K., 1962. Thermal Conductivity of Heterogeneous Two-Component Systems. Industrial & Engineering Chemistry Fundamentals 1, 187–191.

Han, X.-H., Cui, L.-Q., Chen, S.-J., Chen, G.-M., Wang, Q., 2010. A numerical and experimental study of chevron, corrugated-plate heat exchangers. International Communications in Heat and Mass Transfer 37, 1008–1014.

Hemmat Esfe, M., 2018. Thermal conductivity modeling of aqueous CuO nanofluids by adaptive neuro-fuzzy inference system (ANFIS) using experimental data. Periodica Polytechnica Chemical Engineering 62, 202–208.

Hemmat Esfe, M., Afrand, M., Yan, W.M., Akbari, M., 2015a. Applicability of artificial neural network and nonlinear regression to predict thermal conductivity modeling of Al2O3-water nanofluids using experimental data. International Communications in Heat and Mass Transfer 66, 246–249.

Hemmat Esfe, M., Rostamian, H., Afrand, M., Karimipour, A., Hassani, M., 2015b. Modeling and estimation of thermal conductivity of MgO–water/EG (60:40) by artificial neural network and correlation. International Communications in Heat and Mass Transfer 68, 98–103.

Hemmat Esfe, M., Saedodin, S., Akbari, M., Karimipour, A., Afrand, M., Wongwises, S., Safaei, M.R., Dahari, M., 2015c. Experimental investigation and development of new correlations for thermal conductivity of CuO/EG-water nanofluid. International Communications in Heat and Mass Transfer 65, 47–51.

Hemmat Esfe, M., Saedodin, S., Asadi, A., Karimipour, A., 2015d. Thermal conductivity and viscosity of Mg(OH)2-ethylene glycol nanofluids. Journal of Thermal Analysis and Calorimetry 120, 1145–1149.

Hemmat Esfe, M., Saedodin, S., Bahiraei, M., Toghraie, D., Mahian, O., Wongwises, S., 2014. Thermal conductivity modeling of MgO/EG nanofluids using experimental data and artificial neural network. Journal of Thermal Analysis and Calorimetry 118, 287–294.

Heyhat, M.M., Kowsary, F., Rashidi, A.M., Alem Varzane Esfehani, S., Amrollahi, A., 2012. Experimental investigation of turbulent flow and convective heat transfer characteristics of alumina water nanofluids in fully developed flow regime. International Communications in Heat and Mass Transfer 39, 1272–1278.

Ho, C.J., Liu, W.K., Chang, Y.S., Lin, C.C., 2010. Natural convection heat transfer of alumina-water nanofluid in vertical square enclosures: An experimental study. International Journal of Thermal Sciences 49, 1345–1353.

Hojjat, M., Etemad, S.G., Bagheri, R., Thibault, J., 2011. Thermal conductivity of non-Newtonian nanofluids: Experimental data and modeling using neural network. International Journal of Heat and Mass Transfer 54, 1017–1023.

Huang, D., Wu, Z., Sunden, B., 2015. Pressure drop and convective heat transfer of Al2O3/water and MWCNT/water nanofluids in a chevron plate heat exchanger. International Journal of Heat and Mass Transfer 89, 620–626.

Huminic, G., Huminic, A., 2018. The heat transfer performances and entropy generation analysis of hybrid nanofluids in a flattened tube. International Journal of Heat and Mass Transfer 119, 813–827.

Huminic, G., Huminic, A., 2012. Application of nanofluids in heat exchangers: A review. Renewable and Sustainable Energy Reviews 16, 5625–5638.

Hwang, Y., Lee, Jae Keun, Lee, Jong Ku, Jeong, Y.M., Cheong, S. ir, Ahn, Y.C., Kim, S.H., 2008. Production and dispersion stability of nanoparticles in nanofluids. Powder Technology 186, 145–153.

Hwang, Y.J., Ahn, Y.C., Shin, H.S., Lee, C.G., Kim, G.T., Park, H.S., Lee, J.K., 2006. Investigation on characteristics of thermal conductivity enhancement of nanofluids. Current Applied Physics 6, 1068–1071.

Jama, M., Singh, T., Gamaleldin, S.M., Koc, M., Samara, A., Isaifan, R.J., Atieh, M.A., 2016. Critical Review on Nanofluids : Preparation , Characterization , and Applications. Journal of Nanomaterials 1–23.

Jang, R.J.-S., 1991. Fuzzy Modeling Using Generalized Neural Networks and Kalman Filter Algorithm. Proceedings of the 9th National Conference on Artificial Intelligence 91, 762–767.

Javadi, F.S., Sadeghipour, S., Saidur, R., BoroumandJazi, G., Rahmati, B., Elias, M.M., Sohel,

M.R., 2013. The effects of nanofluid on thermophysical properties and heat transfer characteristics of a plate heat exchanger. International Communications in Heat and Mass Transfer 44, 58–63.

Ji, J., Lu, W., Si, C., Zhang, S., Yao, X., Wang, W., Chu, D., 2020. Overview on the Preparation and Heat Transfer Enhancement of Nanofluids. Journal of Physics: Conference Series 1637.

Kabeel, A.E., Abou El Maaty, T., El Samadony, Y., 2013. The effect of using nano-particles on corrugated plate heat exchanger performance. Applied Thermal Engineering 52, 221–229.

Kakac, S., Liu, H.H., 2003. Heat Exchangers selection,Rating, and thermal design, Second Edi. ed. CRC PRESS.

Kanti, P., Sharma, K. V., Ramachandra, C.G., Panitapu, B., 2020a. Stability and thermophysical properties of fly ash nanofluid for heat transfer applications. Heat Transfer 49, 4722–4737.

Kanti, P., Sharma, K. V., Revanasiddappa, M., Ramachandra, C.G., Akilu, S., 2020b. Thermophysical properties of fly ash–Cu hybrid nanofluid for heat transfer applications. Heat Transfer 49, 4491–4510.

Kanti, P., Sharma, K. V., Said, Z., Bellos, E., 2021. Numerical study on the thermo-hydraulic performance analysis of fly ash nanofluid. Journal of Thermal Analysis and Calorimetry.

Khairul, M.A., Alim, M.A., Mahbubul, I.M., Saidur, R., Hepbasli, A., Hossain, A., 2013. Heat transfer performance and exergy analyses of a corrugated plate heat exchanger using metal oxide nanofluids. International Communications in Heat and Mass Transfer 50, 8–14.

Khan, T.S., Khan, M.S., Chyu, M.C., Ayub, Z.H., Chattha, J.A., 2009. Review of heat transfer and pressure drop correlations for evaporation of fluid flow in plate heat exchangers (RP-1352). HVAC and R Research 15, 169–188.

Khdher, A.M., Sidik, N.A.C., Hamzah, W.A.W., Mamat, R., 2016. An experimental determination of thermal conductivity and electrical conductivity of bio glycol based Al2O3 nanofluids and development of new correlation. International Communications in Heat and Mass Transfer 73, 75–83.

Khedkar, R.S., Shrivastava, N., Sonawane, S.S., Wasewar, K.L., 2016. Experimental investigations and theoretical determination of thermal conductivity and viscosity of TiO 2 –ethylene glycol nanofluid. International Communications in Heat and Mass Transfer

73, 54–61.

Khosravi-Bizhaem, H., Abbassi, A., Salimpour, M.R., Zivari-Ravan, A., 2021. Experimental study on heat transfer, entropy generation, and exergy destruction of Ag, MWCNT, and GO water-based nanofluids in helical tubes. Journal of Thermal Analysis and Calorimetry.

Kole, M., Dey, T.K., 2013. Investigation of thermal conductivity, viscosity, and electrical conductivity of graphene based nanofluids. Journal of Applied Physics 113, 084307.

Kotsiantis, S.B., Zaharakis, I.D., Pintelas, P.E., 2006. Machine learning: a review of classification and combining techniques. Artificial Intelligence Review 26, 159–190.

Krishnakumar, T.S., Sheeba, A., Mahesh, V., Jose Prakash, M., 2019. Heat transfer studies on ethylene glycol/water nanofluid containing TiO2 nanoparticles. International Journal of Refrigeration 102, 55–61.

Kulkarni, D.P., Das, D.K., Chukwu, G.A., 2006. Temperature Dependent Rheological Property of Copper Oxide Nanoparticles Suspension (Nanofluid). Journal of Nanoscience and Nanotechnology 6, 1–5.

Kumar, B., Singh, S.N., 2017. Study of pressure drop in single pass U-type plate heat exchanger. Experimental Thermal and Fluid Science 87, 40–49.

Kumar, V., Tiwari, A.K., Ghosh, S.K., 2017. Characterization and performance of nanofluids in plate heat exchanger, in: Materials Today: Proceedings. pp. 4070–4078.

Kumar, V., Tiwari, A.K., Ghosh, S.K., 2015. Application of nanofluids in plate heat exchanger: A review. Energy Conversion and Management 105, 1017–1036.

Kurt, H., Kayfeci, M., 2009. Prediction of thermal conductivity of ethylene glycol-water solutions by using artificial neural networks. Applied Energy 86, 2244–2248.

Kwak, K., Kim, C., 2005. Viscosity and thermal conductivity of copper oxide nanofluid dispersed in ethylene glycol. Korea Australia Rheology Journal 17, 35–40.

Lee, J.-H., Lee, S.-H., Choi, C., Jang, S., Choi, S., 2010. A Review of Thermal Conductivity Data, Mechanisms and Models for Nanofluids. International Journal of Micro-Nano Scale Transport 1, 269–322.

Leong, K.Y., Najwa, Z.A., Ku Ahmad, K.Z., Ong, H.C., 2017. Investigation on Stability and Optical Properties of Titanium Dioxide and Aluminum Oxide Water-Based Nanofluids. International Journal of Thermophysics 38, 1–15.

Li, H., Wang, L., He, Y., Hu, Y., Zhu, J., Jiang, B., 2015. Experimental investigation of thermal

conductivity and viscosity of ethylene glycol based ZnO nanofluids. Applied Thermal Engineering 88, 363–368.

Li, X., Zou, C., Wang, T., Lei, X., 2015. Rheological behavior of ethylene glycol-based SiC nanofluids. International Journal of Heat and Mass Transfer 84, 925–930.

Li, Y., Fernández-Seara, J., Du, K., Pardiñas, Á.Á., Latas, L.L., Jiang, W., 2016. Experimental investigation on heat transfer and pressure drop of ZnO/ethylene glycol-water nanofluids in transition flow. Applied Thermal Engineering 93, 537–548.

Liang, Z., Tsai, H.L., 2011. Thermal conductivity of interfacial layers in nanofluids. Physical Review E - Statistical, Nonlinear, and Soft Matter Physics 83, 1–8.

Longo, G.A., Zilio, C., Ceseracciu, E., Reggiani, M., 2012. Application of Artificial Neural Network (ANN) for the prediction of thermal conductivity of oxide–water nanofluids. Nano Energy 1, 290–296.

LotfizadehDehkordi, B., Kazi, S.N., Hamdi, M., Ghadimi, A., Sadeghinezhad, E., Metselaar, H.S.C., 2013. Investigation of viscosity and thermal conductivity of alumina nanofluids with addition of SDBS. Heat and Mass Transfer 49, 1109–1115.

Lu, S.-Y., Lin, H., 1996. Effective conductivity of composites containing aligned spheroidal inclusions of finite conductivity. Journal of Applied Physics 79, 6761–6769.

Mahbubul, I.M., Saidur, R., Amalina, M.A., 2012. Latest developments on the viscosity of nanofluids. International Journal of Heat and Mass Transfer 55, 874–885.

Mahbubul, I.M., Saidur, R., Amalina, M.A., Elcioglu, E.B., Okutucu-Ozyurt, T., 2015. Effective ultrasonication process for better colloidal dispersion of nanofluid. Ultrasonics Sonochemistry 26, 361–369.

Mahian, O., Kianifar, A., Kleinstreuer, C., Al-Nimr, M.A., Pop, I., Sahin, A.Z., Wongwises, S., 2013. A review of entropy generation in nanofluid flow. International Journal of Heat and Mass Transfer 65, 514–532.

Maxwell, J.C., 1873. Electricity and Magnetism. Clarendon, Oxford, UK.

Mehrabi, M., Sharifpur, M., Meyer, J.P., 2012. Application of the FCM-based neuro-fuzzy inference system and genetic algorithm-polynomial neural network approaches to modelling the thermal conductivity of alumina-water nanofluids. International Communications in Heat and Mass Transfer 39, 971–977.

Meyer, J.P., Adio, S. a., Sharifpur, M., Nwosu, P.N., 2015. The viscosity of nanofluids: a review

of the theoretical, empirical and numerical models. Heat Transfer Engineering 7632, 00–00.

Mishra, P.C., Mukherjee, S., Nayak, S.K., Panda, A., 2014. A brief review on viscosity of nanofluids. International Nano Letters 4, 109–120.

Moffat, R.J., 1988. Describing the uncertainties in experimental results. Experimental Thermal and Fluid Science 1, 3–17.

Mojarrad, M.S., Keshavarz, A., Ziabasharhagh, M., Raznahan, M.M., 2014. Experimental investigation on heat transfer enhancement of alumina/water and alumina/water-ethylene glycol nanofluids in thermally developing laminar flow. Experimental Thermal and Fluid Science 53, 111–118.

Mondragón, R., Segarra, C., Martínez-Cuenca, R., Juliá, J.E., Jarque, J.C., 2013. Experimental characterization and modeling of thermophysical properties of nanofluids at high temperature conditions for heat transfer applications. Powder Technology 249, 516–529.

Mukherjee, S., Panda, S.R., Mishra, P.C., Chaudhuri, P., 2020. Enhancing Thermophysical Characteristics and Heat Transfer Potential of TiO2/Water Nanofluid, International Journal of Thermophysics. Springer US.

Murshed, S.M.S., Estellé, P., 2017. A state of the art review on viscosity of nanofluids. Renewable and Sustainable Energy Reviews 76, 1134–1152.

Nagarajan, P.K., Subramani, J., Suyambazhahan, S., Sathyamurthy, R., 2014. Nanofluids for solar collector applications: A review. Energy Procedia 61, 2416–2434.

Naik, B.A.K., Vinod, A. V, 2018. Rheological Behavior and Effective Thermal Conductivity of Non-Newtonian Nanofluids. Journal of Testing and Evaluation 46, 445–457.

Namburu, P. K., Kulkarni, D.P., Dandekar, A., Das, D.K., 2007. Experimental investigation of viscosity and specific heat of silicon dioxide nanofluids. Micro and Nano Letters 2, 67–71.

Namburu, Praveen K., Kulkarni, D.P., Misra, D., Das, D.K., 2007. Viscosity of copper oxide nanoparticles dispersed in ethylene glycol and water mixture. Experimental Thermal and Fluid Science 32, 397–402.

O'Hanley, H., Buongiorno, J., McKrell, T., Hu, L.W., 2011. Measurement and model correlation of specific heat capacity of water-based nanofluids with silica, alumina and copper oxide nanoparticles. ASME 2011 International Mechanical Engineering Congress

and Exposition, IMECE 2011 10, 1209–1214.

Özerinç, S., Kakaç, S., YazIcIoğlu, A.G., 2010. Enhanced thermal conductivity of nanofluids: A state-of-the-art review. Microfluidics and Nanofluidics 8, 145–170.

Pak, B.C., Cho, Y.I., 1998. Hydrodynamic and heat transfer study of dispersed fluids with submicron metallic oxide particles. Experimental Heat Transfer 11, 151–170.

Pandey, S.D., Nema, V.K., 2012. Experimental analysis of heat transfer and friction factor of nanofluid as a coolant in a corrugated plate heat exchanger. Experimental Thermal and Fluid Science 38, 24–256.

Parashar, N., Seraj, M., Yahya, S.M., Anas, M., 2020. Development of an artificial neural network for the prediction of relative viscosity of ethylene glycol based nanofluids. SN Applied Sciences 2, 1473.

Pastoriza-Gallego, M.J., Lugo, L., Legido, J.L., Piñeiro, M.M., 2011. Rheological non-newtonian behaviour of ethylene glycol-based fe 2o 3 nanofluids. Nanoscale Research Letters 6, 1–7.

Patel, H.E., Sundararajan, T., Das, S.K., 2010. An experimental investigation into the thermal conductivity enhancement in oxide and metallic nanofluids. Journal of Nanoparticle Research 12, 1015–1031.

Paul, G., Chopkar, M., Manna, I., Das, P.K., 2010. Techniques for measuring the thermal conductivity of nanofluids: A review. Renewable and Sustainable Energy Reviews 14, 1913–1924.

Perry, R.H., Green, D.W., 2008. Perry's Chemical Engineers' Handbook, McGraw-Hill.

Popa, C.V., Nguyen, C.T., Gherasim, I., 2017. New specific heat data for Al2O3 and CuO nanoparticles in suspension in water and Ethylene Glycol. International Journal of Thermal Sciences 111, 108–115.

Pourhoseini, S.H., Naghizadeh, N., Hoseinzadeh, H., 2018. Effect of silver-water nanofluid on heat transfer performance of a plate heat exchanger: An experimental and theoretical study. Powder Technology 332, 279–286.

Qiu, L., Zhu, N., Feng, Y., Michaelides, E.E., Żyła, G., Jing, D., Zhang, X., Norris, P.M., Markides, C.N., Mahian, O., 2020. A review of recent advances in thermophysical properties at the nanoscale: From solid state to colloids. Physics Reports 843, 1–81.

Ramezanizadeh, M., Ahmadi, M.H., Nazari, M.A., Sadeghzadeh, M., Chen, L., 2019a. A

review on the utilized machine learning approaches for modeling the dynamic viscosity of nanofluids. Renewable and Sustainable Energy Reviews 114, 109345.

Ramezanizadeh, M., Alhuyi Nazari, M., Ahmadi, M.H., Lorenzini, G., Pop, I., 2019b. A review on the applications of intelligence methods in predicting thermal conductivity of nanofluids. Journal of Thermal Analysis and Calorimetry 138, 827–843.

Rashmi, W., Ismail, A.F., Sopyan, I., Jameel, A.T., Yusof, F., Khalid, M., Mubarak, N.M., 2011. Stability and thermal conductivity enhancement of carbon nanotube nanofluid using gum arabic. Journal of Experimental Nanoscience 6, 567–579.

Ray, D.R., Das, D.K., Vajjha, R.S., 2014. Experimental and numerical investigations of nanofluids performance in a compact minichannel plate heat exchanger. International Journal of Heat and Mass Transfer 71, 732–746.

Razavi, R., Sabaghmoghadam, A., Bemani, A., Baghban, A., Chau, K. wing, Salwana, E., 2019. Application of ANFIS and LSSVM strategies for estimating thermal conductivity enhancement of metal and metal oxide based nanofluids. Engineering Applications of Computational Fluid Mechanics 13, 560–578.

Reddy, M.C.S., Rao, V.V., 2013. Experimental studies on thermal conductivity of blends of ethylene glycol-water-based TiO2 nanofluids. International Communications in Heat and Mass Transfer 46, 31–36.

Sadeghi, R., Etemad, S.G., Keshavarzi, E., Haghshenasfard, M., 2015. Investigation of alumina nanofluid stability by UV--vis spectrum. Microfluidics and Nanofluidics 18, 1023–1030.

Sadi, M., 2017. Prediction of Thermal Conductivity and Viscosity of Ionic Liquid-Based Nanofluids Using Adaptive Neuro Fuzzy Inference System. Heat Transfer Engineering 38, 1561–1572.

Şahin, M., Erol, R., 2017. A Comparative Study of Neural Networks and ANFIS for Forecasting Attendance Rate of Soccer Games. Mathematical and Computational Applications 22, 43.

Sahoo, B.C., Vajjha, R.S., Ganguli, R., Chukwu, G.A., Das, D.K., 2009. Determination of rheological behavior of aluminum oxide nanofluid and development of new viscosity correlations. Petroleum Science and Technology 27, 1757–1770.

Sahooli, M., Sabbaghi, S., Shariaty Niassar, M., 2012. Preparation of CuO/Water Nanofluids Using Polyvinylpyrolidone and a Survey on Its Stability and Thermal Conductivity. Int J Nanosci Nanotechnol 8, 27–34.

Saidur, R., Leong, K.Y., Mohammed, H.A., 2011. A review on applications and challenges of nanofluids. Renewable and Sustainable Energy Reviews 15, 1646–1668.

Saleh, B., Sundar, L.S., 2021. Experimental study on heat transfer, friction factor, entropy and exergy efficiency analyses of a corrugated plate heat exchanger using Ni/water nanofluids. International Journal of Thermal Sciences 165, 106935.

Sarafraz, M.M., Nikkhah, V., Madani, S.A., Jafarian, M., Hormozi, F., 2017. Low-frequency vibration for fouling mitigation and intensification of thermal performance of a plate heat exchanger working with CuO/water nanofluid. Applied Thermal Engineering 121, 388–399.

Shiravi, A.H., Shafiee, M., Firoozzadeh, M., Bostani, H., Bozorgmehrian, M., 2020. Experimental study on convective heat transfer and entropy generation of carbon black nanofluid turbulent flow in a helical coiled heat exchanger. Journal of Thermal Analysis and Calorimetry.

Simpson, S., Schelfhout, A., Golden, C., Vafaei, S., 2018. Nanofluid thermal conductivity and effective parameters. Applied Sciences (Switzerland) 9, 1–56.

Sodagar-Abardeh, J., Ebrahimi-Moghadam, A., Farzaneh-Gord, M., Norouzi, A., 2020. Optimizing chevron plate heat exchangers based on the second law of thermodynamics and genetic algorithm. Journal of Thermal Analysis and Calorimetry 139, 3563–3576.

Soltanimehr, M., Afrand, M., 2016. Thermal conductivity enhancement of COOH-functionalized MWCNTs/ethylene glycol–water nanofluid for application in heating and cooling systems. Applied Thermal Engineering 105, 716–723.

Srinivas, T., Vinod, A.V., 2016. The Effective Thermal Conductivity of Water Based Nanofluids at Different Temperatures. Journal of Testing and Evaluation 44, 280–289.

Suganthi, K.S., Leela Vinodhan, V., Rajan, K.S., 2014. Heat transfer performance and transport properties of ZnO–ethylene glycol and ZnO–ethylene glycol–water nanofluid coolants. Applied Energy 135, 548–559.

Sun, B., Peng, C., Zuo, R., Yang, D., Li, H., 2016. Investigation on the flow and convective heat transfer characteristics of nanofluids in the plate heat exchanger. Experimental Thermal and Fluid Science 76, 75–86.

Sundar, L. Syam, Farooky, M.H., Sarada, S.N., Singh, M.K., Farooky, H., Sarada, S.N., Singh, M.K., 2013. Experimental thermal conductivity of ethylene glycol and water mixture

based low volume concentration of Al2O3 and CuO nanofluids. International Communications in Heat and Mass Transfer 41, 41–46.

Sundar, L.S., Mathew, B., Sefelnasr, A., Sherif, M., Sousa, A.C.M., 2021. Second law of thermodynamic analysis of 40:60% propylene glycol and water mixture based nanodiamond nanofluid under transition flow. Diamond and Related Materials 117, 108480.

Sundar, L.S., Ramana, E.V., Singh, M.K., Sousa, A.C.M., 2014. Thermal conductivity and viscosity of stabilized ethylene glycol and water mixture Al2O3 nano fluids for heat transfer applications : An experimental study. International Communications in Heat and Mass Transfer 56, 86–95.

Sundar, L Syam, Sharma, K. V, Naik, M.T., Singh, M.K., 2013. Empirical and theoretical correlations on viscosity of nanofluids: A review. Renewable and Sustainable Energy Reviews 25, 670–686.

Syam Sundar, L., Mesfin, S., Venkata Ramana, E., Said, Z., Sousa, A.C.M., 2021. Experimental investigation of thermo-physical properties, heat transfer, pumping power, entropy generation, and exergy efficiency of nanodiamond + Fe3O4/60:40% water-ethylene glycol hybrid nanofluid flow in a tube. Thermal Science and Engineering Progress 21, 100799.

Tabari, Z.T., Heris, S.Z., 2015. Heat Transfer Performance of Milk Pasteurization Plate Heat Exchangers Using MWCNT/Water Nanofluid. Journal of Dispersion Science and Technology 36, 196–204.

Taghizadeh-Tabari, Z., Zeinali Heris, S., Moradi, M., Kahani, M., 2016. The study on application of TiO2/water nanofluid in plate heat exchanger of milk pasteurization industries. Renewable and Sustainable Energy Reviews 58, 1318–1326.

Tahani, M., Vakili, M., Khosrojerdi, S., 2016. Experimental evaluation and ANN modeling of thermal conductivity of graphene oxide nanoplatelets/deionized water nanofluid. International Communications in Heat and Mass Transfer 76, 358–365.

Teng, T.P., Hung, Y.H., 2014. Estimation and experimental study of the density and specific heat for alumina nanofluid. Journal of Experimental Nanoscience 9, 707–718.

Tiwari, A.K., Ghosh, P., Sarkar, J., 2015. Particle concentration levels of various nanofluids in plate heat exchanger for best performance. International Journal of Heat and Mass Transfer 89, 1110–1118.

Tiwari, A.K., Ghosh, P., Sarkar, J., 2013a. Performance comparison of the plate heat exchanger using different nanofluids. Experimental Thermal and Fluid Science 49, 141–151.

Tiwari, A.K., Ghosh, P., Sarkar, J., 2013b. Heat transfer and pressure drop characteristics of CeO2/water nanofluid in plate heat exchanger. Applied Thermal Engineering 57, 24–32.

Toghraie, D., Sina, N., Jolfaei, N.A., Hajian, M., Afrand, M., 2019. Designing an Artificial Neural Network (ANN) to predict the viscosity of Silver/Ethylene glycol nanofluid at different temperatures and volume fraction of nanoparticles. Physica A: Statistical Mechanics and its Applications 534, 122142.

Tsai, Y.-C., Liu, F.-B., Shen, P.-T., 2009. Investigations of the pressure drop and flow distribution in a chevron-type plate heat exchanger. International Communications in Heat and Mass Transfer 36, 574–578.

Vajjha, R.S., Das, D.K., 2009. Experimental determination of thermal conductivity of three nanofluids and development of new correlations. International Journal of Heat and Mass Transfer 52, 4675–4682.

Vajjha, R.S., Das, D.K., 2008. Measurements of Specific Heat and Density of Al2O3 Nanofluid. AIP Conference Proceedings 1063, 361–370.

Vajjha, R.S., Das, D.K., Mahagaonkar, B.M., 2009. Density measurement of different nanofluids and their comparison with theory. Petroleum Science and Technology 27, 612–624.

Wang, X. ju, Zhu, D. sheng, yang, S., 2009. Investigation of pH and SDBS on enhancement of thermal conductivity in nanofluids. Chemical Physics Letters 470, 107–111.

Wang, X.J., Li, H., Li, X.F., Wang, Z.F., Lin, F., 2011. Stability of TiO2 and Al2O3 nanofluids. Chinese Physics Letters 28, 4–8.

Wang, Z., Wu, Z., Han, F., Wadsö, L., Sundén, B., 2018. Experimental comparative evaluation of a graphene nanofluid coolant in miniature plate heat exchanger. International Journal of Thermal Sciences 130, 148–156.

Wole-Osho, I., Okonkwo, E.C., Adun, H., Kavaz, D., Abbasoglu, S., 2020. An intelligent approach to predicting the effect of nanoparticle mixture ratio, concentration and temperature on thermal conductivity of hybrid nanofluids. Journal of Thermal Analysis and Calorimetry.

Wong, K. V., De Leon, O., 2010. Applications of nanofluids: Current and future. Advances in

Mechanical Engineering 2010.

Wu, D., Zhu, H., Wang, L., Liu, L., 2009. Critical Issues in Nanofluids Preparation, Characterization Conductivity. Current Nano 5, 103–112.

Xuan, Y., Roetzel, W., 2000. Conceptions for heat transfer correlation of nanofluids. International Journal of Heat and Mass Transfer 43, 3701–3707.

Yang, L., Ji, W., Zhang, Z., Jin, X., 2019a. Thermal conductivity enhancement of water by adding graphene Nano-sheets: Consideration of particle loading and temperature effects. International Communications in Heat and Mass Transfer 109, 104353.

Yang, L., Mao, M., Huang, J. nan, Ji, W., 2019b. Enhancing the thermal conductivity of SAE 50 engine oil by adding zinc oxide nano-powder: An experimental study. Powder Technology 356, 335–341.

Yiamsawas, T., Mahian, O., Dalkilic, A.S., Kaewnai, S., Wongwises, S., 2013. Experimental studies on the viscosity of TiO2 and Al2O3 nanoparticles suspended in a mixture of ethylene glycol and water for high temperature applications. Applied Energy 111, 40–45.

Yu, F., Chen, Y., Liang, X., Xu, J., Lee, C., Liang, Q., Tao, P., Deng, T., 2017. Dispersion stability of thermal nanofluids. Progress in Natural Science: Materials International 27, 531–542.

Yu, W., Xie, H., 2012. A Review onNanofluids: Preparation, StabilityMechanisms, and Applications. Journal of Nanomaterials 87, 1–17.

Yu, W., Xie, H., Li, Y., Chen, L., Wang, Q., 2012. Experimental investigation on the heat transfer properties of Al2O3 nanofluids using the mixture of ethylene glycol and water as base fluid. Powder Technology 230, 14–19.

Zahrani, A.S., Islam, M.S., Saha, S., 2019. A thermo-hydraulic characteristics investigation in corrugated plate heat exchanger. Energy Procedia 160, 597–605.

Zhang, J., Zhu, X., Mondejar, M.E., Haglind, F., 2019. A review of heat transfer enhancement techniques in plate heat exchangers. Renewable and Sustainable Energy Reviews 101, 305–328.

Zhang, T., Zou, Q., Cheng, Z., Chen, Z., Liu, Y., Jiang, Z., 2021. Effect of particle concentration on the stability of water-based SiO2 nanofluid. Powder Technology 379, 457–465.

Zhao, N., Li, Z., 2017. Experiment and Artificial Neural Network Prediction of Thermal Conductivity and Viscosity for Alumina-Water Nanofluids. Materials 10, 552.

Zheng, D., Wang, J., Chen, Z., Baleta, J., Sundén, B., 2020. Performance analysis of a plate heat exchanger using various nanofluids. International Journal of Heat and Mass Transfer 158, 119993.

Zhou, S.Q., Ni, R., 2008. Measurement of the specific heat capacity of water-based Al2 O3 nanofluid. Applied Physics Letters 92, 1–4.

Zhu, H., Lin, Y., Yin, Y., 2004. A novel one-step chemical method for preparation of copper nanofluids. Journal of Colloid and Interface Science 277, 100–103.

Zimparov, V., 2002. Energy conservation through heat transfer enhancement techniques. International Journal of Energy Research 26, 675–696.

Żyła, G., 2017. Viscosity and thermal conductivity of MgO–EG nanofluids: Experimental results and theoretical models predictions. Journal of Thermal Analysis and Calorimetry 129, 171–180.

Appendix-I

Uncertainty analysis

Uncertainty analysis was performed considering the error in measurement caused while measuring the thermal conductivity. Measurement errors in temperature, thermal conductivity and mass of the nanoparticles were considered to calculate the experimental uncertainty. The method proposed by Moffat (1988) was employed to calculate the uncertainty as follows

Thermal conductivity (A1)

$$\frac{\delta k}{k} = \sqrt{\left(\frac{\delta T}{T} \times 100\right)^2 + \left(\frac{\delta k}{k} \times 100\right)^2 + \left(\frac{\delta w}{w} \times 100\right)^2}$$

$$\frac{\delta k}{k} = \sqrt{\left(\frac{0.01}{5} \times 100\right)^2 + \left(\frac{0.001}{0.410} \times 100\right)^2 + \left(\frac{0.0001}{0.02} \times 100\right)^2}$$

$$\frac{\delta k}{k} = \sqrt{(0.02)^2 + (0.243)^2 + (0.5)^2} = 0.56\%$$

Viscosity (A2)

$$\frac{\delta \mu}{\mu} = \sqrt{\left(\frac{\delta T}{T} \times 100\right)^2 + \left(\frac{\delta \mu}{\mu} \times 100\right)^2 + \left(\frac{\delta w}{w} \times 100\right)^2}$$

$$\frac{\delta \mu}{\mu} = \sqrt{\left(\frac{0.01}{5} \times 100\right)^2 + \left(\frac{0.001}{1.163} \times 100\right)^2 + \left(\frac{0.0001}{0.02} \times 100\right)^2}$$

$$\frac{\delta \mu}{\mu} = \sqrt{(0.02)^2 + (0.086)^2 + (0.5)^2} = 0.51\%$$

Heat transfer

Hot-fluid side calculations (A3)

$$Q_h = m_{hf} c_{phf} \left(T_{h,in} - T_{h,out}\right)$$

$$\frac{\delta Q_h}{Q_h} = \sqrt{\left(\frac{\delta m_h}{m_h} \times 100\right)^2 + \left(\frac{\delta c_{phf}}{c_{phf}} \times 100\right)^2 + \left(\frac{\delta (T_{h,in} - T_{h,out})}{(T_{h,in} - T_{h,out})} \times 100\right)^2}$$

$$\frac{\delta Q_h}{Q_h} = \sqrt{\left(\frac{0.1}{10.9} \times 100\right)^2 + (0.5)^2 + \left(\frac{0.1}{(60.1 - 38.1)} \times 100\right)^2}$$

$$\frac{\delta Q_h}{Q_h} = \sqrt{(0.917)^2 + (0.5)^2 + (0.454)^2} = 1.14\%$$

Cold -fluid side calculations (A4)

$$\frac{\delta Q_{nf}}{Q_{nf}} = \sqrt{\left(\frac{\delta m_{nf}}{m_{nf}} \times 100\right)^2 + \left(\frac{\delta c_{pnf}}{c_{pnf}} \times 100\right)^2 + \left(\frac{\delta (T_{nf,in} - T_{nf,out})}{(T_{nf,in} - T_{nf,out})} \times 100\right)^2}$$

$$\frac{\delta Q_{nf}}{Q_{nf}} = \sqrt{\left(\frac{0.1}{12.4} \times 100\right)^2 + (0.5)^2 + \left(\frac{0.1}{(47 - 20.1)} \times 100\right)^2}$$

$$\frac{\delta Q_{nf}}{Q_{nf}} = \sqrt{(0.806)^2 + (0.5)^2 + (0.372)^2} = 1.02\%$$

Overall heat transfer coefficient (A5)

$$U = \frac{Q_{avg}}{A.LMTD}$$

$$LMTD = \frac{(T_{hf,in} - T_{nf,out}) - (T_{hf,out} - T_{nf,in})}{\ln\left(\frac{T_{hf,in} - T_{nf,out}}{T_{hf,out} - T_{nf,in}}\right)}$$

$$Q_{avg} = \frac{Q_{hf} + Q_{nf}}{2}$$

$$Q_{avg} = \frac{1.14+1.02}{2} = 1.08\%$$

$T_{h,in} - T_{nf,out}$ =60-47.1=12.9 ºC and $T_{h,out} - T_{nf,in}$ =38.2-20.1=18.1 ºC

$$T_{b,hf} = \frac{T_{hf,in} + T_{hf,out}}{2} \qquad T_{b,nf} = \frac{T_{nf,in} + T_{nf,out}}{2}$$

$$\frac{\delta U}{U} = \sqrt{\left(\frac{\delta Q_{avg}}{Q_{avg}} \times 100\right)^2 + \left(\frac{\delta A}{A} \times 100\right)^2 + \left(\frac{\delta (LMTD)}{(LMTD)} \times 100\right)^2}$$

$$\frac{\delta U}{U} = \sqrt{\left(\frac{\delta Q_{avg}}{Q_{avg}} \times 100\right)^2 + \left(\frac{0.01}{0.85} \times 100\right)^2 + \left(\frac{0.1}{13.09} \times 100\right)^2}$$

$$\frac{\delta U}{U} = \sqrt{(1.08)^2 + (1.176)^2 + (0.764)^2} = 1.77\%$$

Reynolds number (A6)

$$Re_h = \frac{G_h D_h}{\mu_h}$$

$$\frac{\delta Re}{Re} = \sqrt{\left(\frac{\delta G_h}{G_h} \times 100\right)^2 + \left(\frac{\delta D_h}{D_h} \times 100\right)^2 + \left(\frac{\delta \mu_h}{\mu_h} \times 100\right)^2}$$

$$\frac{\delta Re}{Re} = \sqrt{\left(\frac{0.1}{67.64} \times 100\right)^2 + \left(\frac{0.1}{5.6} \times 100\right)^2 + (0.51)^2}$$

$$\frac{\delta Re}{Re} = \sqrt{(0.148)^2 + (1.78)^2 + (0.51)^2} = 1.85\%$$

Prandtl number (A7)

$$Pr = {}^{\mu c_p}/_{k}$$

$$\frac{\delta Pr}{Pr} = \sqrt{\left(\frac{\delta C_p}{C_p} \times 100\right)^2 + \left(\frac{\delta k}{\mathrm{k}} \times 100\right)^2 + \left(\frac{\delta \mu}{\mu} \times 100\right)^2}$$

$$\frac{\delta Pr}{Pr} = \sqrt{(0.5)^2 + (0.56)^2 + (0.51)^2} = 0.90\%$$

Nusselt number of hot fluid (A8)

$$\frac{\delta Nu_h}{Nu_h} = \sqrt{\left(\frac{\delta Re}{Re} \times 100\right)^2 + \left(\frac{\delta Pr}{Pr} \times 100\right)^2}$$

$$\frac{\delta Nu_h}{Nu_h} = \sqrt{\left(\frac{\delta Re}{Re} \times 100\right)^2 + \left(\frac{\delta Pr}{Pr} \times 100\right)^2}$$

$$\frac{\delta Nu_h}{Nu_h} = \sqrt{(1.85)^2 + (0.9)^2} = 2.06\%$$

Heat transfer coefficient of hot fluid (A9)

$$h_{hf} = {Nu\ D_h}/{k}$$

$$\frac{\delta h_{hf}}{h_{hf}} = \sqrt{\left(\frac{\delta Re}{Re} \times 100\right)^2 + \left(\frac{\delta D_h}{D_h} \times 100\right)^2 + \left(\frac{\delta k}{\mathrm{k}} \times 100\right)^2}$$

$$\frac{\delta h_{hf}}{h_{hf}} = \sqrt{(1.85)^2 + (1.78)^2 + (0.56)^2} = 2.62\%$$

Heat transfer coefficient of nanofluid (A10)

$$\frac{\delta h_{nf}}{h_{nf}} = \sqrt{\left(\frac{\delta U}{U} \times 100\right)^2 + \left(\frac{\delta h_{hf}}{h_{hf}} \times 100\right)^2 + \left(\frac{\delta t}{t} \times 100\right)^2 + \left(\frac{\delta k_p}{k_p} \times 100\right)^2}$$

$$\frac{\delta h_{nf}}{h_{nf}} = \sqrt{(1.77)^2 + (2.62)^2 + (0.2)^2 + \left(\frac{0.1}{16.5} \times 100\right)^2}$$

$$\frac{\delta h_{nf}}{h_{nf}} = \sqrt{(1.77)^2 + (2.62)^2 + (0.2)^2 + (0.6)^2} = 3.22\%$$

Nusselt number of nanofluid (A11)

$$Nu_{nf} = \frac{h_{nf} D_h}{k_{nf}}$$

$$\frac{\delta Nu_{nf}}{Nu_{nf}} = \sqrt{\left(\frac{\delta h_{nf}}{h_{nf}} \times 100\right)^2 + \left(\frac{\delta D_h}{D_h} \times 100\right)^2 + \left(\frac{\delta k_{nf}}{k_{nf}} \times 100\right)^2}$$

$$\frac{\delta Nu_{nf}}{Nu_{nf}} = \sqrt{(3.22)^2 + \left(\frac{0.2}{28} \times 100\right)^2 + (0.56)^2}$$

$$\frac{\delta Nu_{nf}}{Nu_{nf}} = \sqrt{(3.28)^2 + (0.71)^2 + (0.56)^2} = 3.34\%$$

Peclet number (A12)

$$Pe = \frac{u\ D_h}{\alpha} = RePr$$

$$\frac{\delta Pe}{Pe} = \sqrt{(Re)^2 + (Pr)^2}$$

$$\frac{\delta Pe}{Pe} = \sqrt{(1.85)^2 + (0.90)^2} = 2.05\%$$

Frictional factor (A13)

$$f = \frac{\Delta p \, \rho_{nf} \, D_h}{2 N_{cp} L_{eff} {G_{nf}}^2}$$

$$\frac{\delta f}{f} = \sqrt{\left(\frac{\delta \Delta p}{\Delta p} \times 100\right)^2 + \left(\frac{\delta \rho_{nf}}{\rho_{nf}} \times 100\right)^2 + \left(\frac{\delta D_h}{D_h} \times 100\right)^2 + \left(\frac{\delta L_{eff}}{L_{eff}} \times 100\right)^2 + \left(\frac{2 \times \delta G_{nf}}{G_{nf}} \times 100\right)^2}$$

$$\frac{\delta f}{f} = \sqrt{\left(\frac{10}{2320} \times 100\right)^2 + (1.78)^2 + (0.5)^2 + (0.5)^2 + (2 \times 0.148)^2}$$

$$\frac{\delta f}{f} = \sqrt{(0.43)^2 + (1.78)^2 + (0.5)^2 + (0.5)^2 + (2 \times 0.148)^2} = 1.99\%$$

Appendix II

Heat transfer using Al_2O_3 nanofluid: Experimental results

Nanofluid inlet temperature = 20 ºC,

Hot fluid temperature = 60 ºC, Hot fluid flow rate= 10 lpm

Table A1 Outlet temperatures of hot fluid and cold fluid (nanofluid) (ºC)

Concentration	Temperature (ºC)	Nanofluid flow rate (lpm)				
		11	12.5	15	17.5	19
EG:water(35:65)	T_{ho}	37.9	36	34.3	32.9	31.6
	T_{co}	43.9	42.3	40.7	39.2	37.6
0.2 wt.%	T_{ho}	37.6	35.7	33.9	32.5	31.2
	T_{co}	44.2	42.6	41	39.4	37.9
0.5 wt.%	T_{ho}	37.4	35.4	33.7	32.2	30.8
	T_{co}	44.4	42.7	41.2	39.6	38.2
1 wt.%	T_{ho}	37.1	35.2	33.4	32	30.7
	T_{co}	44.8	43.2	41.8	40.3	38.8
1.5 wt.%	T_{ho}	36.8	34.9	33.1	31.6	30.3
	T_{co}	45.1	43.5	42	40.4	38.9
2 wt.%	T_{ho}	36.6	34.7	32.8	31.4	30
	T_{co}	45.5	43.9	42.2	40.6	39.1

Nanofluid inlet temperature = 10 ºC

Hot fluid temperature = 60 ºC, Hot fluid flow rate= 10 lpm

Table A2 Outlet temperatures of hot fluid and cold fluid (nanofluid) (ºC)

Concentration	Temperature (ºC)	Nanofluid flow rate (lpm)				
		11	12.5	15	17.5	19
EG:water(35:65)	T_{ho}	32.5	28.8	26.4	24.9	23.6
	T_{co}	40.2	37.8	35.8	34.4	32.5
0.2 wt.%	T_{ho}	32.3	28.6	26.1	24.5	23.2
	T_{co}	40.5	38.2	36.2	34.8	32.9
0.5 wt.%	T_{ho}	31.9	28.2	25.8	24.3	23
	T_{co}	40.6	38.3	36.4	35	33.1
1 wt.%	T_{ho}	31.7	28	25.4	23.9	22.6
	T_{co}	41.1	38.7	36.8	35.5	33.6
1.5 wt.%	T_{ho}	31.5	27.8	25.2	23.7	22.3
	T_{co}	41.3	39.1	37.2	35.8	33.9
2 wt.%	T_{ho}	31.3	27.5	24.8	23.3	22
	T_{co}	41.8	39.4	37.4	36	34.1

Nanofluid inlet temperature = -5 ºC

Hot fluid temperature = 60 ºC, Hot fluid flow rate= 10 lpm

Table A3 Outlet temperatures of hot fluid and cold fluid (nanofluid) (ºC)

Concentration	Temperature (ºC)	Nanofluid flow rate (lpm)				
		11	12.5	15	17.5	19
EG:water(35:65)	T_{ho}	21.7	19.2	16.8	14.9	12.8
	T_{co}	35.1	32.5	29.6	27.3	24.5
0.2 wt.%	T_{ho}	21.5	19	16.5	14.5	12.4
	T_{co}	35.4	32.9	30	27.7	24.9
0.5 wt.%	T_{ho}	21.1	18.6	16.2	14.3	12.2
	T_{co}	35.5	33	30.2	27.9	25.1
1 wt.%	T_{ho}	20.9	18.4	15.8	13.9	11.8
	T_{co}	36	33.4	30.6	28.4	25.6
1.5 wt.%	T_{ho}	20.7	18.2	15.6	13.7	11.5
	T_{co}	36.2	33.8	31	28.7	25.9
2 wt.%	T_{ho}	20.5	17.9	15.2	13.3	11.2
	T_{co}	36.7	34.1	31.2	28.9	26.1

Nanofluid inlet temperature = 20 ºC

Hot fluid temperature = 60 ºC, Hot fluid flow rate= 12.5 lpm

Table A4 Outlet temperatures of hot fluid and cold fluid (nanofluid) (ºC)

Concentration	Temperature (ºC)	Nanofluid flow rate (lpm)				
		11	12.5	15	17.5	19
EG:water(35:65)	T_{ho}	38	36.9	34.4	33.2	31.7
	T_{co}	47.1	46.2	44.1	42.9	41.2
0.2 wt.%	T_{ho}	37.8	36.6	34	32.8	31.3
	T_{co}	47.4	46.5	44.4	43.2	41.5
0.5 wt.%	T_{ho}	37.6	36.3	33.8	32.5	30.9
	T_{co}	47.6	46.6	44.6	43.4	41.8
1 wt.%	T_{ho}	37.3	36.1	33.5	32.3	30.8
	T_{co}	48	47.1	45.2	44.1	42.4
1.5 wt.%	T_{ho}	37	35.8	33.2	31.9	30.4
	T_{co}	48.3	47.4	45.4	44.2	42.5
2 wt.%	T_{ho}	36.8	35.6	32.9	31.7	30.1
	T_{co}	48.7	47.8	45.6	44.4	42.7

Nanofluid inlet temperature = 10 ºC

Hot fluid temperature = 60 ºC, Hot fluid flow rate= 12.5 lpm

Table A5 Outlet temperatures of hot fluid and cold fluid (nanofluid) (ºC)

Concentration	Temperature (ºC)	Nanofluid flow rate (lpm)				
		11	12.5	15	17.5	19
EG:water(35:65)	T_{ho}	31.6	30.4	27.9	26.9	25.3
	T_{co}	45.7	44.1	40.5	38.7	36.7
0.2 wt.%	T_{ho}	31.4	30.2	27.6	26.5	24.9
	T_{co}	46	44.5	40.9	39.1	37.1
0.5 wt.%	T_{ho}	31	29.8	27.3	26.3	24.7
	T_{co}	46.1	44.6	41.1	39.3	37.3
1 wt.%	T_{ho}	30.8	29.6	26.9	25.9	24.3
	T_{co}	46.6	45	41.5	39.8	37.8
1.5 wt.%	T_{ho}	30.6	29.4	26.7	25.7	24
	T_{co}	46.8	45.4	41.9	40.1	38.1
2 wt.%	T_{ho}	30.4	29.1	26.3	25.3	23.7
	T_{co}	47.3	45.7	42.1	40.3	38.3

Nanofluid inlet temperature = -5 ºC

Hot fluid temperature = 60 ºC, Hot fluid flow rate= 12.5 lpm

Table A6 Outlet temperatures of hot fluid and cold fluid (nanofluid) (ºC)

Concentration	Temperature (ºC)	Nanofluid flow rate (lpm)				
		11	12.5	15	17.5	19
EG:water(35:65)	T_{ho}	21.1	18.9	15.8	14.2	12.8
	T_{co}	43.9	41.1	36.9	34.6	32.8
0.2 wt.%	T_{ho}	20.9	18.7	15.5	13.8	12.4
	T_{co}	44.2	41.5	37.3	35	33.2
0.5 wt.%	T_{ho}	20.5	18.3	15.2	13.6	12.2
	T_{co}	44.3	41.6	37.5	35.2	33.4
1 wt.%	T_{ho}	20.3	18.1	14.8	13.2	11.8
	T_{co}	44.8	42	37.9	35.7	33.9
1.5 wt.%	T_{ho}	20.1	17.9	14.6	13	11.5
	T_{co}	45	42.4	38.3	36	34.2
2 wt.%	T_{ho}	19.9	17.6	14.2	12.6	11.2
	T_{co}	45.5	42.7	38.5	36.2	34.4

Heat transfer using TiO_2 nanofluid: Experimental results

Nanofluid inlet temperature = 20 ºC

Hot fluid temperature = 60 ºC, Hot fluid flow rate= 10 lpm

Table A7 Outlet temperatures of hot fluid and cold fluid (nanofluid) (ºC)

Concentration	Temperature (ºC)	Nanofluid flow rate (lpm)				
		11	12.5	15	17.5	19
EG:water(35:65)	T_{ho}	37.9	36	34.3	32.9	31.6
	T_{co}	43.9	42.3	40.7	39.2	37.6
0.2 wt.%	T_{ho}	37.8	35.9	34.2	32.7	31.4
	T_{co}	44	42.4	40.9	39.3	37.8
0.5 wt.%	T_{ho}	37.6	35.7	34	32.5	31.2
	T_{co}	44.2	42.6	41	39.4	37.9
1 wt.%	T_{ho}	37.3	35.4	33.7	32.2	30.9
	T_{co}	44.4	42.8	41.4	39.8	38.3
1.5 wt.%	T_{ho}	37.2	35.3	33.6	32.1	30.8
	T_{co}	44.7	43.1	41.6	40.1	38.6
2 wt.%	T_{ho}	36.9	35	33.2	31.7	30.4
	T_{co}	45	43.4	41.8	40.3	38.8

Nanofluid inlet temperature = 10 ºC

Hot fluid temperature = 60 ºC,Hot fluid flow rate= 10 lpm

Table A8 Outlet temperatures of hot fluid and cold fluid (nanofluid) (ºC)

Concentration	Temperature (ºC)	Nanofluid flow rate (lpm)				
		11	12.5	15	17.5	19
EG:water(35:65)	T_{ho}	32.5	28.8	26.4	24.9	23.6
	T_{co}	40.2	37.8	35.8	34.4	32.5
0.2 wt.%	T_{ho}	32.4	28.7	26.2	24.7	23.4
	T_{co}	40.3	38	36	34.6	32.7
0.5 wt.%	T_{ho}	32.2	28.5	26.1	24.6	23.2
	T_{co}	40.5	38.1	36.1	34.8	32.9
1 wt.%	T_{ho}	32	28.3	25.8	24.3	22.9
	T_{co}	40.7	38.3	36.4	35.1	33.2
1.5 wt.%	T_{ho}	31.7	28	25.5	24	22.7
	T_{co}	41.1	38.7	36.7	35.3	33.4
2 wt.%	T_{ho}	31.5	27.8	25.3	23.8	22.4
	T_{co}	41.3	38.9	36.9	35.5	33.6

Nanofluid inlet temperature = -5 ºC

Hot fluid temperature = 60 ºC, Hot fluid flow rate= 10 lpm

Table A9 Outlet temperatures of hot fluid and cold fluid (nanofluid) (ºC)

Concentration	Temperature (ºC)	Nanofluid flow rate (lpm)				
		11	12.5	15	17.5	19
EG:water(35:65)	T_{ho}	21.7	19.2	16.8	14.9	12.8
	T_{co}	35.1	32.5	29.6	27.3	24.5
0.2 wt.%	T_{ho}	21.6	19.1	16.6	14.7	12.6
	T_{co}	35.2	32.7	29.8	27.5	24.7
0.5 wt.%	T_{ho}	21.4	18.9	16.5	14.6	12.4
	T_{co}	35.4	32.8	29.9	27.7	24.9
1 wt.%	T_{ho}	21.2	18.7	16.2	14.3	12.1
	T_{co}	35.6	33	30.2	28	25.2
1.5 wt.%	T_{ho}	20.9	18.4	15.9	14	11.9
	T_{co}	36	33.4	30.5	28.2	25.4
2 wt.%	T_{ho}	20.7	18.2	15.7	13.8	11.6
	T_{co}	36.2	33.6	30.7	28.4	25.6

Nanofluid inlet temperature = 20 ºC

Hot fluid temperature = 60 ºC, Hot fluid flow rate= 12.5 lpm

Table A10 Outlet temperatures of hot fluid and cold fluid (nanofluid) (ºC)

Concentration	Temperature (ºC)	Nanofluid flow rate (lpm)				
		11	12.5	15	17.5	19
EG:water(35:65)	T_{ho}	38	36.9	34.4	33.2	31.7
	T_{co}	47.1	46.2	44.1	42.9	41.2
0.2 wt.%	T_{ho}	38	36.8	34.3	33	31.5
	T_{co}	47.2	46.3	44.3	43.1	41.4
0.5 wt.%	T_{ho}	37.8	36.6	34.1	32.8	31.3
	T_{co}	47.4	46.5	44.4	43.2	41.5
1 wt.%	T_{ho}	37.5	36.3	33.8	32.5	31
	T_{co}	47.6	46.7	44.8	43.6	41.9
1.5 wt.%	T_{ho}	37.4	36.2	33.7	32.4	30.9
	T_{co}	47.9	47	45	43.9	42.2
2 wt.%	T_{ho}	37.1	35.9	33.3	32	30.5
	T_{co}	48.2	47.3	45.2	44.1	42.4

Nanofluid inlet temperature = 10 ºC

Hot fluid temperature = 60 ºC, Hot fluid flow rate= 12.5 lpm

Table A11 Outlet temperatures of hot fluid and cold fluid (nanofluid) (ºC)

Concentration	Temperature (ºC)	Nanofluid flow rate (lpm)				
		11	12.5	15	17.5	19
EG:water(35:65)	T_{ho}	31.6	30.4	27.9	26.9	25.3
	T_{co}	45.7	44.1	40.5	38.7	36.7
0.2 wt.%	T_{ho}	31.5	30.3	27.7	26.7	25.1
	T_{co}	45.8	44.3	40.7	38.9	36.9
0.5 wt.%	T_{ho}	31.3	30.1	27.6	26.6	24.9
	T_{co}	46	44.4	40.8	39.1	37.1
1 wt.%	T_{ho}	31.1	29.9	27.3	26.3	24.6
	T_{co}	46.2	44.6	41.1	39.4	37.4
1.5 wt.%	T_{ho}	30.8	29.6	27	26	24.4
	T_{co}	46.6	45	41.4	39.6	37.6
2 wt.%	T_{ho}	30.6	29.4	26.8	25.8	24.1
	T_{co}	46.8	45.2	41.6	39.8	37.8

Nanofluid inlet temperature = -5 ºC

Hot fluid temperature = 60 ºC,Hot fluid flow rate= 12.5 lpm

Table A12 Outlet temperatures of hot fluid and cold fluid (nanofluid) (ºC)

Concentration	Temperature (ºC)	Nanofluid flow rate (lpm)				
		11	12.5	15	17.5	19
EG:water(35:65)	T_{ho}	21.1	18.9	15.8	14.2	12.8
	T_{co}	43.9	41.1	36.9	34.6	32.8
0.2 wt.%	T_{ho}	20.9	18.7	15.6	14	12.6
	T_{co}	44.1	41.3	37	34.7	32.9
0.5 wt.%	T_{ho}	20.8	18.6	15.5	13.8	12.4
	T_{co}	44.2	41.4	37.2	34.9	33.1
1 wt.%	T_{ho}	20.5	18.3	15	13.4	11.9
	T_{co}	44.4	41.6	37.4	35.1	33.3
1.5 wt.%	T_{ho}	20.2	18	14.8	13.2	11.7
	T_{co}	44.7	41.9	37.7	35.4	33.6
2 wt.%	T_{ho}	20	17.7	14.5	12.9	11.5
	T_{co}	45	42.2	38	35.7	33.9

List of publication

Journals

1. Yashawantha, KM, Vinod, AV. Heat transfer characteristics and entropy generation analysis in a plate heat exchanger using ethylene glycol and water mixture-based Al_2O_3 nanofluid. *Heat transfer* (Wiley) 2022; 51:296-322. https://doi.org/10.1002/htj.22308 (Scopus indexed).
2. Marigowda Yashawantha K, Venu Vinod A. ANFIS modelling of effective thermal conductivity of Ethylene Glycol and Water nanofluids for low temperature heat transfer application. *Thermal Science and Engineering Progress* (Elsevier) 2021;24:100936. https://doi.org/10.1016/j.tsep.2021.100936. (SCIE indexed).
3. Yashawantha, K.M., Gurjar, G. & Vinod, A.V. Low Temperature Heat Transfer in Plate Heat Exchanger Using Ethylene Glycol–Water Based Al_2O_3 Nanofluid. *International Journal of Thermophysics* (Springer) 42, 90 (2021). https://doi.org/10.1007/s10765-021-02843-8 (SCI indexed).
4. Yashawantha, K.M., Vinod, A.V. ANN modelling and experimental investigation on effective thermal conductivity of ethylene glycol:water nanofluids. *Journal of Thermal Analysis and Calorimetry* (Springer) 145, 609–630 (2021). https://doi.org/10.1007/s10973-020-09756-y (SCI indexed).

Conference

1. Yashawantha K M, A. Venu Vinod "Thermal conductivity and stability of Al_2O_3 nanorefrigerants" was presented in CHEMCON 2019 on 15th to 17th December 2019 at Indian institute of Technology, New Delhi, (oral presentation).
2. Kyathanahalli Marigowda Yashawantha, Gaurav Gurjar and A. Venu Vinod "Stability and Thermal Conductivity of Ethylene Glycol and Water Nanofluid Containing Graphite Nanoparticles" was presented in first national conference on Innovations in Sustainable Energy and Technology (ISET) on 3rd to 4th December 2020, at Rajiv Gandhi Institute of Petroleum Technology (RGIPT), Bengaluru

Communicated

1. Kyathanahalli Marigowda Yashawantha, Venu Vinod A. "Viscosity of Water and Ethylene Glycol mixture based Al_2O_3 and TiO_2 Nanofluids: Experimental study and Prediction using Artificial Neural Networks", *International Journal of Thermophysics* (SCI) communicated.

Curriculum vitae

Name **:** Yashawantha K M

Gender **:** Male

Nationality **:** Indian

Academic Profile

M.Sc (Engg) by research: Mechanical Engineering from Visvesvaraya Technological University, Belagavi, Karnataka, India (2018)

B.E: Mechanical Engineering from Sahyadri College of Engineering & Management, Mangaluru, Karnataka, India (2011)